

# COMPUTATIONAL AND GEOMETRICAL ASPECTS OF ON-THE-FLY AMBIGUITY RESOLUTION

HASANUDDIN ZAINAL ABIDIN

January 1993



TECHNICAL REPORT  
NO. 164

## PREFACE

In order to make our extensive series of technical reports more readily available, we have scanned the old master copies and produced electronic versions in Portable Document Format. The quality of the images varies depending on the quality of the originals. The images have not been converted to searchable text.

# **COMPUTATIONAL AND GEOMETRICAL ASPECTS OF ON-THE-FLY AMBIGUITY RESOLUTION**

Hasanuddin Zainal Abidin

Department of Geodesy and Geomatics Engineering  
University of New Brunswick  
P.O. Box 4400  
Fredericton, N.B.  
Canada  
E3B 5A3

January 1993  
Latest Reprinting February 1996

© Hasanuddin Z. Abidin, 1992

## PREFACE

This technical report is a reproduction of a dissertation submitted in partial fulfillment of the requirements for the degree of Doctor of Philosophy in the Department of Surveying Engineering, October 1992. The research was supervised by Dr. David E. Wells and Dr. Alfred Kleusberg, and funding was provided by the Canadian International Development Agency.

As with any copyrighted material, permission to reprint or quote extensively from this report must be received from the author. The citation to this work should appear as follows:

Abidin, H.A. (1993). *Computational and Geometrical Aspects of On-the-Fly Ambiguity Resolution*. Ph.D. dissertation, Department of Surveying Engineering Technical Report No. 164, University of New Brunswick, Fredericton, New Brunswick, Canada, 314 pp.

## ABSTRACT

---

---

Precise (centimetre level accuracy) kinematic differential positioning using GPS (Global Positioning System) requires the use of carrier phase observations with correctly resolved integer ambiguities. On-the-fly ambiguity resolution, i.e., ambiguity resolution while the receiver is in motion, is desirable, since it increases the flexibility and reliability of kinematic positioning. On-the-fly ambiguity resolution, however, is not an easy task. A lot of factors will affect the speed and reliability of the ambiguity resolution. In general, these factors can be categorized into three broader groups, namely the ambiguity resolution technique, the effects of the observation errors and biases, and the observation geometry, i.e., the geometry between the satellites, the monitor station(s), and the user.

In this research, the possibility of performing reliable and fast on-the-fly ambiguity resolution of GPS carrier phase signals is studied. An integrated on-the-fly ambiguity resolution technique was developed for this research. This technique was designed to work with either single-frequency, codeless, or dual-frequency GPS data from a minimum of five observed satellites, and it accommodates the use of more than one monitor station. The validity of the technique has been verified using static, simulated kinematic, and kinematic GPS data. The technique has been shown to be capable of resolving initial integer ambiguities on-the-fly reliably and quickly, even instantaneously under certain conditions.

Geometrical and computational aspects of on-the-fly ambiguity resolution have also been studied in this research, particularly related to their effects on the performance of on-the-fly ambiguity resolution. The geometrical aspects studied involve the following geometrical parameters: the wavelength of the signal, selection of primary satellites, number of satellites, observation differencing strategy, location of satellites available, data rate, number of secondary monitor stations, and location of secondary monitor stations. The computational aspects studied involve the ambiguity searching space construction and the process of identifying the correct ambiguities.

## TABLE OF CONTENTS

---

---

ABSTRACT .....	ii
TABLE OF CONTENTS .....	iv
LIST OF TABLES .....	x
LIST OF FIGURES .....	xiii
ACKNOWLEDGEMENTS .....	xviii
Chapter 1. INTRODUCTION .....	1
1.1. Global Positioning System (GPS) .....	1
1.2. Fundamental GPS observations .....	5
1.3. GPS positioning accuracy .....	7
1.4. Precise kinematic applications of GPS .....	7
1.4.1. Attitude and heading determination .....	9
1.4.2. High accuracy sea surface positioning .....	9
1.4.3. Airborne photogrammetric applications .....	11
1.4.4. Precise navigation of agricultural vehicle .....	11
1.5. Motivation .....	12
1.6. Previous studies .....	13
1.7. Methodology and scope of the investigation .....	16
1.8. Outline of the dissertation .....	19
1.9. Contributions of the research .....	21

Chapter 2. ON-THE-FLY AMBIGUITY RESOLUTION .....	22
2.1 Cycle ambiguity resolution .....	22
2.3 Surfaces and lines of ambiguity .....	24
2.3 On-the-fly ambiguity resolution techniques .....	28
2.3.1 General strategy of on-the-fly ambiguity resolution .....	28
2.3.2. Extrawidelaning technique .....	30
2.3.3. Ambiguity mapping function technique .....	34
2.3.4. Least squares ambiguity searching technique .....	38
2.4. Comparison of the techniques .....	41
Chapter 3. INTEGRATED ON-THE-FLY AMBIGUITY RESOLUTION TECHNIQUE .....	43
3.1. Concept of ambiguity resolution .....	44
3.2. Use of more than one monitor station .....	45
3.3. General strategy of the integrated ambiguity resolution technique --	48
3.4. Initial ambiguity estimation .....	50
3.5. Constructing the ambiguity searching space .....	52
3.5.1. Ellipsoidal mathematical ambiguity searching space .....	54
3.5.2. Number of initial ambiguity sets .....	60
3.6. Identification of the correct integer of ambiguities .....	63
3.6.1. Compatibility test between potential coordinates and code-derived coordinates .....	66
3.6.2. Test on L1-norm of the misclosure vector .....	70
3.6.3. Compatibility test between updated coordinates and potential coordinates .....	72
3.6.4. Test on L1-norm of the residual vector .....	74
3.6.5. Test on the quadratic form of the residuals .....	76
3.6.6. Individual ambiguity mapping function test .....	78
3.6.7. Normalized ambiguity mapping function test .....	79



3.6.8. Contrast test on the quadratic forms of the residuals -----	82
3.6.9. Assurance criteria -----	83
3.7. Integer ambiguity estimation of the L1 and L2 signals -----	84
3.7.1. Dual-frequency data -----	84
3.7.2. Codeless data -----	87
 Chapter 4. VALIDATION OF ON-THE-FLY AMBIGUITY RESOLUTION TECHNIQUE -----	 91
4.1. Trimble Geodesist zero baseline results -----	92
4.1.1. Characteristics of the zero baseline data -----	92
4.1.2. On-the-fly ambiguity resolution parameters -----	94
4.1.3. On-the-fly ambiguity resolution results -----	95
4.2. Ashtech codeless static results -----	97
4.2.1. Characteristics of the codeless data -----	97
4.2.2. On-the-fly ambiguity resolution parameters -----	99
4.2.3. On-the-fly ambiguity resolution results -----	100
4.3. Rogue kinematic GPS results -----	102
4.3.1. Characteristics of the real kinematic GPS data -----	102
4.3.2. On-the-fly ambiguity resolution parameters -----	105
4.3.3. On-the-fly ambiguity resolution results -----	108
4.3.4. Verification of on-the-fly ambiguity resolution results ----	110
4.3.5. Cautionary remarks -----	122
 Chapter 5. COMPUTATIONAL ASPECTS OF THE INTEGRATED ON-THE-FLY AMBIGUITY RESOLUTION TECHNIQUE -----	 124
5.1. The ambiguity searching space construction -----	124

5.1.1.	The shape of ambiguity searching space -----	125
5.1.2.	The size of the ellipsoidal searching space -----	127
5.2.	Implementation of the validation and rejection criteria -----	133
Chapter 6.	<b>GEOMETRICAL ASPECTS OF INTEGRATED ON-THE-FLY AMBIGUITY RESOLUTION TECHNIQUE</b> -----	140
6.1.	Geometrical parameters of on-the-fly ambiguity resolution -----	140
6.2.	Physical ambiguity searching space -----	141
6.3.	Signal wavelength -----	145
6.4.	Primary satellites -----	151
6.5.	Number of satellites -----	155
6.6.	Observation differencing strategy -----	158
6.7.	Location of satellites -----	168
6.8.	Data rate -----	174
6.9.	Number of secondary monitor stations -----	179
6.10.	Location of secondary monitor stations -----	185
Chapter 7.	<b>SUMMARY, CONCLUSIONS, AND RECOMMENDATIONS</b> -----	189
7.1.	Summary of research -----	189
7.2.	Conclusions of research -----	194
7.2.1.	Construction of initial ambiguity searching space -----	194
7.2.2.	Implementation of the validation and rejection criteria -----	195
7.2.3.	Effects of the observation geometry -----	197
7.2.4.	Instantaneous on-the-fly ambiguity resolution -----	200
7.3.	Prospects and limitations of on-the-fly ambiguity resolution -----	201
7.3.1.	The prospects -----	202
7.3.2.	The limitations -----	203
7.3.	Suggestions and recommendations for future research -----	204

REFERENCES .....	206
Appendix I. LINEAR COMBINATIONS OF GPS OBSERVATIONS .....	216
I.1. Linear combination of phase observations .....	217
I.2. Wide-lane and narrow-lane combinations .....	223
I.3. Semi, half, and double wide-lane signals .....	226
Appendix II. CODE SMOOTHING USING THE CARRIER PHASES .....	229
Appendix III. COVARIANCE MATRIX OF MULTI STATION DOUBLE-DIFFERENCE OBSERVATIONS .....	232
III.1. Covariance matrix of one-way observations .....	233
III.2. Covariance matrix of between-station single-difference observations .....	234
III.3. Covariance matrix of station-satellite double-difference observations .....	235
Appendix IV. HISTOGRAM AND TIME SERIES OF THE ANTENNAS' DISTANCE DIFFERENCES .....	238
Appendix V. EFFECTS OF GEOMETRICAL PARAMETERS ON AMBIGUITY SEARCHING SPACE .....	250
V.1. Number of secondary monitor stations .....	252
V.2. Number of satellites .....	258
V.3. Primary satellites .....	262
V.4. Observation differencing strategy .....	264
Appendix VI. SIMULATED KINEMATIC GPS DATA .....	268
VI.1. Simulating the code and phase observations .....	268
VI.2. Computing the geometric range between the antenna and satellite .....	270
VI.3. Simulating the satellite ephemeris errors .....	273

VI.4. Simulating the ionospheric biases -----	276
VI.5. Simulating the observation noises -----	277
VI.6. Simulating the integer cycle ambiguity -----	278
Appendix VII. GLOSSARY OF GPS TERMINOLOGY -----	280

V I T A

## LIST OF TABLES

---



---

Tables	page
1.1. Operational GPS satellites -----	3
1.2. Requirements for navigation in agriculture -----	12
2.1. Comparison between on-the-fly ambiguity resolution techniques -----	41
3.1. Some values of Chi-squares percentiles -----	43
3.2. Some values of Normal percentiles -----	45
4.1. Data characteristics -----	93
4.2. Double-differences averaged ambiguities of L1 and L2 signals -----	93
4.3. Standard deviations -----	94
4.4. Parameter values of the identification process for single and dual frequency data -----	95
4.5. On-the-fly ambiguity resolution results of zero baseline data -----	96
4.6. Data characteristics -----	98
4.7. Double-difference averaged ambiguities of half wide-lane, L1, and half-wavelength L2 signals -----	99
4.8. Standard deviations -----	99
4.9. Parameter values of the identification process for codeless data -----	100
4.10. On-the-fly ambiguity resolution results of codeless data -----	101
4.11. Data characteristics -----	102
4.12. Zenith standard deviations -----	107
4.13. Parameter values of the identification process (A for the shorter baselines, B for the longer baselines) -----	108
4.14. Results of on-the-fly ambiguity resolution -----	109
4.15. Double-difference wide-lane integer ambiguities fixed by on-the-fly ambiguity resolution technique -----	109
4.16. Double-difference narrow-lane integer ambiguities fixed by on-the-fly ambiguity resolution technique -----	109

4.17.	Double-difference 22 minute-averaged wide-lane integer ambiguities -----	114
4.18.	Double-difference wide-lane integer ambiguities -----	115
4.19.	Double-difference 22 minute-averaged narrow-lane integer ambiguities -----	117
4.20.	Double-difference narrow-lane integer ambiguities -----	117
5.1.	On-the-fly ambiguity resolution results	
	as a function of the shape of ambiguity searching space -----	126
5.2.	Effects of different confidence levels of the ellipsoidal searching space on the ambiguity resolution times (zero-baseline data) -----	128
5.3.	Effects of different confidence levels of the ellipsoidal searching space on the ambiguity resolution times (Rogue kinematic data) -----	130
5.4.	Effects of the observation precision on the ambiguity resolution times (Trimble Geodesist zero-baseline data) -----	131
5.5.	Effects of the observation precision on the ambiguity resolution times (Rogue kinematic data) -----	131
5.6.	Differences in the identification power of the criteria -----	134
5.7.	Criteria implementation cases -----	135
5.8.	Different cases of the identification process parameter values -----	138
6.1.	Effects of the signal wavelength on the number of initial ambiguity sets -----	147
6.2.	Parameter values of the identification process for L1 and double wide-lane signals -----	149
6.3.	Effects of the signal wavelength on ambiguity resolution times -----	150
6.4.	Effects of different group of primary satellites on observation and computation times of ambiguity resolution -----	154
6.5.	Effects of the reference satellite on the number of initial ambiguity sets -----	164
6.6.	Effects of the observation differencing approach on the epoch of on-the-fly ambiguity resolution -----	165
6.7.	Effects of the observation differencing approach on the epoch of on-the-fly ambiguity resolution (sequential differencing approach) -----	166
6.8.	Effects of the reference satellite on ambiguity resolution times -----	167
6.9.	Effects of the reference satellite on ambiguity resolution times -----	167
6.10.	Time variations of the number of initial ambiguity sets (Rogue kinematic data, baseline UCLU-B3, fixed-reference differencing approach) -----	170
6.11.	Time variations of ambiguity resolution times (Rogue kinematic data, baseline UCLU-B3, fixed-reference differencing approach) -----	172
6.12.	Time variations of ambiguity resolution times (Rogue kinematic data, baseline UCLU-B3, fixed-reference differencing approach) -----	173

6.13.	Effects of data rate on the epoch of on-the-fly ambiguity resolution (Rogue kinematic data with fixed-reference differencing approach) -----	176
6.14.	Effects of data rate on the epoch of on-the-fly ambiguity resolution (Rogue kinematic data with sequential differencing approach) -----	177
6.15.	Standard deviations of L1 C/A-code pseudoranges and phases -----	180
6.16.	The average ratios of the number of initial ambiguity sets with respect to the number of secondary monitor stations -----	181
6.17.	Parameter values of the identification process (A for one monitor, B for two, three, and four monitors) -----	182
6.18.	Zenith standard deviations of pseudoranges and phases -----	186
6.19.	Parameter values of the identification process -----	187
7.1.	Summary of the verification results of the integrated on-the-fly ambiguity resolution technique -----	191
7.2.	Interval values for the identification process parameters -----	196
I.1.	Some examples of linear combination phases of dual-frequency data -----	222
I.2.	Some examples of linear combination phases of codeless data -----	222
V.1.	Effects of the geometrical parameters on the initial mathematical ambiguity searching space -----	251
V.2.	Effects of the geometrical parameters on the initial physical ambiguity searching space -----	251
VI.1.	GPS antenna coordinates of the stations for simulations -----	269
VI.2.	21 primary SV (GPS) constellation ephemerides -----	272
VI.3.	Ionospheric simulation parameters -----	277
VI.4.	Standard deviations of simulated single-frequency data -----	278

## LIST OF FIGURES

---

Figures	page
1.1. The Global Positioning System -----	2
1.2. Factors affecting GPS positioning accuracy -----	8
1.3. Many modes of GPS positioning accuracy -----	8
1.4. Factors affecting the on-the-fly ambiguity resolution -----	16
1.5. Methodology of the research investigation -----	18
2.1. Cycle ambiguity of carrier phase observation -----	23
2.2. Variations of integer ambiguities of double-difference L1-phase observations -	25
2.3. Physical surfaces of ambiguity in 2-D perspective -----	26
2.4. General strategy of on-the-fly ambiguity resolution -----	29
2.5. On-the-fly ambiguity resolution based on extrawidelaning technique -----	33
2.6. On-the-fly ambiguity resolution based on ambiguity mapping function technique -----	36
2.7. Least-squares ambiguity searching technique -----	40
3.1. Conceptual depiction of cycle ambiguity resolution -----	45
3.2. Conceptual depiction of multi monitor station on-the-fly ambiguity resolution -----	47
3.3. Integrated on-the-fly ambiguity resolution technique -----	49
3.4. Cube and ellipsoidal ambiguity searching space -----	53
3.5. Two-dimensional perspective of constructing steps of ellipsoidal ambiguity searching space -----	56
3.6. Ellipsoidal mathematical ambiguity searching space -----	59
3.7. Two-dimensional perspective of constructing mathematical searching space at various epochs -----	60
3.8. The number of initial primary ambiguity sets in the mathematical and physical searching spaces -----	61



3.9.	Flow of estimation process at a certain epoch -----	64
3.10.	Two-dimensional geometrical interpretation of first criteria -----	67
3.11.	Two-dimensional geometrical interpretation of second criteria -----	71
3.12.	Two-dimensional geometrical interpretation of third criteria -----	73
3.13.	Two-dimensional geometrical interpretation of fourth criteria -----	76
3.14.	The real term of individual ambiguity mapping function -----	79
4.1.	Satellite polar plot -----	92
4.2.	Zero-baseline length estimated from the fixed ambiguity solutions -----	97
4.3.	Relative position of stations and satellite polar plot as seen from PEPS -----	98
4.4.	Differences between the known baseline length and the baseline length estimated from the fixed ambiguity solution -----	101
4.5.	Sketch of the survey area and the buoy trajectory -----	103
4.6.	Satellite polar plot -----	104
4.7.	GPS antennas and the buoy -----	104
4.8.	The time series and histogram of the total speed of antenna B1 -----	104
4.9.	Relative positions of antennas B2 and B3 relative to antenna B1 in local geodetic coordinate system along the 22 minute trajectory -----	105
4.10.	Misclosure of relative coordinates -----	111
4.11.	Distance misclosure of the relative coordinates, based on L1 and L2 fixed ambiguity solutions -----	112
4.12.	Epoch-by-epoch and time average wide-lane ambiguities -----	113
4.13.	Epoch-by-epoch and time average narrow-lane ambiguities -----	117
4.14.	Differences of the antennas' distances on the buoy between the distances derived from the fixed ambiguity solution and their 'known' distances -----	119
4.15.	Differences of the antennas' distances on the buoy between the distances derived from the fixed ambiguity solution and their 'known' distances -----	120
4.16.	Differences of the antennas' distances on the buoy between the distances derived from the fixed ambiguity solution and their 'known' distances, in the case that the double-difference integer narrow-lane ambiguities related to antenna B1 and satellites 12 and 15 are in error of 2 cycles -----	122
5.1.	Effects of using ellipsoidal instead of cube ambiguity searching space on on-the-fly ambiguity resolution results -----	127
5.2.	Correlation between the value of the ellipsoid size indicator (NAI1) and the number of ambiguity sets inside the initial ellipsoidal searching space -----	132
5.3.	Effects of the number and type of the applied rejection criteria on the ambiguity resolution times (zero baseline data) -----	137

5.4.	Effects of different values of the identification process parameters on the observation and computation times of ambiguity resolution (Rogue kinematic data) -----	139
6.1.	Geometrical parameters of ambiguity resolution -----	141
6.2.	Two-dimensional depiction of the impacts of the signal wavelength on the number of ambiguity sets inside the physical searching space -----	146
6.3.	Two-dimensional depiction of the impacts of the signal wavelength on the identification process of the correct ambiguities (5 satellites) -----	148
6.4.	Effects of primary satellites on physical searching space -----	152
6.5.	Effects of different group of primary satellites on the number of ambiguity sets inside the initial searching space -----	152
6.6.	Effects of the primary satellites on ambiguity resolution times -----	153
6.7.	Example of the effects of the number of satellites on the size and shape of ellipsoidal searching space and the number of initial ambiguity sets inside the searching space -----	156
6.8.	Two-dimensional depiction of the impacts of satellite numbers on the ambiguity resolution process -----	157
6.9.	Example of the effects of the number of satellites on the ambiguity resolution times -----	158
6.10.	Fixed-reference and sequential differencing approaches -----	159
6.11.	Effect of observation differencing on the number of initial ambiguity sets -----	160
6.12.	Effects of differencing approach on the number of initial ambiguity sets -----	161
6.13.	Effects of differencing approach on the matrix norm $\  \lambda.GP \ $ -----	162
6.14.	Effects of the reference satellite on the number of initial ambiguity sets -----	163
6.15.	Ratio of the ambiguity resolution times between the fixed-reference and sequential differencing approaches -----	165
6.16.	Time variations of the number of initial ambiguity sets -----	169
6.17.	Time variations of PDOP values (Trimble zero baseline data) -----	169
6.18.	Time variations of PDOP values (Rogue kinematic data) -----	170
6.19.	Time variations of ambiguity resolution times (zero baseline data) -----	171
6.20.	Time series of wide-lane residuals -----	172
6.21.	Effects of the observation data interval on the epoch of ambiguity resolution as a function of different temporal location of satellites -----	178
6.22.	Ratio of the number of initial ambiguity sets with respect to the number of secondary monitor stations -----	180
6.23.	Effects of the number of secondary monitor stations on the epochs of	

	ambiguity resolution ( single-frequency, 8 satellites, constellation #2) -----	182
6.24.	Ratios between one monitor and two monitors ambiguity resolution results (single-frequency, eight satellites) -----	183
6.25.	Effects of the number of secondary monitor stations on the epochs of ambiguity resolution ( single-frequency, 7 satellites, constellation #2) -----	184
6.26.	Effects of the number of secondary monitor stations on the epochs of ambiguity resolution ( single-frequency, 6 satellites, constellation #2) -----	184
6.27.	Effects of location of secondary monitor stations on the number of initial ambiguity sets ( single-frequency, 8 satellites, 2 monitor stations, constellation #4) -----	186
6.28.	Effects of location of secondary monitor stations on the epochs of ambiguity resolution -----	188
7.1.	General strategy of integrated on-the-fly ambiguity resolution technique -----	190
7.2.	Computational parameters of on-the-fly ambiguity resolution -----	192
7.3.	Geometrical parameters of on-the-fly ambiguity resolution -----	193
7.4.	Optimal data rate implementation considerations -----	199
IV.1.	Differences of the antennas' distances on the buoy between distances derived from fixed ambiguity solution and their 'known' distances (narrow-lane signal, monitor station : UCLU) -----	240
IV.2.	Differences of the antennas' distances on the buoy between distances derived from fixed ambiguity solution and their 'known' distances (narrow-lane signal, monitor station : PGC) -----	241
IV.3.	Differences of the antennas' distances on the buoy between distances derived from fixed ambiguity solution and their 'known' distances (wide-lane signal, monitor station : UCLU) -----	242
IV.4.	Differences of the antennas' distances on the buoy between distances derived from fixed ambiguity solution and their 'known' distances (wide-lane signal, monitor station : PGC) -----	243
IV.5.	Differences of the antennas' distances on the buoy between distances derived from fixed ambiguity solution and their 'known' distances (ionospheric-free linear combination, monitor station : UCLU) -----	244
IV.6.	Differences of the antennas' distances on the buoy between distances derived from fixed ambiguity solution and their 'known' distances (ionospheric-free linear combination, monitor station : PGC) -----	245
IV.7.	Differences of the antennas' distances on the buoy between distances derived from fixed ambiguity solution and their 'known' distances	

	(L1 - signal, monitor station : UCLU) -----	246
IV.8.	Differences of the antennas' distances on the buoy between distances derived from fixed ambiguity solution and their 'known' distances	
	(L1 - signal, monitor station : PGC) -----	247
IV.9.	Differences of the antennas' distances on the buoy between distances derived from fixed ambiguity solution and their 'known' distances	
	(L2 - signal, monitor station : UCLU) -----	248
IV.10.	Differences of the antennas' distances on the buoy between distances derived from fixed ambiguity solution and their 'known' distances	
	(L2 - signal, monitor station : PGC) -----	249
V.1.	Some values of the scale factor $sf$ -----	254
V.2.	Direction cosines to the satellites -----	260
VI.1.	Relative positions of secondary monitor stations and the simulated trajectory of the moving receiver -----	269
VI.2.	Computing the geometric range between the antenna and the satellite -----	271
VI.3.	GPS satellites polar plot seen from initial position of the moving receiver -----	273
VI.4.	Satellite ephemeris errors -----	274
VI.5.	Smoothed (12-month running averages) monthly mean sunspot numbers -----	277

## ACKNOWLEDGEMENTS

---

---

First of all, I would like to thank God, the Most Beneficent and the Most Merciful, that finally I can finish my Ph.D. program in this 'well-known and tough' Department of Surveying Engineering. Although I work and strive as hard as I can, without His permission, I would not be able to finish my study.

Next, I offer my most sincere thanks to my supervisors Prof. D. E. Wells and Prof. A. Kleusberg for their guidance, constant support, and encouragement throughout my study and this research. Their constructive suggestions, inspiration, and criticism improved the whole manuscript significantly. I express my appreciation to the Canadian International Development Agency (CIDA) and Prof. D. E. Wells for financially supporting my study and research. Acknowledgement should also go to Prof. Sjamsir Mira of the Department of Geodesy, Bandung Institute of Technology, Indonesia, for supporting me in pursuing graduate studies in Canada. I am indebted also to the people and Government of Indonesia for giving me a chance to pursue a higher education while leaving my duty at the Department of Geodesy, Bandung Institute of Technology.

I would also like to thank Jan Kouba of Geophysics Division, Geological Survey of Canada, for providing the Rogue static data; Ken Doucet, of Trimble Navigation, for providing the Trimble zero baseline data; Dr. Rock Santerre, of Centre de Geomatique, Université Laval, Québec City, for providing the Ashtech codeless data; and Dr. Herb

Dragert, of Pacific Geoscience Centre, Sidney, British Columbia, Canada, for providing the Rogue kinematic data used in this research.

The constructive recommendations of the Examining Board have been appreciated and have helped to improve the final version of this thesis. The members of the Board consisted of Prof. D. E. Wells (co-supervisor), Prof. A. Kleusberg (co-supervisor), Prof. A. Hamilton (Surveying Engineering), Prof. W. Knight (Mathematics and Computer Science), Prof. G. Jordan (Forest Resources) and Dr. Benjamin Remondi (National Geodetic Survey, U.S.A).

Last, but not least, I would like also to thank my wife, Budi Mulyanti, for her love, understanding and encouragement. With our daughter, Aulia, and our twin boys, Hanif and Ihsan, they enlighten my days and make this research work much easier to be pursued in this quiet and small town of Fredericton. Finally, I would like to dedicate this thesis to my parents. Their love, their material and spiritual supports, and their concern about my education, have brought me to this stage of achievement.

*In the creation of the heavens and the earth,  
and the alternation of Night and Day,  
there are indeed Signs,  
for men of understanding.*

*(Al-Qur'an, 3 : 190)*

### 1.1. Global Positioning System (GPS)

The NAVSTAR (Navigation System using Time and Ranging) GPS (Global Positioning System) is a passive, all-weather satellite-based radio navigation and positioning system, which is designed to provide precise three dimensional position and velocity, as well as time information on a continuous worldwide basis. The system development began in 1973 by the U.S. Air Force [*Easton*, 1980], and currently the system is being developed by the U.S. Department of Defense. GPS comprises three major segments: the space segment, i.e., GPS satellites, the control system, and the receiver, as depicted in Figure 1.1.

GPS satellites, when fully deployed, will consist of 21 operating Block-II satellites plus 3 active spares. They will be arranged with four satellites in each of six nearly circular orbital planes (denoted as A, B, C, D, E, and F planes), with inclination of 55 degrees. The spacing of the satellites in their orbital planes has been selected to maximize the probability that at least four satellites with good Position Dilution of Precision (PDOP) will always be visible to users at every location on Earth [*Bagley and Lamons*, 1992; *Green*, 1989]. The GPS satellites will have an average orbit altitude of about 20 200 km above the Earth's surface, with the orbital period of 11 hours and 58 minutes.



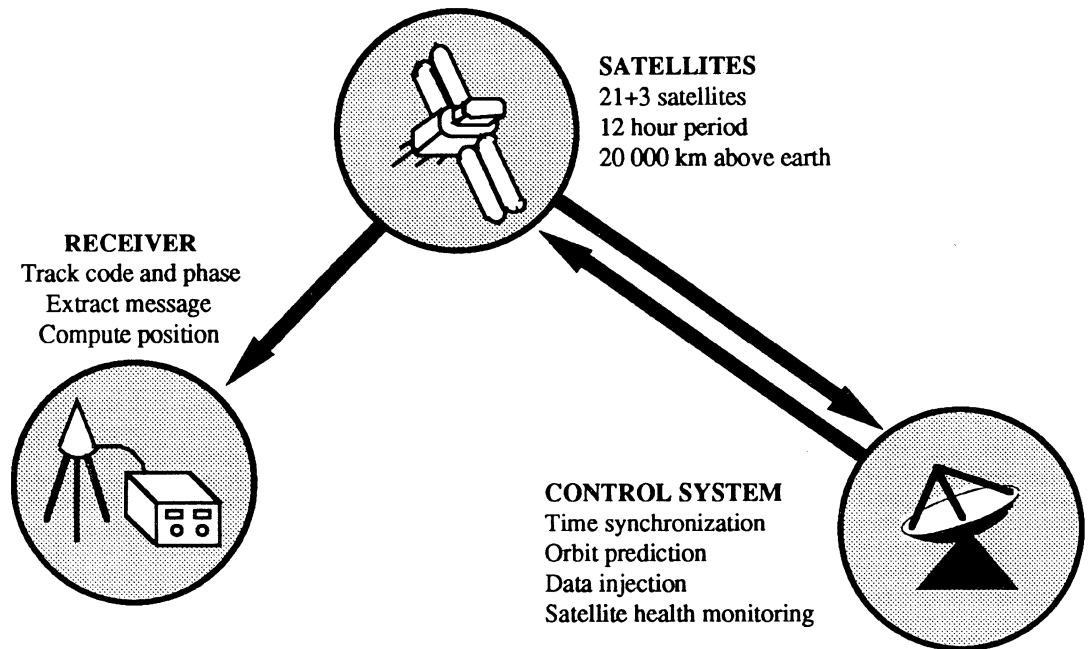


Figure 1.1. The Global Positioning System [*Wells et al.*, 1986].

The first GPS satellite was launched on February 22, 1978, and by October 1992, there were 19 satellites operational of which 4 are prototype Block-I satellites and 15 are Block-II satellites as shown in Table 1.1. The Block-I satellites are at the orbital planes with 63 degree inclination. Since they do not fit within the final GPS constellation, they are used at the present time to augment the coverage provided by the growing complement of Block-II satellites until all 24 satellites of Block-II are on orbit. GPS is expected to be fully operational by late 1993 [*Bagley and Lamons*, 1992].

The operation of GPS satellites is controlled by the GPS control segment. It consists of monitoring stations distributed around the world that continuously track all the satellites in view. More specifically, the control segment consists of Ground Antennas (GAs), Monitor Stations (MSs), the Prelaunch Compatibility Station (PCS), and the Master Control Station (MCS) [*Bagley and Lamons*, 1992]. The GAs are located at Ascension, Diego Garcia, and Kwajalein. The five MSs are the GAs plus Colorado Springs and Hawaii. The PCS is at

Cape Canaveral, and the MCS is at the Consolidated Space Operation Centre at Colorado Springs. The purpose of the control segment is to monitor the health of the satellites, determine their orbits and the behavior of their atomic clocks, and to transmit data to the satellites for re-broadcast to the users which contains the satellite ephemerides, satellite clock synchronization parameters, and satellite health status [Wells *et al.*, 1986].

Table 1.1. Operational GPS satellites (October 1992).

	SVN		PRN	Orbital Plane
<b>Block - I</b> ( 5 satellites )	8		11	C3
	9		13	C1
	10		12	A1
	11		3	C4
	previous	current		
<b>Block - II</b> ( 14 satellites )	13	II-2	2	B3
	14	II-1	14	E1
	15	II-9	15	D2
	16	II-3	16	E3
	17	II-5	17	D3
	18	II-6	18	F3
	19	II-4	19	A4
	20	II-7	20	B2
	21	II-8	21	E2
	23	II-10	23	E4
	24	II-11	24	D1
	25	II-12	25	A2
	26	II-14	26	F2
	27	II-15	27	A3
28	II-13	28	C2	
SVN = Satellite Vehicle Number, PRN = Pseudorandom noise code number. The position of each orbital plane is given in Table VI.2 (Appendix VI).				

Each GPS satellite transmits continuously two spread spectrum L-band radio frequencies: L1 and L2. L1 is centered on 1575.42 MHz (154 x 10.23 MHz) and L2 is centered on 1227.60 MHz (120 x 10.23 MHz). The corresponding wavelengths of these L1 and L2 signals are about 19 cm and 24 cm, respectively. These signals are bi-phase modulated by one or two pseudo-random noise codes. The L1 carrier signal is modulated by both C/A-code (Coarse/Acquisition-code) code and P-code (Precise-code), and the L2 carrier signal is modulated only by the P-code. In addition, the navigation message is modulated on both

signals at a 50 bps (bits per second) rate, and it contains the broadcast ephemeris and the health information of the satellites. The C/A-code is transmitted at the chipping rate of 1.023 MHz with one millisecond repetition, while the P-code is transmitted at the chipping rate of 10.23 MHz with 267 day repetition. Each GPS satellite has a different C/A-code and a different segment of the P-code.

By observing the GPS signals using the GPS receiver(s), the user(s) can obtain information about the times, the range and range rate to the satellites, and the coordinates and velocities of the satellites which, in turn, can be used to derive the position and velocity of the user when enough satellites are observed. GPS, however, is designed to provide its highest accuracy results only to U.S. military and authorized (military allies & civilian) users. When the GPS system is fully operational, most of the civilian users will only have access to the C/A-code, and the P-code will be switched to Y-code which can only be decrypted by the U.S. military and authorized users. This switching to Y-code is referred as Anti-Spoofing (A-S). As well, the civilian range measurements accuracy is also degraded by the so-called Selective Availability (SA). The Selective Availability is implemented by a combination of degraded satellite orbital information ( $\epsilon$ -type SA) and satellite clock dithering ( $\delta$ -type SA). The military and authorized receivers are equipped with the capability to fix the degradation. The current policy dictates that SA and A-S will be activated on all operational Block II satellites after the system has been declared fully operational.

The navigation and positioning service provided by dual-frequency P-code, with the effects of SA and A-S counteracted, is referred to as the Precise Positioning Service (PPS). The navigation and positioning service provided by single-frequency C/A code, affected by SA, is referred to as Standard Positioning Service (SPS). PPS is intended for U.S. military and authorized users, while SPS is intended primarily for civil GPS users.

## 1.2. Fundamental GPS observations

There are two fundamental observations which can be obtained when tracking GPS satellites, namely the pseudoranges (codes) and the carrier phases of the L1 and L2 signals.

The *pseudorange observation* is the difference between the time of transmission (in the satellite time scale) and the time of arrival (in the receiver time scale) of a particular signal transmitted by the satellite [Wells *et al.*, 1986]. This time difference is determined by comparing a receiver-replicated code with the real code received from a particular satellite, and it is the time shift needed to align the two codes. When it is scaled by the speed of light, the pseudorange represents mainly the geometric range between the receiver and the satellite plus the range bias caused by the time difference between the satellite and receiver clocks. The pseudorange observations will also be contaminated by the measurement noise, the multipath (if it exists), and the biases caused by the ionospheric and tropospheric refractions.

The *carrier phase observation* is the phase difference (beat phase) between the phase of the incoming carrier signal from the satellite and an internal receiver-generated carrier signal. When scaled with the wavelength of the signal, the carrier phase observation represents the biased range between the receiver and the satellite, with a portion of range related to certain full cycles of the signal wavelength is unknown. These unknown full cycles of wavelength are usually known as *cycle ambiguity* of the phase observation. As in the case of the pseudorange observation, the phase observation will also be contaminated by the measurement noise, the multipath (if it exists), and the biases caused by the ionospheric and tropospheric refractions.

If the pseudorange and carrier phase observations at a certain frequency are denoted as  $\Delta t$  and  $\phi$ , and the *cycle ambiguities of the carrier phase is denoted as  $N$* , then the following

equations, which relate these observations to the receiver-satellite geometric range and the errors and biases contaminating the observations, can be written as follows :

$$c \cdot \Delta t = \rho + d\rho + dtrop + dion + (dt - dT) + MP + \vartheta P , \quad (1.1)$$

$$\lambda (\phi + N) = \rho + d\rho + dtrop - dion + (dt - dT) + MC + \vartheta C , \quad (1.2)$$

where  $\rho$  is the geometric distance between the receiver and the satellite (m),  $c$  is the speed of light in a vacuum (m/s),  $\lambda$  is wavelength of the signal (m),  $d\rho$  is the range error caused by ephemeris errors (m),  $dtrop$  is the tropospheric delay (m),  $dion$  is the ionospheric bias (m),  $dt$  and  $dT$  are the receiver and satellite clock errors (m),  $MP$  and  $MC$  are the multipath effects in pseudoranges and carrier phases (m), and  $\vartheta P$  and  $\vartheta C$  are noise in pseudoranges and carrier phases (m).

Based on the above equations, it is evident that the accuracy and precision of the pseudorange and carrier phase observations in representing the geometric ranges between the receiver and the satellites depends on the magnitudes of the observation errors and biases and also on the level of observation noise. The level of the observation noise depends on several factors such as the tracking bandwidth, signal-to-noise ratio, and code tracking mechanization parameters [Martin, 1980]. For C/A-code pseudoranges, the noise level is approximately 1 - 5 m, depending on the dynamics of the receiver, signal-to-noise ratio, and sophistication of the signal processing inside the receiver. Due to its higher chipping rate, the noise level of P-code pseudoranges is lower, and it is approximately 10 - 50 cm. The phase observation is much more precise than the pseudorange. Its noise level is about 1 - 2% of the signal wavelength, i.e., about 2 - 4 mm for L1 signal and 2.5 - 5 mm for L2 signal.

Due to its high precision, the carrier phases are the observations which have to be used for accurate and precise positioning using GPS satellites. It should be noted in this case, however, that their cycle ambiguities have to be resolved correctly beforehand in order to convert the carrier phase into the accurate and precise geometric range between the receiver and satellite.

### **1.3. GPS positioning accuracy**

The accuracy of positioning using GPS satellites is affected by several factors such as the accuracy of the observations being used for positioning, the positioning method adopted, the satellite geometry during the survey, and the processing strategy used, as depicted in Figure 1.2. Examples of the many modes of GPS positioning and their accuracies are shown in Figure 1.3. In this research, we are concerned about the precise (centimetre level accuracy) kinematic positioning using GPS. This level of accuracy can be achieved by using the carrier phase observations with the correct cycle ambiguities (see Figure 1.3).

### **1.4. Precise kinematic applications of GPS**

The precise (centimetre level accuracy) kinematic differential positioning using GPS requires the use of the carrier phase observations with correctly resolved integer ambiguities. This implies the need for ambiguity resolution at the beginning of the session (initial ambiguities), times of cycle slip occurrences, and rising of a new satellite which will be included in the positioning process. On-the-fly ambiguity resolution, i.e., ambiguity resolution while the receiver is in motion, is desirable for flexibility and reliability of kinematic positioning, and it is useful for quite a lot of applications. In the following, some of the existing applications and theoretically conceivable applications are outlined.

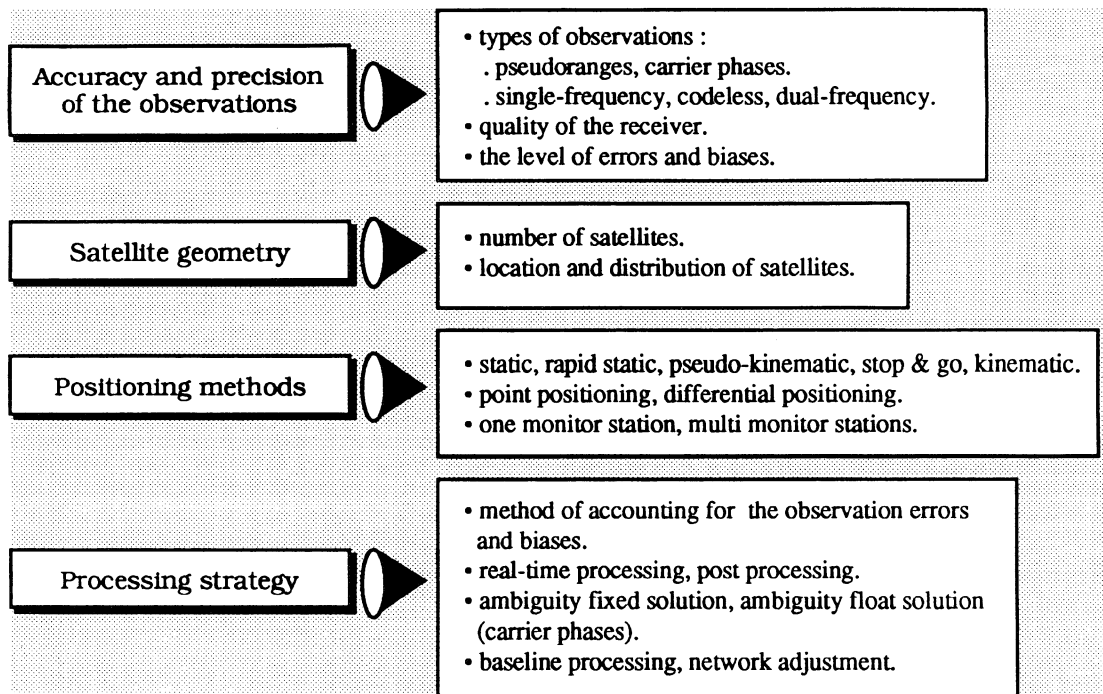


Figure 1.2. The factors affecting GPS positioning accuracy.

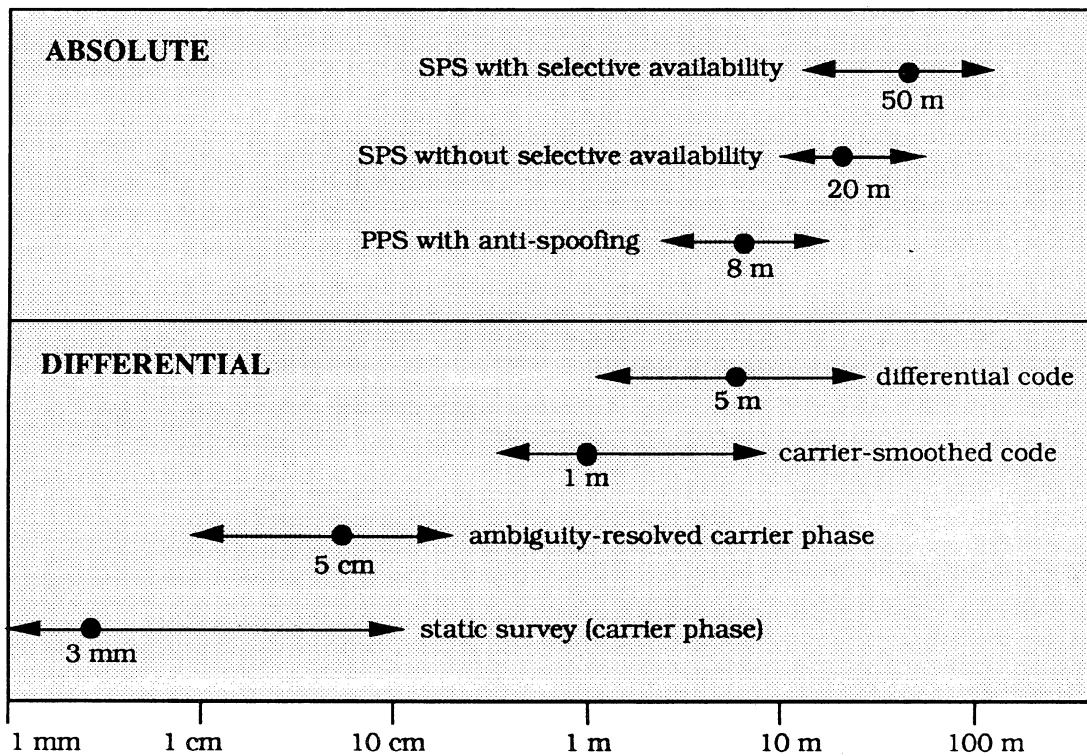


Figure 1.3. Many modes of GPS positioning accuracy [Wells, 1992].

#### **1.4.1. Attitude and heading determination**

The precise and accurate attitude and heading of a moving platform can be determined by differential measurements of GPS carrier phases between two or more independent pairs of antennas on the platform. In this case, however, the integer cycle ambiguities between the pair of antennas have to be resolved beforehand [Nesbo, 1988; Nesbo and Canter, 1990; Brown and Evans, 1990; Knight and Hatch, 1990; Cohen and Parkinson, 1991; Brown, 1992; Jurgen and Rodgers, 1992; van Graas and Braasch, 1991,1992; Wilson and Tonnemacher, 1992, Hwang, 1990b]. On-the-fly precise and accurate heading and attitude information is useful for quite a lot of applications, such as [Braasch and van Graas, 1991; van Graas and Braasch, 1991,1992; Anderman, 1991; Nesbo and Canter, 1990] :

- real-time determination of the attitude and heading of an aircraft or other moving vehicle,
- rapid in-flight alignment and re-initialization of inertial navigation systems,
- precision guidance and/or pointing applications,
- attitude control of space platforms,
- on-line model identification and control of flexible structures, and
- precise positioning of in-sea seismic equipment.

#### **1.4.2. High accuracy sea surface positioning**

Precise differential GPS kinematic positioning will play important roles in high accuracy sea surface positioning, which is required for several applications, such as: precise positioning of the sea floor points (sea floor geodesy), satellite altimeter verification, the study of sea level, ocean waves and currents, offshore tide measurement, and dredging operations.



In the case of **precise positioning of the sea floor points**, the differential kinematic GPS positioning is used to determine the position of the buoy on the sea surface with respect to the monument on land, along with its orientation. The buoy should be equipped with three or more GPS antennas. The acoustic positioning system, which its transducer is attached to the buoy, is then used to connect the GPS derived buoy coordinates to the coordinates of the points on the sea floor where the acoustic transponders are located [Young *et al.*, 1987; McIntyre, 1989; Purcell Jr. *et al.*, 1991]. The precise coordinates of the points on the sea floor are very important information in studying the structure and dynamics of the earth crust beneath the sea, and can also be expected to have an impact on human activities under the sea [Committee on Geodesy, 1983; Spies, 1985, 1990].

The principles of **satellite altimeter verification** using precise differential GPS positioning is explained in Rocken *et al.* [1990]; Hein *et al.* [1991]; and Rocken and Kelecy [1992]. The verification requires the measurement of an independently determined satellite altimetry above sea level to be compared with the satellite altimeter measurement as it passes over the verification region. In this case, the reference GPS receivers are collocated at the (satellite altimetry) laser tracking sites, and the other receivers are mounted on the floaters in the ocean, covering the footprint of the altimeter. By precisely positioning these GPS floaters and simultaneously tracking the satellite position from the laser sites, the height of the satellite altimetry above the local mean sea surface can be determined, and in turn it can be used to verify the altimeter measurement. This technique has been used to verify the altimeter measurements of the first European Remote Sensing Satellite, ERS-1 [Hein *et al.*, 1991; Rocken and Kelecy, 1992].

The high accuracy sea surface GPS positioning will also be useful for studying the sea level, ocean waves, and currents [Hein *et al.*, 1990; Rocken *et al.*, 1990, Geiger and Cocard, 1992], and for efficient and accurate offshore tide measurement. It will also be

beneficial in supporting dredging operations. It will improve the earthwork computation for contract payments, and in the vertical sense, this high positioning accuracy will allow the vessel to serve as its own tide gauge [Geier *et al.*, 1990].

#### **1.4.3. Airborne photogrammetric applications**

Precise differential GPS kinematic positioning will also be useful for airborne photogrammetric applications. One of the applications is to determine the precise coordinates of the camera at exposures times. In this case, the need for the conventional ground control points can be reduced, if not eliminated, leading to the so-called aerotriangulation with minimum ground control or even without ground control [Schwartz *et al.*, 1984; Lucas, 1987; Hintz and Zhao, 1989; Ackermann, 1990; Cannon, 1991]. In order to be viable, the camera in space should be located with a relative accuracy of 3 - 10 cm and it should be repeatable to the same degree [Merrell *et al.*, 1989].

The precise differential GPS positioning can also provide accurate and reliable attitude information which can benefit the photogrammetric block adjustment [Schwartz *et al.*, 1984; Cannon, 1991]. The a priori knowledge of the exposure station obtained from kinematic GPS positioning can also be used for analytical calibration of the airborne photogrammetric system [Lapine, 1991].

#### **1.4.4. Precise navigation of agricultural vehicles**

Precise kinematic differential GPS positioning will also be useful in navigating the agricultural vehicles to accomplish certain tasks [Auernhammer and Muhr, 1991; Petersen, 1991]. Based on the accuracy requirements shown in Table 1.2, precise kinematic positioning can play significant roles in the cases of the navigation of the tractor during

distribution work, the navigation of the harvest machines, and the tractor implement guidance.

Table 1.2. Requirements for navigation in agriculture [Auernhammer and Muhr, 1991].

kind of navigation	examples of the tasks	required accuracy
rough navigation of the vehicle	<ul style="list-style-type: none"> <li>• soil sample acquisition</li> <li>• detection of tram lines</li> </ul>	$\pm 1$ m
navigation of tractor and harvest-machines	<ul style="list-style-type: none"> <li>• mineral fertilizer spreading</li> <li>• liquid manure spreading</li> <li>• solid manure spreading</li> <li>• application of pesticides</li> <li>• soil cultivation</li> </ul>	$\pm 10$ cm
tractor implement guidance	<ul style="list-style-type: none"> <li>• drilling</li> <li>• hoeing</li> <li>• plowing</li> </ul>	$\pm 1$ cm

### 1.5. Motivation

The precise kinematic positioning using GPS satellites, as described in the previous section, has a lot of practical applications. In order to achieve the highest accuracy of positioning, the carrier phase observations should be used instead of the pseudoranges. The inherent cycle ambiguity of carrier phase observations, however, must be correctly resolved beforehand whenever real-time positions are required.

Cycle ambiguity resolution is not a task that can be easily accomplished, even in the case of static differential GPS positioning. A lot of factors will affect the speed and reliability of the ambiguity resolution. In general, these factors can be categorized into three broader groups, namely the ambiguity resolution technique, the effects of the observation errors and biases, and the observation geometry, i.e., the geometry between the satellites, the monitor station(s), and the user. In order to achieve the successful ambiguity resolution, all of the factors have to be judiciously taken into consideration in designing and formulating the ambiguity resolution technique and in performing the ambiguity resolution process. In this

case, besides using a smart and powerful technique, the elimination of the major observation errors and biases and the significant changes in satellite geometry are necessary for reliable ambiguity resolution.

In this research, therefore, the possibility of performing reliable and fast on-the-fly ambiguity resolution will be studied and investigated. Its aspects, particularly its computational and geometrical aspects, will also be elaborated in order to get a better insight into the problem of on-the-fly ambiguity resolution. In the course of the research investigation, some simulated kinematic, static, and real kinematic GPS data will be processed in order to assess the achievable results, the prospects, and the limitations of fast and reliable on-the-fly ambiguity resolution.

#### **1.6. Previous studies**

There have been numerous studies performed in the area of cycle ambiguity resolution of GPS carrier phase observations. In the following, however, only the studies related to the on-the-fly ambiguity resolution technique will be reviewed.

*Wubben* [1989] has proposed *the extrawidelaning technique* of ambiguity resolution, which can be used both for static and moving receivers. The technique requires P-code dual-frequency data, and utilizes the linear combinations of L1 and L2 signals (i.e., wide-lane, narrow-lane, and ionospheric signals) for the ambiguity resolution process [*Wubben*, 1989, 1991]. Although the technique is not affected by the frequency-independent errors and biases such as the clock errors, tropospheric delays, and ephemeris errors, it is sensitive to the frequency-dependent errors and biases such as the ionospheric delay, multipath, and observation noise. The effects of these later errors and biases on the performance of on-the-fly extrawidelaning technique are studied in *Seeber & Wubben*, [1989]; *Abidin & Wells* [1990]; and *Abidin* [1990]. The practical use of the

extrawidelaning technique for on-the-fly ambiguity resolution in the cases of the 3-D ship attitude control investigations and differential kinematic positioning of a photogrammetric plane are also reported in *Seeber & Wubbena* [1989].

*Mader* [1990, 1992] studies the on-the-fly ambiguity resolution using *the ambiguity mapping function technique*. The technique was first described by *Counselman & Gourevitch* [1981], and since then has been applied for the static cases [*Remondi*, 1984; *Mader*, 1992; *Ziegler et.al.*, 1992], pseudo-kinematic cases [*Remondi*, 1990; *Balde et.al.*, 1991], and kinematic cases of positioning [*Mader* , 1990; 1992]. The problem of on-the-fly ambiguity resolution using the ambiguity mapping function are described in *Mader* [1990; 1992], especially with respect to some of its computational aspects and the effects of ionospheric refractions on the ambiguity resolution process. The effects of the observation geometry, however, are only referred to in general in the studies. The studies also present the on-the-fly ambiguity resolution results in conjunction with the kinematic differential positioning to aid airborne gravimetric surveying.

*Hatch* [1989, 1990] has proposed another on-the-fly ambiguity resolution technique which is called *the least-squares ambiguity searching technique*. The geometrical interpretation of the technique is described in *Hatch* [1989], and its mathematical formulations are given in *Hatch* [1990]. Some experimental results of on-the-fly ambiguity resolution related to the single-frequency aircraft positioning are given in *Hatch* [1991], and those related to dual-frequency static data is given in *Hatch et al.* [1992].

*Remondi* [1991, 1992a, 1992b] has also proposed another approach for on-the-fly ambiguity resolution technique, which is called the *kinematic GPS without static initialization* technique. In principle, this technique is similar to the ambiguity mapping function technique. The mathematical formulations of the technique are given in *Remondi*

[1991] and on-the-fly ambiguity resolution results are presented in the aforementioned references.

The studies of on-the-fly ambiguity resolution are also carried out by the group of researchers from the Institute of Astronomical and Physical Geodesy, University FAF Munich and terraSat Inc. in Germany. The mathematical formulations of their on-the-fly ambiguity resolution technique is given in *Landau and Euler* [1992], and the achievable experimental and practical results can be seen in *Landau* [1990]; *Landau and Euler* [1991a, 1991b]; *Euler et.al.* [1991]; *Hein et. al.* [1991]; and *Landau and Euler* [1992].

*Hwang* [1990a, 1990b] has also studied on-the-fly ambiguity resolution of GPS carrier phases. As in the case of [*Loomis*, 1989], he uses the Kalman filter formulation to resolve the ambiguities. In his studies, he also proposes the augmented version of the antenna exchange technique [*Hofmann-Wellenhof and Remondi*, 1988] to be used for on-the-fly ambiguity resolution in certain kinematic applications.

*Cohen and Parkinson* [1992] and *Brown* [1992] have also proposed the on-the-fly ambiguity resolution technique to be used specifically for the attitude determination of a moving platform using GPS carrier phase observations.

The previous reported studies usually describe in general their on-the-fly ambiguity resolution concepts, outline their mathematical formulations, and present some experimental and/or practical results of their techniques. In general, there are no detailed investigations of the computational characteristics of the technique, or on the speed and reliability of on-the-fly ambiguity resolution. Comprehensive investigations of the effects of the observation geometry on the performance of on-the-fly ambiguity resolution are also

usually not given. Moreover, the existing studies do not consider the advantages of using more than one monitor station for speeding up the on-the-fly ambiguity resolution process.

### 1.7. Methodology and scope of the investigation.

The performance of fast and reliable on-the-fly ambiguity resolution will depend on the technique being used, the observation geometry involved, and the level of the observation errors and biases, as depicted in Figure 1.4.

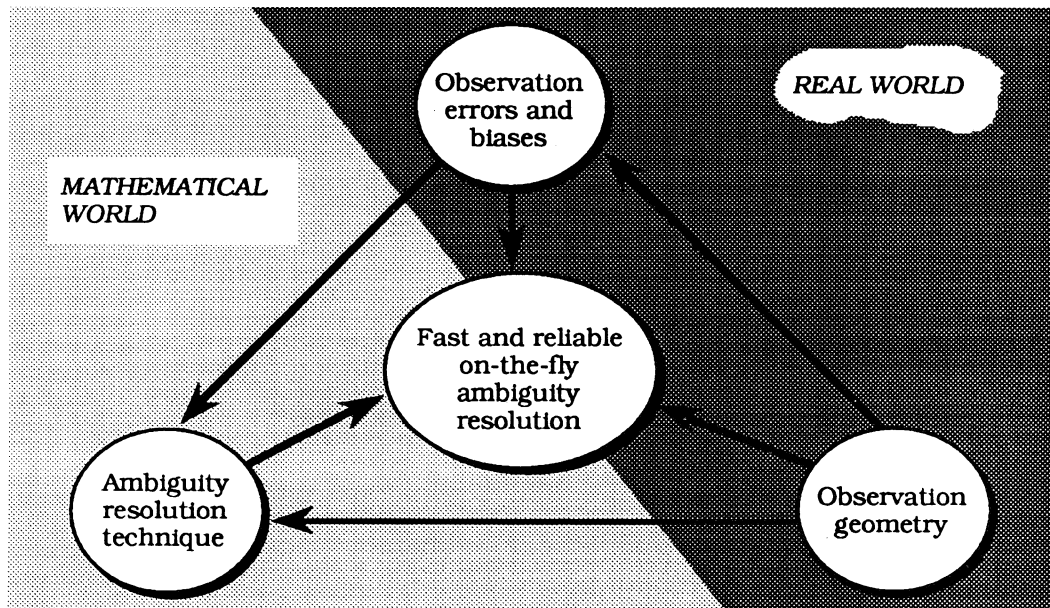


Figure 1.4. The factors affecting the on-the-fly ambiguity resolution.

In order to study and investigate the possibility for the reliable and fast on-the-fly ambiguity resolution, the so-called integrated on-the-fly ambiguity resolution technique is at first developed. The technique is developed by considering the positive features of the three existing on-the-fly ambiguity resolution techniques, i.e., the extrawidelaning technique, the ambiguity mapping function technique, and the least-squares ambiguity searching technique, along with the new features of the integrated technique itself. The integrated

technique is designed and formulated to work with either single-frequency, codeless, or dual-frequency data from at least five satellites, and the double-difference observations are used as the basic observations for the ambiguity resolution. The technique also accommodates the use of more than one (secondary) monitor stations.

The validity of the technique is then tested and verified using the static and kinematic GPS data. The static data used in this case is the zero baseline data collected using the Trimble Geodesist P-receivers (which observes L1-C/A code, L2-P code, and full wavelength L1 and L2 carrier phases), and the codeless data of a 535 m baseline collected using Ashtech LD-XII receivers (which observes L1-C/A code, full wavelength L1 phases, and half wavelength L2 phases). The kinematic data used in this case is the P-code dual frequency GPS data observed using the Rogue receivers, involving two monitor stations and three GPS antennas on a moving buoy.

The computational characteristics of the technique with respects to their effects on the speed and reliability of on-the-fly ambiguity resolution are then studied and investigated. The investigations in this case are concentrated on the two main aspects of the ambiguity resolution technique, namely the ambiguity searching space and the identification process of the correct ambiguities. The static and kinematic GPS data are used in the investigations. This stage of research studies the computational characteristics of the integrated technique in achieving fast and reliable on-the-fly ambiguity resolution.

Observation geometry will also affect the speed and reliability of on-the-fly ambiguity resolution. In this research, the effects of the observation geometry are studied and investigated by considering several geometrical parameters related to GPS satellites, observations, and secondary monitor stations. The static and real kinematic GPS data are used, along with the single-frequency simulated kinematic data from four secondary



monitor stations. This last stage of research studies the requirements for fast and reliable on-the-fly ambiguity resolution with respect to the parameters of the observation geometry.

The observations errors and biases also affect the performance of on-the-fly ambiguity resolution. In this research, however, it is assumed that the user will receive the information to correct the clock errors, satellite ephemeris errors, and ionospheric and tropospheric biases from the wide area differential GPS system [Kee *et.al.*, 1991] which is expected to be operational in the near future. Moreover, the double-differencing between the observations which are used in this research, will also significantly eliminate the effects of some major errors and biases. Therefore, there is no special investigation of the effects of the observation errors and biases on the performance of on-the-fly ambiguity resolution. In summary, the methodology of investigation adopted in this research is depicted by the flowchart in Figure 1.5.

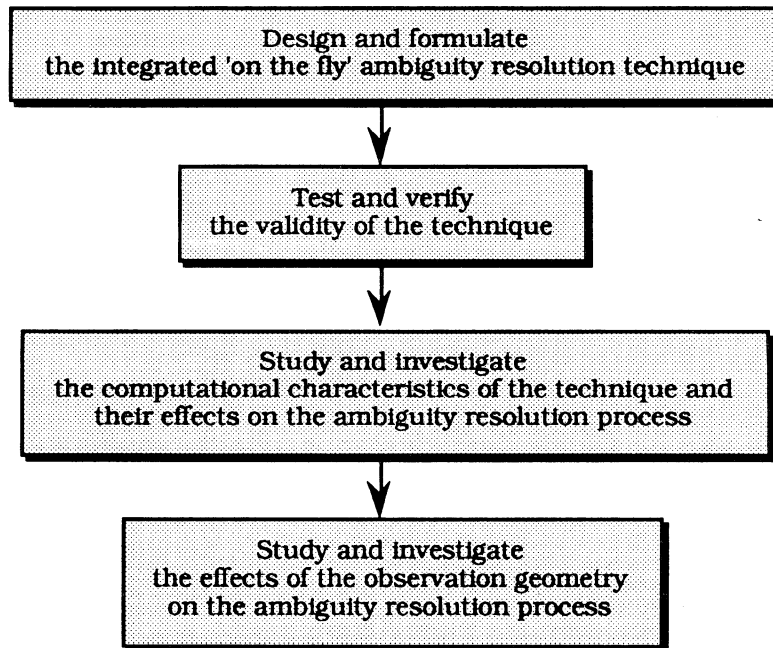


Figure 1.5. The methodology of the research investigation.

## **1.8. Outline of the dissertation.**

The dissertation consists of seven chapters and six appendices. The contents of these chapters and appendices are outlined in the following.

*Chapter 2* introduces the problem of cycle ambiguity resolution of GPS phase observation. The concept of the lines and surfaces of ambiguities are presented along with the notion of the mathematical and physical ambiguity searching spaces. Finally, some of the existing on-the-fly ambiguity resolution techniques are reviewed.

*Chapter 3* describes in detail the concepts and mathematical methodologies of the integrated on-the-fly ambiguity resolution technique developed in this research.

*Chapter 4* presents the on-the-fly ambiguity resolution results obtained by using the integrated on-the-fly ambiguity resolution technique. This chapter proves the validity and efficiency of the integrated technique. The verifications are performed in this case by using both static and kinematic GPS data.

*Chapter 5* discusses the computational characteristics of integrated on-the-fly ambiguity resolution technique and their effects on the speed and reliability of the ambiguity resolution. The discussion is concentrated on the construction of ambiguity searching space and the implementation of validation and rejection criteria. The results based on the static and kinematic GPS data are presented.

*Chapter 6* discusses the effects of the observation geometry on the speed and reliability of on-the-fly ambiguity resolution, with respects to certain geometrical parameters. The geometrical parameters considered in this case are: signal wavelength, primary satellites,

number and location of the satellites, observation differencing strategy, data rate, and number and location of the secondary monitor stations. The results based on static, kinematic, and simulated kinematic GPS data are presented in this case.

*Chapter 7* summarizes findings, makes conclusions, and recommends topics for future investigations. Some points related to the prospects and limitations of on-the-fly ambiguity resolution are also presented.

*Appendix I* contains explanations and mathematical formulations of the linear combinations of GPS observations used in this research.

*Appendix II* contains the mathematical formulation of the code smoothing technique, which smoothes the pseudoranges by using the carrier phase observations.

*Appendix III* gives explanations and mathematical formulations for constructing the covariance matrix of the multi station double-difference observations used in this research.

*Appendix IV* presents the histogram and time series of the distance differences between the computed distances and the corresponding known distances of the three GPS antennas on a moving buoy. The results are related to real kinematic GPS data observed using Rogue receivers.

*Appendix V* contains mathematical explanations for the effects of the observation geometry on the mathematical ambiguity searching space.

*Appendix VI* gives the characteristics of the simulated kinematic GPS data used in this research, and the method used to simulate the data.

## **1.9. Contributions of the research.**

The contributions of this research can be summarized as follows :

- (1). to develop an integrated on-the-fly ambiguity resolution technique, with a strategy and concept quite different from existing on-the-fly ambiguity resolution techniques,
- (2). to introduce and formulate the use of more than one secondary monitor station for on-the-fly ambiguity resolution,
- (3). to introduce some new validation and rejection criteria for on-the-fly ambiguity resolution process,
- (4). to investigate the computational characteristics of integrated on-the-fly ambiguity resolution technique, and their effects on the speed and reliability of on-the-fly ambiguity resolution,
- (5). to investigation of the effects of observation geometry on the speed and reliability of on-the-fly ambiguity resolution, with respect to most of the important geometrical parameters,
- (6). to apply the concept of lines and surfaces of (double-difference) ambiguities in explaining the effects of some geometrical parameters of the ambiguity resolution process,
- (7). to provide a more meaningful geometrical interpretation of the problem of cycle double-difference ambiguity resolution, and
- (8). to provide an assessment of the achievable results, prospects, and limitations of reliable and fast on-the-fly ambiguity resolution.

# ON-THE-FLY AMBIGUITY RESOLUTION

---

---

In this chapter some aspects of on-the-fly ambiguity resolution are introduced and explained. After introducing the cycle ambiguity problems of GPS phase observations, this chapter describes the concepts of lines and surfaces of ambiguity and explains the concepts of mathematical and physical ambiguity searching space. Finally, some of the existing on-the-fly ambiguity resolution techniques are reviewed. Their strengths and weaknesses are identified, and the possibility of synergizing their good features is highlighted.

### 2.1 Cycle ambiguity resolution

Carrier phase and code observations are two types of observations which can be extracted from the GPS signal [Wells *et al.*, 1986]. For positioning purposes, carrier phase observations should be used to achieve the highest accuracy of the estimated differential position because of its higher precision than code observations. However, the inherent cycle ambiguity of carrier phase observations, i.e., the numbers of unobserved full cycles of the phase observations, must be correctly resolved beforehand in order to convert the phases into the precise ranges to the satellites (see Figure 2.1). In the case of real-time differential GPS kinematic positioning using carrier phase observations, the ambiguity resolution is necessary in three occasions: the beginning of the session (initial ambiguity),

cycle slip occurrences, and the rising of a new satellite which will be included in positioning process.

The cycle ambiguity is an integer number. For one-way phase observations between the receiver and the satellite, however, this cycle ambiguity cannot be separated from the clock related errors in the receiver and satellites (see equation I.2). This is also true of single-difference (between-station or between-satellite) phase observations. In the case of station-satellite double-difference observation, clock-related errors in the satellites and receivers are canceled by a differencing process. For resolving the ambiguity, therefore, one should work with the double-difference phase observations.

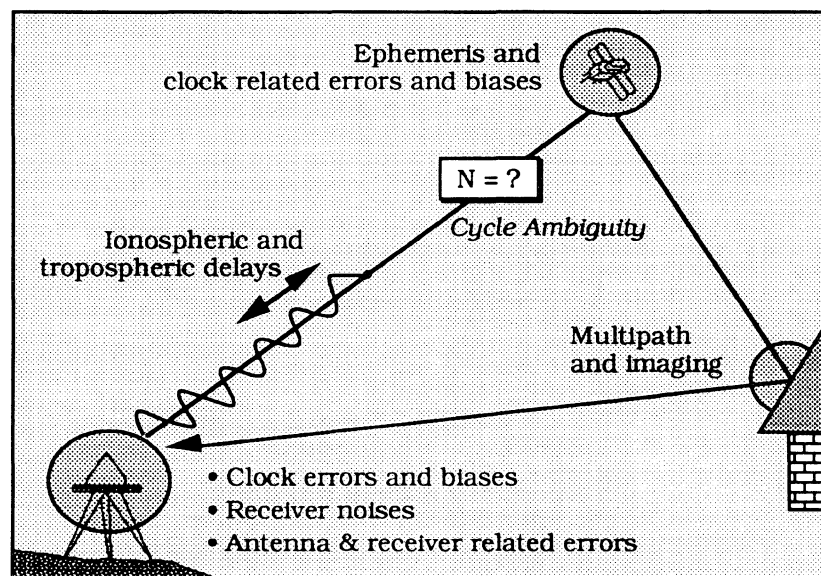


Figure 2.1. Cycle ambiguity of carrier phase observation (the figure is not to scale).

In the case of static differential GPS positioning, isolating the integer ambiguity from the geometric range and the errors and biases in the observations, as depicted in Figure 2.1, requires effort both in observation time and strategy and also in processing schemes. Significant change in satellite geometry and elimination of the major errors and biases in the observations are required for reliable ambiguity resolution. Figure 2.2 gives an example of

how errors and biases in the observation can complicate searching for the correct integer of cycle ambiguity. In this example, the ambiguities are computed using the 'known' coordinates of stations, satellite positions computed using the broadcast ephemeris, and carrier phase observations. If systematic errors and biases in the phase observation can be eliminated, ambiguity can be resolved easily as shown in the case of zero baseline data which is contaminated only by receiver noise. Otherwise, one would have difficulty deciding the correct integer ambiguity as shown in the case of 200 km and 3000 km baselines data, which can be expected to be caused by the effects of the ephemeris errors and ionospheric delays in the phase observations.

Finally, it should also be noted, that besides favorable observation geometry and insignificant observation errors and biases, the smart and reliable algorithm is also very important for fast and reliable on-the-fly ambiguity resolution. Before the existing on-the-fly ambiguity resolution techniques are reviewed, the concepts of the lines and surfaces of ambiguity are introduced in the following sub section in order to give more insight to the ambiguity resolution problem.

## **2.2. Surfaces and lines of ambiguity**

There are two types of the surfaces and lines of ambiguity which will be introduced here, namely the *physical* and *mathematical*. In this research, the physical surface of ambiguity (SOA) is defined as the surface of position (SOP) corresponding to a certain value of ambiguity. Any line on this surface is called the physical line of ambiguity (LOA). The simplified nature of the physical LOA in 2-D perspectives is depicted by Figure 2.3. For the sake of clarity, the carrier phase observations in this case are assumed to be not contaminated by noise, errors and biases. The ranges to satellite represented by  $i$  then can be defined as follows:

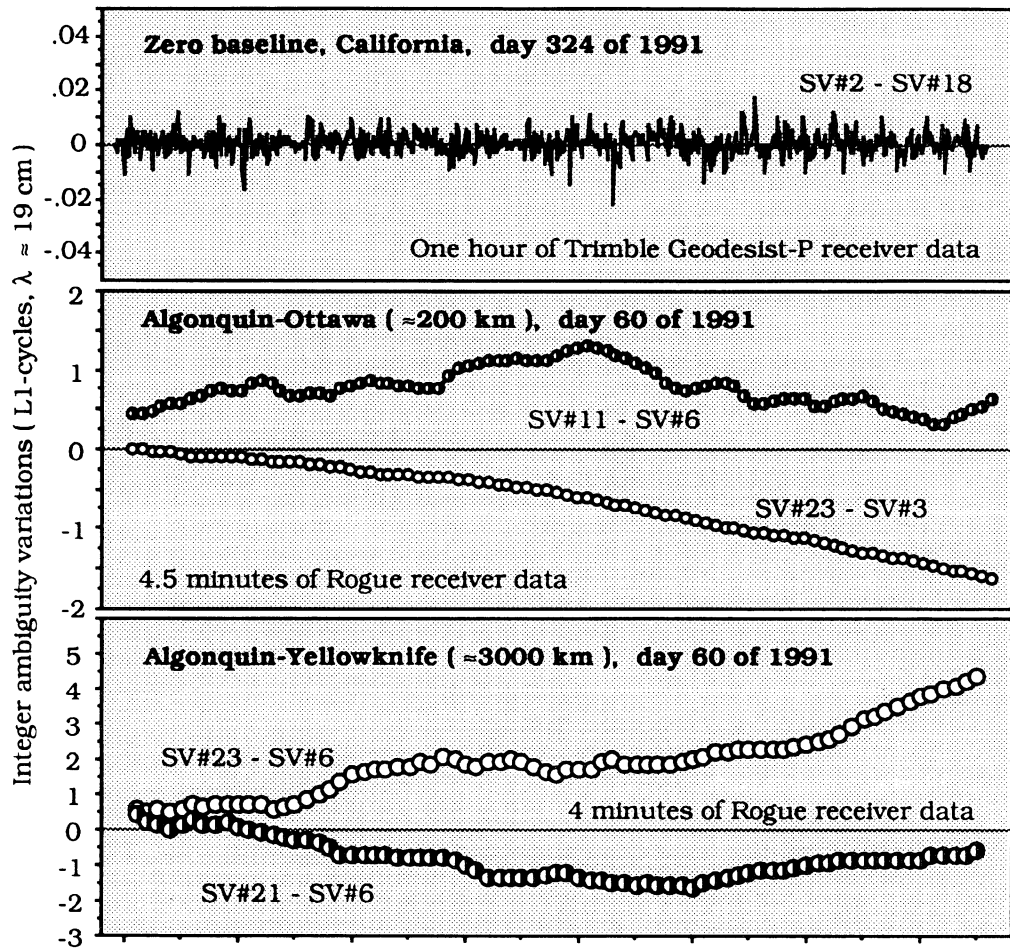


Figure 2.2. Variations of integer ambiguities of double-difference L1-phase observations

$$\rho^i = \lambda (\phi^i + N^i) \quad , \quad (2.1)$$

where  $\rho$ ,  $\lambda$ ,  $\phi$ , and  $N$  denote the range, the wavelength, the observed phase, and the unknown cycle ambiguity, respectively. Note from the above equation that the potential position related to single one-way range is located on the surface of a sphere centered at satellite  $i$ . By changing the values of the ambiguity by one cycle, we basically change the range and create another spherical SOP one cycle apart from the previous one. Therefore, the identification of the correct one-way ambiguity in this case is actually the identification



of the correct spherical SOP. The surface of the ambiguity therefore is also the sphere, and, in a two-dimensional case, it becomes the circle as shown in Figure 2.3.

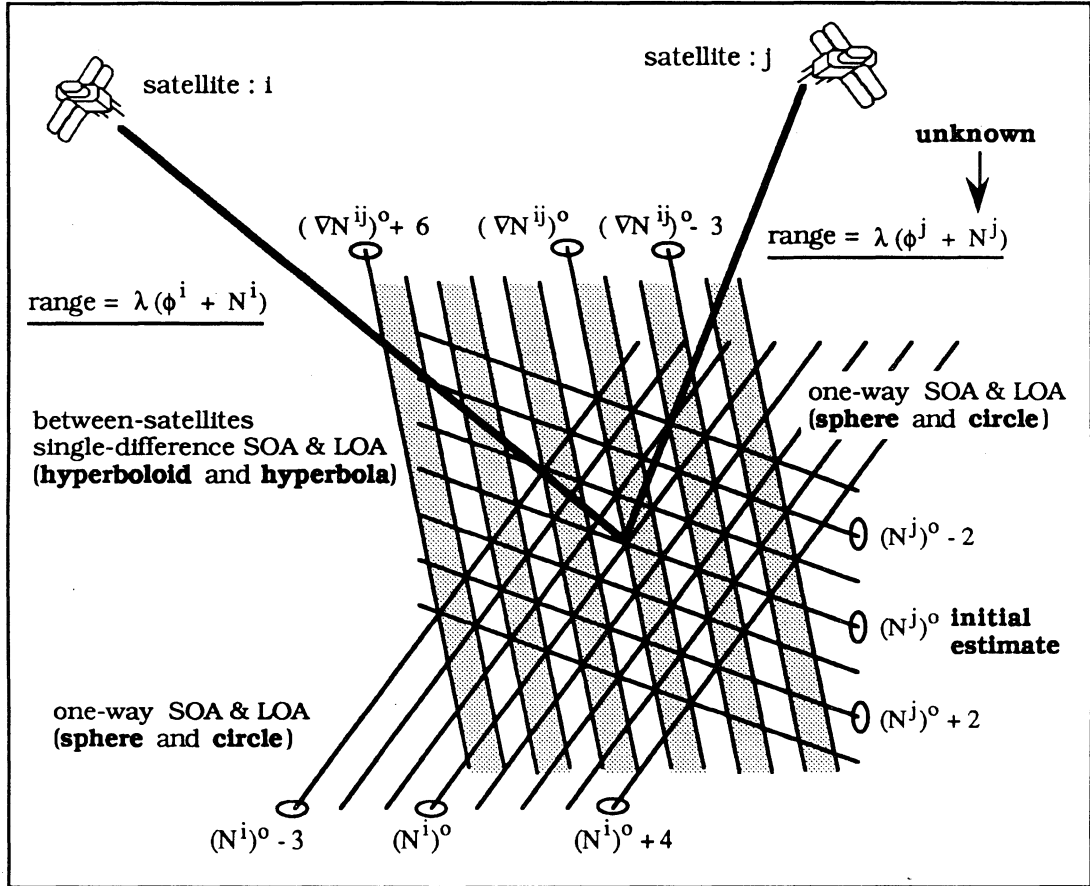


Figure 2.3. The physical surfaces of ambiguity in 2-D perspective.  
 Due to the great distances to the satellites compared to signal wavelength, the parts of the circle and the parabola in the above figure will appear as the straight lines.

If we have another satellite, let's say  $j$ , and we perform the differencing between the satellites, then the following equation is obtained:

$$\nabla \rho^{ij} = \rho^j - \rho^i = \lambda (\nabla \phi^{ij} + \nabla N^{ij}) \quad (2.2)$$

The potential position related to single between-satellite single-difference range expressed by equation (2.2) will be located on the hyperboloid focused on satellites  $i$  and  $j$ . In this

case therefore, the SOA will be also the hyperboloid, or the hyperbola in two-dimensional case, as shown in Figure 2.3.

With *station-satellites double-difference* phase observations, performing the station differencing between the user and the known monitor station observations, is the same as applying the range correction from the monitor station to the between-satellite single-difference observation of the user site. If observations are assumed not to be contaminated by noise, errors, and biases, this correction is the 'known' ambiguity related to a monitor station. Therefore, the SOA and LOA will still be the hyperboloid and the hyperbola, respectively.

The collection of several surfaces of ambiguities constitutes the ambiguity space. In this research, the *physical ambiguity space* is defined as a three-dimensional space constituted by the physical surfaces of ambiguities. It is in the position (cartesian or ellipsoidal) domain, and the ambiguity sets are represented by positions related to the intersections of their corresponding surfaces of ambiguity. The orientation and the pattern of the SOA depends on the observation geometry, such as the location of satellites and the user, the between-satellite differencing approach of observations, and the wavelength of the signal, as indicated in Figure 2.3. Therefore, the ambiguity-set related positions inside the physical ambiguity space will also depend on the aforementioned variables and obviously not be evenly space distributed.

For computational purposes, the physical ambiguity space can be transformed to the *mathematical ambiguity space*: It is defined in the ambiguity domain, and in the case of  $n_s$  number of satellites and double-difference ambiguities, the mathematical ambiguity space is a  $(n_s-1)$  dimensional space. In this space, the positions are represented by  $(n_s-1)$  tuples of integer ambiguities. They are evenly spaced and distributed inside the mathematical

ambiguity space regardless of the observation geometry. The *mathematical SOA and LOA* related to this mathematical ambiguity space will always be the planes and the straight lines.

### **2.3. On-the-fly ambiguity resolution techniques**

There are several techniques that have been proposed for resolving the ambiguity of GPS phase observations. Some of them, however, are intended to be used only for static and rapid static GPS surveying. Among the techniques that can be used for on-the-fly ambiguity resolution, only the extrawidelaning technique [Wubben, 1989], the ambiguity mapping function technique [Remondi, 1984; Mader, 1990, 1992], and the least-squares ambiguity searching approach [Hatch, 1989, 1990] are reviewed in the following. This is because our new strategy for on-the-fly ambiguity resolution, which will be described in the next chapter, will take into consideration some of their positive features. There is also another on-the-fly ambiguity resolution technique worth mentioning, which is called *kinematic GPS without static initialization* technique, proposed by Dr. B.W. Remondi. Since in principle this technique is more or less similar to the ambiguity mapping function technique, it will not be reviewed in this chapter. Interested readers can consult Remondi [1991, 1992a, 1992b] for the formulation and the performance of this technique.

#### **2.3.1. General strategy of on-the-fly ambiguity resolution**

Except for the extrawidelaning technique, the aforementioned on-the-fly ambiguity resolution techniques have a more or less similar strategy for resolving ambiguity, which can be depicted in Figure 2.4. Basically, the ambiguity resolution is performed by testing many combinations of ambiguity sets or positions representing the ambiguity sets inside a certain predetermined searching space. The searching space is usually centered at a certain initial estimate of the ambiguity set or the position, and it could be either the *mathematical*

*space*, i.e., defined in the ambiguity domain, or *physical space*, i.e., defined in the position domain.

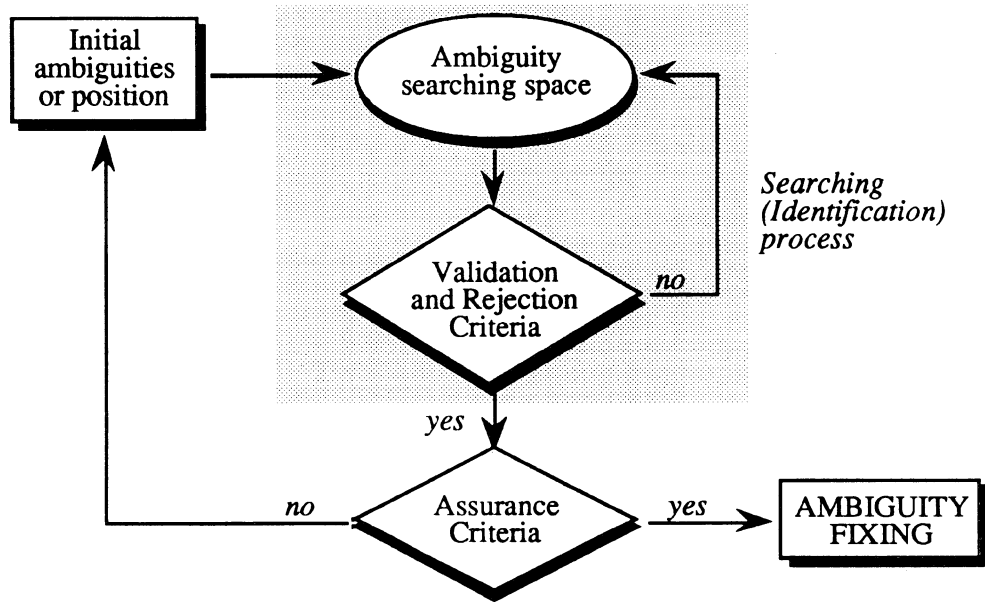


Figure 2.4. General strategy of on-the-fly ambiguity resolution.

The process of searching integer ambiguities is performed by applying certain validation and rejection criteria to the ambiguities or positions being tested. The searching process is stopped and the ambiguities are fixed whenever certain assurance criteria are fulfilled. The on-the-fly ambiguity resolution techniques usually differ from each other in the validation and rejection criteria used in the searching process and in the assurance criteria used to stop searching. Differences could be in the types and numbers of criteria, and/or in their formulations and application sequences. The techniques might also differ in the underlying philosophy of the ambiguity resolution process, and in approaches used to construct the searching space and to estimate the initial ambiguities or position. These differences usually lead to the differences in the computation and observation times of ambiguity resolution, and sometimes to differences in the reliability of resolution.

### 2.3.2. Extrawidelaning technique

The extrawidelaning technique of ambiguity resolution is proposed by *Wubbena* [1989] for dual-frequency GPS data. It can be used both for static and moving receivers. The technique is not affected by frequency-independent errors and biases, such as clock errors, tropospheric effect, and ephemeris error. However, it is sensitive to frequency-dependent errors and biases, such as ionospheric effects, multipath and observation noise. The technique does not directly use actual GPS observations in resolving the ambiguities. Instead, linear combinations of the actual observations, the so-called wide-lane, narrow-lane, and ionospheric signal observations, are used (see Appendix I).

In the extrawidelaning technique, the resolution of the cycle ambiguities of wide-lane and narrow-lane carrier phases is accomplished through *five steps*. In the **first step**, pseudoranges are smoothed using carrier phase observations [*Hatch*, 1982] in order to reduce the noise and multipath effect on pseudoranges (the smoothing formulation is given in Appendix II). The **second step** is to obtain the a priori wide-lane ambiguity. The cycle ambiguity of the wide-lane signal is first estimated because of its relatively long wavelength (86.25 cm), which can be resolved more easily. Here, the a priori wide-lane ambiguity is estimated using the combination of wide-lane carrier range ( $L_{\Delta}$ ) and smoothed 'narrow-lane' pseudorange observations ( $\hat{P}_{\Sigma}$ ). To eliminate most of the effects of the errors and therefore simplify the working model, the receiver-satellite double-difference ambiguities are estimated. By using equations (I.23) and (I.24) from Appendix I, the following relation for estimating the a priori wide-lane ambiguity is obtained :

$$\nabla\Delta N_{\Delta} = \frac{(\nabla\Delta\hat{P}_{\Sigma} - \nabla\Delta L_{\Delta}) + (\nabla\Delta MC_{\Delta} - \nabla\Delta M\hat{P}_{\Sigma}) + (\nabla\Delta vC_{\Delta} - \nabla\Delta v\hat{P}_{\Sigma})}{\lambda_{\Delta}} \quad (2.3)$$

The last two terms in the above equations are related to the multipath and the observation noise (see Appendix I for a more detailed explanation). Since the epoch-by-epoch magnitude of these two terms is usually difficult to know, these terms are usually neglected in computing the a priori wide-lane ambiguity. When there is no multipath and the pseudoranges are smoothed using carrier phases, the neglect can be tolerated. When strong multipath occurs, however, it can be expected that it will bias the a priori wide-lane ambiguity estimates. To further reduce the effects of the remaining noise and multipath, sequential time averaging can be performed on the a priori ambiguity estimates.

After estimating the a priori wide-lane ambiguity, the **third step** is to estimate the narrow-lane ambiguity using the help of ionospheric signal observations ( $L_{is}$ ). Based on equations (I.24) to (I.27) from Appendix I, the double-difference ionospheric signal observations can be formulated as follows :

$$\begin{aligned}
\nabla\Delta L_{is} &= \nabla\Delta L_{\Sigma} - \nabla\Delta L_{\Delta} \\
&= - 2.\nabla\Delta\text{dion}_{\Delta/\Sigma} - \nabla\Delta NR_{\Sigma} + \nabla\Delta NR_{\Delta} + \nabla\Delta(MC_{\Sigma} - MC_{\Delta}) + \nabla\Delta(\vartheta C_{\Sigma} - \vartheta C_{\Delta}) \\
&= - 2.\nabla\Delta\text{dion}_{\Delta/\Sigma} - \lambda_{\Sigma}.\nabla\Delta N_{\Sigma} + \lambda_{\Delta}.\nabla\Delta N_{\Delta} + \nabla\Delta MC_{is} + \nabla\Delta\vartheta C_{is} \quad , \quad (2.4)
\end{aligned}$$

where  $\text{dion}$  denotes the effect of ionospheric refraction (see also Appendix I). By rearranging the above equation, the formula for estimating the double-difference narrow-lane ambiguity can be established as follows :

$$\begin{aligned}
\nabla\Delta N_{\Sigma} &= \frac{\lambda_{\Delta}.\nabla\Delta N_{\Delta} - (\nabla\Delta L_{is} + 2.\nabla\Delta\text{dion}_{\Delta/\Sigma} - \nabla\Delta MC_{is} - \nabla\Delta\vartheta C_{is})}{\lambda_{\Sigma}} \\
&= 8.059.\nabla\Delta N_{\Delta} - \frac{(\nabla\Delta L_{is} + 2.\nabla\Delta\text{dion}_{\Delta/\Sigma} - \nabla\Delta MC_{is} - \nabla\Delta\vartheta C_{is})}{\lambda_{\Sigma}} \quad (2.5)
\end{aligned}$$

If the a priori wide-lane ambiguity can be estimated with the accuracy level of  $\pm 2$  cycles ( $0.059 \cdot \nabla \Delta N_{\Delta} = 0.12$  cycles), and the ionospheric effects, carrier multipath, and phase noise are negligible or can be reduced to a negligible level, then the ionospheric signal will have the integer ambiguity with a wavelength equal to the narrow-lane wavelength. The first requirement in estimating the a priori wide-lane ambiguity is not difficult to satisfy by using smoothed pseudorange or time averaging. The differential ionospheric effect, however, can be considered negligible only for baseline lengths up to a few kilometres. For longer baselines, it should be somehow reduced so the ionospheric signal ambiguity can be fixed. The effects of the noise and multipath on the ionospheric signal can be reduced by time averaging, the reliability of which will depend on the magnitudes and signatures of the noise and multipath.

It should be emphasized here that this third step is the most important step of the extrawidelaning technique. The resolving times and the reliability of the ambiguity resolution depends on how long and how reliably the ionospheric signal ambiguity can be 'fixed'. In this case, the accuracy of the ionospheric signal is used as a criteria for the fixing [Wubben, 1989; Seeber & Wubben, 1989].

In the **fourth step** of extrawidelaning technique, by using the double-difference narrow-lane ambiguities estimates on equation (2.5), the double-difference wide-lane ambiguities are fixed using the *even-odd relation* between the wide-lane and narrow-lane ambiguities. In this case, when the narrow-lane ambiguity is an even integer number then the a priori wide-lane ambiguity is fixed to the nearest even integer number, and, when the narrow-lane ambiguity is an odd integer number, then the a priori wide-lane ambiguity is fixed to the nearest odd integer number. Note that this even-odd relation increases the effective wavelength of wide-lane signal by a factor of two to 172.5 cm; a process which is termed *extrawidelaning*. Finally, as the **fifth stage**, after the wide-lane ambiguity is fixed based

on this extrawidelaning, it is used in equation (2.5) to fix the narrow-lane ambiguity. This process of ambiguity resolution using the extrawidelaning technique is depicted in Figure 2.5.

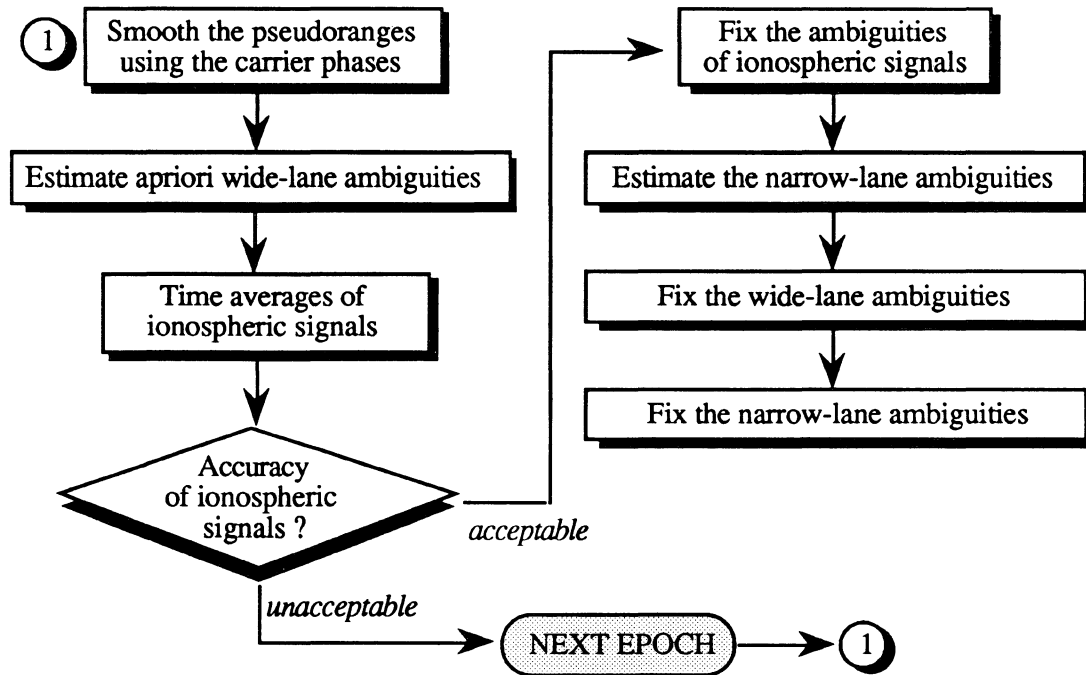


Figure 2.5. On-the-fly ambiguity resolution based on extrawidelaning technique.

As mentioned before, the extrawidelaning technique of ambiguity resolution uses the accuracy of the ionospheric signal as criterion for fixing the ambiguities. Therefore, the times (needed) and success to resolve the ambiguities is dependent on the magnitude of the residual frequency-dependent errors and biases in the observations, such as ionospheric delay, multipath error, and observation noise. The technique usually requires a few minutes to resolve the ambiguity if the ionospheric refraction is negligible and the data is not contaminated by multipath effects [Seeber & Wubbena, 1989; Abidin & Wells, 1990; Abidin, 1990].



### 2.3.3. Ambiguity mapping function technique

The ambiguity mapping function technique was first described by *Counselman & Gourevitch* [1981]. The technique has been applied for the static case [*Remondi*, 1984; *Mader*, 1992; *Ziegler et.al.*, 1992], the pseudo-kinematic case [*Remondi*, 1990; *Balde et.al.*, 1991], and the kinematic case [*Mader*, 1990, 1992]. The ambiguity function is defined as follows:

$$\text{AMF}(\vec{r}) = \sum_{i=1}^{ne} \left| \sum_{k=1}^{ns} \sum_{l=1}^{nf} \exp\{ i [\phi_{\text{obs}}^{j,k,l} - \phi_{\text{calc}}^{j,k,l}(\vec{r})] \} \right| , \quad (2.6)$$

where  $\vec{r}$  is the position vector (cartesian or ellipsoidal coordinates),  $\phi_{\text{obs}}$  is the observed single-difference or double-difference phase (in radians),  $\phi_{\text{calc}}$  is the calculated single-difference or double-difference phase at position  $\vec{r}$  (in radians),  $ne$  is the number of epochs,  $ns$  is the number of satellites, and  $nf$  is the number of frequencies. Finally, it should be noted in this equation that:

$$\exp(i\phi) = \cos(\phi) + i.\sin(\phi) . \quad (2.7)$$

In equation (2.6), the integer cycle ambiguity of the observed phase does not have an effect on the ambiguity mapping function value since

$$\exp(i\phi) = \exp [i(\phi + 2\pi.N)] , \quad (2.8)$$

with  $N$  as the cycle ambiguity integer. Changes in the ambiguity integer will also have no effect. This insensitivity of the ambiguity mapping function is a positive point in the case of

cycle slips. In the case of choosing the correct ambiguity from several possible values, however, it is a negative point since more than one ambiguity may yield almost the same values of the ambiguity mapping functions.

As can be seen from equation (2.6), the ambiguity mapping function measures the agreement between the measurements and their calculated values. The unaccounted errors and biases in the observed phases therefore will affect the value of the mapping function. If the value is normalized with the number of measurements used to compute the ambiguity mapping function, then considering there are no observation errors and biases, the ambiguity mapping function will have the values between zero and one. The value of one represents the perfect agreement among the measurements, i.e., the most constructive interference among the observed signals, and the value of zero represents the most destructive interferences.

The ambiguity mapping function technique can be used to resolve the cycle ambiguity by trying to find a position corresponding to the maximum value ( $\approx 1$ ) of the normalized ambiguity mapping function. This position, along with the satellite position, is then used to compute the cycle ambiguity. In the case of on-the-fly ambiguity resolution, the correct ambiguities are resolved by searching through positions inside the three-dimensional position searching space as shown in Figure 2.6. With enough measurements at different frequencies from different satellites and different epochs, it can be expected that, without significant measurement errors and biases, the observed phases will interfere constructively at the correct position and interfere destructively at other positions.

In searching for the correct integer ambiguities, the ambiguity mapping function technique employs two rejection criteria, namely *the magnitude of the real term of the individual ambiguity mapping function* which is formulated as:

$$AMF_{real}^{j,k,l}(\vec{r}) = \cos(\phi_{obs}^{j,k,l} - \phi_{calc}^{j,k,l}(\vec{r})) > \text{minimum threshold} . \quad (2.9)$$

and the magnitude of the normalized ambiguity mapping function which is formulated as:

$$NAMF(\vec{r}) = \frac{AMF(\vec{r})}{nf \cdot ns \cdot ne} > \text{minimum threshold} . \quad (2.10)$$

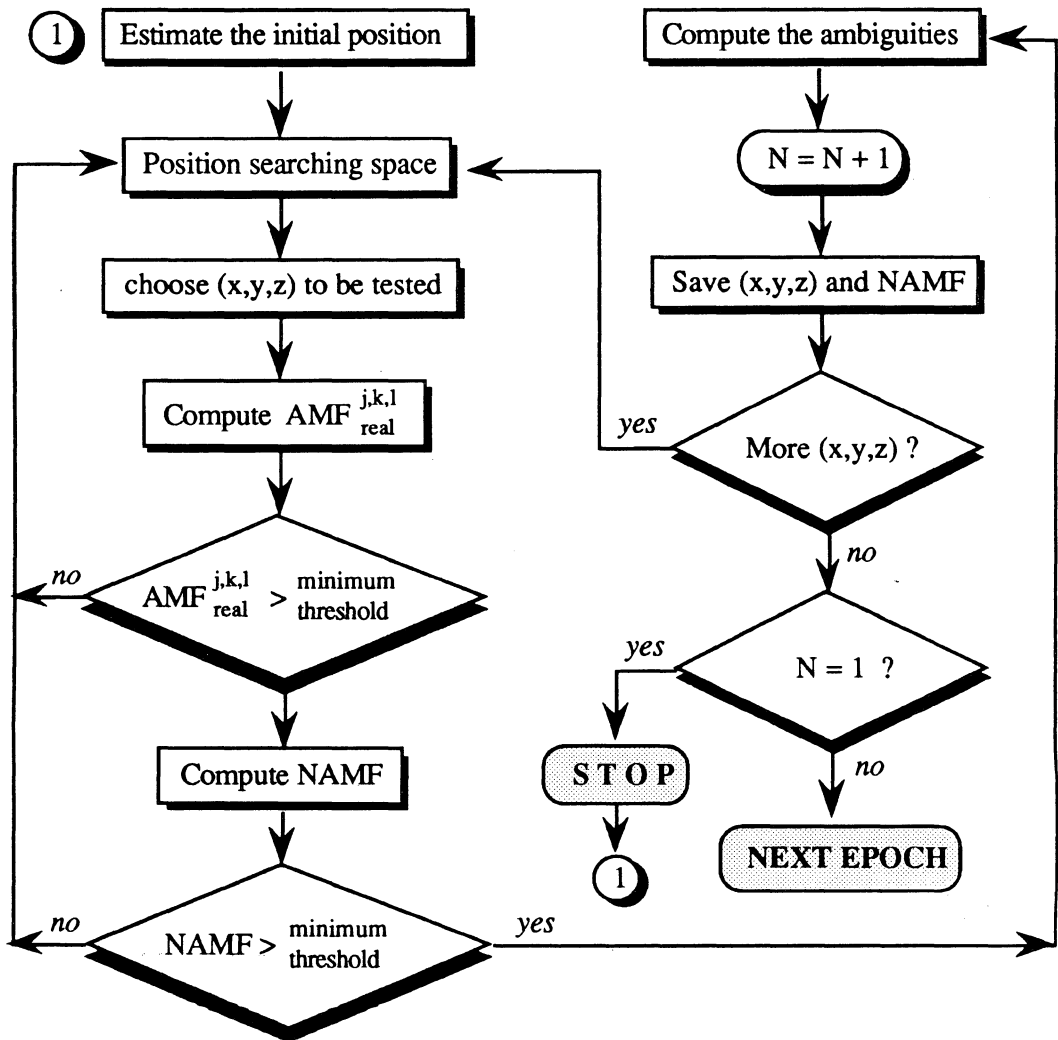


Figure 2.6. On-the-fly ambiguity resolution based on ambiguity mapping function technique (N in this figure is the number of potentially correct ambiguities).

For ambiguity searching, the increments in each coordinate should be chosen in proportion to the signal wavelength. In general, they should be less than half a wavelength. The increments should not, however, be too small since it will lead to too many positions to be tested and therefore will burden the computational efforts. It should also not be too large, in order not to miss the correct position and in turn the correct ambiguities. From this tradeoff, it is obvious that it is preferable to work with a signal with longer wavelength. In the case of dual frequency data, it is preferable to use the wide-lane signal rather than L1 and L2 signals, and, in the case of codeless data, it is better to use the semi or double wide-lane signals (see Appendix I for the definition of these signals).

In the case of the moving receiver, it should be noted that when more than one epoch is needed to resolve the ambiguity, the change in the antenna position should be taken properly into account in order to 'move' the searching space from epoch to epoch. In this case, considering there are no cycle slips between the epochs, the change in the observed phases can be utilized.

As can be realized from equation (2.6), both frequency-dependent and frequency-independent errors and biases in the phase observations will affect the ambiguity mapping function value. Obviously, they will have an impact on the ambiguity resolution process, and, for reliable ambiguity resolution, should be somehow eliminated or properly taken into account.

In order to account for the ionospheric refraction effects, *Mader* [1992] has modified the searching strategy of the ambiguity mapping function technique. Instead of searching in the position domain (physical searching space), the new strategy is searching in the ambiguity spaces of L1 and L2 signals (mathematical searching space). The ability to vary by a small amount each of the integers generated is also incorporated to account for more severe

effects of the ionospheric refractions. The problem with this approach, however, is the tremendous number of the ambiguity sets to be tested and it is therefore not efficient for on-the-fly ambiguity resolution.

Based on his investigations, *Mader* [1992] suggested that the ambiguity resolution technique needs about 14 observations to resolve ambiguities. In the context of on-the-fly ambiguity resolution, it could mean instantaneous ambiguity resolution with seven L1 and L2 phase observations, or second-epoch resolution with seven L1 phases, or any resolution epochs corresponding to other combinations of single or dual frequency data and number of satellites which yield at least 14 observed phases.

#### **2.3.4. Least squares ambiguity searching technique**

The least squares ambiguity searching technique is described in *Hatch* [1989, 1990]. The technique is based on the least square adjustment technique [*Vanicek and Krakiwsky*, 1986], and uses the least squares residuals of the observation to measure the disagreement between the phase measurements corresponding to different ambiguity sets being tested. The measure of disagreement, which is the estimated variance factor, is used to isolate the correct ambiguities from the wrong ambiguities. In searching for the correct ambiguities, the technique exploits the facts that the ambiguities corresponding to four chosen satellites, i.e., *primary ambiguities*, mathematically determine the other ambiguities corresponding to remaining satellites, i.e., *secondary ambiguities*. Therefore, it is only necessary to search for the primary ambiguities regardless of the available number of satellites. With using double-difference observations, this means only three-dimensional searching space should be considered. In this case, the estimates of initial ambiguities is required along with a description of the volume over which the search is to be conducted. The initial code-derived position is usually used to estimate these initial ambiguities.

In the least-squares searching technique, the primary ambiguities are used to generate potential (trial) positions. Secondary ambiguities are then used to identify potentially correct trial positions and hence the correct ambiguities, and, at the same time to reject the incorrect ones. The mathematical formulations of the technique can be seen in *Hatch* [1990] and ambiguity resolution concept of the technique can be depicted as shown in Figure 2.7. In this flowchart, the estimated variance factor is computed using the following relation:

$$\hat{\sigma}_0^2 = \frac{\mathbf{v}^T \cdot \mathbf{C}^{-1}(\text{Obs}) \cdot \mathbf{v}}{ns - 4} \quad , \quad (2.11)$$

where  $\mathbf{v}$  is the residual vector of the phase observations,  $ns$  is the number of satellites, and  $\mathbf{C}^{-1}(\text{Obs})$  is the covariance matrix of the phase observations. *Hatch* [1990] did not mention precisely how it is decided whether the estimated variance factor is to be kept or rejected. However, one way to decide is by applying the chi-squares statistical testing on estimated variance factor [*Vanicek and Krakiwsky*, 1986].

As mentioned before, the least squares ambiguity searching technique depends on the residual of observations for isolating the correct ambiguities and rejecting the wrong ones. Therefore, the incorrect mathematical model, the unaccounted errors and biases in the observations, and the incorrect a priori covariance matrix of the observations can make the searching technique fail to find the correct ambiguities.

From a computational point of view, however, this technique is more efficient than the ambiguity mapping function technique. The increase in the number of satellites will not increase the processing time as in the case of the ambiguity mapping function technique. Instead, it will decrease the processing time.

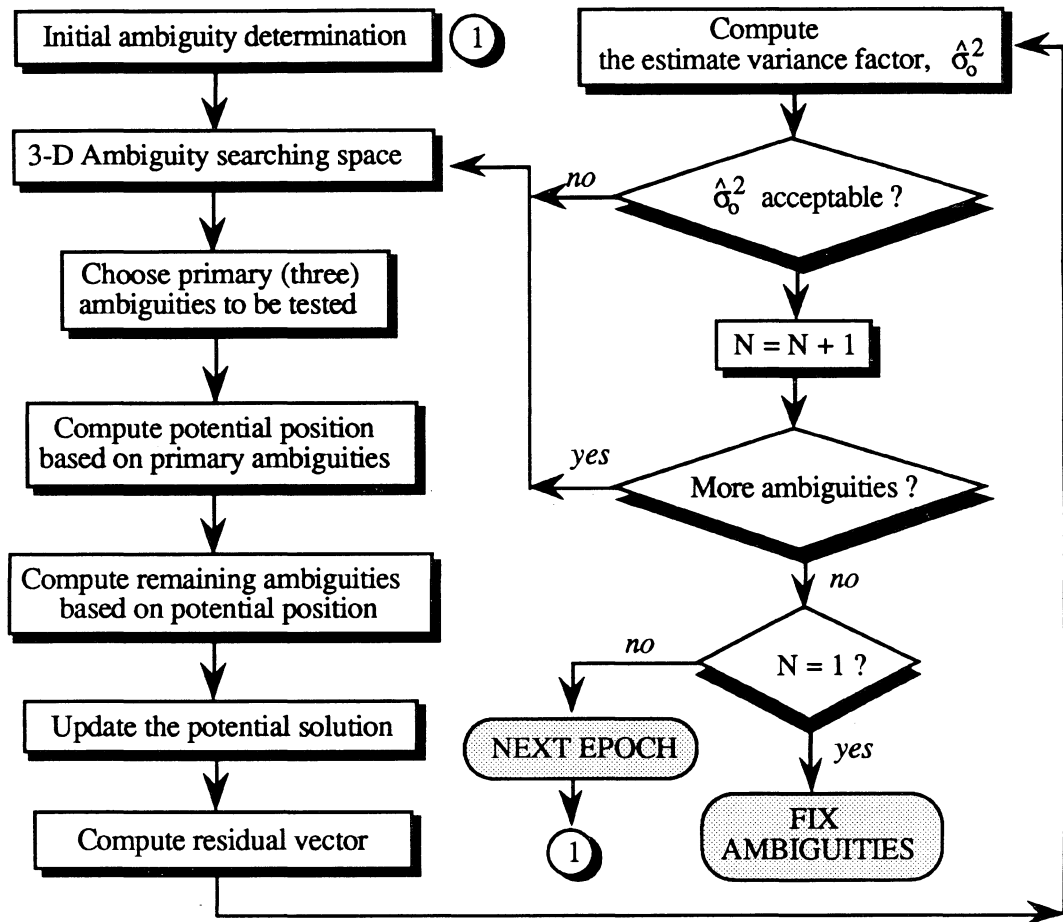


Figure 2.7. Least squares ambiguity searching technique.  
(N in this figure is the number of potentially correct ambiguities).

Based on static data processed in kinematic mode and simulated kinematic data, *Hatch* [1990] concluded that the least-squares ambiguity searching technique can resolve the ambiguity instantaneously if dual-frequency data is used, seven satellites or more are available, and the ionospheric effects are insignificant. If six satellites are available, the ambiguity can usually be resolved under two minutes of observation times and, in the case of five satellites, it will rarely exceed five minutes. With single frequency data, five to six observed satellites, and significant tropospheric and ionospheric refractions, the resolution of the ambiguities, however, becomes more difficult and several tens-of-minutes of observation times are required to resolve the ambiguity [*Hatch*, 1991].

## 2.4. Comparison of the techniques

The aforementioned on-the-fly ambiguity resolution techniques, have their own characteristics, advantages and disadvantages. The general features of these three techniques are summarized in Table 2.1.

Table 2.1. Comparisons between on-the-fly ambiguity resolution techniques

Features	<i>Extrawidelaning technique</i>	<i>Ambiguity mapping function</i>	<i>Least-squares ambiguity searching</i>
<i>Data required (frequency)</i>	dual	single or dual	single or dual
<i>Number of satellites</i>	any	at least 4	more than 4
<i>Ambiguity searching</i>	none	yes (position domain)	yes (ambiguity domain)
<i>Ambiguity searching shape</i>	none	cube	cube
<i>Assurance criteria</i>	accuracy of ionospheric signal	ambiguity mapping function value	estimated variance factor
<i>Frequency-dependent biases &amp; errors</i>	affect	affect	affect
<i>Frequency-independent biases &amp; errors</i>	no effects	affect	affect
<i>Computation time per epoch</i>	fastest	slowest	moderate
<i>Correlation between computational time and number of satellites</i>	positive	positive	negative



This research seeks to bring together the positive features of these techniques in developing a new strategy for on-the-fly ambiguity resolution. The proposed technique is called integrated on-the-fly ambiguity resolution technique and some of its aspects have been described in *Abidin* [1991, 1992]; and *Abidin et al.* [1991, 1992]. A more detailed and complete explanation of the technique will be given in Chapter 3, and the detailed analysis of its performance will be given in Chapters 4, 5, and 6.

## Chapter 3

# INTEGRATED ON-THE-FLY AMBIGUITY RESOLUTION TECHNIQUE

---

---

In this chapter, the concepts and mathematical methodologies related to the integrated on-the-fly ambiguity resolution technique proposed in this investigation are explained. The technique is formulated by considering the use of more than one monitor station with a single moving receiver. The elimination of errors and biases, however, is not integrated with the ambiguity resolution technique algorithm since it is assumed that the elimination is done partly by observation differencing and partly by using correction parameters obtained from somewhere else such as a master monitor station [Brown, 1989]. The explanations in this chapter, therefore, are done by assuming that the remaining errors and biases in the observations are insignificant.

This chapter will explain the concept of ambiguity resolution adopted in this research. The reason and advantages of using more than one monitor station is then explained and the rest of the chapter is allocated for outlining the algorithm of the integrated on-the-fly ambiguity resolution technique. In this chapter, the term *initial ambiguities* is used to represent the initial estimates of the ambiguities which are used to locate the centre of ambiguity searching space. The term *potential positions (ambiguities)* used in the context of the ambiguity searching process, may also be called the *trial positions (ambiguities)*.

### 3.1. The concept of ambiguity resolution

Resolving the cycle ambiguity of GPS carrier phase signal is not an easy task to accomplish, particularly when resolution is on-the-fly and as quickly as possible. Besides requiring a good station-satellite relative geometry and low level of observation errors and biases, fast on-the-fly ambiguity resolution also requires fast and reliable algorithm.

With integrated on-the-fly ambiguity resolution technique, the ambiguity resolution process is mathematically accomplished by using the mutual combination of *estimation* and *identification* processes, as conceptually depicted in Figure 3.1. The estimation process is used to estimate the initial ambiguities and to construct the initial ambiguity searching space for the identification process. It also provides the parameters for validating and rejecting the ambiguities in the identification process. The estimation process is based primarily on the least-squares adjustment technique [Vanicek & Krakiwsky, 1986].

The identification process is designed to identify the correct ambiguities from many combinations of ambiguities given inside the searching space. This process consists of several criteria for validating the potentially correct ambiguities and, at the same time also for rejecting the supposedly incorrect ones. The more detailed formulation and methodologies involved in this estimation and identification processes will be explained later.

The success and failure of resolving the ambiguities will be affected by our ability to understand, formulate, and model the real world problem of ambiguity resolution, as indicated in Figure 3.1. The errors and biases in the observations and the station-satellite relative geometry deserve special consideration due to their significant impact on the ambiguity resolution process.

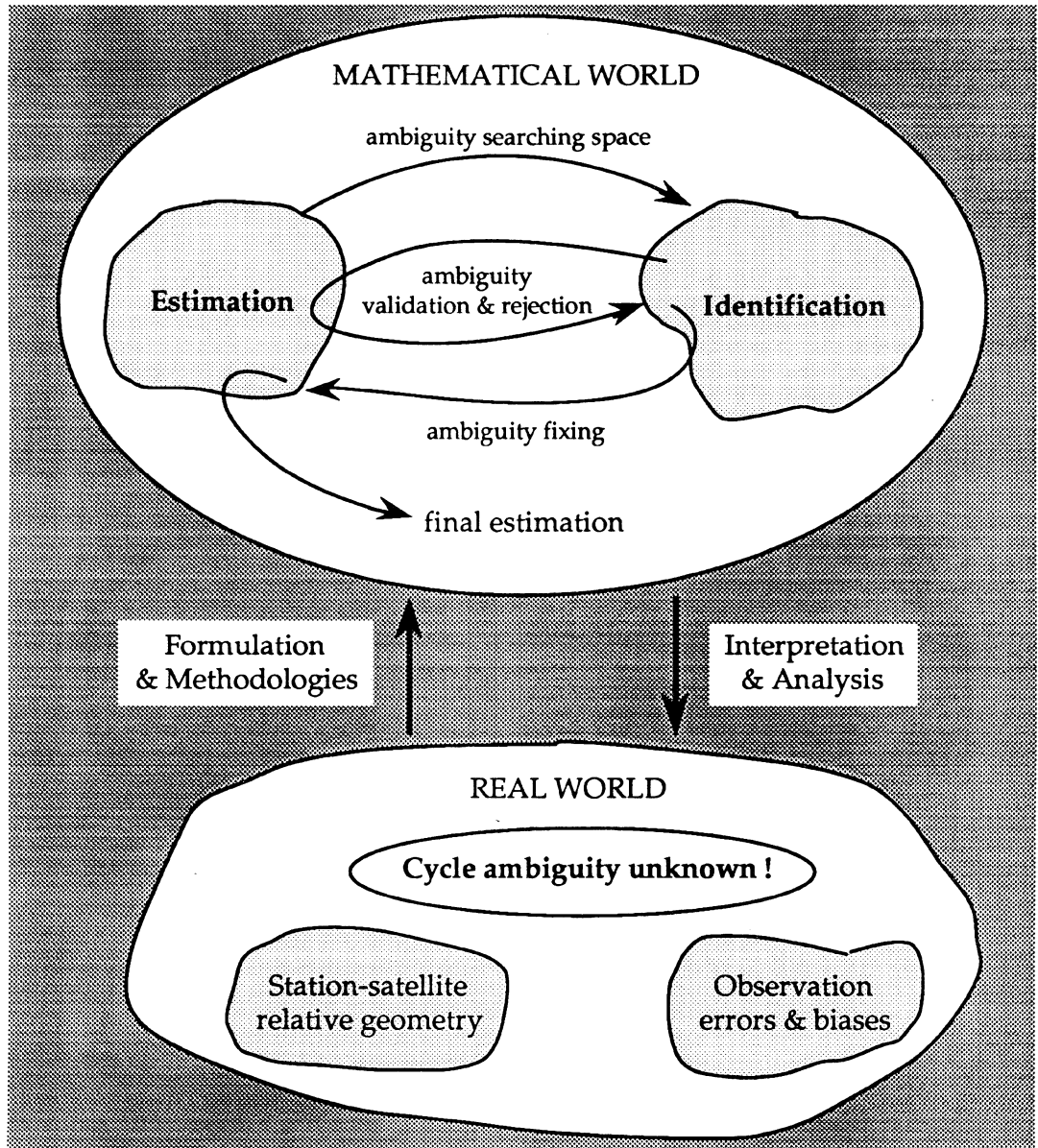


Figure 3.1. Conceptual depiction of cycle ambiguity resolution system

### 3.2. The use of more than one monitor station

With a fast, smart, and reliable ambiguity resolution algorithm along with favourable geometry of the satellites and insignificant residual errors and biases in the observations, on-the-fly ambiguity resolution can usually be done quickly enough even when depending

on only one monitor station. This is usually the case when the monitor station and the moving receiver are close together and the dual-frequency receiver is used. The ambiguity resolution, however, becomes more difficult with unfavourable geometry and significant residual errors and biases (as in the case of longer distances between the monitor station and the moving receiver), and with the use of single-frequency receivers. In these situations, the use of more than one monitor station becomes necessary.

There are two main advantages of using more than one monitor station for on-the-fly ambiguity resolution. The first one is that, with the observations from multi monitor stations, one can estimate more reliably the biases affecting the observations such as the ephemeris errors and the ionospheric refractions. By removing these biases, ambiguity resolution becomes more reliable and much easier. The second advantage is that, considering that the observations have been corrected for the biases and are mainly contaminated by the noise, the use of multi monitor stations also speeds up ambiguity resolution. Increased resolution speed is mainly due to the reduction in the size of initial ambiguity searching space and an increase in contrast level between the potentially correct and incorrect ambiguities.

In this thesis, two groups of monitor stations are considered. The first group is user-independent monitor stations, which are well-established, operated on a permanent basis, and cover a wide area. This group of primary monitor stations, which can be called "active control system networks" [Delikaraoglou *et.al.*, 1990], or an "extended differential GPS system" [Brown, 1989], or a "wide-area differential GPS system" [Kee *et.al.*, 1991], is assumed to provide users with information about the observation biases, such as satellite ephemeris error components and ionospheric and tropospheric model parameters. The primary group of monitor stations is assumed to utilize dual-frequency receivers.

The second group of monitor stations, which will be called "the secondary monitor stations" is established by users to better suit their own interests for faster on-the-fly ambiguity resolution. With secondary monitor stations, the users more or less control the type of receiver used, the kind of data sent, the data interval adopted, the locations of the monitor stations with respect to the survey area, the antenna placement, etc. Since observation biases are assumed to be taken care of by the primary monitor stations, the secondary monitor stations can safely observe using either single, codeless, or dual frequency receivers. The roles of these two groups of monitor stations for on-the-fly ambiguity resolution is conceptually depicted in Figure 3.2.

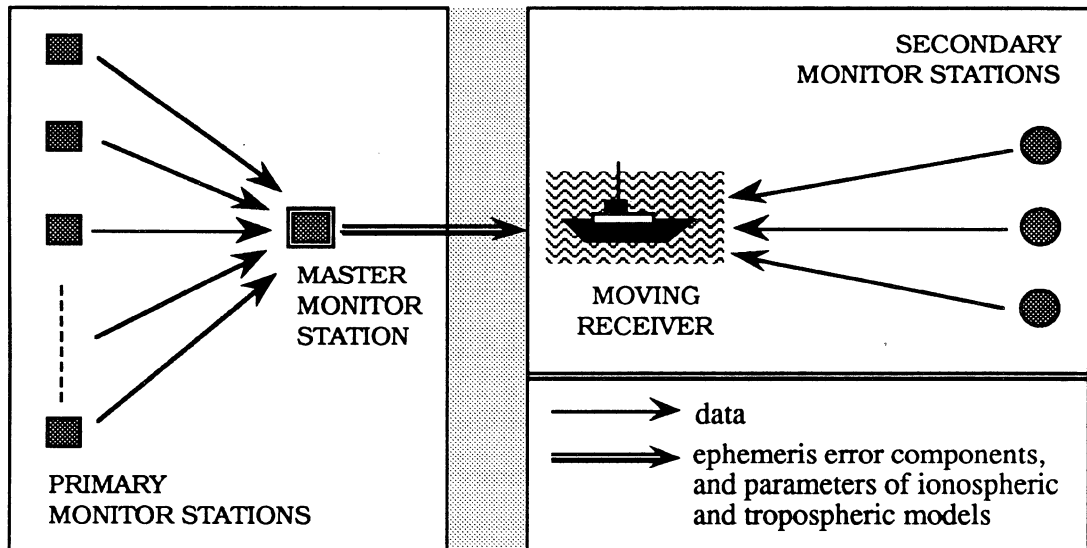


Figure 3.2. Conceptual depiction of multi monitor station on-the-fly ambiguity resolution.

In the following subchapters, the integrated on-the-fly ambiguity resolution technique utilizing more than one secondary monitor station is explained. It is assumed that only the noises remain in the observations after the users apply the corrections sent by the master monitor station of the primary group of monitor stations.

### **3.3. General strategy of the integrated ambiguity resolution technique**

The integrated on-the-fly ambiguity resolution technique used in this research is based on the synergism of the three ambiguity resolution techniques explained in Chapter 2. The process of searching the ambiguities follows the framework of the least squares ambiguity searching technique. Besides the other new criteria, the ambiguity mapping function is used as one of the validation and rejection criterion. The extrawidelaning technique is used when dual frequency data is available to determine the initial ambiguities and the ambiguities at each epoch to be considered along with other tested ambiguities. In order to reduce or eliminate some of the systematic errors and also to reduce the ambiguity searching space, the technique uses station-satellite double-difference observations. The signal used for ambiguity resolution are wide-lane and narrow-lane in the case of dual frequency data; semi, half or double wide-lane (wavelength of about 34 cm, 43 cm, and 163 cm, respectively) in the case of codeless data, and L1-signal in the case of single frequency data. In general, the technique tries to identify the correct ambiguity set through the following steps :

- Estimate the initial ambiguities,
- Construct the three-dimensional ambiguity space centered on the initial ambiguities,
- Search the correct ambiguities inside the ambiguity space by employing certain validation and rejection criteria, and
- Fix the ambiguities when certain assurance criteria are fulfilled.

More detailed steps are given by the flow-chart in Figure 3.3. Searching the correct ambiguities in the integrated technique is done by utilizing eight validation and rejection (VR) criteria, namely :

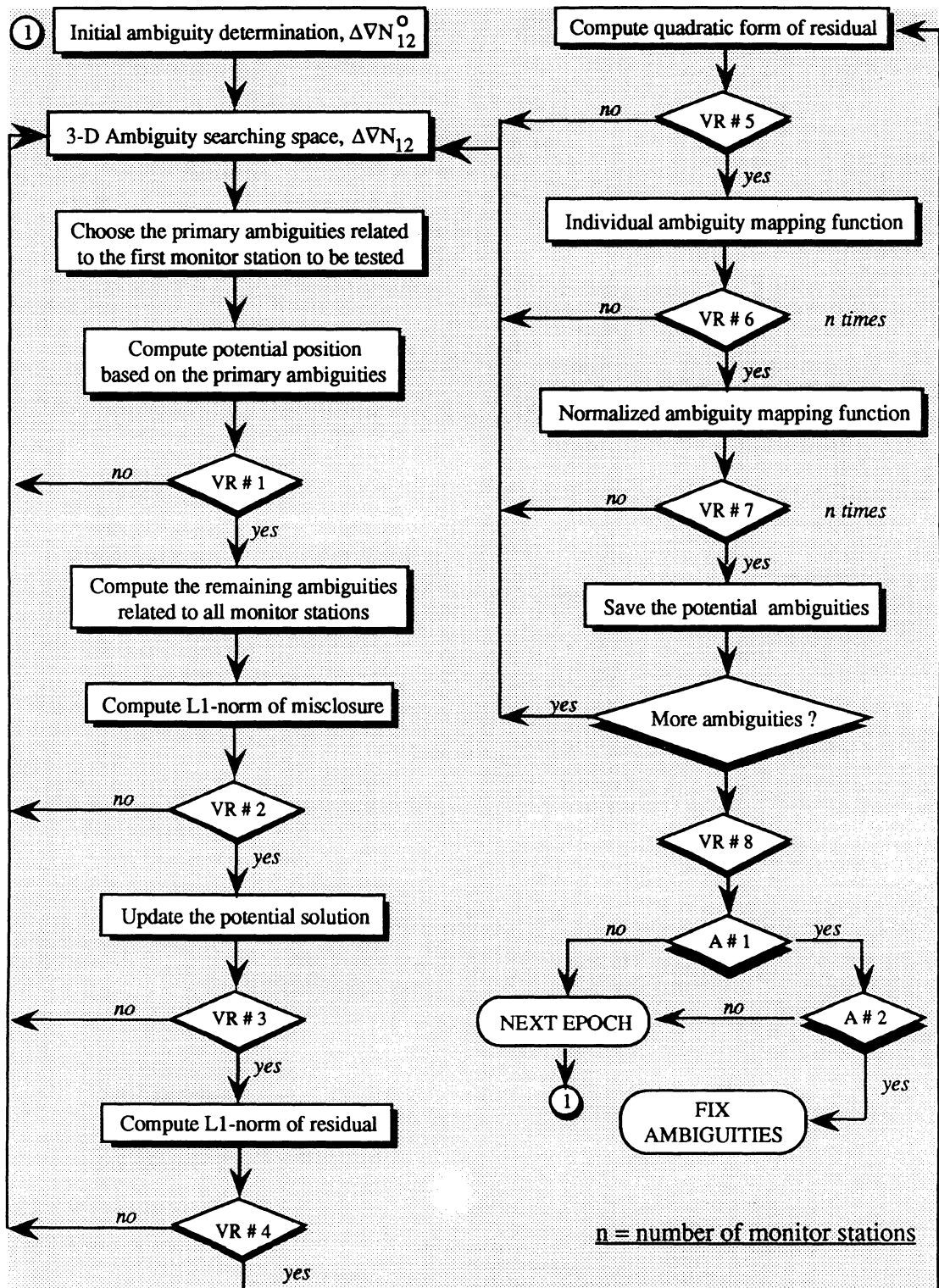


Figure 3.3. Integrated on-the-fly ambiguity resolution technique.



- VR #1 : Compatibility test between the potential and code-derived positions.
- VR #2 : Test on L1-norm of the misclosure vector.
- VR #3 : Compatibility test between the updated and code-derived positions.
- VR #4 : Test on L1-norm of the residual vector.
- VR #5 : Test on the quadratic form of the residuals.
- VR #6 : Individual ambiguity mapping function test .
- VR #7 : Normalized ambiguity mapping function test .
- VR #8 : Contrast test on quadratic form of the residuals.

and two assurance criteria, namely :

- A#1 : Number of potential ambiguity set = 1, and
- A#2 : Its corresponding value of normalized ambiguity mapping function is greater than a certain predetermined threshold.

### 3.4. Initial ambiguity estimation

The initial estimates of ambiguities will be used to centre the initial ambiguity searching space. In this case, the necessary initial ambiguities to be determined are three double difference ambiguities from four observed satellites related to the first monitor station. These satellites will be called the *primary satellites*, since the ambiguities related to the remaining satellites and monitor stations are mathematically dependent on their ambiguities. Correspondingly, the ambiguities related to these primary satellites are denoted as the *primary ambiguities*. If n monitor stations are involved and they are numbered as 1,3,4,

..., n, and the moving receiver is numbered as 2, then the initial primary ambiguities which should be determined are  $(\nabla\Delta N_{12}^o(i), i = 1,3)$ .

For faster and reliable ambiguity resolution, the integers of the initial primary ambiguities should be as close as possible to their correct integers. The initial primary ambiguities  $\nabla\Delta N_{12}^o$  can be determined in several ways. In this technique, for dual-frequency data, these initial ambiguity estimates are computed either using the extrawidelaning technique of ambiguity resolution or using satellite positions and the position of a moving receiver. The moving receiver position is derived using smoothed narrow-lane pseudoranges from all satellites and all monitor stations (if more than one). In the case of codeless and single-frequency data, since the extrawidelaning technique cannot be employed, only the second technique is used by utilizing smoothed L1-C/A code pseudoranges. The pseudoranges are smoothed using carrier phase observations based on the techniques described in *Hatch* [1982] with slight modification in assigning weights to the involved observations (see Appendix II).

The use of extrawidelaning technique for ambiguity resolution is explained in Chapter 2 and Appendix I. When using a code-derived position, the initial estimates for the double-difference ambiguities  $\nabla\Delta N_{12}^o$  are computed as follows :

$$\nabla\Delta N_{12}^o(i) = \text{ININT} \frac{\nabla\Delta\rho_{12}^o(i) - \nabla\Delta L_{12}(i)}{\lambda}, (i = 1,3) \quad , \quad (3.1)$$

where  $\nabla\Delta\rho_{12}^o(i)$  are the double-difference theoretical ranges computed using satellite position and the code-derived position of a moving receiver.  $\nabla\Delta L_{12}(i)$  are the double-difference phase observations in length units.  $\lambda$  is the wavelength of the working signal,

which could be wide-lane, L1 signal, semi wide-lane, half wide-lane or double wide-lane signal. ININT denotes the rounding of the values to the nearest integer number.

The initial ambiguities should be determined accurately as possible in order to construct the ambiguity searching space which would include the correct ambiguity set. Initial ambiguities are computed using the code-derived position. Considering that all code observations have more or less the same precision, the use of observations from more than one secondary monitor station will increase the accuracy of initial ambiguities, compared to the case of using only one monitor station.

### **3.5. Constructing the ambiguity searching space**

The integrated on-the-fly ambiguity resolution technique uses mathematical searching space instead of physical one. The mathematical ambiguity searching space contains the primary ambiguity sets to be tested. Ideally, it should contain the correct ambiguity set and at the same time, should be as small as possible in order to be computationally efficient. The ambiguity searching space should not be too large, since it will include too many ambiguities to be tested. Too large of searching space burdens the computations and prolongs the time of ambiguity resolution. On the other hand, the space should not be too small since then it might not include the correct ambiguity set. Too small of space will usually lead to failure in ambiguity resolution or at best, will slowdown the resolution of ambiguity. The trade-off between these two parameters should always be exercised in constructing the optimal ambiguity searching space.

With integrated technique, searching for the correct ambiguities is performed in three-dimensional primary searching space, constructed by the ambiguities of the primary satellites related to the first monitor station,  $(\nabla\Delta N_{12}(i), i=1,3)$ . The shape and the size of

the three-dimensional ambiguity searching space could be determined by several ways. The common and indeed the simplest way of constructing it is by using the *cube* centered at certain initial ambiguity estimates. The size of the cube can be arbitrarily determined based on experience or by statistical measures.

Even though it is simple to construct, the cube is not an optimal ambiguity searching space. When its size is arbitrarily set at certain constant parameters, it ignores the spatial and temporal impact of station-satellite relative geometry and correlations between the ambiguities, which theoretically affect the ambiguity searching space. When some statistical measures (usually standard deviations) are used to size the cube, the correlations between the ambiguities are still left out. In the integrated technique, the spatial and temporal impacts of the geometry and mathematical correlations are taken into consideration in constructing the ambiguity searching space, so that it will lead to an ellipsoidal searching space instead of a cube (see Figure 3.4).

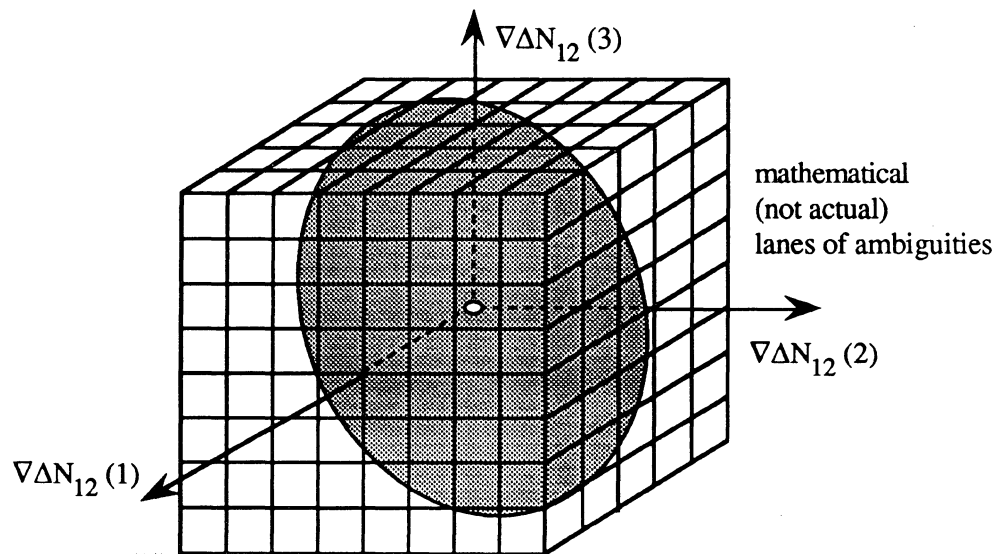


Figure 3.4. Cube and ellipsoidal ambiguity searching space.

### 3.5.1. The ellipsoidal mathematical ambiguity searching space.

In the integrated technique, the ellipsoidal mathematical ambiguity searching space of the primary ambiguities ( $\nabla\Delta N_{12}(i)$ ,  $i=1,3$ ) is centered at the initial ambiguities ( $\nabla\Delta N_{12}^0(i)$ ,  $i=1,3$ ), and it is expressed by the following equation:

$$(\nabla\Delta N_{12} - \nabla\Delta N_{12}^0)^T \cdot C^{-1}(\nabla\Delta N_{12}^0) \cdot (\nabla\Delta N_{12} - \nabla\Delta N_{12}^0) < \chi^2_{3,1-\alpha} \quad , \quad (3.2)$$

where  $C(\nabla\Delta N_{12}^0)$  is the covariance matrix of the initial primary ambiguities and  $\chi^2_{3,1-\alpha}$  is the chi-squares percentile for degrees of freedom 3 and confidence level  $(1-\alpha)$ . The values of  $\chi^2_{3,1-\alpha}$  for some confidence levels are shown in Table 3.1.

Table 3.1. Some values of Chi-squares percentiles,  $\chi^2_{3,1-\alpha}$ .

(1- $\alpha$ )	90.0 %	95.0 %	97.0 %	98.0 %	99.0%	99.5 %	99.9 %
$\chi^2_{3,1-\alpha}$	6.25	7.82	8.95	9.84	11.34	12.84	16.27

When *dual-frequency data* is available and the extrawidelaning technique is used to estimate the initial (wide-lane) ambiguity, the covariance matrix of the initial ambiguities is computed as:

$$C(\nabla\Delta N_{12}^0) = \frac{1}{\lambda^2} \cdot \{ C(\nabla\Delta P_{p12}) + C(\nabla\Delta L_{p12}) \} \quad , \quad (3.3)$$

where  $\nabla\Delta P_{p12}$  and  $\nabla\Delta L_{p12}$  are the smoothed double-difference narrow-lane pseudoranges and the double-difference wide-lane carrier ranges related to the primary satellites and  $\lambda$  is

the wavelength of the wide-lane signal. When a code-derived position is used to determine the initial (wide-lane) ambiguity, this covariance matrix is computed as:

$$C(\nabla\Delta N_{12}^o) = \frac{1}{\lambda^2} \cdot \{ A_p \cdot C(X_c)_n \cdot A_p^T + C(\nabla\Delta L_{p12}) \} \quad , \quad (3.4)$$

where  $A_p$  is the design matrix related to the coordinates parameter involving the primary satellites related to the first monitor station, and  $C(X_c)_n$  is covariance matrix of the position computed based on all double-difference smoothed narrow-lane pseudoranges related to all  $n$  monitor stations. The covariance matrix is computed as follows:

$$C(X_c)_n = \{ D_c^T \cdot C^{-1}(\nabla\Delta P)_n \cdot D_c \}^{-1} \quad , \quad (3.5)$$

where  $D_c$  and  $C(\nabla\Delta P)_n$  are the design matrix and the covariance matrix of the observations related to all satellites and  $n$  monitor stations. The design matrix  $D_c$  , with dimension  $n(ns-1)$  by 3 is formulated as:

$$D_c = \begin{bmatrix} A_c \\ A_c \\ \dots \\ A_c \end{bmatrix} \quad , \quad (3.6)$$

and the covariance matrix  $C(\nabla\Delta P)_n$  with dimension  $n(ns-1)$  by  $n(ns-1)$  is formulated as:

$$C(\nabla\Delta P)_n = \begin{bmatrix} C(\nabla\Delta P_{12}) & \text{COR} & \text{COR} & \text{COR} \\ & C(\nabla\Delta P_{32}) & \text{COR} & \text{COR} \\ & & \dots & \dots \\ \text{symmetric} & & & C(\nabla\Delta P_{n2}) \end{bmatrix} \quad . \quad (3.7)$$

In equation (3.7) above, COR is the mathematical correlation matrix because of the differencing between the observations (see Appendix III for more detailed formulation).

With *codeless* or *single-frequency data*, the construction of ambiguity searching space is determined using code-derived position. Its determination is similar to dual-frequency data as expressed by equations (3.4) and (3.5) except for the types of observation used. With codeless data, smoothed C/A-code pseudorange and semi, half, or double wide-lane phase observations (see Appendix I) are used; and, with single-frequency data, smoothed C/A-code pseudorange and L1 phase observations are used. It should be noted here that, in the case of single frequency data, the smoothing of pseudorange using carrier phase observations (see Appendix II) will be biased by the residual ionospheric refraction in the observations.

In order to be computationally more efficient, the selection of the primary ambiguities ( $\nabla\Delta N_{12}(i)$ ,  $i=1,3$ ) which satisfy equation (3.4), is done in a few consecutive steps which can be depicted in the two-dimensional perspective in Figure 3.5.

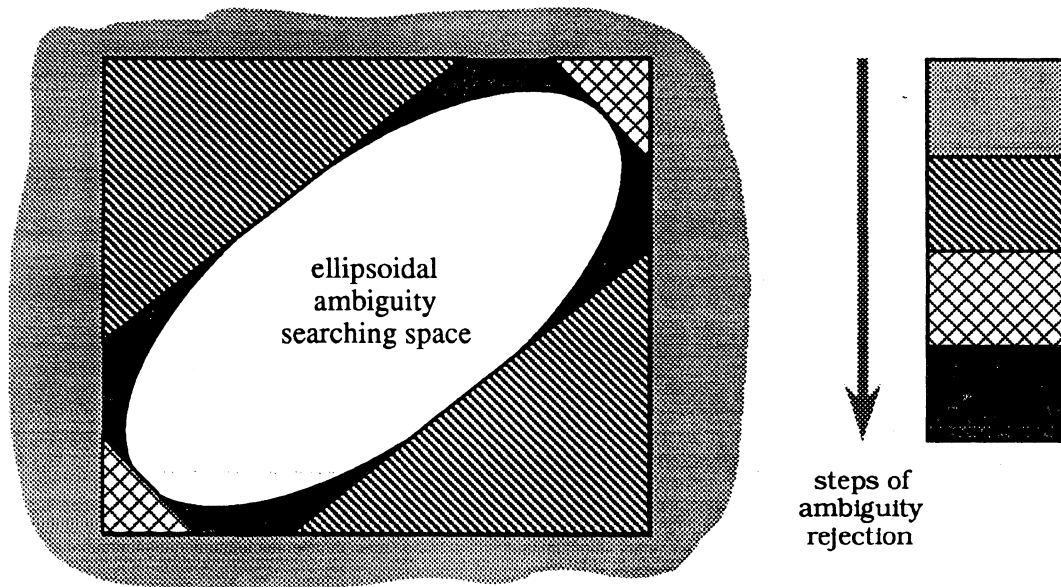


Figure 3.5. Two dimensional perspective of constructions steps of the ellipsoidal ambiguity searching space.

The *first step* of selection is done by constructing the cube around the initial ambiguity estimates using the following formula :

$$\begin{aligned}
 \text{1st step : } \quad & | \nabla \Delta N_{12}(i) - \nabla \Delta N_{12}^o(i) | \leq d \nabla \Delta N_{12}(i) , \quad \text{for } (i=1,3) \\
 & d \nabla \Delta N_{12}(i) = \mathcal{R}(0,1)_{1-\alpha/2} \cdot \sigma(\nabla \Delta N_{12}^o(i)) ,
 \end{aligned}
 \tag{3.8}$$

where  $\mathcal{R}(0,1)_{1-\alpha/2}$  is the standardized gaussian (normal) percentiles with confidence level  $(1-\alpha)$  and  $\sigma(\cdot)$  denotes the standard deviation of  $(\cdot)$  . The confidence level in this case should be chosen so that the whole ellipsoidal searching space is completely inside the cube. Table 3.2 shows the values of  $\mathcal{R}(0,1)_{1-\alpha/2}$  for some confidence levels  $(1-\alpha)$ .

Table 3.2. Some values of Normal percentiles,  $\mathcal{R}(0,1)_{1-\alpha/2}$ .

$(1-\alpha)$	90.0 %	95.0 %	97.0 %	98.0 %	99.0%	99.5 %	99.9 %
$\mathcal{R}(0,1)$	1.65	1.96	2.17	2.33	2.58	2.81	3.03

In order to formulate the next steps of the ambiguity selection, the quadratic form of the ambiguities in the left hand side of the inequality expressed by equation (3.2) should be reformulated to have a more explicit ellipsoid equation. This is done by decomposing  $C(\nabla \Delta N_{12}^o)$  based on the *spectral decomposition* theorem [Strang, 1980] as:

$$C(\nabla \Delta N_{12}^o) = E \cdot \Lambda \cdot E^T , \tag{3.9}$$

and rotating the vector  $(\nabla \Delta N_{12} - \nabla \Delta N_{12}^o)$  into vector  $Y (y_1, y_2, y_3)$  as:

$$Y = E^T \cdot (\nabla \Delta N_{12} - \nabla \Delta N_{12}^o) . \tag{3.10}$$



In these equations, E is a 3 by 3 orthogonal matrix in which its columns are the normalized eigenvectors ( $e_1, e_2, e_3$ ) of  $C(\nabla\Delta N_{12}^o)$  and  $\Lambda$  is a 3 by 3 diagonal matrix with the eigenvalues of  $C(\nabla\Delta N_{12}^o)$ , i.e., ( $\kappa_1, \kappa_2, \kappa_3$ ), as the diagonal elements. Mathematically, it can be written as :

$$\begin{aligned} E &= [ e_1 \quad e_2 \quad e_3 ] , \\ \Lambda &= \text{diag. } [ \kappa_1 , \kappa_2 , \kappa_3 ] . \end{aligned} \quad (3.11)$$

If the above equations are substituted into equation (3.4), then equation (3.4) can be expressed as:

$$\frac{y_1^2}{\kappa_1} + \frac{y_2^2}{\kappa_2} + \frac{y_3^2}{\kappa_3} < \chi^2_{3,1-\alpha} . \quad (3.12)$$

This equation represents the ellipsoid depicted in Figure 3.6. Using equation (3.12), the next steps of the ambiguity selection are performed by testing the ambiguities inside the cube defined by equation (3.8) with the following relations:

$$\text{2nd step :} \quad e_1^T \cdot (\nabla\Delta N_{12} - \nabla\Delta N_{12}^o) < \sqrt{(\chi^2_{3,1-\alpha} \cdot \kappa_1)} , \quad (3.13)$$

$$\text{3rd step :} \quad e_2^T \cdot (\nabla\Delta N_{12} - \nabla\Delta N_{12}^o) < \sqrt{(\chi^2_{3,1-\alpha} \cdot \kappa_2)} , \quad (3.14)$$

$$\text{4th step :} \quad e_3^T \cdot (\nabla\Delta N_{12} - \nabla\Delta N_{12}^o) < \sqrt{(\chi^2_{3,1-\alpha} \cdot \kappa_3)} . \quad (3.15)$$

Finally, the next step is to apply equation (3.12). In the above equations the operator ( $\cdot$ ) denotes the dot product between two vectors.

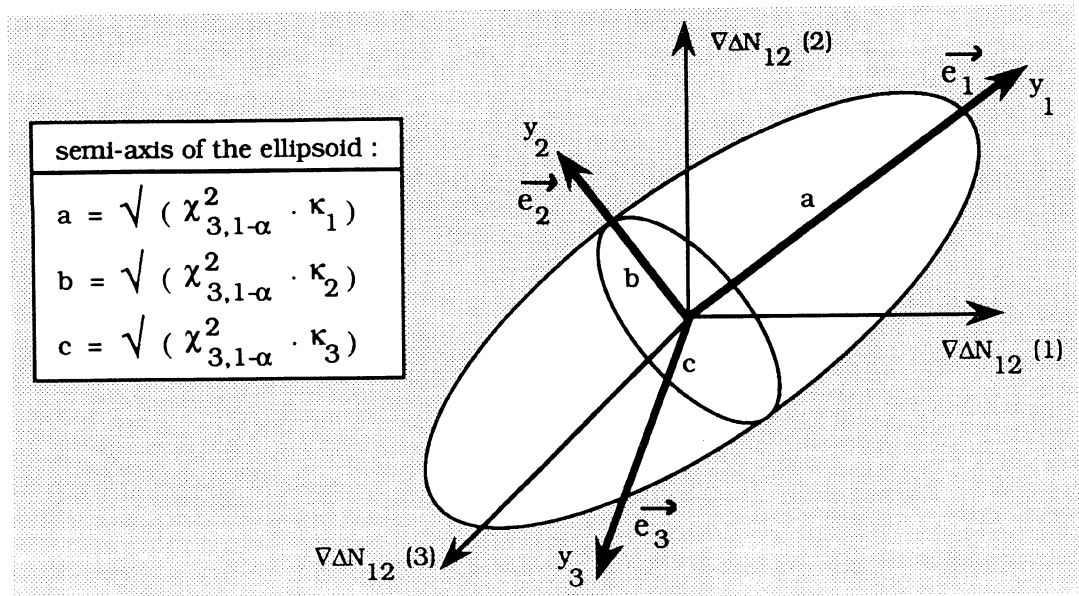


Figure 3.6. Ellipsoidal mathematical ambiguity searching space

It should be mentioned here that equation (3.2) is used to define the mathematical searching space at the initial epoch and at the re-initialization epochs, i.e., the epochs where their previous epochs reject all the potential ambiguity sets or the epoch after cycle slip occurrences. Other than these two epochs, the ambiguity searching space is constructed by the potential ambiguities which pass the identification process at the previous epoch and, at the same time, satisfy equation (3.2) for that epoch. In this latter case, the searching space will not have a particular geometric shape. In 2-D perspective, this approach of constructing the searching space can be depicted in Figure 3.7.

With dual-frequency data, besides these ambiguity sets, the ambiguity set determined using the extrawidelaning technique at the corresponding epoch, is always included and considered in the identification process of the correct ambiguity set.

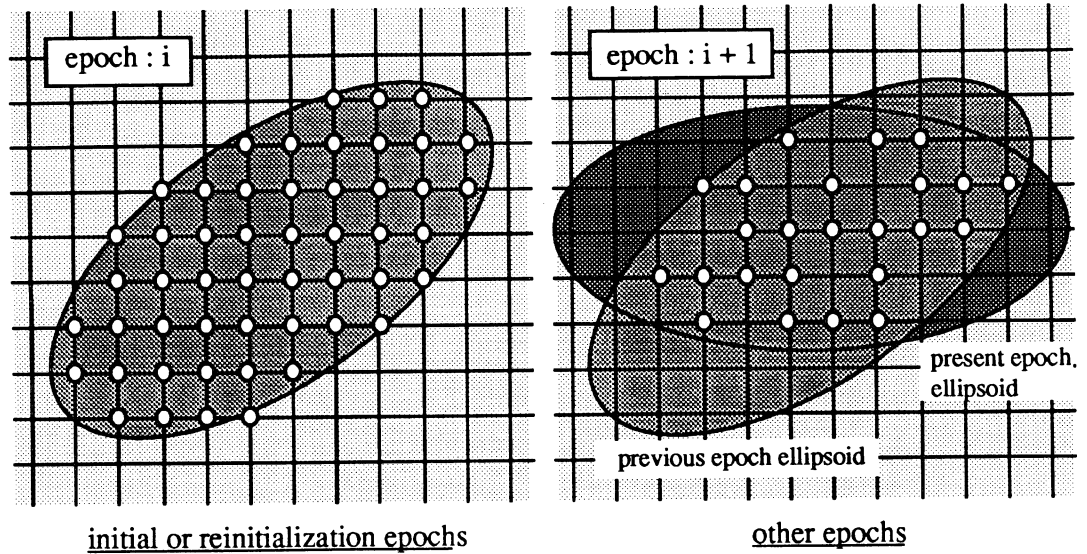


Figure 3.7. Two-dimensional perspective of constructing the mathematical searching spaces at various epochs.

### 3.5.2. The number of initial ambiguity sets

The number of the initial primary ambiguity sets inside the mathematical ellipsoidal ambiguity searching space will affect both the computation and observation times of on-the-fly ambiguity resolution. As stated before, for fast and reliable ambiguity resolution, the number of ambiguity sets should not be too few or too many. The optimal number of the ambiguity sets corresponds to the fastest and most reliable ambiguity resolution. This optimal number of sets, however, is difficult to know beforehand, since it depends on several factors such as the data characteristics, satellite geometry, and the processing options used for ambiguity resolution.

In the case of *mathematical searching space*, since the surfaces of ambiguities are regularly spaced, the number of ambiguity sets will be determined by the size, shape, and orientation of the ellipsoidal searching space. These parameters of the ellipsoid itself depend on several

factors, such as signal wavelength, satellite geometry, the number of secondary monitor stations, and the confidence level used in sizing the ellipsoid. In the case of *physical searching space*, however, besides the size, shape, and orientation of the ellipsoid, the pattern and spacing of the surfaces of ambiguities also play important roles, as indicated in Figure 3.8. It is important to note here that the number of primary ambiguity sets in the mathematical searching space is equal to the number of potential positions related to these primary ambiguity sets in the physical searching space. The sizes, shapes, and orientations of the two ellipsoids, however, will be different in general.

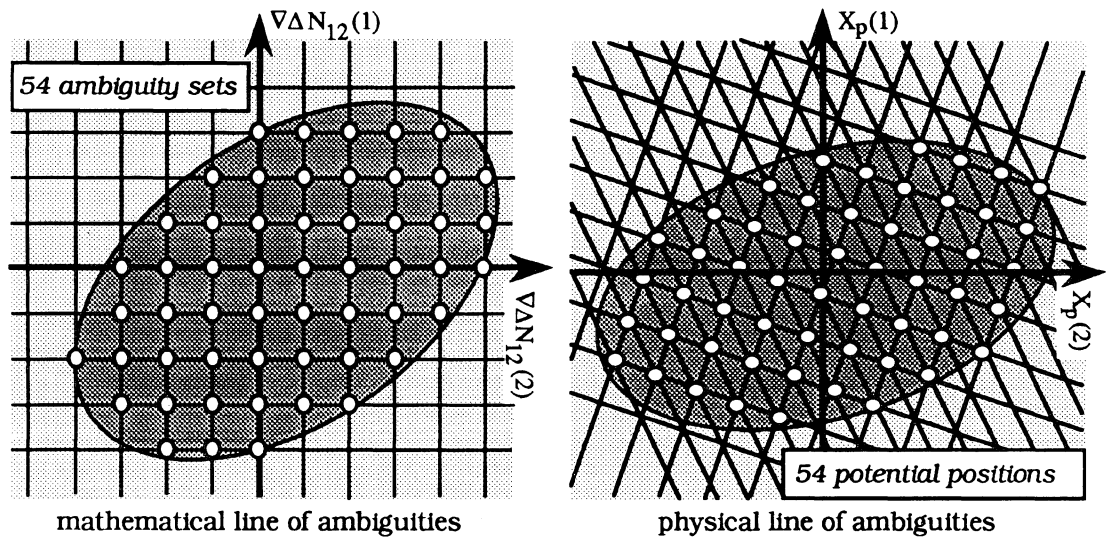


Figure 3.8. The number of initial primary ambiguity sets in the mathematical and physical searching spaces.

The number of ambiguity sets inside the initial searching space can be predicted beforehand using the indicators, which are called the *Number of Ambiguity Indicator* (NAI). The volume of the ellipsoid is used to establish the first indicator related to the size of the ellipsoid at certain confidence level  $(1-\alpha)$ . In the mathematical searching space, the volume of ellipsoid can be expressed as:

$$\text{Volume} = \frac{4}{3} \cdot \pi \cdot (\chi^2_{3,1-\alpha})^{3/2} \cdot \sqrt{\kappa_1 \cdot \kappa_2 \cdot \kappa_3} , \quad (3.16)$$

where  $\kappa_1, \kappa_2$ , and  $\kappa_3$  are the eigenvalues of the covariance matrix  $C(\nabla \Delta N_{12}^o)$ , arranged from the largest to smallest. Since the multiplication product of the eigenvalues is equal to the determinant of the matrix, equation (3.16) can be rewritten as follows:

$$\text{Volume} = \frac{4}{3} \cdot \pi \cdot (\chi^2_{3,1-\alpha})^{3/2} \cdot \sqrt{\det.\{ C(\nabla \Delta N_{12}^o) \}} . \quad (3.17)$$

Based on the above equation, the first *number of ambiguity indicator* (NAI1) is defined as:

$$\text{NAI1} = \sqrt{\det.\{ C(\nabla \Delta N_{12}^o) \}} , \quad (3.18)$$

with the *unit variances* of observations used to construct the covariance matrix. In this case, the larger the value of NAI1, the more ambiguity sets can be expected inside the searching space. NAI1 is the primary indicator that will be used in this investigation.

Depending on their shapes, the same volume of ellipsoids may lead to a different number of ambiguity sets. Therefore the second number of ambiguity indicator (NAI2) is introduced to confront this situation. NAI2 indicates the elongation of the ellipsoid and it is defined as follows:

$$\text{NAI2} = \sqrt{\kappa_{\max} / \kappa_{\min}} = \sqrt{\kappa_1 / \kappa_3} . \quad (3.19)$$

In this case, the larger the value of NAI2 the more elongated the ellipsoid will be. Depending on the orientation, size of ellipsoid, and length of the medium axis, larger NAI2 could either mean the smaller or larger number of ambiguity sets. In general, however, it can be expected that the largest value of NAI2 will correspond to a relatively small number of ambiguity sets. The orientation of the ellipsoid will also affect the number of ambiguity sets. For prediction purposes, however, the NAI1 and NAI2 values are sufficient to indicate the relative number of initial ambiguity sets inside the searching space as a function of its affecting factors. Therefore, the indicator related to the orientation of the ellipsoid is not used in this case.

It should be noted also that in the case of physical searching space, two main indicators can also be used to indicate the number of potential positions, i.e., the number of primary ambiguities inside the searching space. The first one characterizes the volume of the ellipsoid as defined by equation (3.18) with the different in the covariance matrix used. The second one is the position dilution of precision, PDOP [Wells et al., 1986]. The PDOP value indicates the spread of the potential positions. The larger the value of PDOP, the larger the separations of potential positions and the smaller the number of ambiguity sets there will be inside the searching space.

### **3.6. Identification of the correct ambiguities**

After constructing the ambiguity searching space, the next step is to try to identify the correct ambiguities from the given primary integer ambiguity sets inside the searching space. Some validation and rejection criteria are employed, which are based on the synergism of the identification and estimation processes indicated in Figure 3.1. The estimation process is based on the unweighted and weighted parametric least squares adjustment [Vanicek & Krakiwsky, 1986] (see Figure 3.9).

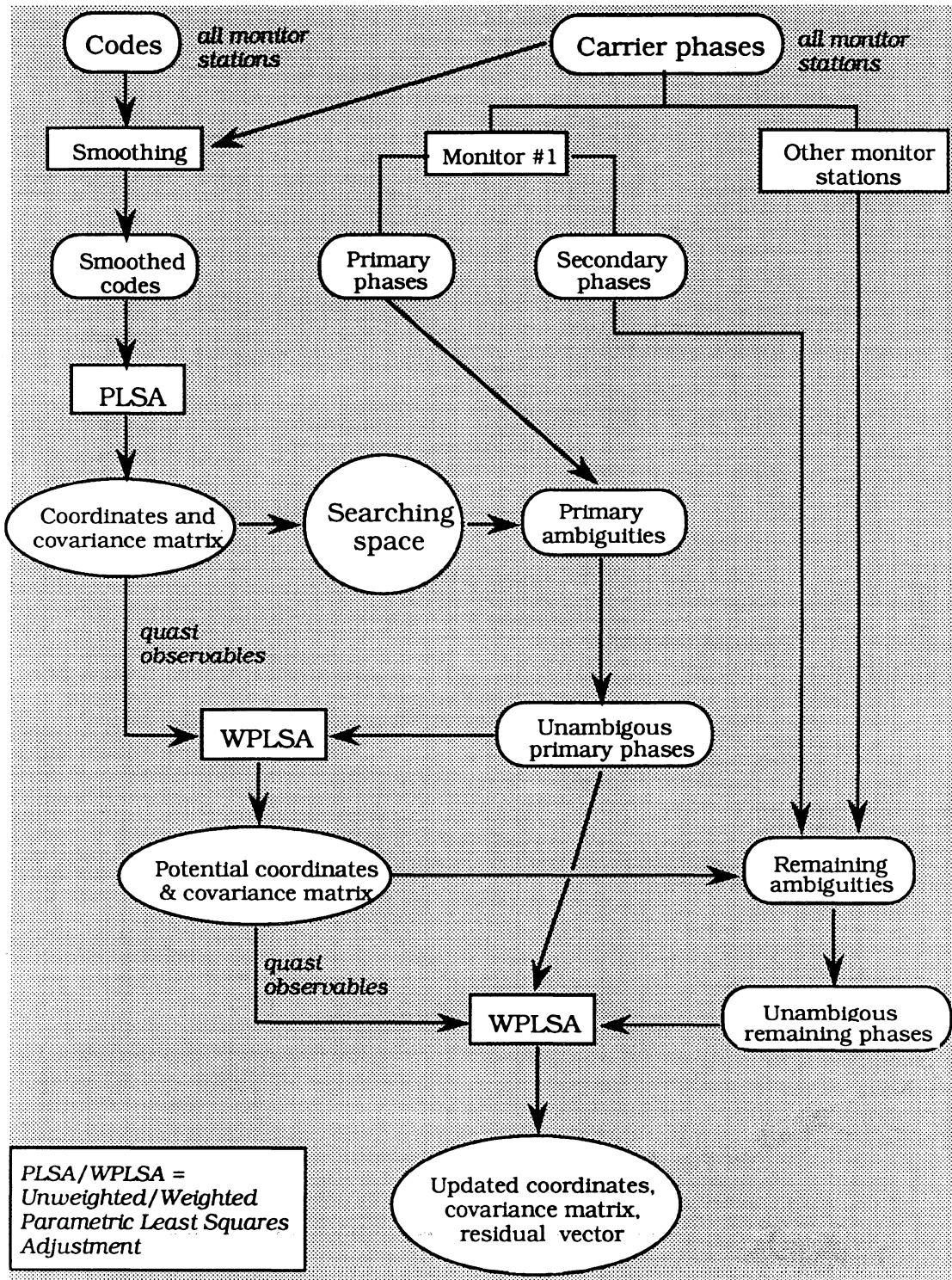


Figure 3.9. The flow of the estimation process at a certain epoch.

The identification process assumes that the phase observations with the correct integer ambiguities should satisfy certain mathematical and statistical criteria when they are used in the position estimation process. Phase observations should yield the 'acceptable' properties of position estimates, corresponding misclosures, and residuals. These expected theoretical properties can then be used for validating or otherwise rejecting the ambiguity sets being tested, i.e., used to formulate the rejection and validation criteria.

In this identification process, searching for the correct integer ambiguities is done on three double-difference ambiguities of primary satellites related to a certain pair of monitor stations and a moving receiver. The other (secondary) ambiguities related to the other (secondary) satellites and monitor stations are mathematically dependent on these three primary ambiguities. Every three-ambiguity set is tested individually. At each epoch, only the ambiguity sets who pass all the validation and rejection criteria are saved and considered for the next epoch testing. Moreover, one ambiguity set will be considered as the correct ambiguity if it also fulfills some assurance criteria. As has been stated before, when the ambiguity searching and fixing needs more than one epoch, the number of ambiguity sets tested at the second and subsequent epochs is equal to the number of potentially correct ambiguity sets which passed all rejection criteria at previous epochs, and are present inside the ellipsoidal searching space of that particular epoch. The ambiguity searching space has to be reinitialized, however, whenever cycle slips occur or whenever the previous epoch rejects all potential ambiguity sets. With dual-frequency data, the ambiguity set determined using extrawidelaning technique is always included and considered for testing at each epoch .

There are eight validation and rejection criteria used by the integrated technique. These criteria are sequenced according to the flow of the estimation process (see Figure 3.9) in order to reject the potentially incorrect integer of ambiguities as soon as possible, which



then will minimize the computation times and usually lead to faster ambiguity resolution. In the following, all of the validation and rejection criteria used in the identification process is explained in more detail. General terms of code and phase observations are used and should be read as smoothed narrow-lane pseudoranges and wide-lane carrier phases in the case of dual-frequency data; smoothed L1-C/A code pseudoranges and semi, half, or double wide-lane carrier phases in the case of codeless data; and smoothed L1-C/A code pseudoranges and L1 - carrier phases in the case of single-frequency data.

### 3.6.1. Compatibility test between the potential coordinates and the code derived coordinates

The potential (trial) position is computed using the primary phase observations, taking into account the primary ambiguities being tested. If the primary ambiguities used are correct, then the corresponding estimated position should differ with the code-derived position in a statistically predictable manner. The coordinates differences in this case will be caused by the differences in precision between the code and phase observations, coupled with the effect of the satellite geometry.

Mathematically speaking, these expected differences in coordinates, which are used as the first validation and rejection criteria, is formulated as follows :

$$\begin{aligned} \delta_{xpc(i)} &= X_p(i) - X_c(i) , \\ |\delta_{xpc(i)}| &< \mathcal{R}(0,1)_{1-\alpha/2} \cdot \sigma_{\delta_{xpc(i)}} , \quad i = 1,3 , \end{aligned} \quad (3.20)$$

where  $X_p$  is the potential position computed using the primary phase observations with the primary ambiguities being tested ( $\nabla\Delta N_{12}(i)$ ,  $i = 1,3$ ) and  $X_c$  is the position computed

using all double-difference smoothed pseudoranges related to all monitor stations. In computing the potential position  $X_p$ , the coordinates  $X_c$  are considered as quasi-observables.  $\sigma_{\delta x_{pc}(i)}$  is the standard deviation of  $\delta x_{pc}(i)$ .  $\mathcal{R}(0,1)_{1-\alpha/2}$  is the standardized gaussian (normal) percentiles with confidence level  $(1-\alpha)$ .

Geometrically speaking, the acceptance volume of the criteria as expressed by equation (3.20) is the cube centered at the code-derived position. Its two-dimensional depiction in physical searching space is shown in Figure 3.10. To be computationally more efficient, the ellipsoidal acceptance volume which is mathematically more rigorous but computationally more time consuming, is not used in this case, since at the very beginning of the identification process the number of the ambiguity sets to be tested is usually the largest.

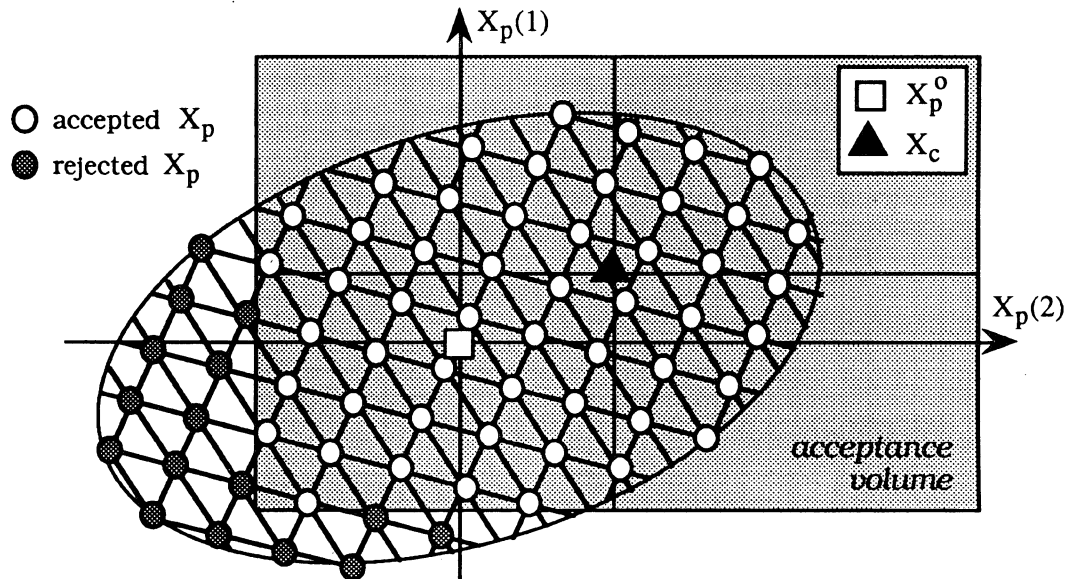


Figure 3.10. Two-dimensional geometrical interpretation of the first criteria.

Using this rejection and validation criteria, the size of the cube shown in Figure 3.10 is determined not only by the assigned confidence level, but also by the satellite geometry and the values assigned to represent the precision of the observations. In this step of

identification, the primary ambiguities related to the potential position which do not satisfy the above criteria will not be passed to the next step of identification. Therefore all integer ambiguity sets with this primary ambiguity set will automatically also be rejected.

In equation (3.20), the potential position vector  $X_p$  is computed as:

$$X_p = X_p^0 + \lambda \cdot GP \cdot (\nabla\Delta N_{12} - \nabla\Delta N_{12}^0) . \quad (3.21)$$

In the above equation,  $X_p^0$  is the initial potential position computed using the initial primary ambiguities  $\nabla\Delta N_{12}^0$ , based on the following weighted least squares adjustment formulae:

$$X_p^0 = X_c + GP \cdot \omega_p . \quad (3.22)$$

By substituting equation (3.22) to equation (3.21), the vector of coordinate differences,  $\delta x_{pc}$ , in equation (3.20) can be formulated as:

$$\delta x_{pc} = GP \cdot \{ \omega_p + \lambda \cdot (\nabla\Delta N_{12} - \nabla\Delta N_{12}^0) \} . \quad (3.23)$$

In equations (3.21) - (3.23) above, the gain matrix  $GP$  and the misclosure vector  $\omega_p$  related to the primary satellites are formulated as:

$$GP = \{ A_p^T \cdot C^{-1}(\nabla\Delta L_{p12}) \cdot A_p + C^{-1}(X_c)_n \}^{-1} \cdot A_p^T \cdot C^{-1}(\nabla\Delta L_{p12}) , \quad (3.24)$$

$$\omega_p = A_p \cdot X_c - \nabla\Delta L_{p12} . \quad (3.25)$$

In the above equations,  $\nabla\Delta L_{p12}$  is the phase observation vector (in ranges units) related to first monitor station and the primary satellites.

The standard deviations of coordinate differences,  $\sigma_{\delta x_{pc(i)}}$  in equation (3.20) are computed based on covariance matrix of position difference  $C(\delta x_{pc})_n$ . The covariance matrix can be computed using the following relation :

$$C(\delta x_{pc})_n = GP \cdot C(\omega_p) \cdot GP^T \quad , \quad (3.26)$$

where  $C(\omega_p)$  is the covariance matrix of misclosure vector and be formulated as:

$$C(\omega_p) = A_p \cdot C(X_c)_n \cdot A_p^T + C(\nabla\Delta L_{p12}) \quad . \quad (3.27)$$

If the following matrix lemma for arbitrary matrix A and positive definite matrices B and C [Vanicek & Krakiwsky, 1986]:

$$(C^{-1} + A^T B^{-1} A)^{-1} A^T B^{-1} = CA^T (B + ACA^T)^{-1} \quad , \quad (3.28)$$

is applied to equation (3.24) and the new formulation of  $GP_n$  is substituted into equation (3.26), the covariance matrix  $C(\delta x_{pc})_n$  can also be formulated as follows:

$$C(\delta x_{pc})_n = GP \cdot A_p \cdot C(X_c)_n \quad . \quad (3.29)$$

The above equation is computationally more efficient to than equation (3.26) and it is therefore used in executing this rejection and validation criteria. Notably, the gain matrix GP at a certain epoch is the same for all primary ambiguity sets being tested, and therefore

should be computed only once outside the computational searching loop in order to save the computation time.

### 3.6.2. Test on L1-norm of the misclosure vector

The next validation and rejection criteria to further identify the correct integer ambiguities is the test on L1-norm of the misclosure vector of all double-difference carrier phase observations related to all monitor stations and satellites. Since the correct primary ambiguities should correspond to the correct secondary ambiguities, assuming that there are no significant residual errors and biases in the observations, then the L1-norm of the misclosure vector related to all phase observations should be relatively small, and its magnitude will be primarily governed by the noise and remaining errors and biases in the observations. In this case, the test on L1-norm of the misclosure vector is:

$$\| \omega_{c,n} \|_1 < \text{constant} \cdot \lambda \cdot [ n(ns-1)-3 ] , \quad (3.30)$$

where  $\| \omega_{c,n} \|_1$  is the L1-norm of the misclosure vector  $\omega_{c,n}$ , constant is a fraction of wavelength, and n and ns represent the number of monitor stations and satellites, respectively. The L1-norm of this misclosure vector is formulated as:

$$\| \omega_{c,n} \|_1 = \sum_{i=4}^{ns-1} | \omega_{12}(i) | + \sum_{i=1}^{ns-1} | \omega_{32}(i) | + \dots + \sum_{i=1}^{ns-1} | \omega_{n2}(i) | , \quad (3.31)$$

where  $\omega_{12}$ ,  $\omega_{32}$ , ..., and  $\omega_{n2}$  are the misclosure vectors related to each monitor station, respectively. These misclosure vectors are computed using the following vector relations :

$$\omega_{k2} = \nabla\Delta L_{k2} + \lambda \cdot \nabla\Delta N_{k2} - \nabla\Delta\rho_{k2}, \quad \{k = 1,3,4, \dots, n\}. \quad (3.32)$$

In the above equation,  $\nabla\Delta L_{k2}$  denotes the phase observation vectors (in ranges units) related to all satellites and monitor station  $k$  ( $k = 1,3,\dots,n$ ). The double difference geometric range vectors  $\nabla\Delta\rho_{k2}$  are computed using the potential position  $X_p$ , and the ambiguity vectors  $\nabla\Delta N_{k2}$  are computed using an equation similar to equation (3.1). The geometrical interpretation of this second rejection and validation criteria in two-dimensional physical searching space is shown in Figure 3.11.

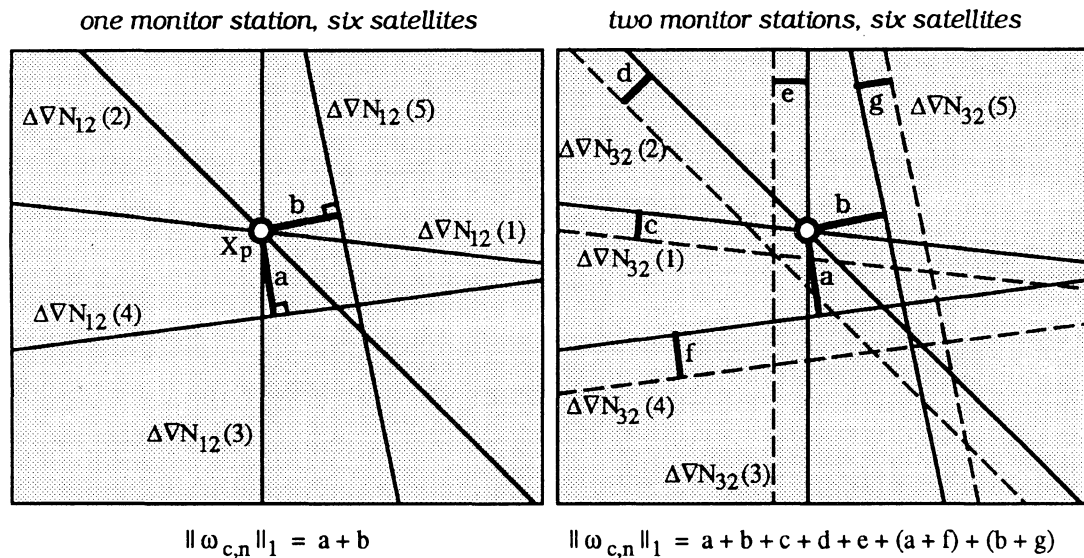


Figure 3.11. Two-dimensional geometrical interpretation of the second criteria.

From Figure 3.11 and equation (3.31), it can be realized that, with the increase in the number of monitor stations, the L1-norm of the misclosure vectors related to incorrect ambiguities can be expected to be larger and, theoretically speaking, should be easier to detect and reject. Finally, it should be noted that the value of constant variable in equation (3.30) should be set by considering the expected level of the noise and the remaining errors and biases in observations, signal wavelength, and the number of satellites and monitor stations.

### 3.6.3. Compatibility test between the updated coordinates and potential coordinates.

The potential position which passes the previous two validation and rejection criteria is then considered as the quasi-observables in the position estimation process, and, along with all 'unambiguous' phase observations from all satellites and all monitor stations, is used to estimate the so-called updated position. If the potential position corresponds to the correct primary ambiguities, then corresponding secondary ambiguities can also be expected to be correct. In this case, then the updated position should be theoretically more accurate than the potential position, and their coordinate differences should be mathematically predictable. The validation and rejection criteria therefore can be established based on this rationale.

Similar to the first criteria, the criteria to test the compatibility between the updated and the potential coordinates is formulated as follows:

$$\begin{aligned} \delta x_{up}(i) &= X_u(i) - X_p(i) , \\ |\delta x_{up}(i)| &< \mathcal{R}(0,1)_{1-\alpha/2} \cdot \sigma_{\delta x_{up}(i)} , \quad i = 1,3 \quad . \end{aligned} \quad (3.33)$$

In the above equation, the updated position,  $X_u$ , is computed by updating the potential solution,  $X_p$ , using the 'unambiguous' secondary carrier phase observations from all monitor stations. As with the first criteria, the acceptance volume of this criteria as expressed by the above equation is a cube centered at each potential position. Its geometrical interpretation is depicted in two-dimensional fashion in Figure 3.12.

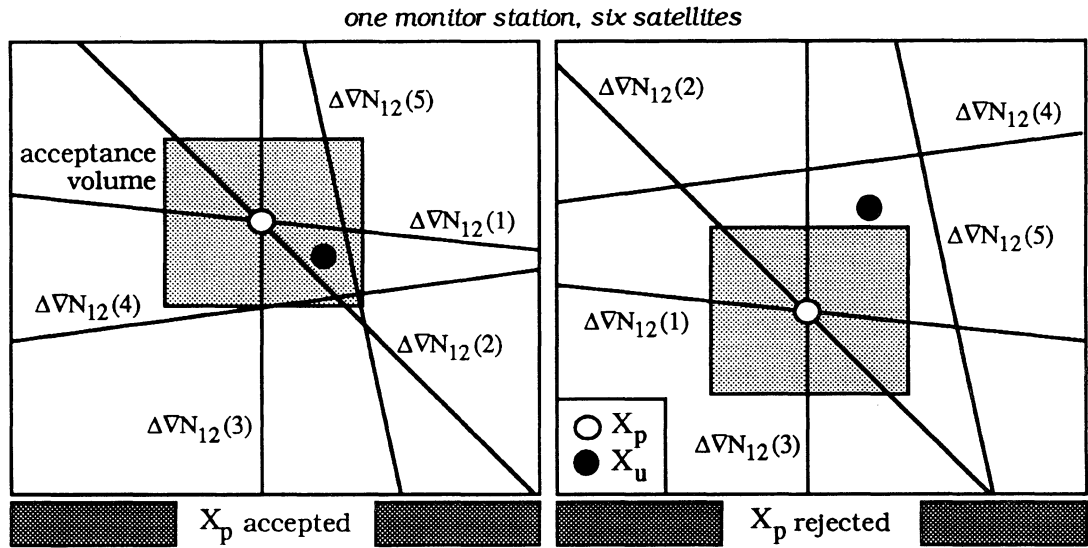


Figure 3.12. Two-dimensional geometrical interpretation of the third criteria.

In equation (3.33), the updated position is computed using the following formulae :

$$X_u = X_p + GC_n \cdot \omega_{c,n} \quad (3.34)$$

In the above equation,  $GC_n$  is the gain matrix related to all monitor stations and all satellites, and  $\omega_{c,n}$  is the corresponding misclosure vector computed by basing on equation (3.32). The matrix  $GC_n$  and vector  $\omega_{c,n}$  are formulated as follows:

$$GC_n = \{ D_c^T \cdot C^{-1}(\nabla \Delta L)_n \cdot D_c + C(X_p) \}^{-1} \cdot D_c^T \cdot C^{-1}(\nabla \Delta L)_n, \quad (3.35)$$

$$\omega_{c,n} = \left[ \omega_{12}^T, \omega_{32}^T, \dots, \omega_{n2}^T \right]^T \quad (3.36)$$

In equation (3.35),  $D_c$  is the design matrix of the observations expressed by equation (3.6),  $C(\nabla \Delta L)_n$  is covariance matrix of the phase observations, and  $C(X_p)$  is covariance matrix



of the potential position. The covariance matrix of the phase observations,  $C(\nabla\Delta L)_n$ , will have the same structure as equation (3.7) with the only difference that equation (3.7) represents code observations. The covariance matrix of the potential position  $C(X_p)$  is computed using the following formulae:

$$C(X_p) = \{ A_p^T \cdot C^{-1}(\nabla\Delta L_{p12}) \cdot A_p + C^{-1}(X_c)_n \}^{-1} \quad , \quad (3.37)$$

and the covariance matrix  $C(X_c)_n$  is expressed by equation (3.5).

The standard deviations ( $\sigma_{\delta x_{up}(i)}$ ,  $i=1,3$ ) are computed from the covariance matrix of position difference  $C(\delta x_{up})_n$ . This covariance matrix is computed as follows:

$$C(\delta x_{up})_n = GC_n \cdot D_c \cdot C(X_p)_n \quad . \quad (3.38)$$

The gain matrix  $GC_n$  at a certain epoch is the same for all primary ambiguity sets being tested, and therefore, to be computationally efficient, should be computed only once outside the computational searching loop.

#### 3.6.4. Test on L1-norm of the residual vector.

The next step in identifying the correct integer ambiguities is to examine the L1-norm of the residual vector obtained from the updated position estimation process. In this case only the residual related to the real observations, i.e., the phase observations, is considered. The quasi-residual related to the quasi-observations (i.e. the potential position) has been partly considered in the previous rejection and validation criteria, and also will be considered in the next criteria. In case the correct integer ambiguities are used in the estimation, then

assuming there are no significant errors and biases in the observations, the resulting residual should be relatively small. Therefore similar to the misclosure vector, the validation and rejection criteria can be established by assuming that the L1-norm of the residual vector related to the potentially correct integer ambiguities should vary only in a certain expected interval. It is formulated as:

$$\| \mathbf{v}_n \|_1 < \text{constant} \cdot \lambda \cdot n(ns-1) \quad , \quad (3.39)$$

where  $\| \mathbf{v}_n \|_1$  is the L1-norm of the residual vector  $\mathbf{v}_n$ , constant is a fraction of wavelength, and n and ns is the number of monitor stations and satellites, respectively. In the case of n monitor stations, the residual vector  $\mathbf{v}_n$  is computed as follows:

$$\mathbf{v}_n = D_c \cdot \delta x_{up} - \omega_{c,n} \quad . \quad (3.40)$$

If equations (3.6) and (3.36) are substituted to the above equation, then the residual vector with dimension  $n(ns-1)$  can be expressed :

$$\mathbf{v}_n = \begin{bmatrix} v_{12} \\ v_{32} \\ \dots \\ v_{n2} \end{bmatrix} = \begin{bmatrix} \nabla \Delta \rho_{12} + A_c \cdot \delta x_{up} - \nabla \Delta L_{12} - \lambda \cdot \nabla \Delta N_{12} \\ \nabla \Delta \rho_{32} + A_c \cdot \delta x_{up} - \nabla \Delta L_{32} - \lambda \cdot \nabla \Delta N_{32} \\ \dots \\ \nabla \Delta \rho_{n2} + A_c \cdot \delta x_{up} - \nabla \Delta L_{n2} - \lambda \cdot \nabla \Delta N_{n2} \end{bmatrix} \quad . \quad (3.41)$$

where  $v_{12}$ ,  $v_{32}$ , ..., and  $v_{n2}$  are the residual vectors related to each monitor station, respectively. The L1-norm of the residual can then be formulated as follows:

$$\| \mathbf{v}_n \|_1 = \sum_{i=1}^{ns-1} |v_{12}(i)| + \sum_{i=1}^{ns-1} |v_{32}(i)| + \dots + \sum_{i=1}^{ns-1} |v_{n2}(i)| \quad . \quad (3.42)$$

The geometrical interpretation of this criteria is depicted in Figure 3.13 in two-dimensional physical searching space. It is quite similar with geometrical interpretation of the test on L1-norm of the misclosure vectors shown in Figure 3.11. The main difference is in the use of updated position  $X_u$  instead of the potential position  $X_p$  in evaluating the parameters. Figure 3.13 indicates that the L1-norm of the residual vectors related to incorrect ambiguities can be expected to be larger with an increase in the number of monitor stations and, theoretically speaking, should be easier to be detected and rejected. The value of the constant parameter in equation (3.39) should be set by always considering the expected remaining observation errors and biases, the signal wavelength, and the satellite geometry.

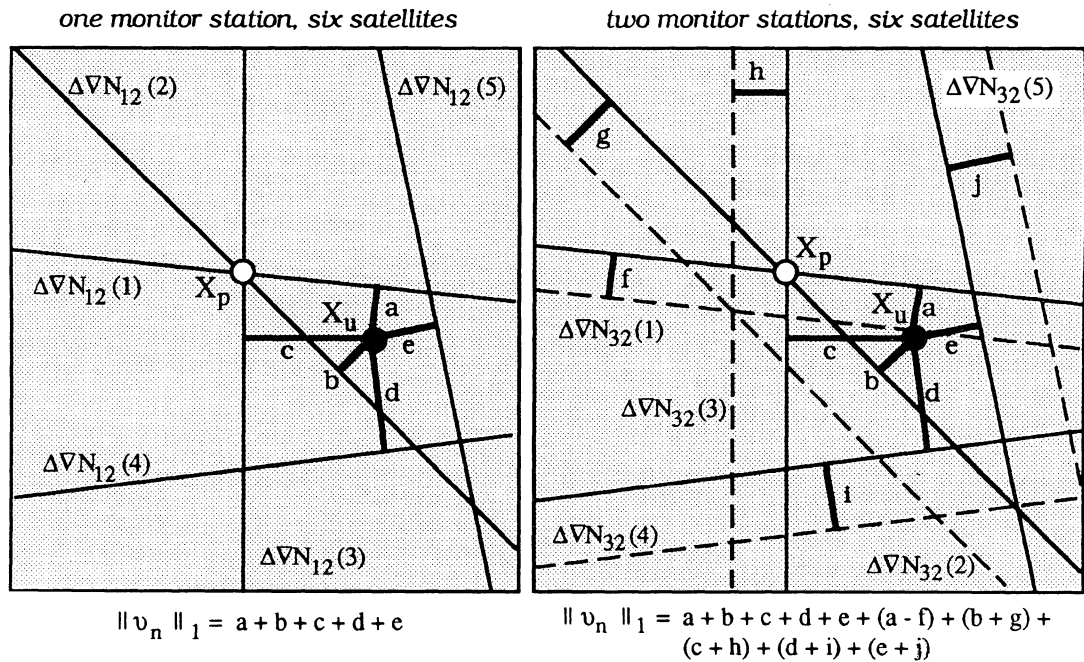


Figure 3.13. Two-dimensional geometrical interpretation of the fourth criteria.

### 3.6.5. Test on the quadratic form of the residuals.

The next properties of the residual vector that can be used to validate or reject the integer ambiguities are its quadratic form since, in the context of the least-squares adjustment, it is the quantity which is to be minimized by the adjustment process. This quadratic form is

formulated in this case of weighted parametric least-squares adjustment by taking into account both the actual residual related to the phase observations and the quasi-residuals related to the quasi-observations, i.e., the potential position. It is expressed as follows :

$$QF(v) = v_n^T \cdot C^{-1}(\nabla \Delta L)_n \cdot v_n + \delta x_{up}^T \cdot C^{-1}(X_p)_n \cdot \delta x_{up} \quad , \quad (3.43)$$

where  $QF(v)$  denotes the quadratic form of the residuals. In this case, the value of the quadratic form can be expected to increase with increases in the number of satellites and/or the monitor stations. The values assigned to describe the observation precision will also affect the value of the quadratic form. This criteria is applied only to the residual vector which pass the previous L1-norm test defined by equation (3.39).

The higher cost of computation time is the main reason that the quadratic form of the residuals is used after the L1-norm as the criteria. If the correct integer ambiguities are involved and assuming that only the random errors are present in the observations, then the values of the quadratic form of the residuals should be statistically predictable and smaller than a certain parameter. These expected values are used as one of the criteria for validating or rejecting the integer ambiguities. One-sided statistical testing is applied in this case, and it is formulated as follows :

$$QF(v) < \chi^2_{n(ns-1),1-\alpha} \quad , \quad (3.44)$$

where  $\chi^2_{n(ns-1),1-\alpha}$  is the chi-squares percentile for degrees of freedom  $n(ns-1)$  and confidence level  $(1-\alpha)$ . The values of  $\chi^2_{n(ns-1),1-\alpha}$  will increase with the increases in the number of satellites and/or the monitor stations, and so does the acceptance volume of the

criteria. Note from equation (3.43) and (3.44) that, geometrically speaking, the acceptance volume of this criteria is a hyper ellipsoid with dimension  $n(ns-1)+3$ .

### 3.6.6. Individual ambiguity mapping function test.

After the previous two criteria, the finer examination of the residual of the phase observations can still be beneficial in trying to identify the correct integer ambiguities. One avenue to do this is by using the concept of ambiguity mapping function, as explained in Chapter 2. The first property of the ambiguity mapping function that will be used in this sixth step of ambiguity validation and rejection is the value of the real term of the individual ambiguity mapping function (see equation 2.6). This criteria is applied to test agreement between the individual double-difference phase observation with its corresponding computed theoretical value based on the updated position. In the case of  $n$  monitor stations, it is formulated as follows:

$$\left\{ \begin{array}{l} d\nabla\Delta\phi_{k2}(i) = \nabla\Delta\phi_{k2}^{obs}(i) - \nabla\Delta\phi_{k2}^{calc}(i) \\ \cos\{d\nabla\Delta\phi_{k2}(i)\} > \text{minimum threshold \#1} \end{array} \right., \{ (i = 1, ns-1), k = 1, 3, \dots, n \} . \quad (3.45)$$

In equation (3.45), superscript *obs* denotes the individual observed double-difference phase observation related to monitor station  $k$ , and superscript *calc* denotes the individual calculated double-difference phase observation based on the updated position and the satellite coordinates. In this case, the ambiguity set being tested must satisfy all conditions expressed by equation (3.45) in order to pass the next validation and rejection criteria. Compared to the single monitor station case, it is indeed more difficult for the incorrect ambiguity set to pass this validation and rejection criteria.

The value of cosine of the phase residual  $d\nabla\Delta\phi_{k2}(i)$  in equation (3.45) lies between -1.0 and 1.0. The values of the minimum threshold, however, should be set somewhere between 0.7 and 1.0 depending on the expected magnitude of noise and the residual errors and biases in the observations and wavelength of the signal. Figure 3.11 shows the values of the cos term correspond to the phase residuals values of 0.0, 0.05, 0.075, 0.10, 0.125 and 0.15 cycles, respectively. The figure shows the advantage of working with longer wavelength signal in which an increase in the phase residual does not decrease the value of the cos term too rapidly as in the case of the signal with shorter wavelength.

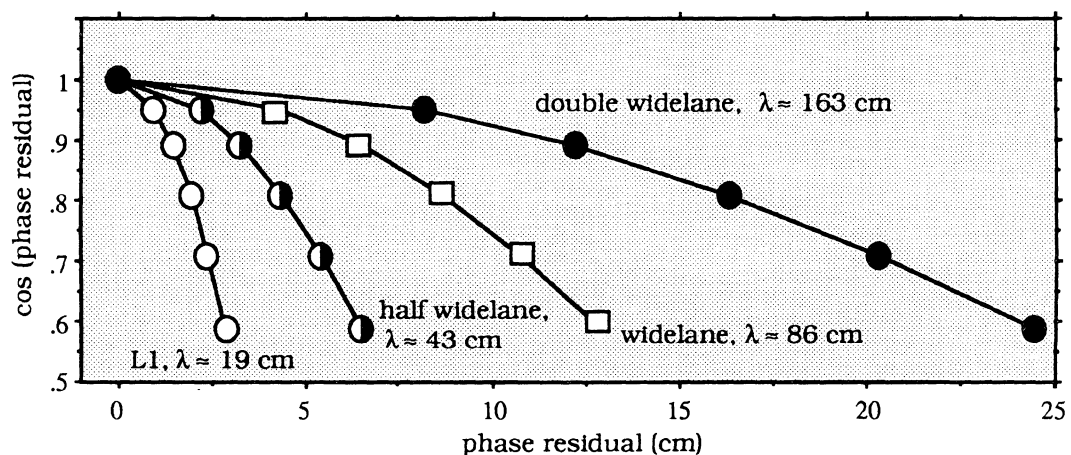


Figure 3.14. The real term of individual ambiguity mapping function.

### 3.6.7. Normalized ambiguity mapping function test.

The validation and rejection criteria called the normalized ambiguity mapping function value test is applied to test the group agreement between the phase observations which pass the previous test criteria, and their corresponding computed theoretical values based on the updated position ( $X_U$ ). The normalized ambiguity mapping function test consists primarily of three criteria which are used to check spatial and temporal agreement between the observed and the calculated phases, i.e., the phase residuals. Compared to previous tests

on the phase residuals, this normalized ambiguity function test has a finer resolution, i.e., higher identification power.

At certain epoch  $t$ , the normalized ambiguity mapping function test is formulated as:

$$\text{NAMF}_{t,k} (X_u) > \text{minimum threshold \#2}, \quad (k = 1, 3, \dots, n), \quad (3.46)$$

$$\text{NAMF}_{t,n} (X_u) > \text{minimum threshold \#3}, \quad \text{and} \quad (3.47)$$

$$\text{NAMF}_{1,t,n} (X_u) > \text{minimum threshold \#4}. \quad (3.48)$$

In equation (3.46),  $\text{NAMF}_{t,k}$  is the normalized ambiguity mapping function based on the observations related to monitor station  $k$  at epoch  $t$ , and it is formulated as :

$$\text{NAMF}_{t,k} = \frac{1}{ns-1} \sqrt{x_k^2 + y_k^2}, \quad (3.49)$$

where :

$$x_k = \sum_{i=1}^{ns-1} \cos\{d\nabla\Delta\phi_{k2}(i)\}; \quad y_k = \sum_{i=1}^{ns-1} \sin\{d\nabla\Delta\phi_{k2}(i)\}. \quad (3.50)$$

In equation (3.47),  $\text{NAMF}_{t,n}$  is the normalized ambiguity mapping function based on the observations related to all monitor stations at epoch  $t$ , and it is computed as follows:

$$\text{NAMF}_{t,n} = \frac{1}{n.(ns-1)} \sqrt{x_{\text{all}}^2 + y_{\text{all}}^2}, \quad (3.51)$$

where :

$$x_{\text{all}} = x_1 + \sum_{k=3}^n x_k; \quad y_{\text{all}} = y_1 + \sum_{k=3}^n y_k. \quad (3.52)$$

Finally,  $NAMF_{1,t,n}$  in equation (3.48) is the normalized ambiguity mapping function based on the observations related to all monitor stations from the first epoch up to epoch  $t$ . It can be computed sequentially as follows:

$$NAMF_{1,t,n} = NAMF_{1,t-1,n} + \frac{1}{t} (NAMF_{t,n} - NAMF_{1,t-1,n}) \quad (3.53)$$

It should be noted here that, with more observations, the value of the normalized mapping function related to the correct ambiguity set can be expected to be much closer to 1.0. Therefore, the values of the minimum thresholds used in equation (3.45) to (3.47) can be set as follows:

$$mt \#1 < mt \#2 < mt \#3 < mt \#4, \quad (mt = \text{minimum threshold}). \quad (3.54)$$

Besides the number of observations involved, the expected residual errors and biases in the observations and the wavelength of the signal should also be considered in choosing the values of the minimum threshold. Typically, values between 0.7 and 0.8 can be assigned to minimum threshold#1 and between 0.9 and 0.99 to minimum thresholds #2, #3, and #4.

With the changes in satellite geometry, the normalized ambiguity mapping function value,  $NAMF_{1,t,n}$ , related to incorrect ambiguities, can be expected to decrease, while the mapping function value related to correct ambiguities can be expected to be more or less steady, approaching the value of 1.0. Therefore, identifying the correct integer ambiguities should become easier as the observation time progresses and the observation geometry changes.



At this stage, the integer ambiguity set which passes all previous seven validation and rejection criteria is saved as the *potentially correct ambiguity set*. The corresponding values of the quadratic form of the residuals (equation 3.43) and the normalized ambiguity mapping function values  $NAMF_{1,t,n}$ , are also saved at this time. The next ambiguity set is then considered and tested using the procedures described above until all ambiguity sets at that epoch are tested.

### 3.6.8. Contrast test on quadratic form of the residuals

After all integer ambiguity sets inside the searching space are tested at a particular epoch, there are usually some ambiguity sets which still remain as candidates for the correct ambiguity set. Before continuing to the next epoch testing, another criterion is used to validate or reject these remaining ambiguity sets. A test is done on the corresponding values of the quadratic form of the residuals.

This test stems from the principles of the least squares adjustment used in the estimation process. The least squares adjustment yields the estimates of the parameters by minimizing the quadratic form of the residuals. In this case of the correct ambiguity identification, it can be expected that the quadratic form of the residuals related to the correct integer ambiguities should be relatively small or smaller than other values. The contrast among the quadratic form values can then be used to validate or reject certain ambiguity sets related to that quadratic forms. This contrast test is formulated as follows:

$$\frac{QF(v)_i}{QF(v)_{\min}} < F_{n(ns-1),n(ns-1),1-\alpha} , (i = 1,np-1) . \quad (3.55)$$

In the above equation  $QF(v)_{\min}$  and  $QF(v)_i$  are the minimum and  $i$ th quadratic form values of the residuals.  $F_{n(ns-1),n(ns-1),1-\alpha}$  is the Fisher percentile for degrees of freedom  $n(ns-1)$  and  $n(ns-1)$  and confidence level  $(1-\alpha)$ .  $n_p$  is the number of the quadratic forms. The values of the Fisher percentiles will increase with increases in the number of the satellites and/or the monitor stations as does the acceptance volume of the criteria.

If after this criteria some of the integer ambiguity sets still remain, then the validation process will be continued to the next epoch and the same validation and rejection procedures described above will be repeated until certain assurance criteria are fulfilled.

### 3.6.9. Assurance criteria

The identification process of the correct integer ambiguity set is stopped if the following two assurance criteria are satisfied :

- a) the number of potentially correct ambiguity sets after all validation and rejection criteria is only one, and
- b) its corresponding value of normalized ambiguity mapping function,  $NAMF_{1,t,n}$ , is larger than a certain predetermined threshold.

The ambiguity set which fulfills the above conditions will be fixed as the correct ambiguity. It should be emphasized in this case, however, that these fixed integer ambiguities could be either really the correct integers or the incorrect one. Fixing the ambiguities to the incorrect integers, which will be termed in this thesis as the failure in ambiguity resolution, could be caused by several factors. One of them is the use of the validation and rejection

criteria parameters which do not represent the state of satellite geometry, the level of the noise, and the remaining errors and biases in the observations. This fact will be highlighted later when the computational and geometrical aspects of ambiguity resolution are discussed in Chapters 5 and 6.

### **3.7. The integer ambiguity estimation of the L1 and L2 signals**

In the position estimation process using carrier phases, for better position accuracy, it is preferable to use the signal with the shortest possible wavelength if the observations are mainly contaminated by noise. It is due to the fact that the shorter the wavelength, the higher the precision of the phase observation will be, and vice versa. When the ionospheric effect is quite significant, then it is preferable to use the ionospheric free linear combination. In both cases, when one deals with dual-frequency and codeless GPS data, after fixing the wide-lane, and semi, half, or double wide-lane ambiguity, the ambiguities of L1 and L2 signals should also be fixed.

#### **3.7.1. Dual-frequency data**

In the case of dual-frequency data, when the double-difference wide-lane ambiguities ( $\nabla\Delta N_{\Delta}$ ) can be fixed, the double-difference ambiguities of L1 and L2 signals ( $\nabla\Delta N_1$  and  $\nabla\Delta N_2$ ) have to also be fixed. Theoretically speaking, the next longer wavelength signal, i.e., L2 signal, should be fixed. In this investigation, however, due to its lower noise level and ionospheric effect, and its even-odd relation with the previously fixed wide-lane ambiguities, the narrow-lane ambiguities ( $\nabla\Delta N_{\Sigma}$ ) will be fixed first. Then based on the wide-lane and narrow-lane ambiguities, the ambiguities of L1 and L2 signals are fixed using the following relations:

$$\nabla\Delta N_1 = (\nabla\Delta N_\Delta + \nabla\Delta N_\Sigma)/2 \quad , \quad (3.56)$$

$$\nabla\Delta N_2 = (\nabla\Delta N_\Sigma - \nabla\Delta N_\Delta)/2 \quad . \quad (3.57)$$

There are two methods for computing the narrow-lane ambiguities in this case. The first one is by simply utilizing the final updated position of the moving receiver and the second one is by using the ionospheric free linear combination of phase observations.

In the *first method*, the double difference narrow-lane ambiguities are computed using an equation similar to (3.1) as follows:

$$\nabla\Delta N_\Sigma = \frac{1}{\lambda_\Sigma} \cdot (\nabla\Delta\rho - \nabla\Delta L_\Sigma) \quad , \quad (3.58)$$

where  $\nabla\Delta\rho$  is the double-difference geometric ranges computed by basing on the final updated coordinates derived using the unambiguous wide-lane carrier phases.  $\nabla\Delta L_\Sigma$  is the ambiguous double-difference narrow-lane phases in range units. The closeness of these estimated real ambiguities to the integer numbers depends on the magnitudes of the observation noise and the residual errors and biases in the observations, which all are neglected in equation (3.58) above. If the wide-lane ambiguity is an even integer number, then the corresponding narrow-lane ambiguities is rounded to the nearest even integer number and, if the wide-lane integer ambiguity is the odd number, then the narrow-lane ambiguity is fixed to the nearest odd integer number.

In the *second method*, the ionospheric free linear combination of the double-difference phase observation is used in combination with the double-difference wide-lane integer ambiguities to compute the double-difference integer ambiguities of the L1 and L2 signals.

The double-difference ionospheric free linear combination,  $\nabla\Delta L_{if}$ , is formulated in this case as follows:

$$\nabla\Delta L_{if} = \frac{f_1^2 \cdot \nabla\Delta L_1 - f_2^2 \cdot \nabla\Delta L_2}{f_1^2 - f_2^2}, \quad (3.59)$$

where  $f_1$  and  $f_2$  are the frequencies of the L1 and L2 signals, respectively. This ionospheric free linear combination is related to the ambiguities of L1 and L2 signals through the following equation:

$$\nabla\Delta\rho = \nabla\Delta L_{if} + \frac{f_1^2 \cdot \lambda_1 \cdot \nabla\Delta N_1 - f_2^2 \cdot \lambda_2 \cdot \nabla\Delta N_2}{f_1^2 - f_2^2}, \quad (3.60)$$

where  $\lambda_1$  and  $\lambda_2$  denote the wavelength of L1 and L2 signals, respectively. By substituting equations (3.56) and (3.57) to equation (3.60), the following formulation for double-difference ambiguities of narrow-lane signal can be established:

$$\nabla\Delta N_{\Sigma} = \frac{2 \cdot (f_1 + f_2)}{f_2} \cdot \left( \frac{\nabla\Delta\rho - \nabla\Delta L_{if}}{\lambda_2} \right) - \frac{(f_1 + f_2)}{(f_1 - f_2)} \cdot \nabla\Delta N_{\Delta} \quad (3.61)$$

By inserting the frequencies of L1 and L2 signals, the above equation can be rewritten as:

$$\nabla\Delta N_{\Sigma} = \frac{137}{30} \cdot \left( \frac{\nabla\Delta\rho - \nabla\Delta L_{if}}{\lambda_2} \right) - \frac{137}{17} \cdot \nabla\Delta N_{\Delta} \quad (3.62)$$

The narrow-lane ambiguities are then fixed by employing their even-odd relation with the corresponding wide-lane ambiguities, and the ambiguities of L1 and L2 signals are computed afterward using equations (3.56) and (3.57).

Since the narrow-lane phase observations have lower observation noise than the ionospheric free linear combinations, the first method should be used when the ionospheric effect is expected to be low, as in the case of low ionospheric activity and/or short separation between the monitor station and the moving receiver. In the case of high ionospheric activity, however, the second method should be used.

### 3.7.2. Codeless data

In the case of **codeless data**, the observation types available are the L1-C/A code pseudoranges, full-wavelength L1 phases, and half-wavelength L2 phases resulting from the squaring process [Wells *et al.*, 1986]. For ambiguity resolution, the semi, half or double wide-lane signals (see Appendix I) can be used. The double wide-lane signal has a longer wavelength, i.e., 162.8 cm compared to 34.1 cm and 43.1 cm of the semi and half wide-lane signals, which is useful for ambiguity resolution. However, it is more affected by the ionospheric refraction and also has the highest noise level compared to semi and half wide-lane signals. Among the three, the semi wide-lane is the least affected by the ionosphere and has also the lowest noise level. Its wavelength, however, is the shortest. One therefore has to trade-off these factors in choosing the signal to be used in the ambiguity resolution process. In both cases, after fixing the semi, half, or double wide-lane ambiguities, the cycle ambiguity resolution of L1 and L2 signals are accomplished using the help of the ionospheric free linear combination. It should be noted here that the frequency and wavelength of the half-wavelength L2 phases ( $f_{2c}$  and  $\lambda_{2c}$ ) are related to the original frequency and wavelength of L2 signal ( $f_2$  and  $\lambda_2$ ) as follows:

$$f_{2c} = 2 \cdot f_2 \quad \text{and} \quad \lambda_{2c} = \lambda_2 / 2 \approx 12.2 \text{ cm} \quad . \quad (3.63)$$

In the case of codeless data, the double-difference ionospheric free linear combination,  $\nabla\Delta L_{if}$ , can be formulated as follows:

$$\nabla\Delta L_{if} = \frac{f_{2c}^2 \cdot \nabla\Delta L_{2c} - f_1^2 \cdot \nabla\Delta L_1}{f_{2c}^2 - f_1^2} = \frac{4f_2^2 \cdot \nabla\Delta L_{2c} - f_1^2 \cdot \nabla\Delta L_1}{4f_2^2 - f_1^2} \quad , \quad (3.64)$$

where :

$$\nabla\Delta L_{2c} = \lambda_{2c} \cdot \nabla\Delta\phi_{2c} \quad . \quad (3.65)$$

In the above equation,  $\phi_{2c}$  is the observed half-wavelength L2 phases in cycles units. This ionospheric free linear combination is related to the ambiguities of L1 and L2 signals ( $\nabla\Delta N_1$  and  $\nabla\Delta N_{2c}$ ) through the following equation:

$$\nabla\Delta\rho = \nabla\Delta L_{if} + \frac{2f_2^2 \cdot \lambda_2 \cdot \nabla\Delta N_{2c} - f_1^2 \cdot \lambda_1 \cdot \nabla\Delta N_1}{4f_2^2 - f_1^2} \quad . \quad (3.66)$$

If the ambiguities of the semi, half and double wide-lane signals are denoted as  $\nabla\Delta N_{s\Delta}$ ,  $\nabla\Delta N_{\Delta/2}$  and  $\nabla\Delta N_{2\Delta}$  then the following ambiguity relations exist (see Appendix I):

$$\nabla\Delta N_{s\Delta} = -\nabla\Delta N_1 + \nabla\Delta N_{2c} \quad , \quad (3.67)$$

$$\nabla\Delta N_{\Delta/2} = 2\nabla\Delta N_1 - \nabla\Delta N_{2c} \quad , \quad (3.68)$$

$$\nabla\Delta N_{2\Delta} = -3\nabla\Delta N_1 + 2\nabla\Delta N_{2c} \quad . \quad (3.69)$$

In the case of *semi wide-lane signal*, substituting equation (3.67) into equation (3.66), the following formula for the double-difference integer ambiguities of L1 signal is obtained:

$$\nabla\Delta N_1 = \frac{(4.f_2^2 - f_1^2)}{(2.f_1.f_2 - f_1^2)} \cdot \left( \frac{\nabla\Delta\rho - \nabla\Delta L_{if}}{\lambda_1} \right) - \frac{2.f_2}{(2.f_2 - f_1)} \cdot \nabla\Delta N_{s\Delta} \quad (3.70)$$

By inserting the frequencies of L1 and L2 signals, the above equation can be rewritten as:

$$\nabla\Delta N_1 = \frac{8471}{3311} \cdot \left( \frac{\nabla\Delta\rho - \nabla\Delta L_{if}}{\lambda_1} \right) - \frac{120}{43} \cdot \nabla\Delta N_{s\Delta} \quad (3.71)$$

In the case of *half wide-lane signal*, substituting equation (3.68) to equation (3.66) above, the following formulation for the double-difference integer ambiguities of L1 signal is obtained:

$$\nabla\Delta N_1 = \frac{(4.f_2^2 - f_1^2)}{(4.f_1.f_2 - f_1^2)} \cdot \left( \frac{\nabla\Delta\rho - \nabla\Delta L_{if}}{\lambda_1} \right) + \frac{2.f_2}{(4.f_2 - f_1)} \cdot \nabla\Delta N_{\Delta/2} \quad (3.72)$$

By inserting the frequencies of L1 and L2 signals, the above equation can be rewritten as:

$$\nabla\Delta N_1 = \frac{8471}{12551} \cdot \left( \frac{\nabla\Delta\rho - \nabla\Delta L_{if}}{\lambda_1} \right) + \frac{120}{163} \cdot \nabla\Delta N_{\Delta/2} \quad (3.73)$$



In the case of *double wide-lane signal*, substituting equation (3.69) to equation (3.66), the following formula for the double-difference integer ambiguities of L1 signal can be established :

$$\nabla\Delta N_1 = \frac{(4.f_2^2 - f_1^2)}{(3.f_1.f_2 - f_1^2)} \cdot \left( \frac{\nabla\Delta\rho - \nabla\Delta L_{if}}{\lambda_1} \right) - \frac{f_2}{(3.f_2 - f_1)} \cdot \nabla\Delta N_{2\Delta} \quad (3.74)$$

By inserting the frequencies of L1 and L2 signals, the above equation can be rewritten as:

$$\nabla\Delta N_1 = \frac{8471}{7931} \cdot \left( \frac{\nabla\Delta\rho - \nabla\Delta L_{if}}{\lambda_1} \right) - \frac{60}{103} \cdot \nabla\Delta N_{2\Delta} \quad (3.75)$$

In all the cases of using semi, half or double wide-lane signals, by knowing the ambiguities of L1 phases, then the ambiguities of the half-wavelength L2 phases can be computed by basing on equation (3.67), (3.68), or (3.69).

## Chapter 4

# VALIDATION OF ON-THE-FLY AMBIGUITY RESOLUTION TECHNIQUE

---

---

This chapter is intended to prove the validity of the integrated on the fly ambiguity resolution technique which has been described and outlined in the previous chapter. The verification is performed using both static and kinematic real GPS data. The static data, particularly the zero baseline data, is used to ensure that the algorithm is working properly. The real GPS kinematic data is then processed to show that the validity of the on-the-fly ambiguity resolution technique. The results are presented along with discussions and analysis on these results. All the computation is executed using the IBM ES9000 MOD320 mainframe computer.

It should be noted that the parameter values of the identification process, the standard deviations of the observations, and primary satellites used in the examples shown in this chapter are chosen based on a trial and error process. In the case of the parameter values of the identification process and the standard deviations of the observations, the set of values which corresponds to the best performance of ambiguity resolution in all combinations of the primary satellites, in terms of speed and resolution success, is used. In terms of primary satellites, the one which yields the fastest ambiguity resolution is used for the example. Since the actual standard deviations of the observations are difficult to know

exactly, some values are considered by taking into account their theoretical measurement precision and also the expected level of the remaining errors and biases in the observations. In choosing the optimal parameter values of the identification process, some trial sets of values are tested by considering several factors such as the standard deviations of the observation used, satellite geometry, signal used, and expected remaining errors and biases in the observations. It should be noted that the effects of different parameter values of the identification process, different standard deviations of the observations, and different primary satellites on the performance of on-the-fly ambiguity resolution will be discussed in Chapters 5 and 6.

#### 4.1. TRIMBLE GEODESIST ZERO-BASELINE RESULTS.

##### 4.1.1. Characteristics of the zero baseline data.

The zero baseline data used here was collected using two Trimble Geodesist P-receivers which observe L1-C/A code, L2-P code, and full wavelength carrier phases on L1 and L2 frequencies. The data was collected at a known station in California on 21st of November 1991 (day 324). A maximum of six satellites were visible during the one hour test and a five second update rate was used. The

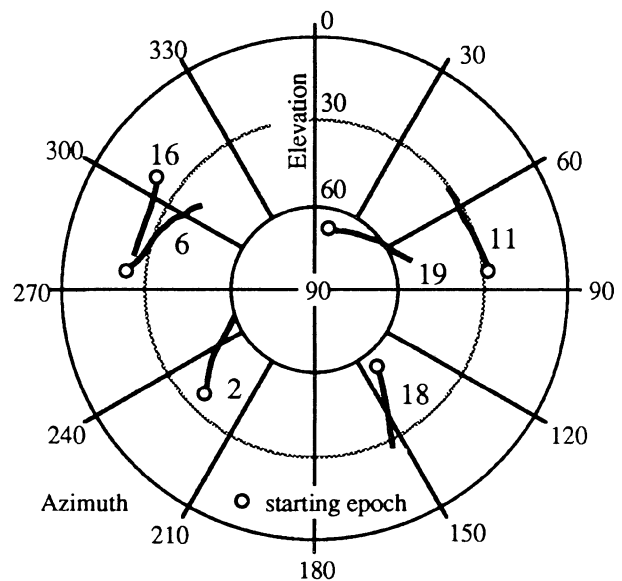


Figure 4.1. Satellite polar plot.

satellite constellation during the session is shown by polar plot in Figure 4.1. In summary, the general characteristics of the data are given in Table 4.1. In performing on-the-fly

ambiguity resolution computation, one receiver is considered as a monitor station, and the other as a moving receiver.

The double-difference reference integer ambiguities are computed by using the known coordinates of the station and the broadcast ephemeris of satellites. Since in this case the double-difference phases are only contaminated by the observation noise, these reference ambiguities can be easily and reliably determined, as shown

Table 4.1. Data characteristics

Location	California
Date	21 November 1991
Time period	≈ 1 hour
Local times	≈ 6:00 - 7:00 a.m.
GPS receivers	Trimble Geodesist
Data interval	5 second
Satellites, PRNs #	2, 6, 11, 16, 18, 19

by the example in Figure 2.2. If equation similar to (3.1) is used to compute the double-difference ambiguities of L1 and L2 signals, the precise and accurate reference ambiguities can be obtained. Table 4.2 shows the estimated double-difference real-ambiguities of L1 and L2 signals averaged over the whole observation period along with their standard deviations. The reference integer ambiguities are established by rounding these real ambiguities to the nearest integer, which are obvious in this case.

Table 4.2. Double-differences averaged ambiguities of L1 and L2 signals.

Satellite differencing	L1 - ambiguities	L2 - ambiguities
PRN 2 - PRN 18	0.0005 ± 0.0002	5421.0002 ± 0.0001
PRN 11 - PRN 18	0.0000 ± 0.0002	5422.0000 ± 0.0001
PRN 6 - PRN 18	0.0009 ± 0.0002	5421.9991 ± 0.0001
PRN 19 - PRN 18	0.0016 ± 0.0002	5421.9994 ± 0.0001
PRN 16 - PRN 18	0.0002 ± 0.0002	5421.0003 ± 0.0002

#### 4.1.2. On-the-fly ambiguity resolution parameters.

As was explained in the previous chapter, in order to execute the integrated on-the-fly ambiguity resolution techniques, the values of the ambiguity resolution parameters have to be chosen or assigned. These parameters will include the four satellites chosen as the primary satellites, the observation differencing between satellites, the standard deviations of the pseudoranges and phases observations, and the values of the rejection and validation criteria parameters.

In this case, PRNs 2, 11, 6, and 16 are chosen as the primary satellites, and PRN 2 is chosen as the reference satellite for differencing. The Position Dilution of Precision (PDOP) value for the whole satellite is about 3.8 and for the primary satellites is about 4.1. Since with zero baseline, the systematic errors in the observations are completely eliminated by the differencing, the precision of certain type of observations (code or phase) to all satellites is characterized by the same standard deviation. The standard deviations of the pseudoranges and carrier phases observations listed in Table 4.3 are used in this case.

Table 4.3. The standard deviations of Trimble Geodesist zero-baseline data.

	L1-C/A code	L2-P code
pseudoranges	1.5 m	1.0 m
carrier phases	5.00 mm	7.00 mm

For the identification process of the correct ambiguities, the parameter values of the searching space, the rejection and validation criteria, and the assurance criteria are listed in Table 4.4. Two sets of parameter values are used, for the single and dual frequency cases. In the dual-frequency case, all types of available observations are used. But in the case of single frequency, only L1-C/A code and L1 signal are considered. The wide-lane signal is

used as a signal for the ambiguity resolution in the case of dual-frequency data, and the L1 signal for single-frequency data. With dual-frequency data, after the wide-lane ambiguities are fixed, the narrow-lane ambiguities are then resolved by utilizing the ionospheric free linear combination of phase observations (see section 3.7.1).

Table 4.4. The parameter values of the identification process for single and dual frequency data.

The parameters	Single	Dual
Confidence level of ellipsoidal searching space	0.99	0.99
Confidence level of the first criteria	0.99	0.99
The constant value of the second criteria	0.20	0.20
Confidence level of the third criteria	0.99	0.99
The constant value of the fourth criteria	0.10	0.10
Confidence level of the fifth criteria	0.99	0.99
Minimum individual mapping function value of the sixth criteria	0.90	0.85
Minimum normalized mapping function values of the seventh criteria	0.98 & 0.99	0.96 & 0.97
Confidence level of the eight criteria	0.99	0.99
Minimum normalized mapping function value of the assurance criteria	0.99	0.98

#### 4.1.3. On-the-fly ambiguity resolution results.

On-the-fly ambiguity resolution is executed in simulated kinematic mode by considering one receiver as a monitor station and another receiver as a moving receiver. In this case, the observation and computation times needed to resolve the ambiguities are presented in Table 4.5.

Table 4.5. The on-the-fly ambiguity resolution results of zero baseline data.

Data	number of initial ambiguity sets	CPU times in milliseconds	epoch of ambiguity resolution (5 second data interval)
Single	1029	527	16
Dual # 1	97	73	2
Dual # 2	1159	127	2

The results related to dual frequency data in Table 4.5 are categorized into two cases based on the approach used to compute the initial primary ambiguities. In the dual # 1 case, the initial ambiguities are computed based on the code-derived position; while in the dual # 2 case, extrawidelaning is used. Notably, the use of the extrawidelaning technique leads to a larger searching space, and consequently slower computation times than the use of code-derived position. The epochs of ambiguity resolution, however, are the same for both cases.

It should also be noted that in the case of single frequency data, the identification process of the correct ambiguities is started at epoch #10, not at the first epoch as is the case with dual frequency data. Up to this epoch, the code smoothing process is done to reduce the noise level in the code observations in order to obtain a smaller and more reliable ambiguity searching space.

The success of the on-the-fly ambiguity resolution can also be verified by estimating the length of the zero baseline using fixed-ambiguity phase observations. The results obtained by using the narrow-lane and L1 signals are shown in Figure 4.2. Note from the figure that the time average of the baseline length is about 1 % of the wavelength of the signal, i.e., about 1.1 mm and 1.9 mm, respectively, for the narrow-lane and L1 signals.

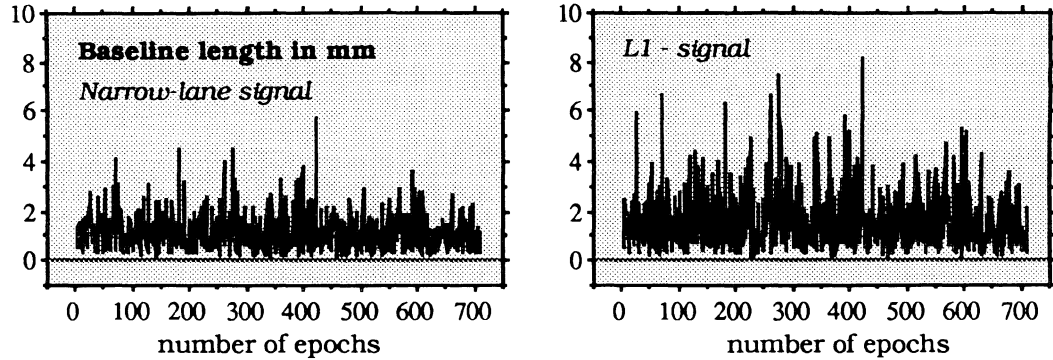


Figure 4.2. The zero-baseline length estimated from the fixed ambiguity solutions.

#### 4.2. ASHTECH CODELESS STATIC RESULTS.

This data set is processed to verify the validity of the integrated on-the-fly ambiguity resolution technique in processing the codeless GPS data which consist of L1-C/A code, full wavelength L1-phases, and half-wavelength L2-phases.

##### 4.2.1. Characteristics of the codeless data.

The codeless GPS data processed in this case was collected at 30 second data interval on 12 June 1991 (day 163), using Ashtech LD-XII receivers at two known stations (DOME and PEPS) on Université Laval campus, Québec City, Canada. The baseline length was around 535 metres. Five satellites were observed, i.e., PRNs 2, 6, 11, 15, and 19 for about one hour. The relative position of stations DOME and PEPS and the satellite constellation during the session is shown by polar plot in Figure 4.3. In summary, the general characteristics of the data is given in Table 4.6.

For the ambiguity resolution computation, PRNs 2, 6, 11, and 15 were used as the primary satellites, and PRN 2 was used as the reference satellite for observation differencing.



Station DOME was used as the monitor station, and station PEPS was considered the moving receiver. The half wide-lane signal is used as a working signal for resolving the ambiguities.

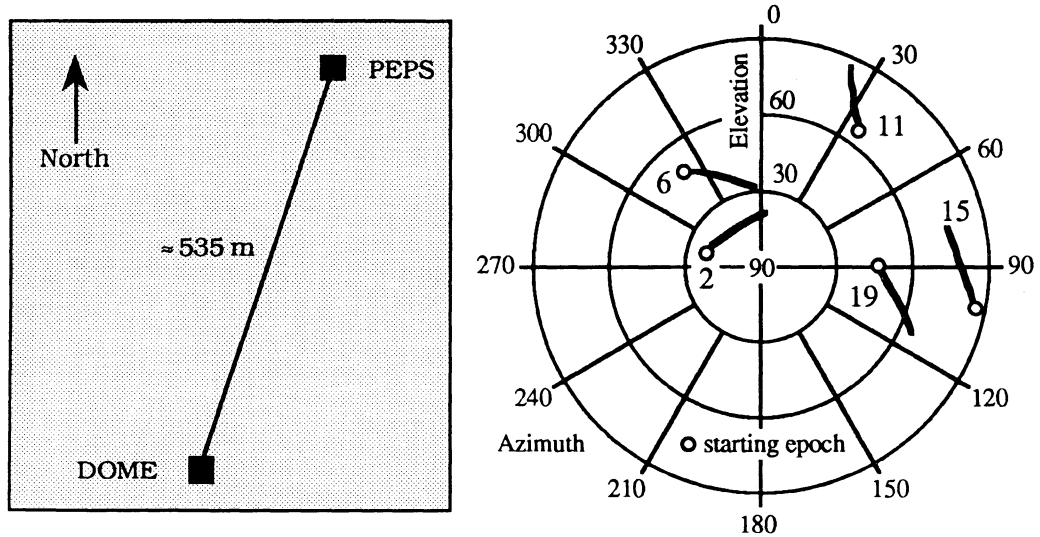


Figure 4.3. Relative position of the stations and satellite polar plot as seen from PEPS.

The double-difference reference integer ambiguities are computed by using the known coordinates of the station and the broadcast ephemeris of satellites in an equation similar to (3.1). Table 4.7 shows the estimated double-difference real-ambiguities of half wide-lane, full wavelength L1 and half-wavelength L2

Table 4.6. Data characteristics

Location	Quebec City
Date	12 June 1991
Time period	≈ 1 hour
Local times	≈ 6:38 - 6:40 p.m.
GPS receivers	Ashtech LD-XII
Data interval	30 seconds
Satellites, PRNs #	2, 6, 11, 15, 19

signals averaged over the whole epochs along with their standard deviations. The reference integer ambiguities are established by rounding these real ambiguities to the nearest integer, which are quite obvious in this case.

Table 4.7. Double-differences averaged ambiguities of half wide-lane, L1 and half-wavelength L2 signals.

Satellite differencing	half wide-lane ambiguities	L1 - ambiguities	half-wavelength L2 - ambiguities
PRN 6 - PRN 2	-36303.987 ± 0.004	-82217.996 ± 0.003	-128132.005 ± 0.005
PRN 11 - PRN 2	245768.975 ± 0.004	556593.020 ± 0.003	867417.066 ± 0.005
PRN 15 - PRN 2	100947.011 ± 0.004	228613.998 ± 0.003	356280.986 ± 0.004
PRN 19 - PRN 2	235269.978 ± 0.005	532815.005 ± 0.003	830360.032 ± 0.006

#### 4.2.2. On-the-fly ambiguity resolution parameters.

For on-the-fly ambiguity resolution, PRNs 2, 6, 11, and 15 are chosen as the primary satellites, and PRN 2 is chosen as the reference satellite for between-satellite observation differencing. The Position Dilution of Precision (PDOP) value for the whole satellite is about 4.4 and, for the primary satellites, is about 8.7. Because of its relatively short baseline length, the precision of a certain type of observations to all satellites is characterized by the same standard deviation. The standard deviations of pseudoranges and carrier phases observations listed in Table 4.8 are used.

Table 4.8. The standard deviations of Ashtech codeless static data.

	L1-signal	L2-signal
pseudoranges	1.0 m	-
carrier phases	3.00 mm	8.00 mm

For the identification process of the correct ambiguities, the parameter values of the searching space, the rejection and validation criteria, and the assurance criteria are listed in

Table 4.9. The half wide-lane signal with wavelength of about 43 cm is used as a working signal for the ambiguity resolution. After fixing the ambiguities of the half wide-lane signal, the ambiguities of L1 signal and half-wavelength L2 signal are resolved by utilizing the ionospheric free linear combination of phase observations, based on equations (3.71) and (3.67) given in the previous chapter.

Table 4.9. The parameter values of the identification process for codeless data.

The parameters	Values
Confidence level of ellipsoidal searching space	0.950
Confidence level of the first criteria	0.950
The constant value of the second criteria	0.100
Confidence level of the third criteria	0.950
The constant value of the fourth criteria	0.050
Confidence level of the fifth criteria	0.990
Minimum individual mapping function value of the sixth criteria	0.900
Minimum normalized mapping function values of the seventh criteria	0.97 & 0.98
Confidence level of the eight criteria	0.999
Minimum normalized mapping function value of the assurance criteria	0.990

#### 4.2.3. On-the-fly ambiguity resolution results.

On-the-fly ambiguity resolution is executed in simulated kinematic mode by considering station DOME as a monitor station and station PEPS as a moving receiver. The observation and computation times needed to correctly resolve the ambiguities of half wide-lane, L1, and half-wavelength L2 signals are given in Table 4.10.

Table 4.10. On-the-fly ambiguity resolution results of codeless data.

Data	number of initial ambiguity sets	CPU times in milliseconds	epoch of ambiguity resolution (30 second data interval)
Codeless	2729	501	4

The success of on-the-fly ambiguity resolution can also be verified by comparing the 'known' baseline length with the epoch-by-epoch baseline lengths estimated using the fixed-ambiguity phase observations. The results obtained by using the L1 and half-wavelength L2 signals are shown in Figure 4.4. The time averages of the baseline length differences in this case are about 2.7 mm and 3.8 mm for the L1 and half-wavelength L2 signals, respectively. These averages indicate the correctness of their corresponding integer ambiguities. The figure also shows that the epoch-by-epoch baseline lengths estimated using the half-wavelength L2 signal are noisier than those estimated using L1 signal despite the shorter wavelength of the half-wavelength L2-signal. This is due to the squaring process in the receiver for obtaining the half-wavelength L2 signal which increases the noise level of the yielded signal by a factor of two times greater than the original full-wavelength L2-signal [Wells *et al.*, 1986].

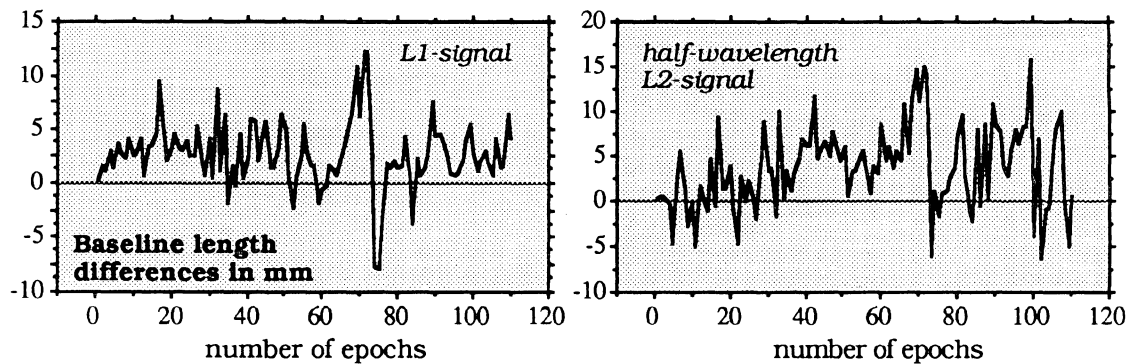


Figure 4.4. The differences between the 'known' baseline length and the baseline length estimated from the fixed ambiguity solution.

### 4.3. ROGUE KINEMATIC GPS RESULTS.

#### 4.3.1. Characteristics of the kinematic GPS data.

The kinematic GPS data used is part of the data from the marine sea-floor geodetic experiment conducted off the shore of Vancouver Island, British Columbia, Canada, from May 28 to June 6, 1991. This integrated GPS-acoustic system survey was performed to measure the real-time relative motion between the Juan de Fuca and the North American plates in the Cascadia subduction zone [Dragert, 1992]. Four institutions were involved in this survey, namely Scripps Institution of Oceanography, Jet Propulsion Laboratory, Geodetic Survey of Canada, and United States Geological Survey.

The GPS data in this survey is the P-code dual frequency GPS data observed using *Rogue* GPS receivers. Two monitor stations and three antennas on the moving buoy are involved. The two monitor stations are PGC at the Pacific Geoscience Centre, Sidney, B.C, and UCLU (Ucluelet) at the west coast of central Vancouver Island. The three antennas were rigidly mounted on a buoy which was towed about 100 m behind the ship. The antennas floated about 1.5 m above the water (when it was calm).

To show the validity of the integrated on-the-fly ambiguity resolution technique explained in the previous chapter, some of the GPS data from the survey is processed. The general characteristics of the data processed in this chapter are shown in Table 4.11. It was collected on June 6, 1991 with one second data interval. From the whole-day data set

Table 4.11. Data characteristics

Location	off the shore of Vancouver Island
Date	6 June 1991
Time period	≈ 22 minutes
Local times	≈ 9:38 - 10:00 a.m.
GPS receivers	Rogue
Data interval	1 second
Satellites, PRNs #	11, 12, 15, 21, 23

only about 22 minutes worth of data (1365 epochs) has been processed. This sample data set is chosen because of the following factors: the same five satellites are continuously tracked, the ionospheric refraction can be expected to be relatively small since the data was collected in the morning, and also it is free of cycle slips. For this time period, the buoy is about 167 km from station PGC and about 61 km from station UCLU as depicted in Figure 4.5, and five satellites (PRNs : 11, 12, 15, 21, and 23) were observed. The satellite constellation during this 22 minute period is shown in Figure 4.6 by the satellite polar plot as seen from station UCLU.

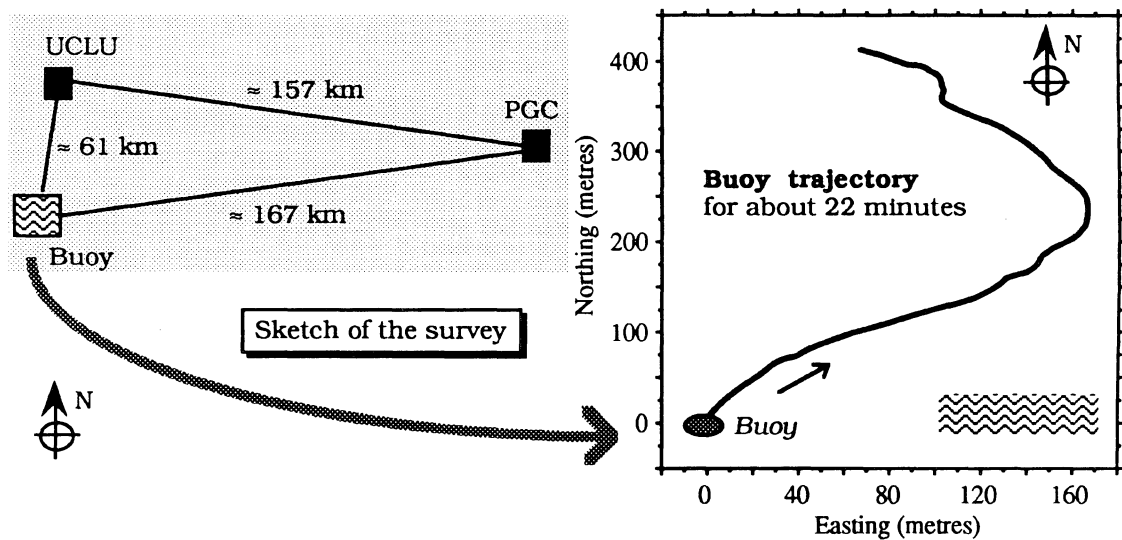


Figure 4.5. Sketch of the survey area and the buoy trajectory.

The buoy system used in this survey consists of a steel framework enclosing a doughnut buoy. Within the framework, bracing members connect a central stem to an upper equilateral triangular platform. The entire structure is quite rigid, due to its heavy-duty construction. The three GPS antennas (which will be denoted as B1, B2, and B3) are located just inside the vertex of the triangle, as shown in Figure 4.7. The centre-to-centre distances for the antennas were as follows:

B1 to B2 = 2643.6 mm ,  
 B1 to B3 = 2642.5 mm , and  
 B2 to B3 = 2652.6 mm .

These distances were measured between the screws which are used to hold the antennas. These distances will be used as one of the criteria in verifying the success of the ambiguity resolution.

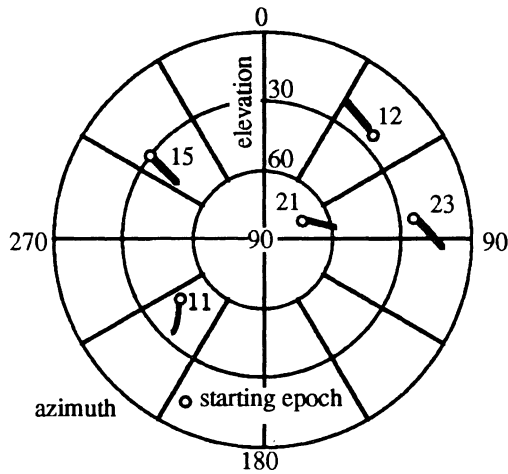


Figure 4.6. Satellite polar plot .

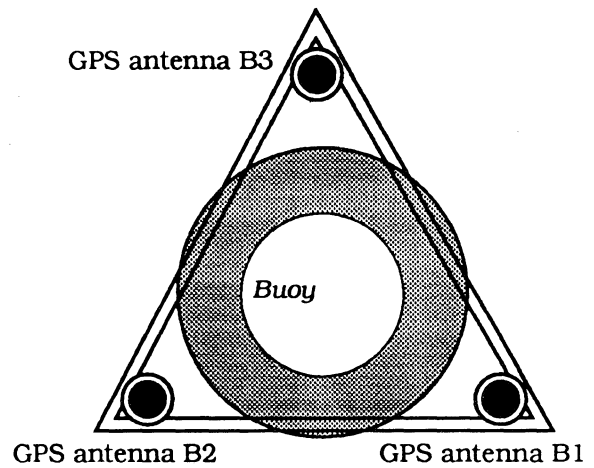


Figure 4.7. GPS antennas and the buoy

The speed of the buoy during the 22 minute trajectory considered in this case is quite slow. Figure 4.8 shows the total speed of antenna B1 computed based on GPS phase observations. In average, it was about 1m/sec.

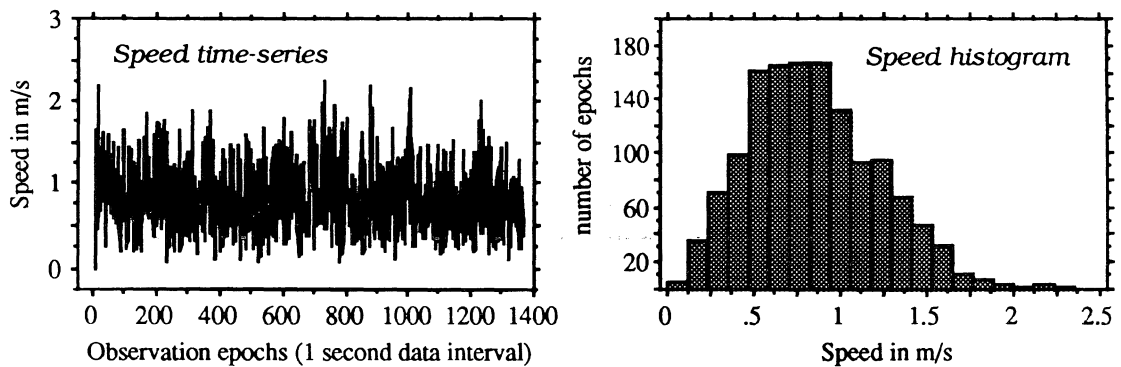


Figure 4.8. The time series and histogram of the total speed of antenna B1.

As expected, along the trajectory the antennas were always in motion. As shown in Figure 4.9, the relative positions of the antennas between each other were changing with time. No single cycle slip, however, occurred during this period.

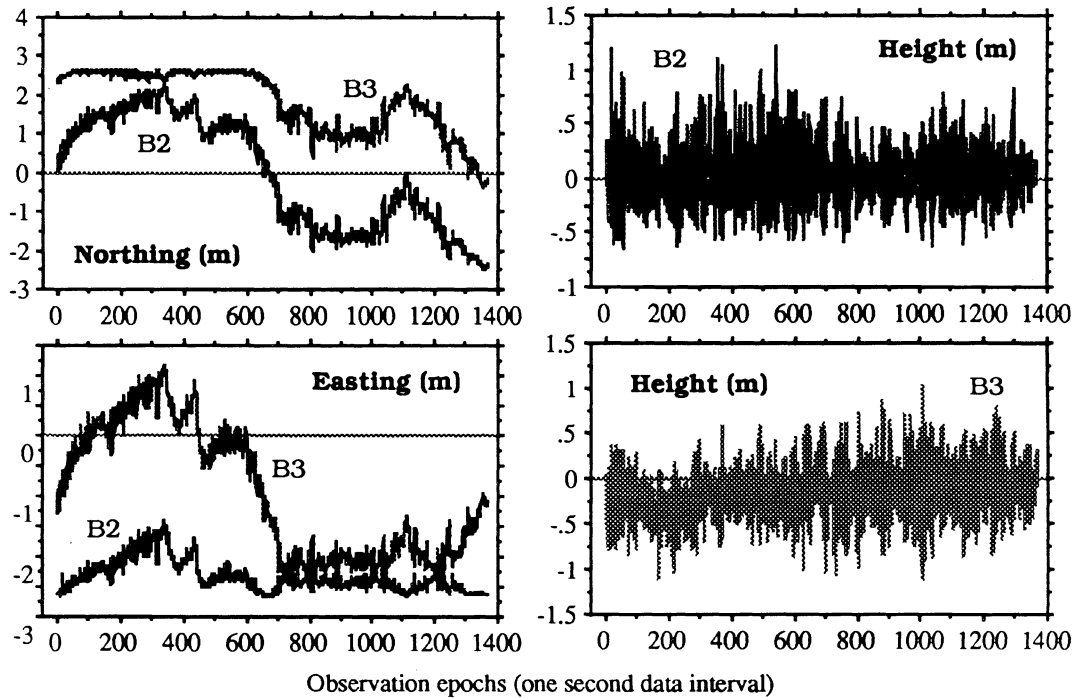


Figure 4.9. The relative positions of antennas B2 and B3 relative to antenna B1 in local geodetic coordinate system (northing, easting, height) along the 22 minute trajectory.

#### 4.3.2. On-the-fly ambiguity resolution parameters.

As was explained in the previous chapter, in order to execute the integrated on-the-fly ambiguity resolution techniques, the values of the ambiguity resolution parameters have to be chosen or assigned. These values include the four satellites chosen as the primary satellites, observation differencing between satellites, standard deviations of the pseudoranges and phases observations, and values of the rejection and validation criteria parameters.



For ambiguity resolution, PRNs 12, 15, 21, and 23 are chosen as the primary satellites, and PRN 12 is chosen as the reference satellite for differencing. The Position Dilution of Precision (PDOP) value for the all satellites is about 4.2 and for the primary satellites is about 5.4. Due to relatively long baseline lengths (60 - 170 km), it can be expected that the effects of the looking direction dependent errors and biases, such as ionospheric refraction, will not be the same for all satellite observations.

Considering the finding by *Euler and Goad* [1991], the standard deviation of the pseudoranges and phases observations at each epoch  $t$  are considered to be elevation-dependent, and they are computed using the following exponential relations :

$$\sigma_P(h(t)) = \sigma_P(90) \cdot \exp\left(\frac{90 - h(t)}{90}\right), \quad (4.1)$$

$$\sigma_L(h(t)) = \sigma_L(90) \cdot \exp\left(\frac{90 - h(t)}{90}\right), \quad (4.2)$$

where  $\sigma_P$  and  $\sigma_L$  denote the standard deviation of the pseudoranges and phases observations and  $h(t)$  is the satellite elevation at epoch  $t$  in degrees. In this formula,  $\sigma_P(90)$  and  $\sigma_L(90)$  are the standard deviations of the observations at the zenith direction which should be assigned by the user.

According to *Thomas* [1988], based on the nominal system parameters, the system noise errors of the Rogue GPS receiver are less than 0.1 mm in phase observation and a centimeter or less in P-code pseudoranges for a 5-minute integration time. Furthermore, excluding the system-noise errors and errors outside the receiver (e.g. multipath and antenna errors), the between-satellite systematic errors are about 0.2 mm or less for the phases and about 1 cm or less for the P-code pseudoranges.

Considering the baseline lengths, the possibility of multipath occurrences and the sizing of the ambiguity searching space, rather pessimistic values are used for standard deviations of the observations. In this case, the zenith standard deviations listed in Table 4.12 are used to compute the standard deviations of the observations at each epoch for both L1 and L2 frequencies. It should be noted that, in the identification process of the correct ambiguities, the standard deviations of the observations will also determine the identification power of some rejection and validation criteria as well as affecting the size of the ambiguity searching space.

Table 4.12. Zenith standard deviations.

	L1	L2
$\sigma_p(90)$	0.25m	0.40m
$\sigma_L(90)$	2.00 mm	3.00 mm

For the identification process of the correct ambiguities, the parameter values of the searching space, the rejection and validation criteria, and the assurance criteria are listed in Table 4.13. Two sets of parameter values are used in this case, one for the shorter baselines, namely UCLU-B1, UCLU-B2, and UCLU-B3, and another for the relatively longer baselines, namely PGC-UCLU, PGC-B1, PGC-B2, and PGC-B3. Since the observations related to the longer baselines can be expected to have larger remaining errors and biases, the acceptance volume of some rejection criteria related to the longer baselines are made relatively larger than those related to the shorter baselines. The initial ambiguities are estimated by basing on the narrow-lane pseudorange derived position.

The wide-lane signal is used as a basic signal for the ambiguity resolution. After the wide-lane ambiguities are fixed, the narrow-lane ambiguities are then resolved by utilizing the ionospheric free linear combination of phase observations (see section 3.7.1).

Table 4.13. The parameter values of the identification process  
(A for the shorter baselines, B for the longer baselines).

The parameters	A	B
Confidence level of ellipsoidal searching space	0.99	0.99
Confidence level of the first criteria	0.95	0.95
The constant value of the second criteria	0.20	0.40
Confidence level of the third criteria	0.95	0.95
The constant value of the fourth criteria	0.05	0.10
Confidence level of the fifth criteria	0.99	0.99
Minimum individual mapping function value of the sixth criteria	0.80	0.70
Minimum normalized mapping function values of the seventh criteria	0.96 & 0.97	0.95 & 0.96
Confidence level of the eight criteria	0.99	0.99
Minimum normalized mapping function value of the assurance criteria	0.98	0.97

#### 4.3.3. On-the-fly ambiguity resolution results.

On-the-fly ambiguity resolution is performed by considering one monitor station at a time, namely PGC or UCLU. Double-difference ambiguities related to all three antennas on the buoy are the ambiguities to be resolved. The double-difference ambiguities involving stations PGC and UCLU are also resolved, to be used for ambiguity resolution verification.

The results of on-the-fly ambiguity resolution are given in Table 4.14. and the integer wide-lane and narrow-lane ambiguities are given in Tables 4.15 and 4.16.

Table 4.14. The results of on-the-fly ambiguity resolution

Baseline	number of initial ambiguity sets	CPU times in milliseconds	epoch of ambiguity resolution (1 second data interval)
PGC - B1	37	79	4
PGC - B2	37	77	4
PGC - B3	37	78	4
UCLU - B1	37	68	3
UCLU - B2	37	74	4
UCLU - B3	37	55	1
PGC - UCLU	37	79	4

Table 4.15. Double-difference wide-lane integer ambiguities fixed by on-the-fly ambiguity resolution technique.

Baseline	PRNs : 15 - 12	PRNs : 21 - 12	PRNs : 23 - 12	PRNs : 11 - 12
PGC - B1	-783968	-1081646	5559792	-1677891
PGC - B2	-520118	-1331438	5692825	-1966103
PGC - B3	-175456	-1144857	5049569	-1767813
UCLU - B1	-2367457	-2075740	4570391	-2634163
UCLU - B2	-2103607	-2325532	4703424	-2922375
UCLU - B3	-1758945	-2138951	4060168	-2724085
PGC - UCLU	1583489	994094	989401	956272

Table 4.16. Double-difference narrow-lane integer ambiguities fixed by on-the-fly ambiguity resolution technique.

Baseline	PRNs : 15 - 12	PRNs : 21 - 12	PRNs : 23 - 12	PRNs : 11 - 12
PGC - B1	-6317840	-8716770	44805330	-13521763
PGC - B2	-4191494	-10729770	45877435	-15844395
PGC - B3	-1413944	-9226171	40693557	-14246431
UCLU - B1	-19078911	-16727964	36831929	-21228167
UCLU - B2	-16952565	-18740964	37904034	-23550799
UCLU - B3	-14175015	-17237365	32720156	-21952835
PGC - UCLU	12761071	8011194	7973401	7706404

As shown in Table 4.14, the ambiguities are resolved quickly, even instantaneously, in the case of baseline UCLU - B3. The quick ambiguity resolution is mainly due to the precise and accurate pseudoranges and phases observations of the Rogue GPS receivers as well as the relatively small remaining errors and biases at this time period. Because of the precise and accurate pseudoranges, a small but reliable ambiguity searching space can be established which in turn leads to fast and reliable resolution of the ambiguities. Note also from Table 4.14 that the same number of initial ambiguity sets to be tested and the same epoch of ambiguity resolution do not necessarily lead to the same CPU times. Finally, the main question here is whether the fixed integer ambiguities given in Tables 4.15 and 4.16 are really the correct ones. In the following, several verification techniques are utilized to answer this question.

#### 4.3.4. Verification of on-the-fly ambiguity resolution results.

There are few methods that can be used to verify the correctness of the integer ambiguities fixed by the on-the-fly ambiguity resolution technique as listed in Tables 4.15 and 4.16. The correctness of the wide-lane and narrow-lane integer ambiguities will be investigated by employing all possible methods.

The *first method* is to check the misclosure of the integer ambiguities. It is obvious that, for the correct double-difference integer ambiguities either wide-lane or narrow-lane, each of them will satisfy the following relation:

$$\begin{aligned}
 \nabla\Delta N(\text{PGC-UCLU}) - \nabla\Delta N(\text{PGC-B1}) + \nabla\Delta N(\text{UCLU-B1}) &= 0, \\
 \nabla\Delta N(\text{PGC-UCLU}) - \nabla\Delta N(\text{PGC-B2}) + \nabla\Delta N(\text{UCLU-B2}) &= 0, \\
 \nabla\Delta N(\text{PGC-UCLU}) - \nabla\Delta N(\text{PGC-B3}) + \nabla\Delta N(\text{UCLU-B3}) &= 0.
 \end{aligned}
 \tag{4.3}$$

If each of the wide-lane or narrow-lane ambiguities from Tables 4.15 and 4.16 are inserted into the above equations, all of the ambiguities satisfy the equations, i.e., all the ambiguity misclosures are equal to zero. This means that the integer ambiguities are probably the correct ones. Theoretically speaking, zero misclosure of the ambiguities will also lead to a relatively small misclosure of the relative coordinates. Figure 4.11 shows that this is indeed the case. In this figure, the misclosure of the relative coordinates are represented by the distance between two relative coordinates of the antenna as shown by the example in Figure 4.10.

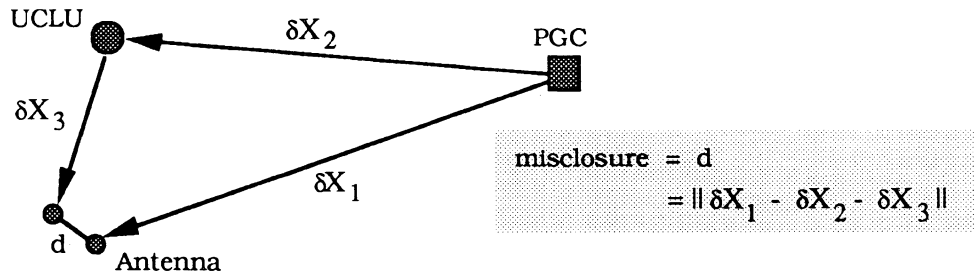


Figure 4.10. The misclosure of the relative coordinates.

The misclosures shown in Figures 4.11 are computed using L1 and L2 fixed ambiguity solutions. The integer ambiguities of L1 and L2 signals in this case are computed from the wide-lane and narrow-lane integer ambiguities given in Tables 4.15 and 4.16, using equations (3.55) and (3.56). Note from Figure 4.11 that the misclosures are in the order of a few millimetres, which are consistent with the expected noise level of the phase observations.

It should be emphasized here, however, that equation (4.3) and the results shown in Figure 4.11 cannot definitely assure the correctness of the integer ambiguities since certain error combinations in the integer ambiguities can still yield zero ambiguity misclosures and relatively small misclosures of the relative coordinates. Therefore, other verification methods have to be employed to ensure the correctness of the integer ambiguities.

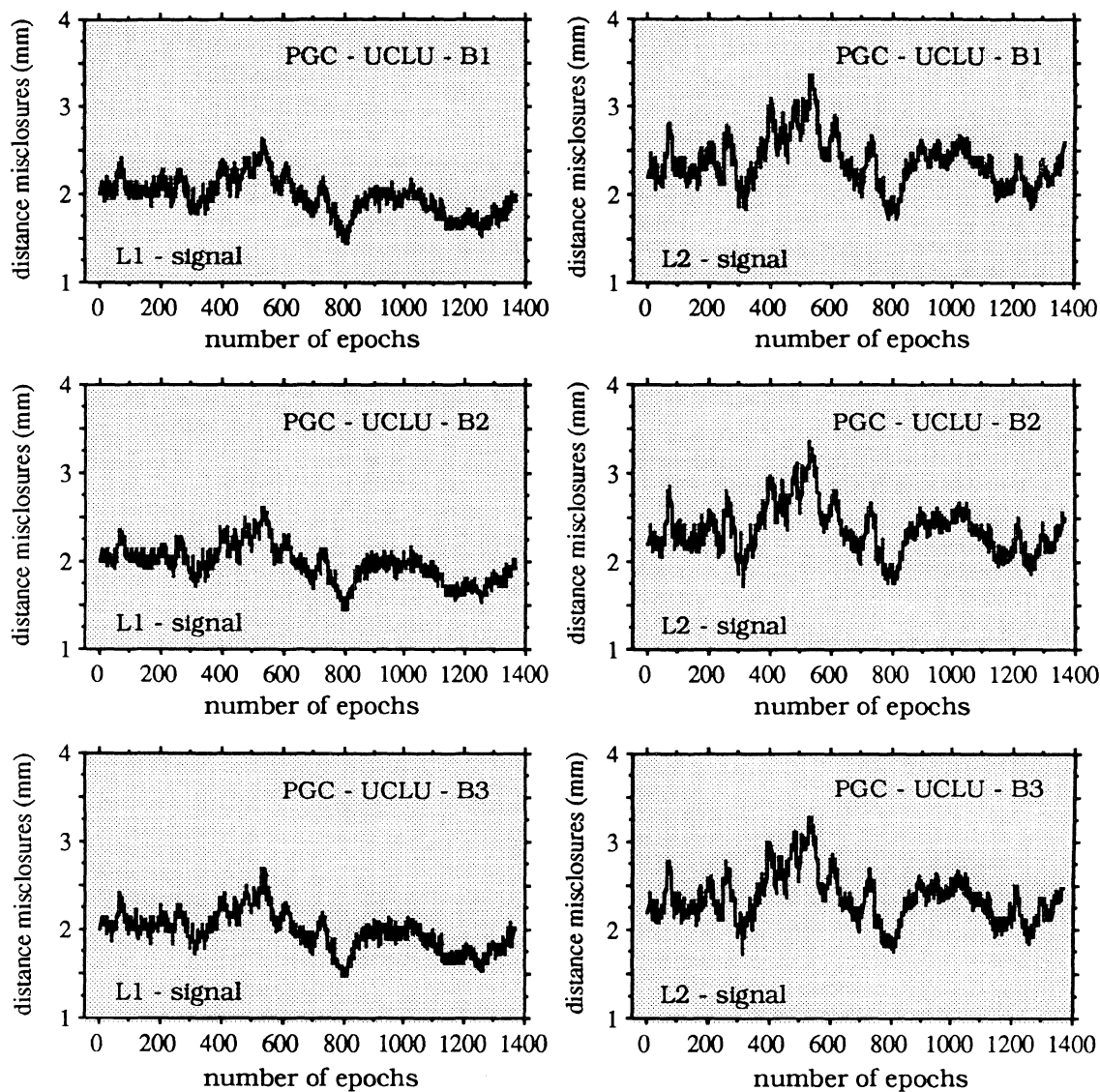


Figure 4.11. The (distance) misclosures of the relative coordinates, based on L1 and L2 fixed ambiguity solutions.

The *second method* of ambiguity verification is used to check the correctness of the wide-lane and narrow-lane integer ambiguities by using only the whole 22 minutes of GPS data available. This is done firstly for the wide-lane ambiguities related to all baselines. Because of its relatively long wavelength ( $\approx 86.2$  cm), the wide-lane ambiguities are more reliable and much easier to fix. Using these integer wide-lane ambiguities and the

geometric-free linear combination of phase observations, the narrow-lane ambiguities related to the three antennas are then estimated.

In this verification method, the wide-lane ambiguities computed based only on the narrow-lane pseudoranges ( $P_{\Sigma}$ ) and wide-lane carrier ranges ( $L_{\Delta}$ ), averaged over 22 minute time period (1365 epochs), are used for comparison. At each epoch  $t$ , the wide-lane ambiguities is computed using the following relation:

$$\nabla\Delta N_{\Delta}(t) = \frac{\nabla\Delta P_{\Sigma}(t) - \nabla\Delta L_{\Delta}(t)}{\lambda_{\Delta}} \quad (4.4)$$

The ambiguities estimated using the above equation will be mainly contaminated by the pseudoranges noise and multipath if it exists. The geometric ranges, ephemeris errors, and the tropospheric and ionospheric delays are canceled out by the differencing between the narrow-lane pseudoranges and wide-lane carrier ranges, as can be seen from equations (I.23) and (I.24) in Appendix I. Time averaging is employed in this case to suppress the effects of pseudoranges noise and multipath (if it exists), as can be shown by an example in Figure 4.12.

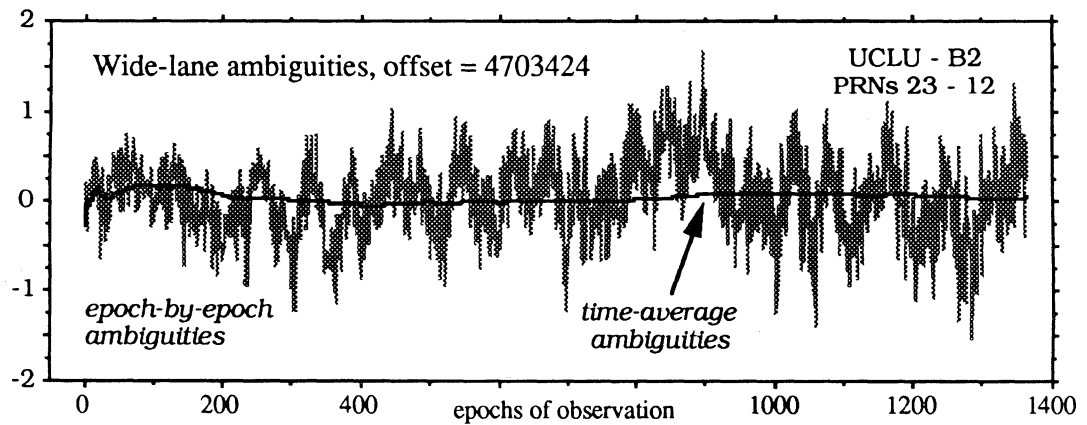


Figure 4.12. Epoch-by-epoch and time average wide-lane ambiguities.



Note from this figure that time averaging significantly reduces the effects of the noise and multipath-like signatures in the observations. The other double-difference wide-line ambiguities, related to all baselines and all satellites, exhibit more or less the same characteristics as the example shown in figure 4.12. The real values of the 22 minute averages are tabulated in Table 4.17. Notably, these real ambiguities are very close to the corresponding integer ambiguities given in Table 4.15, indicating that the wide-lane integer ambiguities listed in Table 4.15 should be the correct ones.

Table 4.17. Double-difference 22 minute-averaged wide-lane ambiguities.

Baseline	PRNs : 15 - 12	PRNs : 21 - 12	PRNs : 23 - 12	PRNs : 11 - 12
PGC - B1	-783967.91	-1081645.91	5559792.14	-1677890.94
PGC - B2	-520117.83	-1331437.90	5692825.15	-1966102.83
PGC - B3	-175455.90	-1144856.92	5049569.15	-1767812.94
UCLU - B1	-2367457.01	-2075739.97	4570391.04	-2634162.94
UCLU- B2	-2103606.94	-2325531.96	4703424.05	-2922374.83
UCLU - B3	-1758945.07	-2138950.98	4060168.05	-2724084.95
PGC - UCLU	1583489.10	994094.06	989401.10	956272.00
B1 - B2	263850.07	-249791.98	133033.01	-288211.89
B1 - B3	608512.00	-63211.01	-510222.99	-89922.00
B2 - B3	344661.93	186580.98	-643256.00	198289.89

The estimated double-difference wide-lane real-ambiguities related to all antennas (B1, B2, and B3) on the buoy given in Table 4.17 can also be used to verify the wide-lane ambiguities fixed by the on-the-fly ambiguity resolution technique. Table 4.18 lists the ambiguities related to antennas B1, B2, and B3 computed from the ambiguities in Table 4.15 as follows:

$$\begin{aligned}
\nabla\Delta N(B1-B2) &= \nabla\Delta N(PGC-B2) - \nabla\Delta N(PGC-B1) = \nabla\Delta N(UCLU-B2) - \nabla\Delta N(UCLU-B1) , \\
\nabla\Delta N(B1-B3) &= \nabla\Delta N(PGC-B3) - \nabla\Delta N(PGC-B1) = \nabla\Delta N(UCLU-B3) - \nabla\Delta N(UCLU-B1) , \\
\nabla\Delta N(B2-B3) &= \nabla\Delta N(PGC-B3) - \nabla\Delta N(PGC-B2) = \nabla\Delta N(UCLU-B3) - \nabla\Delta N(UCLU-B2) .
\end{aligned}
\tag{4.5}$$

The comparison of the double-difference wide-lane integer ambiguities listed in Table 4.18 and the corresponding real-ambiguities in Table 4.17 again suggests that the integer wide-lane ambiguities fixed by the on-the-fly ambiguity resolution technique as listed in Table 4.15 should be the correct integers.

Table 4.18. Double-difference wide-lane integer ambiguities.

Baseline	PRNs : 15 - 12	PRNs : 21 - 12	PRNs : 23 - 12	PRNs : 11 - 12
B1 - B2	263850	-249792	133033	-288212
B1 - B3	608512	-63211	-510223	-89922
B2 - B3	344662	186581	-643256	198290

The narrow-lane ambiguities related to the three antennas can be estimated by using the wide-lane ambiguities given in Table 4.18 and the geometric-free linear combination of phase observations. The double-difference geometric free linear combination ( $\nabla\Delta L_{gf}$ ) of L1 and L2 phases can be by:

$$\nabla\Delta L_{gf} = \nabla\Delta L_1 - \nabla\Delta L_2 = \lambda_1 \cdot \nabla\Delta\phi_1 - \lambda_2 \cdot \nabla\Delta\phi_2 . \tag{4.6}$$

In the above equation, the geometric ranges are eliminated by differencing the L1 with the L2 carrier ranges. When the baselines are very short, as in the case of antennas B1, B2, and B3 here, the geometric free linear phase combinations will mainly be contaminated by

the phase noise, assuming there is no multipath. In this case, the following relation can then be established :

$$\lambda_1 \cdot \nabla \Delta \phi_1 - \lambda_2 \cdot \nabla \Delta \phi_2 \approx \lambda_2 \cdot \nabla \Delta N_2 - \lambda_1 \cdot \nabla \Delta N_1 \quad . \quad (4.7)$$

By combining the above equation with equations (3.55) and (3.56), the following relation for estimating epoch-by-epoch narrow-lane ambiguities can be formulated:

$$\nabla \Delta N_{\Sigma} = \frac{2 \cdot f_2}{(f_1 - f_2)} \cdot \nabla \Delta \phi_1 - \frac{2 \cdot f_1}{(f_1 - f_2)} \cdot \nabla \Delta \phi_2 + \frac{(f_1 + f_2)}{(f_1 - f_2)} \cdot \nabla \Delta N_{\Delta} \quad . \quad (4.8)$$

By inserting the frequencies of L1 and L2 signals into the above equation, the following formulation is obtained:

$$\nabla \Delta N_{\Sigma} = \frac{1}{17} \cdot (120 \cdot \nabla \Delta \phi_1 - 154 \cdot \nabla \Delta \phi_2 + 137 \cdot \nabla \Delta N_{\Delta}) \quad . \quad (4.9)$$

In order to suppress the effects of the observation noise and multipath (if it exists), the time averaging on the epoch-by-epoch estimates of the narrow-lane ambiguities are performed. An example of the two estimates as a function of time is shown in Figure 4.13.

The real-values of the 22 minute averaged narrow-lane ambiguities related to the three antennas and all satellites are tabulated in Table 4.19. These real ambiguities are very close to their corresponding integer ambiguities, computed with equation (4.5) and given in Table 4.20. These results indicate that the narrow-lane integer ambiguities listed in Table 4.16 are most likely the correct ones.

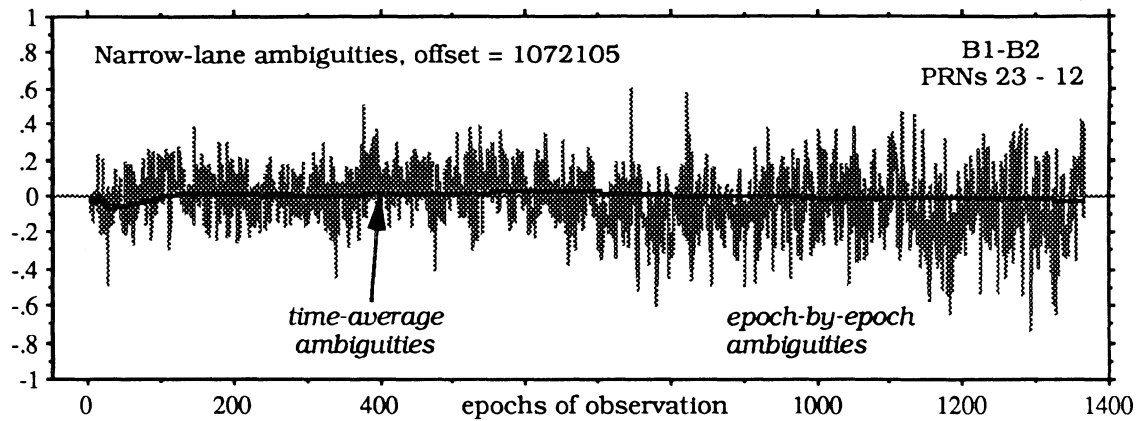


Figure 4.13. Epoch-by-epoch and time average narrow-lane ambiguities.

Table 4.19. Double-difference 22 minute-averaged narrow-lane ambiguities.

Baseline	PRNs : 15 - 12	PRNs : 21 - 12	PRNs : 23 - 12	PRNs : 11 - 12
B1 - B2	2126345.93	-2013000.03	1072104.98	-2322632.14
B1 - B3	4903896.00	-509401.01	-4111773.04	-724667.99
B2 - B3	2777550.06	1503599.02	-5183878.01	1597964.15

Table 4.20. Double-difference narrow-lane integer ambiguities.

Baseline	PRNs : 15 - 12	PRNs : 21 - 12	PRNs : 23 - 12	PRNs : 11 - 12
B1 - B2	2126346	-2013000	1072105	-2322632
B1 - B3	4903896	-509401	-4111773	-724668
B2 - B3	2777550	1503599	-5183878	1597964

The *third method* that is used to further verify the correctness of the integer ambiguities utilizes the known distances between the antennas on the buoy. Using the integer ambiguities listed in Tables 4.15 and 4.16, the epoch-by-epoch coordinates of the three

antennas are computed independently with respect to monitor stations PGC and UCLU, respectively. These coordinates of the antennas are then used to compute the distances between the antenna at every epoch. The epoch-by-epoch differences between the computed distances and the corresponding known distance between the antennas are used to assess the correctness of the ambiguities. Theoretically speaking, the correct ambiguities should lead to relatively small distance differences, and the incorrect ambiguities should lead to relatively large distance differences.

In order to make sure that the wide-lane and narrow-lane ambiguities have been both correctly resolved, the five signals, i.e., wide-lane, narrow-lane, L1-signal, L2-signal, and ionospheric free linear combination are used to analyze these distance differences. The time series and histogram of the distance differences off all these signals and baselines are given in Appendix IV. As an example, the histograms of the distance differences related to L1 and L2 signals are shown in Figures 4.14 and 4.15.

The figures show that the distance differences related to L1 and L2 signals in all baselines are always less than a centimetre at all epochs, and their mean values are in the order of a few millimetres. This fact suggests the correctness of the wide-lane and narrow-lane integer ambiguities fixed by the on-the-fly ambiguity resolution technique. If the integer wide-lane and narrow-lane ambiguities are incorrect as many as  $\delta\nabla\Delta N_{\Delta}$  and  $\delta\nabla\Delta N_{\Sigma}$  cycles, then the L1 and L2 integer ambiguities will also be incorrect with the following number of cycles :

$$\begin{aligned}\delta\nabla\Delta N_1 &= (\delta\nabla\Delta N_{\Delta} + \delta\nabla\Delta N_{\Sigma})/2 \quad , \\ \delta\nabla\Delta N_2 &= (\delta\nabla\Delta N_{\Sigma} - \delta\nabla\Delta N_{\Delta})/2 \quad .\end{aligned}\tag{4.10}$$

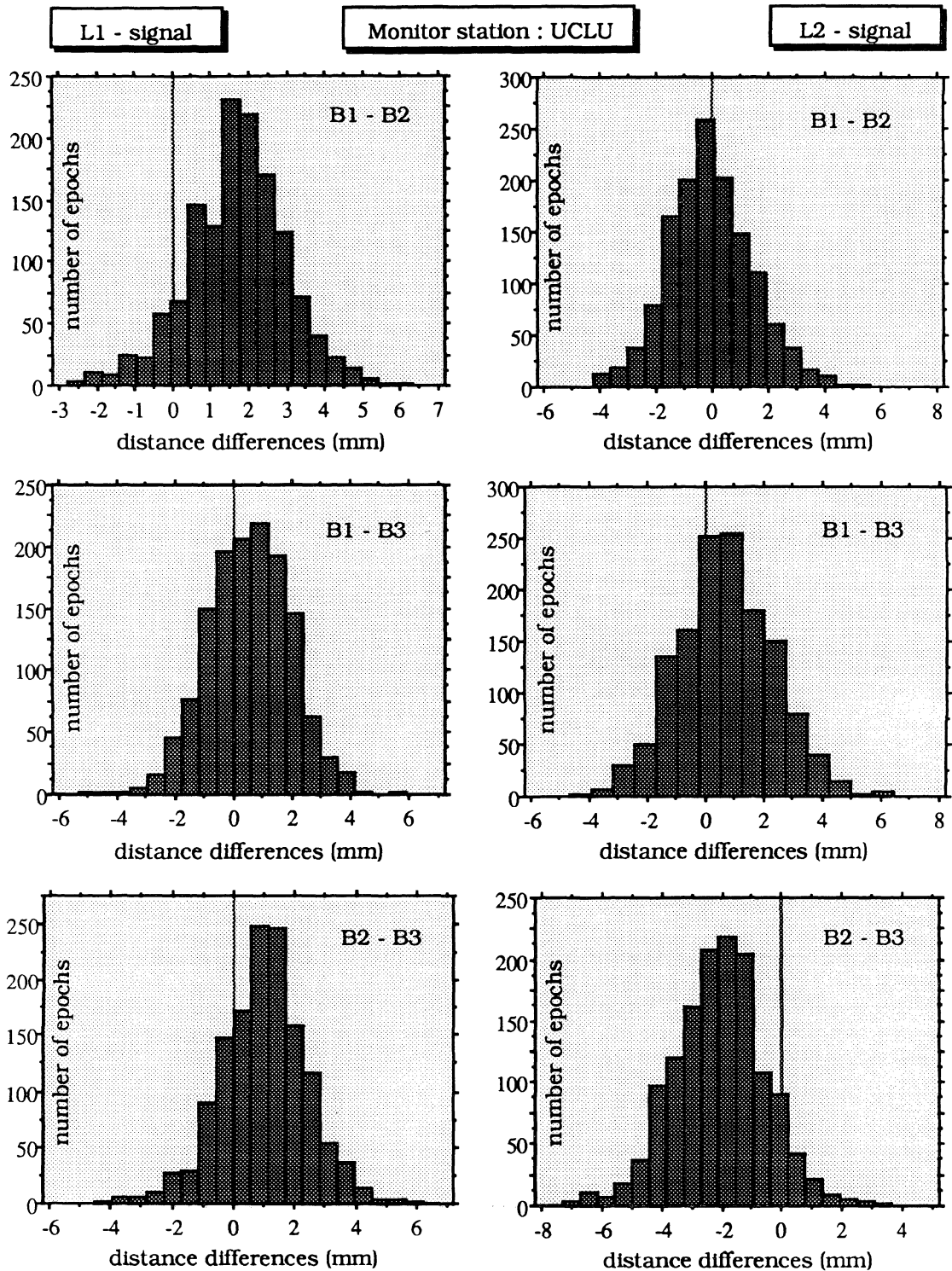


Figure 4.14. The differences of the antennas' distances on the buoy between the distances derived from the fixed ambiguity solution and their 'known' distances (left : L1-signal, right : L2-signal, monitor station : UCLU).

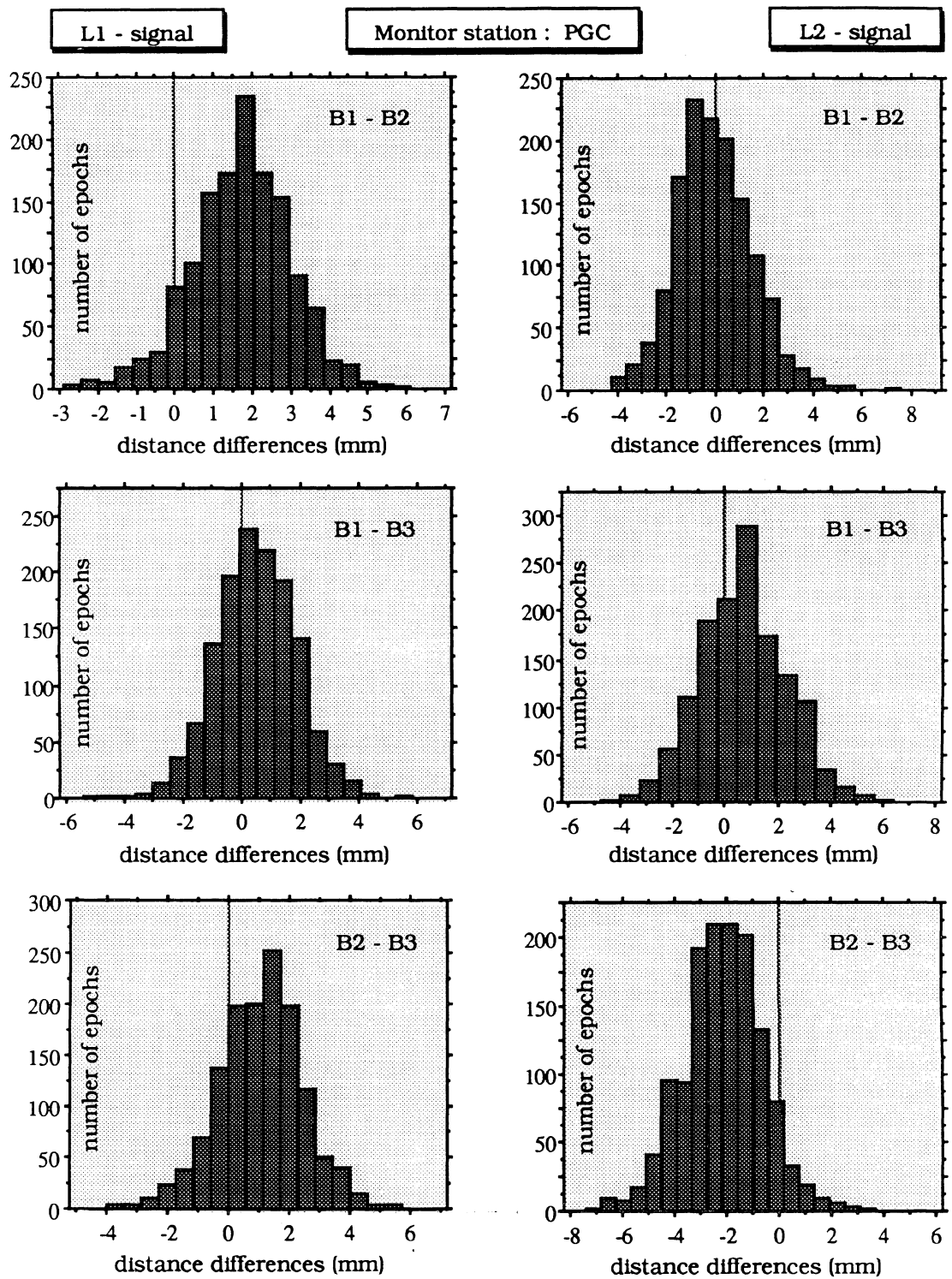


Figure 4.15. The differences of the antennas' distances on the buoy between the distances derived from the fixed ambiguity solution and their 'known' distances (left : L1-signal, right : L2-signal, monitor station : PGC).

In the above equations, the even-odd relation also exists between the errors in wide-lane and narrow-lane integer ambiguities as in the case of the nominal integer ambiguities itself. From the above equation, it can be seen that any combination of errors in wide-lane and/or narrow-lane integer ambiguities will always lead to an error in at least L1 or L2 integer ambiguities. The integer ambiguities of L1 and L2 signals will both be correct only when both the wide-lane and narrow-lane ambiguities are also correct.

In order to appreciate the results shown in Figures 4.14 and 4.15, the histogram and time series of the distances differences related to the incorrect integer ambiguities are also shown in Figure 4.16. These distance differences are related to monitor station UCLU, antennas B1 and B2, and L1 and L2 signals. The correct double-difference wide-lane integer ambiguities are used, but the double-difference narrow-lane integer ambiguities related to antenna B1 and satellites 12 and 15 are intentionally set to be in error of 2 cycles. This is the smallest error that can occur with narrow-lane integer ambiguities. This will lead to an error of 1 cycle in the integer ambiguities of L1 and L2 signals, respectively. Note from Figure 4.16 that the error of only one cycle in the ambiguities of L1 and L2 signals enlarges the differences of the antenna's distances up to about 15 to 20 cm and destroy the 'normality' of the histogram as shown in Figure 4.14.

Finally, it should be noted that the ambiguity verification techniques are transparent to certain case of ambiguity resolution failure. The verification techniques cannot detect failure when the fixed integer ambiguities related to all baselines (PGC-UCLU, PGC-B1, PGC-B2, PGC-B3, UCLU-B1, UCLU-B2, and UCLU-B3) and the same satellites, are simultaneously in error with the same signs and magnitudes. Although this scenario of ambiguity resolution failure is unlikely to happen in our example, however, one should keep this problem in mind when processing similar data sets.



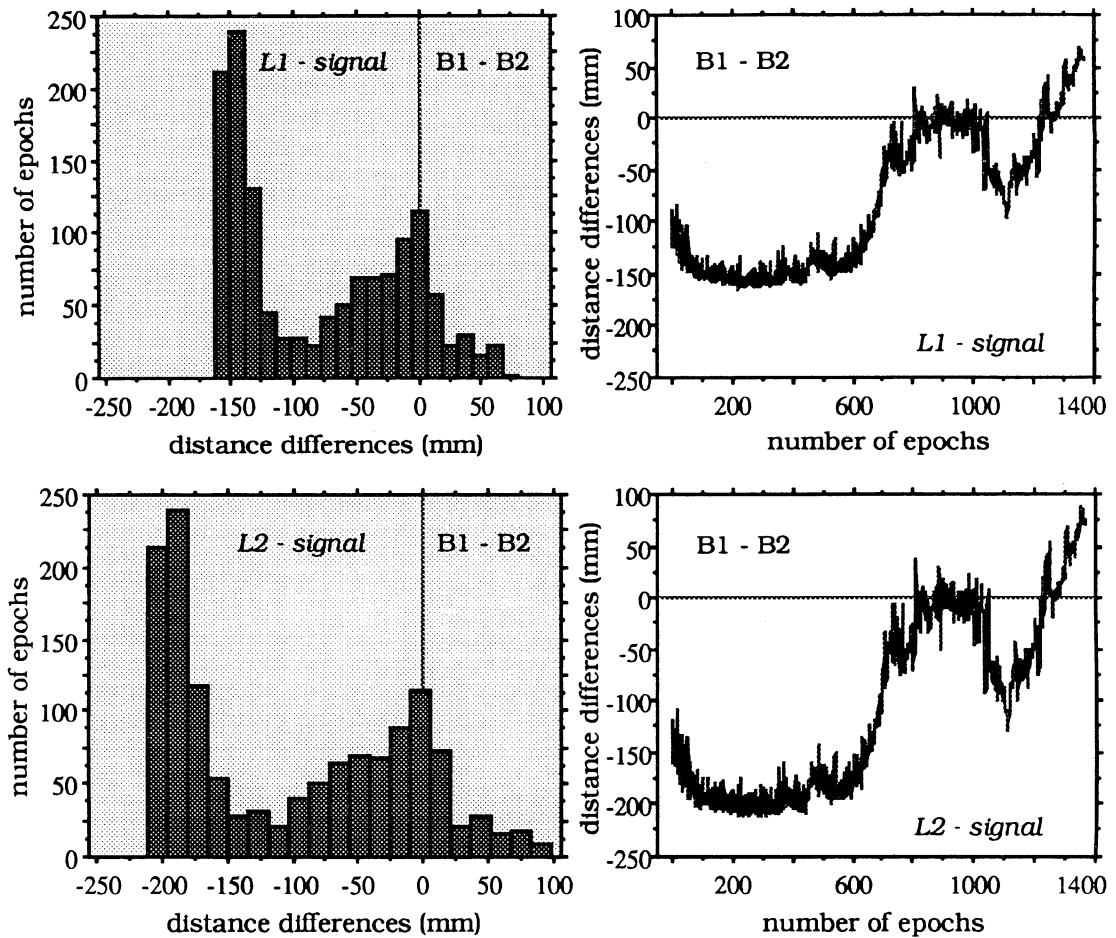


Figure 4.16. The differences of the antennas' distances on the buoy between the distances derived from the fixed ambiguity solution and their 'known' distances, in the case that the double-difference integer narrow-lane ambiguities related to antenna B1 and satellites 12 and 15 are in error of 2 cycles (monitor station : UCLU).

#### 4.3.5. Cautionary remarks.

It should be emphasized that the quick ambiguity resolution of Rogue kinematic data is due to the mutual combination of several factors. Some of them are the precise and accurate dual-frequency P-code pseudoranges and phases observations collected by the Rogue GPS receivers, low residual observation errors and biases during the first period of the session, correct choice of the primary satellites and between-satellite differencing strategy, and appropriate values of the parameters used for identifying the correct ambiguities. For

appropriate values of the parameters used for identifying the correct ambiguities. For different processing scenarios with respect to these factors, the results could be different. In this case, slow ambiguity resolution or even failure in resolving the correct ambiguities could occur. This fact will be investigated and analyzed in the following two chapters.

## Chapter 5

# COMPUTATIONAL ASPECTS OF THE INTEGRATED ON-THE-FLY AMBIGUITY RESOLUTION TECHNIQUE

---

---

This chapter discusses the computational characteristics of the integrated on-the-fly ambiguity resolution technique. The construction of the ambiguity searching space and the implementation of the validation and rejection criteria are two parts of the algorithm which will be examined. Their influences on the computation and observation times of the ambiguity resolution are investigated. In order to get results which closely reflect the algorithmic impacts, the real GPS zero baseline data is used for investigation. The Rogue real-kinematic data processed in the previous chapter, however, will also be utilized in this case. All the computation is executed using IBM ES9000 MOD320 mainframe computer.

The speed of ambiguity resolution is explained in terms of *observation times* and *computation times*. The observation times are the number of observations (epochs) required to resolve the ambiguities, and the computation times are the CPU times required for the processing.

### **5.1. The ambiguity searching space construction.**

As stated in the previous chapter, constructing the optimal ambiguity searching space is important for fast and reliable on-the-fly ambiguity resolution. In addition to containing the

correct ambiguity sets, the shape and size of the ambiguity searching space should be carefully chosen. Their interactions with influencing parameters such as the satellite geometry, should be properly taken into consideration.

### **5.1.1. The shape of ambiguity searching space**

In terms of *the shape of ambiguity searching space*, it was conceptually explained in Chapter 3 that the ellipsoid is more optimal than the cube, and therefore should be used. Mathematically speaking, it is more rigorous and realistic in representing the effects of the observation (satellite-user-signal) geometry. Furthermore, the ellipsoidal searching space contains fewer ambiguity sets to be tested, which results in faster computation time, and usually leads to faster observation times of ambiguity resolution.

Table 5.1 shows the on-the-fly ambiguity results for the zero-baseline data and Rogue kinematic data shown in previous chapter in comparison with the results obtained if a cube instead of an ellipsoid is used as the shape of the ambiguity searching space. With zero-baseline data, the initial ambiguities are estimated either using the code-derived position (dual-frequency # 1) or the extrawidelaning technique (dual-frequency #2). With Rogue kinematic data, only the code-derived position is used to estimate the initial ambiguities.

The results in Table 5.1 show that the ellipsoidal searching space always leads to faster computation times of ambiguity resolution. The observation times of resolution, however, are not always faster, particularly in the case of dual-frequency data. The advantages of the ellipsoidal over the cube searching space varies as a function of several factors, such as the size of the searching spaces, the wavelength of the signal, the primary satellites used, and satellite geometry. The effects of the primary satellites in this case are shown in Figure 5.1. The results are given for both, single and dual-frequency cases from the zero-baseline data, and they are computed using the same values of the identification process parameters used

in Chapter 4. The results in this figure show that the advantages of the ellipsoidal over the cube searching space will vary as a function of the primary satellites used. This in a way suggests that for fast ambiguity resolution, one should judiciously choose the primary satellites to be used, which will be explained later in the next chapter. The other effects of the primary satellites on the ambiguity resolution will also be investigated in more detail in the next chapter.

Table 5.1. The on-the-fly ambiguity resolution results as a function of the shape of ambiguity searching space

Trimble Geodestist zero-baseline data and Rogue kinematic data	number of initial ambiguity sets		CPU times in milliseconds		epoch of ambiguity resolution	
	<i>Cube</i>	<i>Ellipsoid</i>	<i>Cube</i>	<i>Ellipsoid</i>	<i>Cube</i>	<i>Ellipsoid</i>
Single-frequency	7875	1029	879	527	33	16
Dual-frequency # 1	693	97	103	73	2	2
Dual-frequency # 2	2197	1159	150	127	2	2
PGC - B1	125	37	94	79	5	4
PGC - B2	125	37	87	77	5	4
PGC - B3	125	37	89	78	5	4
UCLU - B1	125	37	72	68	3	3
UCLU - B2	125	37	77	74	4	4
UCLU - B3	125	37	58	55	1	1
PGC - UCLU	125	37	84	79	4	4

It should be emphasized that, for different values of the identification process parameters, different sizes of the searching space, and different satellite geometry, the results shown in Table 5.1 and Figure 5.1 could be different. The general trend, however, will remain more or less the same, and therefore, for fast ambiguity resolution, the ellipsoidal ambiguity searching space should always be used rather than the cube.

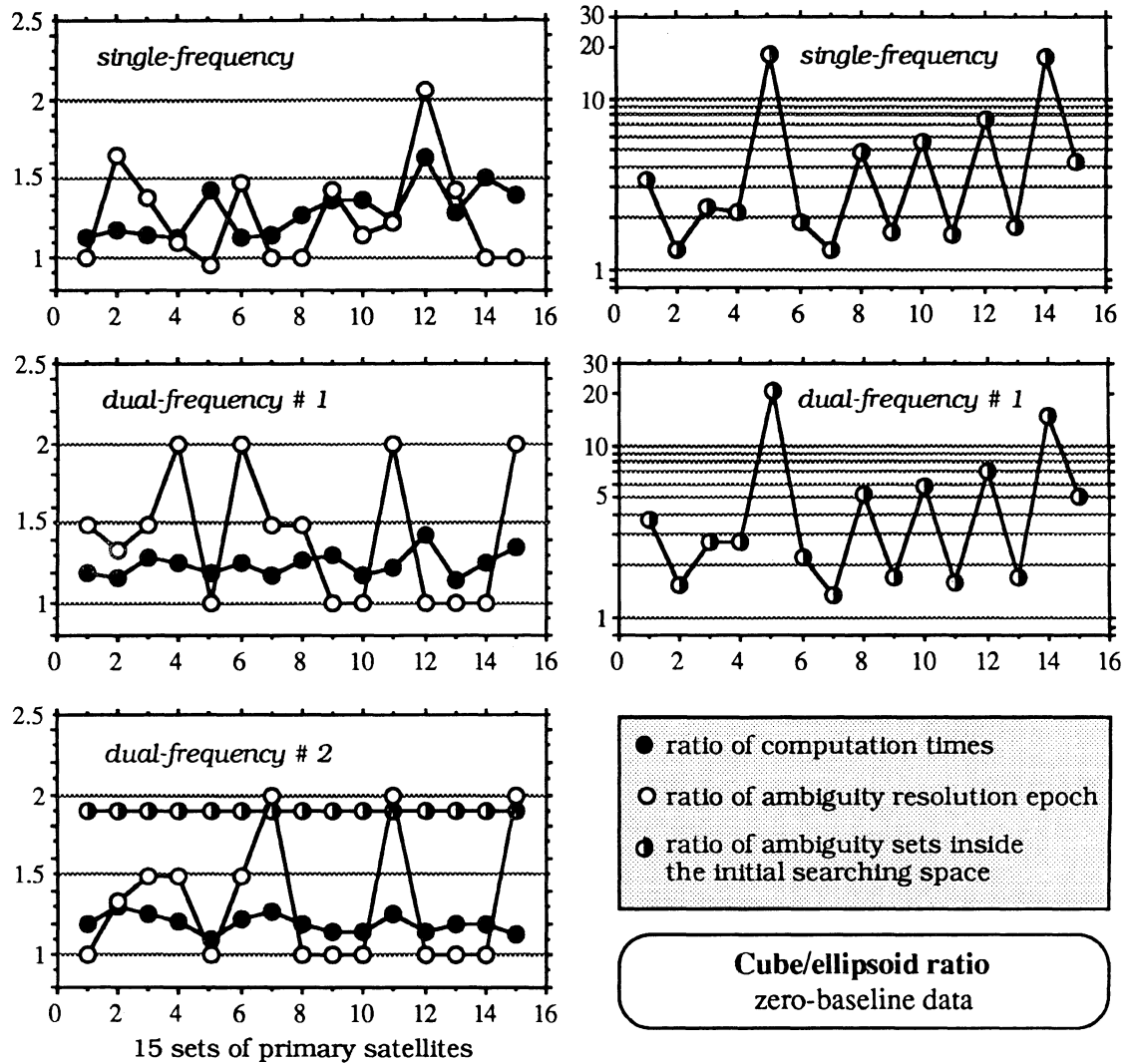


Figure 5.1. The effects of using the ellipsoidal instead of the cube ambiguity searching space on on-the-fly ambiguity resolution results.

### 5.1.2. The size of the ellipsoidal searching space.

Besides the shape, the size of the searching space is also an important parameter in the ambiguity resolution process. The size determines the number of ambiguity sets to be tested, and therefore affects the computation and observation times of ambiguity resolution. The size of ellipsoidal searching space depends on several parameters, mainly the

confidence level used to size the ellipsoid, precision of the observations, and observation geometry.

The impact of different *confidence levels* of the ellipsoid on the size of the searching space and the ambiguity resolution times is shown by the example given in Tables 5.2 and 5.3.

The primary satellites and the parameter's values of the validation and rejection criteria used in deriving this example are the same as those used in Chapter 4.

Table 5.2. The effects of different confidence levels of the ellipsoidal searching space on the ambiguity resolution times (zero-baseline data).

confidence level	zero-baseline data single-frequency			zero-baseline data dual-frequency # 1			zero-baseline data dual-frequency # 2		
	A	B	C	A	B	C	A	B	C
70.0 %	205	213	14	25	52	1*	229	67	1
80.0 %	309	264	14	29	53	1*	331	83	2
90.0 %	475	331	14	41	53	1*	531	97	2
95.0 %	651	411	15	59	65	2	725	105	2
96.0 %	709	449	16	65	66	2	749	108	2
97.0 %	777	467	16	73	66	2	869	112	2
98.0 %	877	493	16	79	67	2	941	116	2
99.0 %	1029	527	16	97	73	2	1159	127	2
99.5 %	1231	597	18	125	77	2	1279	129	2
99.9 %	1817	728	18	177	84	2	1875	152	2

\* denotes the resolution failures, i.e. the ambiguities are fixed to the incorrect integers.  
A = number of initial ambiguity sets inside the initial searching space.  
B = CPU times in milliseconds. C = epoch of ambiguity resolution.

Note from Tables 5.2 and 5.3 that increasing the size of the searching space leads to slower computation time of ambiguity resolution, and vice versa. The corresponding observation times of resolution, however, is not always faster with a decrease in the searching space

size. The size of the searching space should not be too small, since it may not encompass the correct ambiguities, which in turn may lead to the ambiguity resolution failure, as shown in Table 5.2. However, it should not also be too large, since it will slow down the computation times, and in some cases lead to the slower observation times of ambiguity resolution, as shown in Tables 5.2 and 5.3. Based on the data processing done during the investigations, the confidence level between 0.95 to 0.99, in general, seems to be the most appropriate to use, both from the views of efficiency and reliability.

Note also from Table 5.2 that, at a certain confidence level, the size of the ellipsoidal searching space is larger when the extrawidelaning technique is used to estimate the initial ambiguities than when the code-derived position is used. From an efficiency point of view, therefore, the extrawidelaning technique is less preferable for constructing the initial searching space.

The size of the ellipsoidal searching space will also depend on *the standard deviations* used to represent the precision of the observations, particularly the code (pseudorange) observations. The actual standard deviations of the observations are difficult to know exactly, although their values may be predicted based on the theoretical precision of the observation and the expected level of the remaining errors and biases in the observations. In this case, it can be expected that different users may assign different standard deviations to the same set of observations, depending on their understanding and experience.

Tables 5.4 and 5.5. give the examples of the effects of different chosen values of standard deviations of the pseudoranges on the size of initial ambiguity searching space and their corresponding computation and observation times of ambiguity resolution. The results are based on the zero-baseline data and Rogue kinematic data. The same primary satellites and the same values of the validation and rejection criteria parameters, as in the case of Tables



5.2 and 5.3, are used in this case. The code-derived position is used to estimate the initial ambiguities and a 99 % confidence level is used to size the ellipsoidal searching space.

Table 5.3. The effects of different confidence levels of the ellipsoidal searching space on the ambiguity resolution times (Rogue kinematic data).

confidence level	PGC - antenna B1			UCLU - antenna B1		
	A	B	C	A	B	C
70.0 %	7	59	2	7	50	1
80.0 %	13	62	2	13	59	2
90.0 %	15	63	2	15	59	2
95.0 %	19	71	3	19	66	3
96.0 %	21	71	3	21	66	3
97.0 %	23	71	3	23	66	3
98.0 %	27	78	4	27	66	3
99.0 %	37	79	4	37	68	3
99.5 %	47	90	5	47	69	3
99.9 %	65	93	5	65	71	3

\* denotes the resolution failures, i.e. the ambiguities are fixed to the incorrect integers.  
A = number of initial ambiguity sets inside the initial searching space.  
B = CPU times in milliseconds. C = epoch of ambiguity resolution.

The results in Tables 5.4 and 5.5 show that different chosen values used to represent the standard deviation of the observations quite significantly affect the searching space size and consequently the speed and reliability of ambiguity resolution. These values not only affect the searching space, but also the acceptance volume of the validation and rejection criteria. The different values of standard deviations could lead to either fast or slow ambiguity resolution and even failure in ambiguity resolution. Therefore, their values should always be chosen judiciously to represent as close as possible the real precision of the observations in order to achieve not only fast but also reliable ambiguity resolution.

Table 5.4. The effects of the observation precision on the ambiguity resolution times (Trimble Geodesist zero-baseline data).

standard deviations in m		single-frequency			dual-frequency		
L1-C/A code	L2-P code	A	B	C	A	B	C
0.50	0.25	39	109	11*	3	79	4
0.75	0.50	131	246	23	15	67	3
1.00	0.75	297	221	14	37	57	2
1.50	1.00	1029	527	16	97	73	2
2.00	1.50	2357	1227	33	237	110	3
2.50	2.00	4507	2083	33	485	207	5

\* denotes the resolution failures, i.e. the ambiguities are fixed to the incorrect integers.  
A = number of initial ambiguity sets inside the initial searching space.  
B = CPU times in milliseconds. C = epoch of ambiguity resolution.

Table 5.5. The effects of the observation precision on the ambiguity resolution times (Rogue kinematic data).

standard deviations in m		FGC - antenna B1			UCLU - antenna B1		
L1-P code	L2-P code	A	B	C	A	B	C
0.10	0.15	1	45	1	1	44	1
0.20	0.30	17	69	3	17	59	2
0.25	0.40	37	94	4	37	68	3
0.30	0.45	59	96	5	59	78	4
0.40	0.60	129	149	9	129	100	5
0.50	0.75	237	233	15	237	111	4
0.60	0.90	429	341	21	429	134	2
0.70	1.00	587	461	28	587	175	3
0.80	1.20	919	557	15	917	271	3
1.00	1.5	1781	935	16	1783	457	4

Finally, it should also be noted that the size of the ellipsoidal searching space will also depend on the precision of different observations to different satellites is formulated. In the case of the zero-baseline data in Table 5.4, all observations are considered to have the same

precision. In the case of Rogue kinematic data in Table 5.5, however, the precision of the observations are formulated to be elevation-dependent. The other assumptions can be expected to yield different sizes of ellipsoidal searching spaces.

As stated, the size of the ellipsoidal searching space will also be governed by observation geometry parameters, such as the primary satellites used, number of satellites and monitor stations, location of satellites, etc. The combined effects of these geometrical parameters on the size of the searching space can be predicted using the values of the ellipsoidal size indicator NAI1 defined by equation (3.17), which is proportional to the volume of the ellipsoid. In computing the values of NAI1, the signal wavelength of 1 m is assumed. Figure 5.2 shows the example of the correlation between the values of the size indicator and the number of the ambiguity sets inside the initial ellipsoidal searching space (NOA).

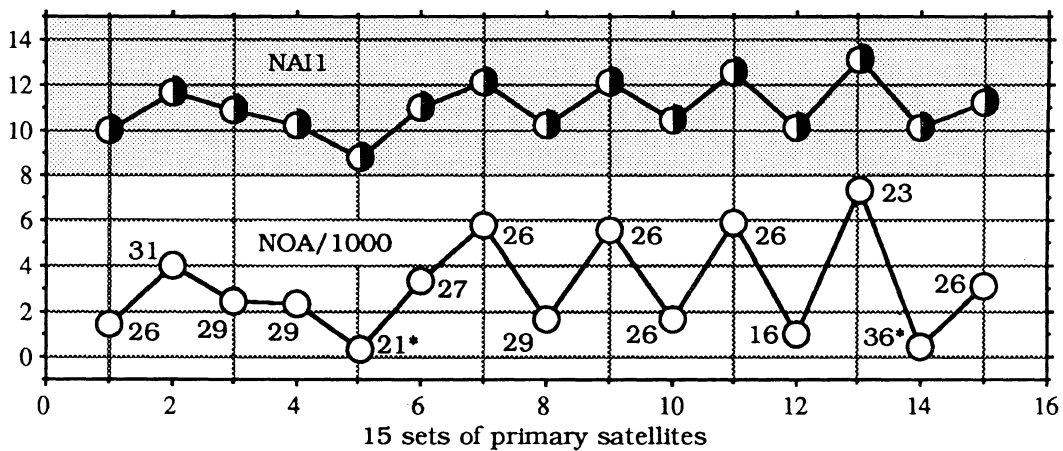


Figure 5.2. The correlation between the values of the ellipsoid size indicator (NAI1) and the number of the ambiguity sets inside the initial ellipsoidal searching space (NOA). The numbers inside the figure are the epoch of ambiguity resolution related to the particular primary satellites. The ambiguity resolution failure is denoted in this case by \*.

The single-frequency zero-baseline data is used with the same values of the identification process parameters, as in the case of Table 5.1. As expected, the results show a positive strong correlation between the values of NAI1 and NOA. It should be noted that the similar

values of NAI1 do not always mean the similar values of NOA, as is shown by the primary satellite sets #1, #4, #12 and #14 in Figure 5.2. This fact is understandable since the number of the ambiguity sets does not depend solely on the size of the ellipsoid, as indicated by the correlation coefficient of the two parameters which is not exactly equal to 1, but 0.966. The shape and orientation of the ellipsoid will also affect the number of ambiguity sets, although their roles are not as major as the role of the ellipsoidal size. Note also from Figure 5.2 that a smaller ellipsoidal searching space does not automatically mean faster observation times of ambiguity resolution. In fact, the smallest size of the searching space causes failure of ambiguity resolution in this case.

More detailed investigation on the geometrical aspects of on-the-fly ambiguity resolution will be presented in the next chapter. At this point, it can be concluded that the size of ambiguity searching space depends on the observation geometry and, for fast and reliable ambiguity resolution, the trade off among the geometrical parameters always has to be exercised.

## **5.2. Implementation of the validation and rejection criteria.**

The proper implementation of the validation and rejection criteria is an important aspect of fast and reliable on-the-fly ambiguity resolution. The most important aspect in this regard is related to the determination of the optimal values for the parameters of the criteria. In order to be optimal, the parameter values should represent the state of satellite geometry, level of noise, and remaining errors and biases in the observations. The other aspect that will also have an effect is the number and type of the rejection criteria being used. Since every criterion can be expected to have a different *identification power*, the number and type of rejection criteria applied will affect the ambiguity resolution times. It should be noted that the identification power of the validation and rejection criterion not only

characterizes how strongly the criterion can reject the incorrect ambiguities, but also how well it can validate and keep the correct ambiguities.

The differences in the power of identification among the criteria are shown by the example given in Table 5.6. It is difficult, however, to quantify the power level of each criterion with respect to the other since it most likely will change with the nature of the satellite geometry and the noise, errors, and biases in the observations. This example is based on Trimble zero-baseline data, and is computed using the same values of the identification process parameters as the example shown in Table 5.1, except that 95 % confidence level is used to size the ellipsoidal searching space, and 0.10 and 0.05 are used as the values of constant in the second and fourth criteria. In this case, PRNs 18, 2, 11, and 6 are used as the primary satellites, and PRN 18 is used as a reference for differencing. With different parameters and different satellite geometry, the figures of the identification power could be different. The general trend, however, is quite difficult to establish in this case.

Table 5.6. The differences in the identification power of the criteria.

NUMBER OF AMBIGUITY SETS	1st epoch of searching	2nd epoch of searching
searching space	937	38
after criteria # 1	910	37
after criteria # 2	445	37
after criteria # 3	442	37
after criteria # 4	208	37
after criteria # 5	196	32
after criteria # 6	158	32
after criteria # 7	84	32
after criteria # 8	55	31

Note also from Table 5.6 that most of the potentially incorrect ambiguities are rejected in the first epoch. At the subsequent epochs therefore the criteria mainly act as the validation criteria of the potentially correct ambiguities. Note also in this table that the number of ambiguities which remain at the first epoch after all validation and rejection criteria is not the same as the number of initial ambiguity sets inside the searching space of the second epoch. This is because some of these first epoch remaining ambiguities are not inside the second epoch ellipsoidal searching space, and therefore they are not considered anymore, as illustrated by Figure 3.7.

Since *different rejection and validation criteria* have different identification power, the number and types of the criteria applied will affect the ambiguity resolution times. The example from 14 cases, as outlined in Table 5.7, is shown in Figure 5.3. The results are based on Trimble zero-baseline data and Rogue kinematic data. The same values of the validation and rejection criteria parameters, as in the case of Tables 5.1, are used in this case. The code-derived position is used to estimate the initial ambiguities and two sets of the primary satellites are considered in this example.

Table 5.7. The criteria implementation cases.

Case #	Application of the criteria (1 = yes, 0 = no) The criteria are ordered from #1 to #8							
1	1	1	1	1	1	1	1	1
2	1	1	1	1	1	1	1	0
3	1	1	1	1	1	1	0	0
4	1	1	1	1	1	0	0	0
5	1	1	1	1	0	0	0	0
6	0	1	1	1	1	1	1	1
7	0	0	1	1	1	1	1	1
8	0	0	0	1	1	1	1	1
9	0	0	0	0	1	1	1	1
10	0	0	0	0	1	0	0	1
11	0	0	0	1	1	0	0	1
12	1	0	1	1	1	0	0	1
13	0	0	0	0	0	1	1	0
14	1	0	1	0	0	1	1	0

From the example shown in Figure 5.3, it can be seen that different criteria will usually lead to different computation times and, quite frequently, to different epochs of ambiguity resolution, especially in the case of single frequency data. Compared to the use of all criteria, the use of some criteria could either mean the same or a slower speed of ambiguity resolution. In certain cases, it could even cause the ambiguity resolution to fail, as shown by the example in Figure 5.3. The failure in this case could happen because a certain incorrect ambiguity set which actually could be rejected by a certain criterion, if this criterion is activated, appears to have the characteristics of the correct ambiguities to the criteria being used. Then, for certain parameter values of the identification process it can be mistakenly fixed as the correct ambiguities. Some criteria only affect the computation times of ambiguity resolution, while others could affect both the computation and observation times. Finally, it should also be pointed out that with different values of the identification process parameters and different observation geometry, the numbers shown in Figure 5.3 will be different. The general trend, however, will be more or less the same, i.e., the use of all rejection criteria will usually lead to the fastest ambiguity resolution, both in terms of computation and observation times.

The parameter values used to execute the validation and rejection criteria will also affect the ambiguity resolution times. Different parameter values will lead to different figures of computation and observation times. Values which yield the fastest computation and observation times should be used. These optimal parameter values, however, are not easy to determine exactly since they depend on several factors. Their estimate values, however, can be predicted by considering the satellite geometry, the wavelength of the working signal, and the expected level of the noise and remaining errors and biases in the observations. The example of the effects of the different sets of the identification process parameter values, as listed in Table 5.8, on the ambiguity resolution times is shown in Figure 5.4. This example is based on Rogue kinematic data. PRNs 11, 12, 21, and 23 are

used as the primary satellites, and PRN 11 is used as a reference for between-satellite observation differencing.

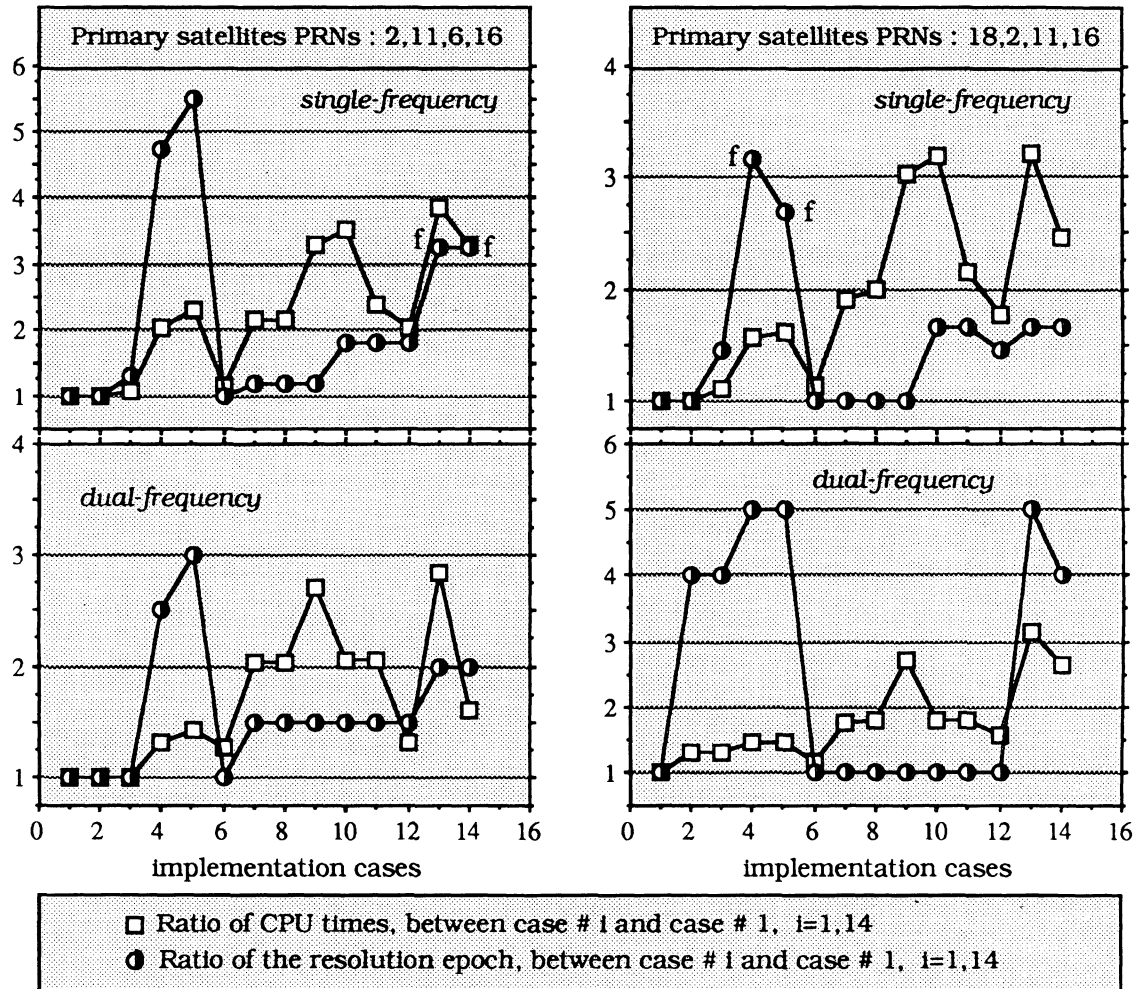


Figure 5.3. The effects of the number and type of the applied rejection criteria on the ambiguity resolution times (zero-baseline data). Letter f in the figure denotes the ambiguity resolution failure for the corresponding implementation case.

Note in Table 5.8 that case #1 is used to represent the *optimistic approach* of assigning the parameter values, and case #9 is used to represent the *pessimistic approach*. The other cases are used to represent the other options between the two extremes. In the optimistic approach, the parameter values of the criteria are set to make the identification process as



tight as possible, in order to reject as many as possible of the potentially incorrect ambiguity sets; while in the pessimistic approach, the parameter values are chosen to make the acceptance volume of the criteria as large as possible in order to avoid rejecting the correct ambiguities at any time.

Table 5.8. The different cases of the identification process parameter values.

Case #	The parameter values of the searching space, the validation & rejection criteria, and the assurance criteria.									
	S	VR #1	VR #2	VR #3	VR #4	VR #5	VR #6	VR #7	VR #8	A
1	0.950	0.950	0.10	0.950	0.05	0.950	0.90	0.970 & 0.980	0.950	0.980
2	0.990	0.950	0.20	0.950	0.05	0.990	0.80	0.960 & 0.970	0.990	0.970
3	0.990	0.950	0.20	0.950	0.05	0.950	0.80	0.960 & 0.970	0.950	0.970
4	0.990	0.950	0.20	0.950	0.05	0.990	0.70	0.950 & 0.960	0.990	0.970
5	0.990	0.960	0.20	0.960	0.05	0.960	0.80	0.960 & 0.970	0.960	0.980
6	0.990	0.970	0.20	0.970	0.05	0.970	0.80	0.960 & 0.970	0.970	0.980
7	0.990	0.980	0.25	0.980	0.05	0.980	0.80	0.960 & 0.970	0.980	0.980
8	0.990	0.990	0.25	0.990	0.05	0.990	0.80	0.960 & 0.970	0.990	0.980
9	0.999	0.990	0.50	0.999	0.25	0.999	0.70	0.950 & 0.960	0.999	0.990

S = the searching space, VR = the validation & rejection criteria, A = the assurance criteria

The results in Figure 5.4 show that different values of the identification parameters lead to different figures of the ambiguity resolution times. Notably from this particular example, neither the optimistic nor the pessimistic approach yield the fastest ambiguity resolution. In both cases, their computation and observation times of ambiguity resolution are longer than the other cases of the identification parameter values. As expected, the CPU times related to the pessimistic approach is the largest. Note also from the figure that assigning the

optimistic values to the parameters of certain criteria, i.e., making the acceptance volume of the criteria relatively small could lead to failure in ambiguity resolution, as shown in cases #3, #5, and #8. Therefore, one should neither be too pessimistic nor too optimistic in assigning the values to each parameter of the identification process. The trade off between the reliability and the speed of the ambiguity resolution should always be exercised in this regard, by considering not only the computational characteristics of the algorithm, but also the satellite geometry and the remaining errors and biases in the observations.

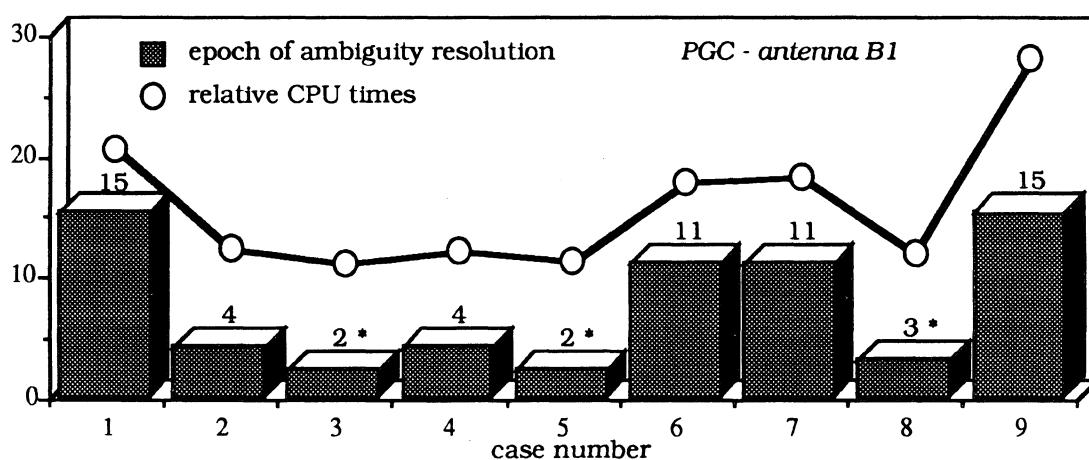


Figure 5.4. The effects of different values of the identification process parameters on the observation and computation times of ambiguity resolution (Rogue kinematic data). The asterisk sign \* denotes the ambiguity resolution failure.

# GEOMETRICAL ASPECTS OF ON-THE-FLY AMBIGUITY RESOLUTION

---

---

The performance of on-the-fly ambiguity resolution is not only affected by the ambiguity resolution algorithm and the parameters used to execute it, but theoretically speaking, it should also be affected by observation geometry. In this chapter, the geometrical aspects of on-the-fly ambiguity resolution are investigated and analyzed. The investigation is done with respect to certain geometrical parameters, which will be outlined in the following sub chapter. The real static and kinematic GPS data which have been partly processed in the previous chapters are used to show the effects of these geometrical parameters on on-the-fly ambiguity resolution.

### **6.1. Geometrical parameters of on-the-fly ambiguity resolution**

The performance of the integrated on-the-fly ambiguity resolution technique will depend on the geometry of observation, i.e., the geometry related to all components of observation, such as satellites, monitor stations, user, and signal being observed. In order to investigate the impacts of the observation geometry on on-the-fly ambiguity resolution, some parameters are introduced to represent the geometry of observation system. These geometrical parameters are depicted and listed in Figure 6.1, and most of them will be

considered in this research. These geometrical parameters affect the ambiguity resolution at different stages of the ambiguity resolution process and with different power. Besides affecting the size, shape, and orientation of the ambiguity searching space, the parameters also affect the power of identification and rejection criteria. The impacts caused by certain geometrical parameters usually coupled with the impacts caused by other parameter(s). In the following, however, in order to get more insight into the problem, the effects of each parameter will be separately investigated, and the coupling effects will be mentioned and investigated whenever necessary.

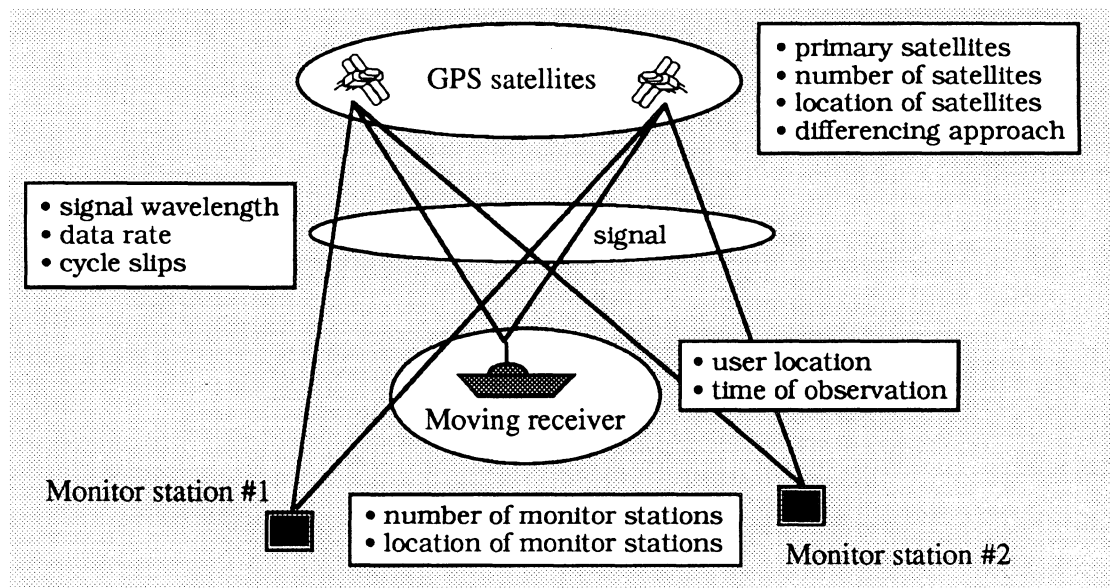


Figure 6.1. Geometrical parameters of ambiguity resolution.

## 6.2. Physical ambiguity searching space

The physical ambiguity searching space is the searching space in the position domain. In chapter 2, the general concept of physical surfaces and lines of ambiguity, and the physical ambiguity searching space were introduced. In chapter 3, the mathematical ambiguity searching space was introduced, discussed, and formulated. To get more insight into the

effects of observation geometry on the ambiguity resolution process, the mathematical formulation for the physical searching space is established in the following.

The *mathematical ambiguity searching space* was defined by equation (3.2) which will be rewritten in the following:

$$(\nabla\Delta N_{12} - \nabla\Delta N_{12}^{\circ})^T \cdot C^{-1}(\nabla\Delta N_{12}^{\circ}) \cdot (\nabla\Delta N_{12} - \nabla\Delta N_{12}^{\circ}) < \chi^2_{3,1-\alpha} \quad , \quad (6.1)$$

where all parameters were defined in Chapter 3. If the initial estimate of primary ambiguities  $\nabla\Delta N_{12}^{\circ}$  is related to the potential position  $X_p^{\circ}$  and the potential (trial) primary ambiguities  $\nabla\Delta N_{12}$  is related to the potential positions  $X_p$ , then based on equation (3.20), the following relation exists:

$$(\nabla\Delta N_{12} - \nabla\Delta N_{12}^{\circ}) = \frac{1}{\lambda} \cdot GP^{-1} \cdot (X_p - X_p^{\circ}) \quad , \quad (6.2)$$

where  $\lambda$  is the signal wavelength and GP is the gain matrix which is formulated by equation (3.22). If equation (6.2) is substituted to equation (6.1), the following equation for the physical ambiguity searching space is obtained:

$$(X_p - X_p^{\circ})^T \cdot C^{-1} \cdot (X_p - X_p^{\circ}) < \chi^2_{3,1-\alpha} \quad , \quad (6.3)$$

where C is the covariance matrix which has the following formulation:

$$C = \lambda^2 \cdot GP \cdot C(\nabla\Delta N_{12}^{\circ}) \cdot GP^T \quad (6.4)$$

Equation (6.3) represents the ellipsoid centered at  $X_p^o$  and its size, shape, and orientation is governed by the covariance matrix  $C$ . The confidence level  $(1-\alpha)$  will also determine the size of the ellipsoid. If the initial ambiguities are determined using the *extrawidelaning technique*, then by substituting equation (3.3) to equation (6.4), the covariance matrix  $C$  can be written as:

$$C = GP \cdot \{ C(\nabla\Delta P_{p12}) + C(\nabla\Delta L_{p12}) \} \cdot GP^T \quad (6.5)$$

When the *code-derived position* is used to estimate the initial ambiguities, then by substituting equation (3.4) to equation (6.4), the covariance matrix  $C$  can be formulated as:

$$C = GP \cdot \{ A_p \cdot C(X_c)_n \cdot A_p^T + C(\nabla\Delta L_{p12}) \} \cdot GP^T \quad (6.6)$$

Applying *the matrix lemma* expressed by equation (3.27), equation (6.6) can be reformulated to state :

$$C = GP \cdot A_p \cdot C(X_c)_n \cdot \quad (6.7)$$

From equations (6.5) and (6.7), it can be seen that the size, shape, and orientation of the ellipsoidal physical ambiguity searching space will be affected by the geometry of all satellites and the four satellites used as primary satellites. The size, shape, and orientation of the ellipsoidal physical searching space will be most likely different with those of the ellipsoidal mathematical searching space. More detail characteristics of the searching spaces are described in Appendix V. The number of potential positions inside the physical searching space, however, will be equal to the number of primary ambiguity sets inside the mathematical searching space. Unlike a mathematical searching space, the distances between the surfaces of ambiguities in the physical space will not always be the same or

regular. The distances will change with the signal wavelength, geometry of all satellites, primary satellites used, and observation differencing strategy adopted, as indicated by equation (6.2).

The distances between the surfaces of ambiguities can be represented by the norm of matrix  $(\lambda.GP)$ . The norm of a matrix measures the largest amount by which any vector is amplified by matrix multiplication [*Strang*, 1980], i.e., it indicates the ‘amplification factor’ of the matrix. The larger the norm of matrix  $(\lambda.GP)$ , the larger will be the distances between the surfaces of ambiguities, and vice versa. The norm of the matrix is computed using the following relation [*Strang*, 1980]:

$$\| \lambda.GP \| = \sqrt{\kappa_{\max} \text{ of } (\lambda^2.GP^T.GP)} \quad , \quad (6.8)$$

where  $\kappa_{\max}$  is the largest eigenvalue of the matrix  $(\lambda^2.GP^T.GP)$ . The gain matrix GP is defined in equation (3.23) and is rewritten in the following:

$$GP = \{ A_p^T.C^{-1}(\nabla\Delta L_{p12}).A_p + C^{-1}(X_c)_n \}^{-1} . A_p^T.C^{-1}(\nabla\Delta L_{p12}) \quad . \quad (6.9)$$

From the above equation, it can be realized that the value of  $\| \lambda.GP \|$  and therefore the distances between the ambiguity surfaces will be affected by several factors such as the signal wavelength, primary satellites used, standard deviation ratio between the pseudoranges and phase observations, number of satellites, approach used for differencing the observations, location of satellites, and number of monitor stations. Note that the value of Position Dilution Precision (PDOP) [*Wells et. al.*, 1986] related to primary satellites can also be used to indicate the distances between the surfaces of ambiguities. The larger PDOP value indicates the larger distances between the ambiguity surfaces, and vice versa. PDOP values, however, cannot be used to explain the differences in distances of the ambiguity

surfaces as a function of different signal wavelength or different observation differencing approach. PDOP values will remain the same in these cases.

### 6.3. The wavelength of the signal

The speed of on-the-fly ambiguity resolution will depend on the wavelength of the signal used, as indicated by some results shown in the previous chapters. In principle, the longer the wavelength, the faster the ambiguity resolution will be. The signal wavelength will affect the number of the potential primary ambiguities inside the initial searching space and the validation and rejection power of the identification process.

With *mathematical searching space*, the wavelength of the working signal will primarily affect the volume of the ellipsoidal searching space, although its shape and orientation will also be affected. Based on equations (3.3), (3.4), and (3.16), the volumes of the ellipsoids related to two signals with wavelengths  $\lambda_1$  and  $\lambda_2$  can be related as :

$$\text{Volume}(\lambda_1) \approx (\lambda_2 / \lambda_1)^3 \cdot \text{Volume}(\lambda_2) \quad . \quad (6.10)$$

The equation shows that the smaller the wavelength, the larger the volume of the ellipsoidal mathematical searching space will be and vice versa. The value from the left side of the equation is not exactly equal to the right side value because different signals with different wavelengths will have different covariance matrix  $C(\nabla\Delta L_{P_{12}})$  as shown in equations (3.3) and (3.4). Since the mathematical searching space has a regular spacing of the surfaces of ambiguities, the smaller volume of the searching space leads to smaller number of ambiguity sets inside the searching space. The relation between these two numbers of ambiguity sets, however, will not be exactly in accordance with equation (6.10), since the



number of ambiguity sets will not be determined only by the volume, but also by the shape and orientation of the ellipsoid.

In the case of *physical searching space*, the wavelength of the signal will primarily affect the distances between the potential positions inside the searching space, although the size, shape, and orientation of the searching space will also be affected. Based on equation (6.2), the distances between two potential positions  $dX_p$  related to two primary ambiguity sets of two signals with wavelengths  $\lambda_1$  and  $\lambda_2$  can be expressed as follows:

$$dX_p(\lambda_1) \approx (\lambda_1 / \lambda_2) \cdot dX_p(\lambda_2) \quad (6.11)$$

The above equation shows that the smaller wavelength corresponds to smaller distances between the potential positions which lead to larger number of potential positions and vice versa for a longer wavelength. This fact is two-dimensionally depicted in Figure 6.2 in the physical searching space.

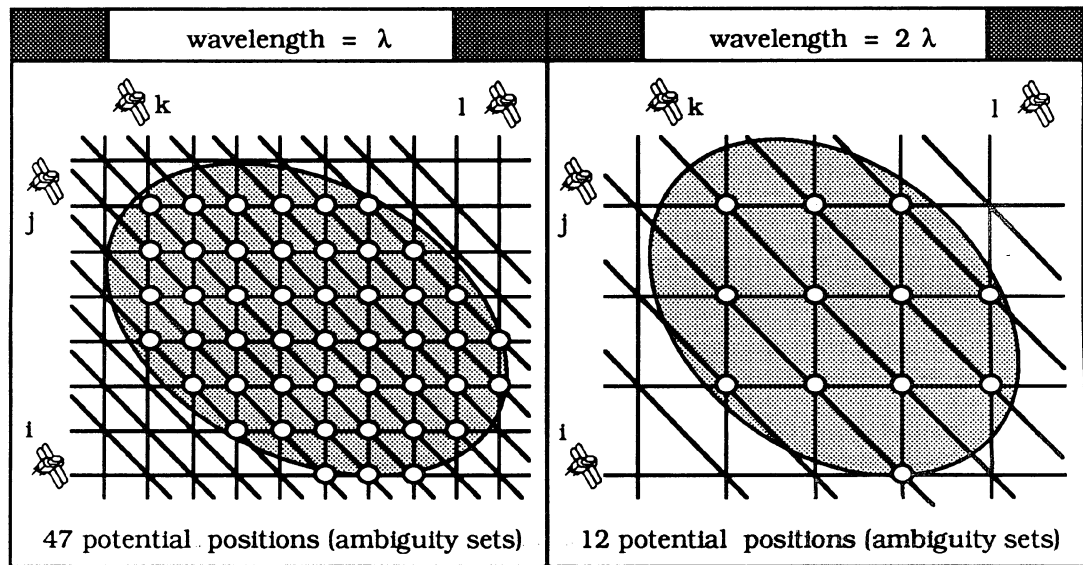


Figure 6.2. Two dimensional depiction of the impacts of the signal wavelength on the number of ambiguity sets inside the *physical searching space*. The satellites are positioned only to indicate the orientation of the hyperbolas. The satellite differencing : j-i, k-j, l-k, and m-l.

Results based on the Ashtech codeless data described in Chapter 4 are shown in Table 6.1. The table shows the number of initial ambiguity sets related to three types of signal, namely L1, half wide-lane, and double wide-lane signals, with wavelength of 19.0 cm, 43.1 cm, and 162.8 cm, respectively. In this case, the ellipsoidal searching space is sized with 95% confidence level and the observation standard deviations listed in Table 4.8 are used.

Table 6.1. The effects of the signal wavelength on the number of initial ambiguity sets.

Primary satellites, PRNs #	Number of initial ambiguity sets			Ratio of ambiguity sets		
	L1 signal	half widelane	double widelane	A <sup>1/3</sup>	B <sup>1/3</sup>	C <sup>1/3</sup>
2,6,11,15	31075	2729	61	7.99	3.55	2.25
2,6,11,19	4115	417	29	5.22	2.43	2.14
2,6,15,19	25439	2225	51	7.93	3.52	2.25
2,11,15,19	50197	4375	95	8.08	3.58	2.26
6,11,15,19	52041	4533	95	8.18	3.63	2.26
A = L1-signal/double widelane, B = half widelane/double widelane, C = L1-signal/half widelane,				wavelength ratio = 8.57. wavelength ratio = 3.78. wavelength ratio = 2.27.		

The examples in Table 6.1 show that the numbers of initial ambiguity sets related to different signal wavelength also depend on the primary satellites used. In this particular example, it can be seen that the ratio of the number of ambiguity sets between two signals are approximately equal to the cube of their wavelength ratio as also indicated by equation (6.10), except for primary satellites with PRNs # 2, 6, 11, and 19.

As well as affecting the number of ambiguity sets inside the searching space, the wavelength of the signal will also affect the *identification process of the correct*

*ambiguities*. Mathematically speaking, the signal wavelength will affect the identification power of the validation and rejection criteria. Geometrically speaking, when the longer signal wavelength is used, due to the larger separation between the surfaces of ambiguities, the ambiguity surfaces related to all satellites will intersect at fewer positions compared to the shorter signal wavelength, as depicted in Figure 6.3. The longer wavelength usually results in faster computation and observation times of ambiguity resolution. The ratio of improvement with respect to the signal wavelength ratio, however, is difficult to quantify, since it will change with the satellite geometry and the primary satellites used.

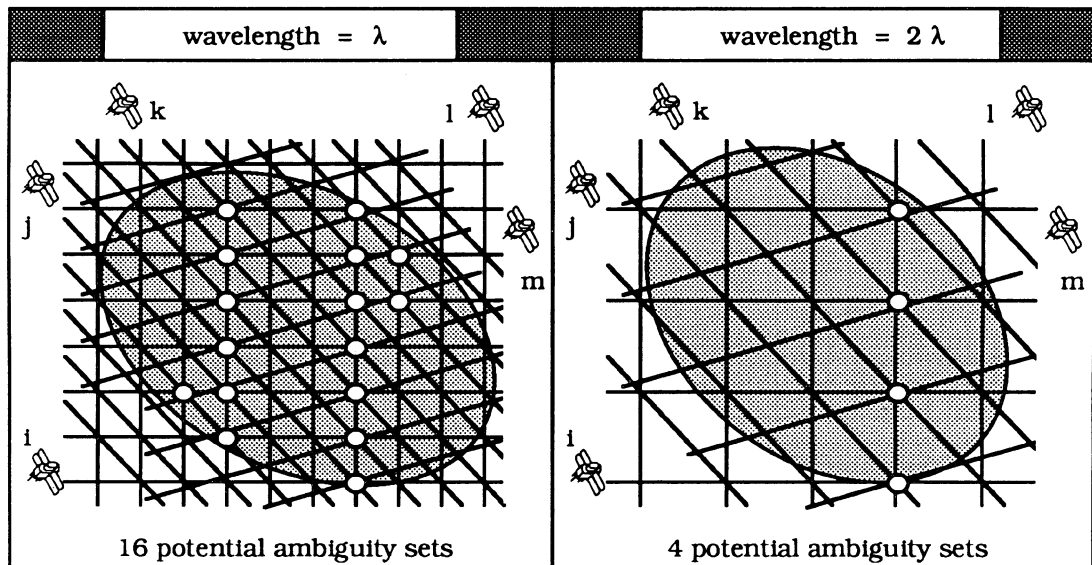


Figure 6.3. Two dimensional depiction of the impacts of the signal wavelength on the identification process of the correct ambiguities (5 satellites).

The Ashtech codeless data used in obtaining the results shown in Table 6.1 is used to show the effects of the signal wavelength on the ambiguity resolution. The on-the-fly ambiguity resolution is performed by considering three types of signal, namely L1, half wide-lane, and double wide-lane signals. In all three cases, PRNs 2, 6, 11, and 15 are used as primary satellites, and PRN 2 is used as the reference satellite for observation differencing. The standard deviations listed in Table 4.8 are used in this case. Three sets of parameter

values are used for the identification process, each for every signal. The parameter values for the half wide-lane signal has been given in Table 4.9, while the parameter values for the L1 and double wide-lane signals are given in Table 6.2. The computation and observation times of on-the-fly ambiguity resolution for all the three signals are given in Table 6.3.

Table 6.2. The parameter values of the identification process for L1 and double wide-lane signals.

The parameters	L1-signal	Double wide-lane signal
Confidence level of ellipsoidal searching space	0.950	0.950
Confidence level of the first criteria	0.950	0.950
The constant value of the second criteria	0.100	0.400
Confidence level of the third criteria	0.950	0.950
The constant value of the fourth criteria	0.050	0.050
Confidence level of the fifth criteria	0.990	0.990
Minimum individual mapping function value of the sixth criteria	0.900	0.900
Minimum normalized mapping function values of the seventh criteria	0.97 & 0.98	0.97 & 0.98
Confidence level of the eight criteria	0.9999	0.999
Minimum normalized mapping function value of the assurance criteria	0.990	0.980

The results in Table 6.3 show that the longer wavelength will lead to faster ambiguity resolution times, both in observation and computation times and vice versa. Note with the L1 signal, when the searching of the correct ambiguities is started at the first epoch of observation, many ambiguity sets have to be tested, and, in this case, the ambiguities are fixed to the wrong integers. When the searching process is started after smoothing the pseudoranges for five epochs, however, the ambiguities can be correctly resolved. On top

of it, the number of ambiguity sets to be tested and the computation times of ambiguity resolution can also be significantly reduced. Note also in Table 6.3 that as expected, the values of the matrix norm  $\| \lambda.GP \|$  are increasing with the increase in the signal wavelength. With the L1 signal, the different values of the matrix norms, with respect to different first epochs of searching, are caused by different standard deviation ratios between the pseudoranges and the phase observations at those two epochs.

Table 6.3. The effects of the signal wavelength on the ambiguity resolution times.

Working signal	$\lambda$ in cm	first epoch of searching	A	B	C	D
L1 signal	19.0	1st	31075	5991	6*	0.92
	19.0	5th	2781	585	7	0.98
Half wide-lane	43.1	1st	2729	501	4	2.07
Double wide-lane	162.8	1st	61	69	2	6.20
<p>* denotes the resolution failures,  i.e. the ambiguities are fixed to the incorrect integers.  A = number of initial ambiguity sets inside the initial searching space.  B = CPU times in milliseconds.  C = epoch of ambiguity resolution (30 sec. data interval).  D = the norm of matrix <math>\lambda.GP = \  \lambda.GP \ </math></p>						

The results presented in Table 6.3 are based on certain parameter values of the identification process and certain satellite geometry. For different values of the parameters and different satellite geometry, it can be expected that different numbers from those in the table will be obtained. The general trend, however, will remain the same. It should be noted also here that, even though the signals with longer wavelength are preferable for ambiguity resolution, for estimating the final position of the moving receiver, they are less favorable than the signals of shorter wavelength due to their higher noise level. The magnitude of the ionospheric advance on the longer wavelength signal is also larger than on the shorter wavelength signal.

#### 6.4. The primary satellites.

In the integrated technique of on-the-fly ambiguity resolution, the primary satellites being used will have a strong effect on the ambiguity resolution process, as has been shown in the previous chapters. The primary satellites will affect both the number of ambiguity sets inside the initial searching space and the identification process of the correct ambiguities. When the precision of certain types of observations to all satellites is characterized by the same standard deviation and the initial ambiguities are estimated using the extrawidelaning technique, however, the number of ambiguity sets to be tested are the same for different primary satellites.

In the context of *mathematical searching space*, when the code derived position is used to estimate the initial ambiguities, different groups of primary satellites will lead to different size of the searching space and to a different shape and orientation of the ellipsoid. As shown by equation (3.4), different primary satellites correspond to different design matrix  $A_p$ , which then lead to a different covariance matrix of the initial ambiguities used to construct the searching space. In the context of *physical searching space*, different group of primary satellites will primarily affect the distances between the potential positions inside the searching space and the patterns of the surfaces of ambiguities as well as the size, shape, and orientation of the searching space as two dimensionally depicted in Figure 6.4. These effects usually lead to a different number of ambiguity sets (potential positions) inside the searching space.

Figure 6.5 gives an example of the effects of a different group of primary satellites on the number of ambiguity sets inside the initial searching space. The results are based on the Rogue kinematic data described in the previous chapter. The standard deviations of the observations and the size of the ellipsoidal searching space used here are the same as those used in chapter 4 and listed in Tables 4.12 and 4.13.

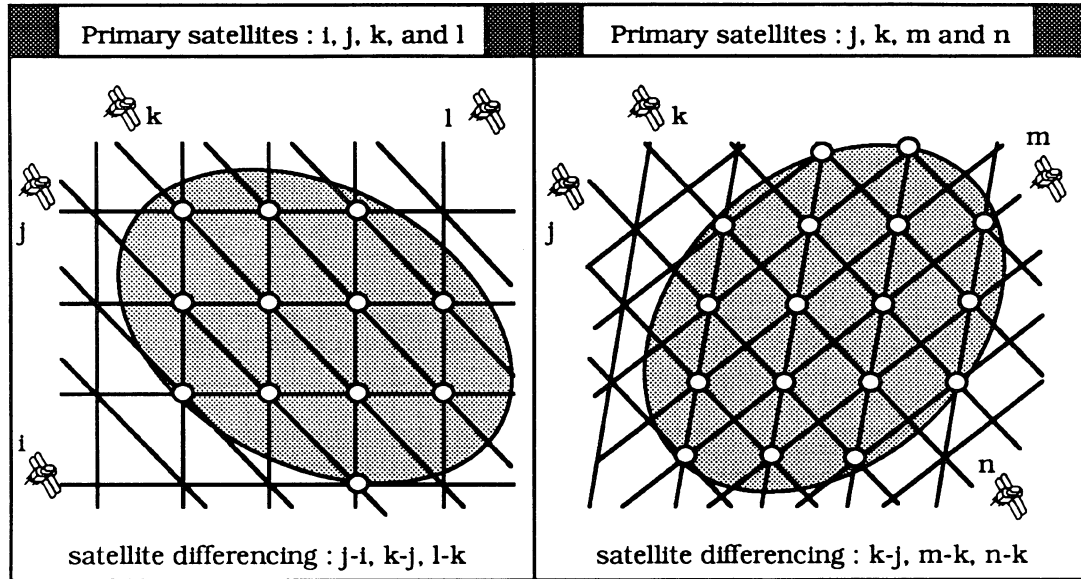


Figure 6.4. The effects of the primary satellites on the physical searching space.

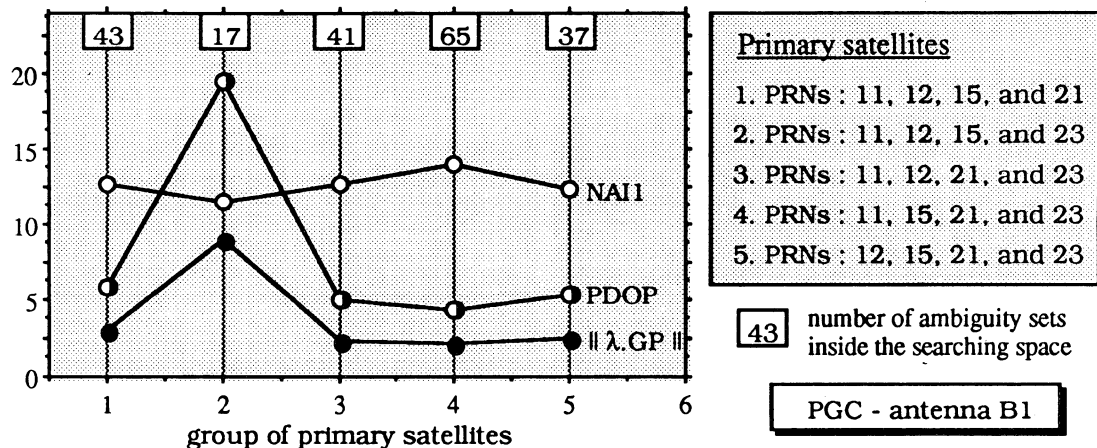


Figure 6.5. The effects of different group of primary satellites on the number of ambiguity sets inside the initial searching spaces.

The results in Figure 6.5 show that different group of primary satellites lead to different volume of ellipsoidal mathematical searching space expressed by parameter NAI1 which is defined by equation (3.17). As expected, the larger value of NAI1 corresponds to a larger number of ambiguity sets. In the context of physical searching space, the values of the matrix norm  $\|\lambda.GP\|$  or PDOP can also be used instead of NAI1 to predict the number of

ambiguity sets, since they indicate the spread of the positions. Since the larger  $\| \lambda.GP \|$  or PDOP indicates the wider spread of the positions, the larger  $\| \lambda.GP \|$  or PDOP indicates a smaller number of potential positions (ambiguity sets) inside the searching space, as confirmed by results in Figure 6.5.

Different groups of primary satellites not only lead to different numbers of ambiguity sets to be tested or different numbers of potential positions, but they also yield different accuracy and precision of potential positions. Since potential positions are used to estimate secondary ambiguities used for computing the updated positions and their covariance matrices, then the primary satellites used will affect all the validation and rejection criteria used in identifying the correct ambiguity set. It can be expected that different primary satellites will lead to different computation and observation times of ambiguity resolution, as shown by the example in Figure 6.6. The effect of different primary satellites on the identification power of each criteria, however, is quite difficult to quantify. The results shown in Figure 6.6 are based on the same Rogue kinematic data and the same processing parameters as used in deriving the results shown in Figure 6.5.

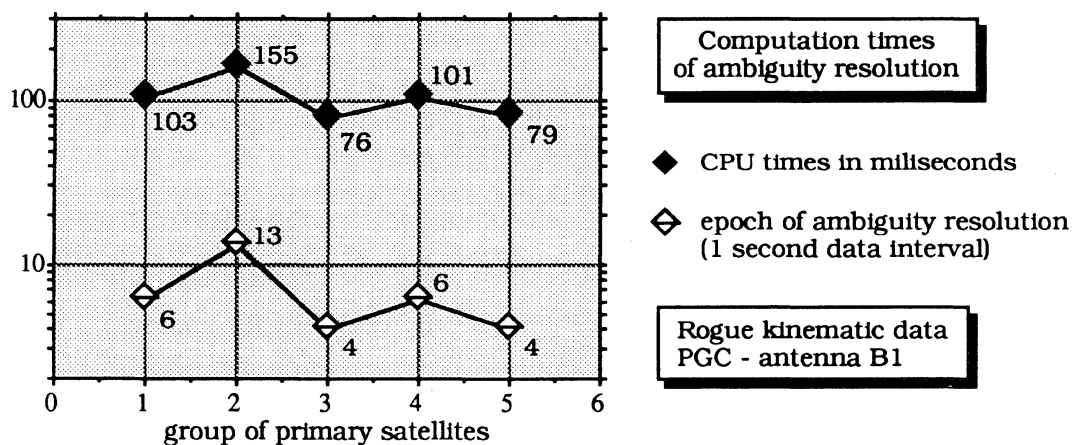


Figure 6.6. The effects of the primary satellites on ambiguity resolution times.



Note from Figures 6.5 and 6.6 that, in this particular example, the primary satellites with the smallest number of initial ambiguity sets yield the slowest ambiguity resolution times, while the fastest ambiguity resolution times are related to the groups of primary satellites with a moderate number of ambiguity sets. In the case of antenna B3 and the same monitor station PGC, however, the primary satellites with the smallest number of ambiguity sets yield the fastest ambiguity resolution as shown in Table 6.4. Results in Table 6.4, which are derived using the same values of identification process parameters given in Chapter 4, also show that a different group of primary satellites could also lead to the same epoch of ambiguity resolution, even though their computation times are usually still different.

Table 6.4. The effects of different group of primary satellites on the observation and computation times of ambiguity resolution.

PRN number of primary satellites	number of ambiguities	PGC-B2		PGC-B3		UCLU-B1		UCLU-B2		UCLU-B3	
		A	B	A	B	A	B	A	B	A	B
11, 12, 15, 21	43	5	91	4	83	1	61	2	67	2	61
11, 12, 15, 23	17	12	146	3	65	3	63	2	59	2	51
11, 12, 21, 23	41	5	80	5	79	4	74	4	74	2	55
11, 15, 21, 23	65	6	99	4	85	3	69	2	63	2	57
12, 15, 21, 23	37	4	77	4	78	3	68	4	74	1	55
A = epoch of ambiguity resolution,      B = CPU times in milliseconds											

The fact that the three antennas B1, B2, and B3 are very close together, but the ambiguity resolution times with respect to certain primary satellites and certain monitor station are different, indicates that the characteristics of their measurement noises and errors are different. Theoretically speaking, for the low observation noise and errors, the smallest number of ambiguity sets will most likely still contain the correct ambiguity sets, which in turn can be expected to yield the fastest ambiguity resolution times. In general, however,

for a fast and also reliable on-the-fly ambiguity resolution, one should not use the primary satellites with the smallest or the largest number of ambiguity sets. Instead, the one with average number of ambiguity sets should be used.

### **6.5. The number of satellites.**

The number of observed satellites will strongly affect the computation and observation times of ambiguity resolution since it will affect both the ambiguity searching space and the identification process of the correct ambiguity. When using the code derived position to determine the initial ambiguities, the number of satellites will affect the centre position, size, shape and orientation of the mathematical ellipsoidal ambiguity searching space.

In general, the more satellites available, the smaller the ellipsoidal searching space will be (refer to equations (3.4) - (3.6) and Appendix V for the mathematical reasoning). Therefore, for the same primary satellites and probability level of the ellipsoid, more satellites usually means a smaller number of ambiguity sets to be tested, which usually in turn leads to faster computation and observation times of ambiguity resolution. The example of the effects of the number of satellites on the ellipsoidal mathematical searching space are shown in Figure 6.7.

The example is based on the dual-frequency zero-baseline data described in Chapter 4. The ellipsoidal searching space is sized with 99 % confidence level, and the standard deviations of observations as listed in Table 4.3 are used in this case. This example shows that the volumes of the ellipsoidal searching spaces and the number of ambiguity sets inside the spaces related to five satellites are always larger than those related to six satellites for all 15 groups of primary satellites used.

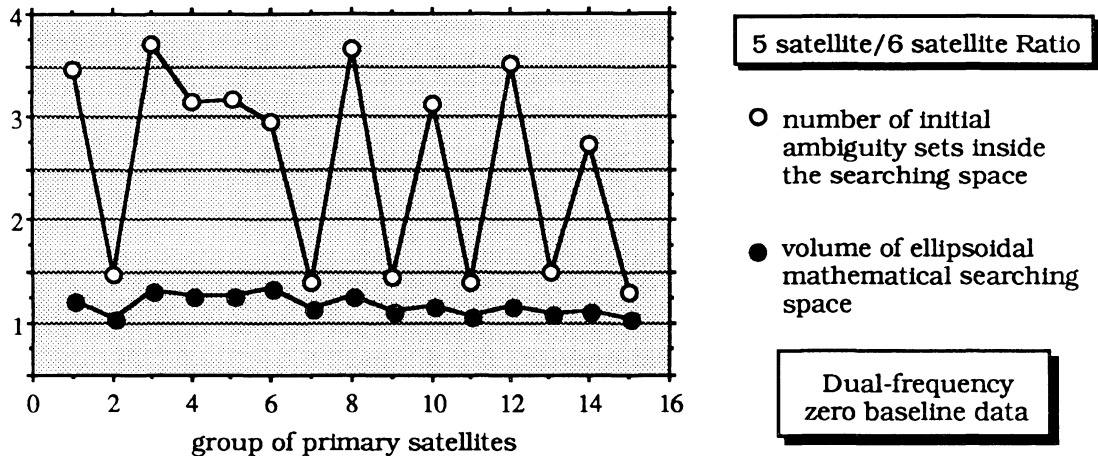


Figure 6.7. Example of the effects of the number of satellites on the size and shape of the searching space and the number of initial ambiguity sets inside the searching space.

The number of satellites will also affect the identification process of ambiguity resolution. With the use of more satellites, the correct ambiguity set has to satisfy more geometrical constraints and more stringent validation and rejection criteria. This makes the potentially correct ambiguities more distinguishable from the potentially incorrect ones, as depicted in two-dimensional physical searching space in Figure 6.8. This, in turn, usually leads to faster observation and computation times of ambiguity resolution. The speed improvement, however, can be expected to depend also on the primary satellites used and the relative location of the observed satellites, as also indicated by Figure 6.8. The example of the effects of the number of satellites on the ambiguity resolution times are shown in Figure 6.9. This example is based the same dual-frequency zero-baseline data used in deriving the results shown in Figure 6.7. The values of the identification process parameters as listed in Table 4.4 are used except that confidence levels of 0.95 are used for the first and third criteria, instead of 0.99.

Note from Figure 6.9 that, in general, the use of more satellites will lead to the faster observation and also shorter computation times of ambiguity resolution. The example also

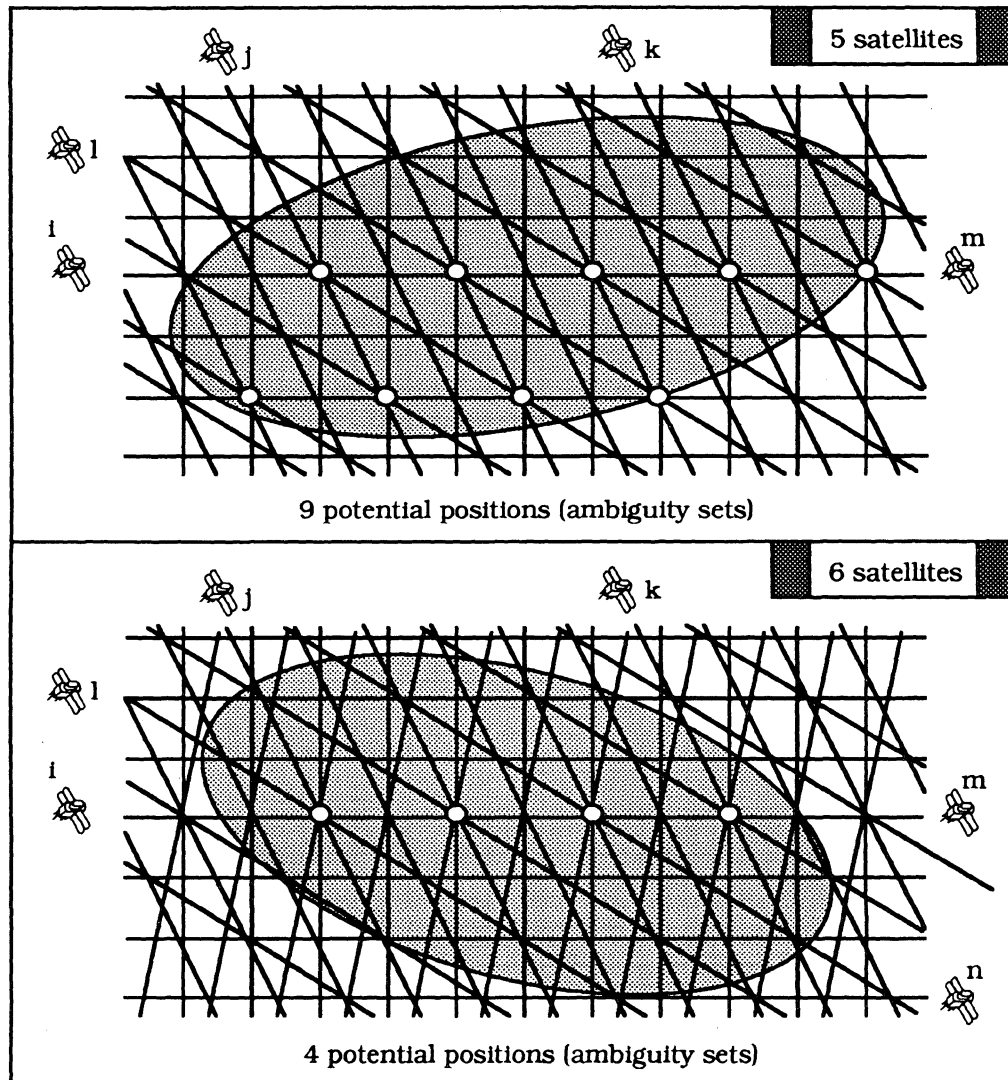


Figure 6.8. Two-dimensional depiction of the impacts of the satellite numbers on the ambiguity resolution process. The satellites are positioned only to indicate the orientation of the hyperbolas. The satellite *differencing* :  $j-i$ ,  $k-i$ ,  $l-i$ ,  $m-i$ , and  $n-i$ .

shows that the different groups of primary satellites have more pronounced effect on the epochs of ambiguity resolution related to five satellites, compared to those related to six satellites. The results presented in Figures 6.7 and 6.9 are related to a certain satellite constellation and certain parameter values of the identification process. For different satellite constellation and different parameter values of the identification process, the

numbers shown in the figures could be different. The general trend with respect to the number of satellites, however, will remain the same.

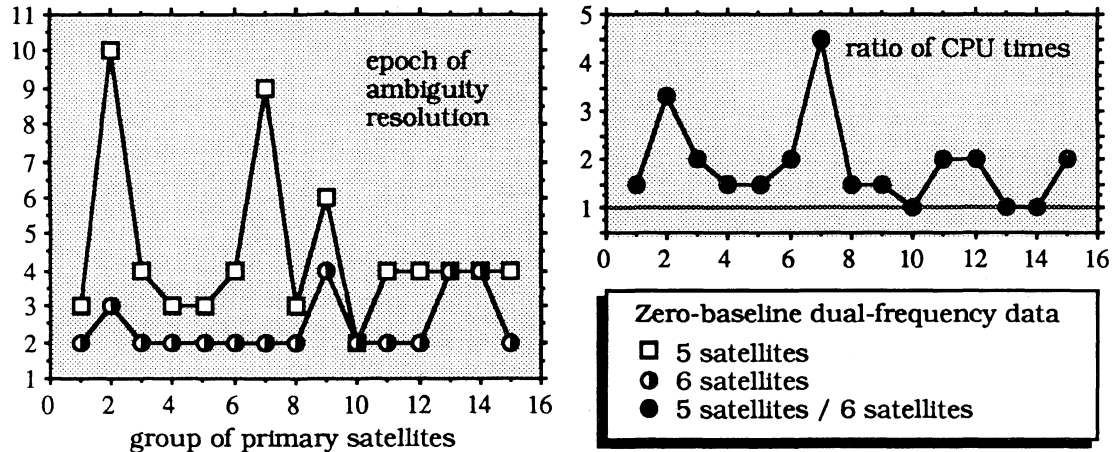


Figure 6.9. Example of the effects of the number of satellites on the ambiguity resolution times.

### 6.6. The observation differencing strategy.

In performing the double-difference observations, there are basically three approaches that can be used for differencing the observations between satellites, namely *sequential differencing*, *fixed-reference differencing*, and *orthonormalized differencing* [Wells et al., 1987]. The orthonormalized differencing [Bock et al., 1985], not like the other two approaches, destroys the integer nature of the ambiguities, and therefore is not considered. Only the sequential and fixed-reference differencing approaches are investigated here.

If  $n_s$  satellites are observed and ordered as 1,2,3, ...,  $n_s$ ; the sequential differencing is performed as (2-1), (3-2), (4-3), ..., and so on; and the fixed-reference differencing with satellite no. 1 as a reference is performed as (2-1), (3-1), ....., and ( $n_s$ -1). The examples of these two differencing approaches are shown in Figure 6.10. As indicated in this figure,

the observation differencing approach will affect the observation geometry, i.e., the pattern and spacing of surfaces of positions. It will also affect the level and characteristics of the errors and biases in the double-differences, particularly the looking-direction dependent errors and biases, such as the ionospheric and tropospheric delays, and ephemeris errors.

The two effects of the observation differencing obviously will also affect the ambiguity resolution process. With the integrated technique of on-the-fly ambiguity resolution, the observation differencing will affect both the ambiguity searching space and the identification process of the correct ambiguities.

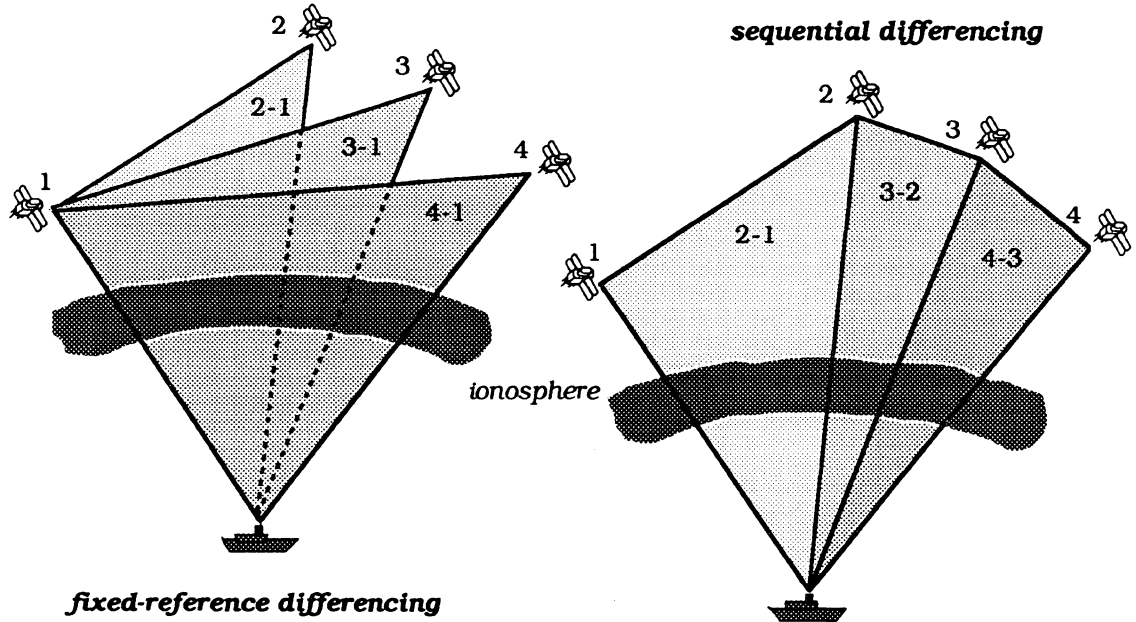


Figure 6.10. Fixed-reference and sequential differencing approaches.

As described in Appendix V, the different observation differencing strategy will not affect the volume of mathematical searching space, but it will affect the shape and orientation of the space. In the context of physical searching space, the volume, shape, and orientation of the space will all not be affected by different observation differencing strategy. The pattern and spacing of the ambiguity surfaces, however, will be affected. This in turn affects the

number of initial positions (ambiguity sets) inside the searching space, as two-dimensionally illustrated in Figure 6.11.

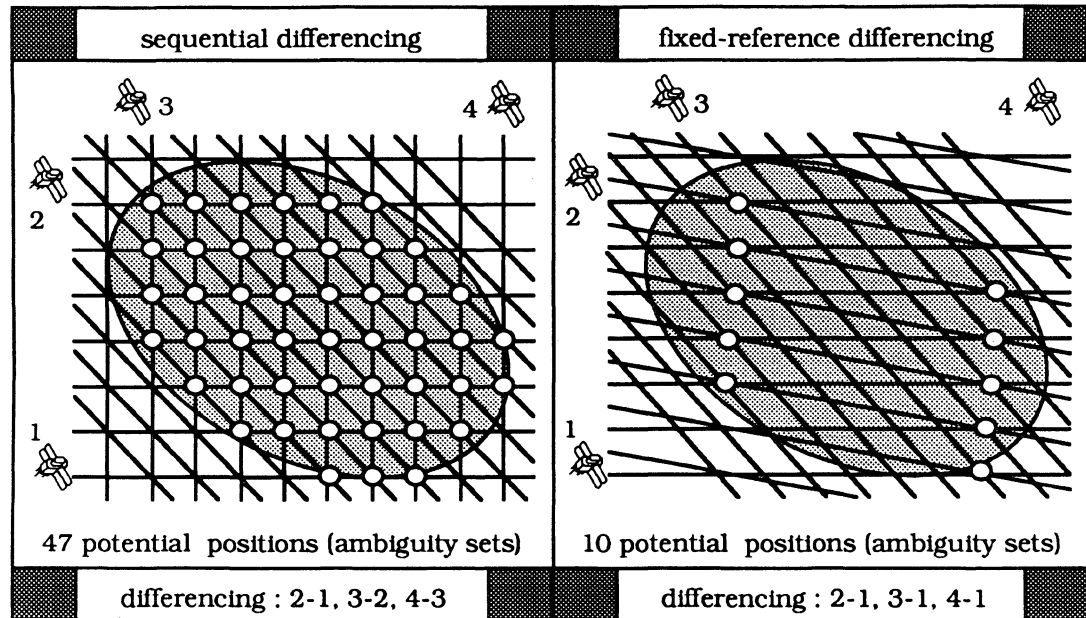


Figure 6.11. The effect of the observation differencing on the number of initial ambiguity sets.

These differences in number of ambiguity sets, however, will vary as function of several variables such as the primary satellites used, number of observed satellites, wavelength of the working signal, and nominal size of the ellipsoidal searching space. The example for this fact is shown in Figure 6.12. This example is based on the Trimble zero-baseline data described in Chapter 4. The ellipsoidal searching space is sized with 99% confidence level and the standard deviations of observations as listed in Table 4.3 are used. The percentages of the ambiguity differences in Figure 6.12 are computed as :

$$\% \text{ of difference} = \frac{\# \text{fixed} - \# \text{sequential}}{\# \text{fixed}} \cdot 100 \%,$$

where #fixed is the number of initial ambiguities related to fixed-reference differencing and #sequential is the number of initial ambiguities related to sequential differencing approach.

In the case of fixed-reference differencing, the reference satellite is the first satellite in the order.

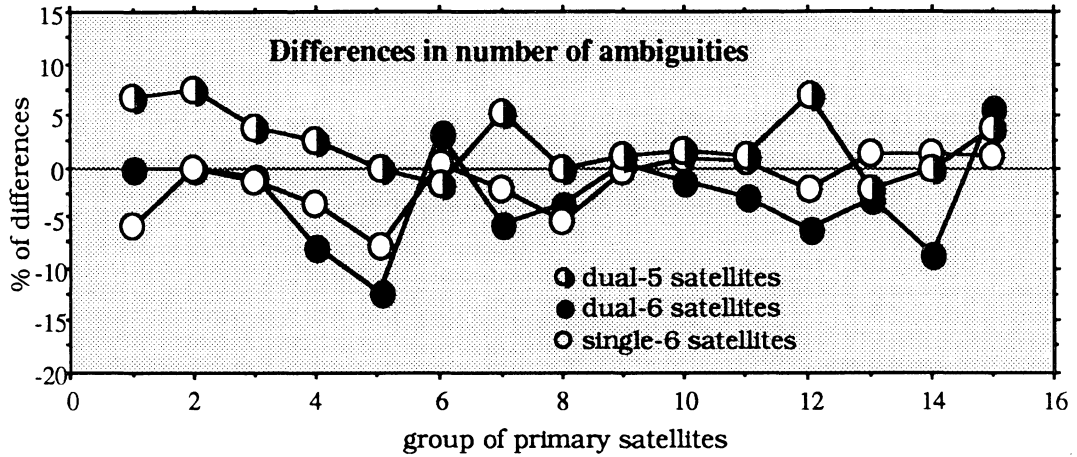


Figure 6.12. The effects of differencing approach on the number of initial ambiguity sets.

Note from the above figure that the differences in the number of ambiguity sets could be zero, positive, or negative numbers. This suggests that, in terms of obtaining the small ambiguity sets to be tested, one should not always adhere to a certain observation differencing approach since either fixed-reference or sequential differencing approach could be the most appropriate one, depending on the primary satellites used. However, when the nominal size of the ellipsoid is small, due to the use of small standard deviations of the observations and/or relatively small confidence level of the ellipsoid, and the wavelength of the working signal is relatively long, then it can be expected that the number of initial ambiguities will not be significantly affected by the differencing approach.

With certain primary satellites used, the values of PDOP cannot be used to explain the differences in the number of ambiguity sets caused by the use of different observation differencing approach as indicated in Figure 6.12. In the context of physical searching space, these differences can be explained by the matrix norm  $\|\lambda.GP\|$ . Figure 6.13 shows



the values on the matrix norm related to the results shown in Figure 6.12. The percentages of differences in the matrix norm values shown in Figure 6.13 are computed as:

$$\% \text{ of difference} = \frac{\| \lambda.GP \| \text{ fixed} - \| \lambda.GP \| \text{ sequential}}{\| \lambda.GP \| \text{ fixed}} \cdot 100 \%,$$

where  $\| \lambda.GP \| \text{ fixed}$  is the matrix norms related to fixed-reference differencing and  $\| \lambda.GP \| \text{ sequential}$  is the matrix norms related to sequential differencing approach.

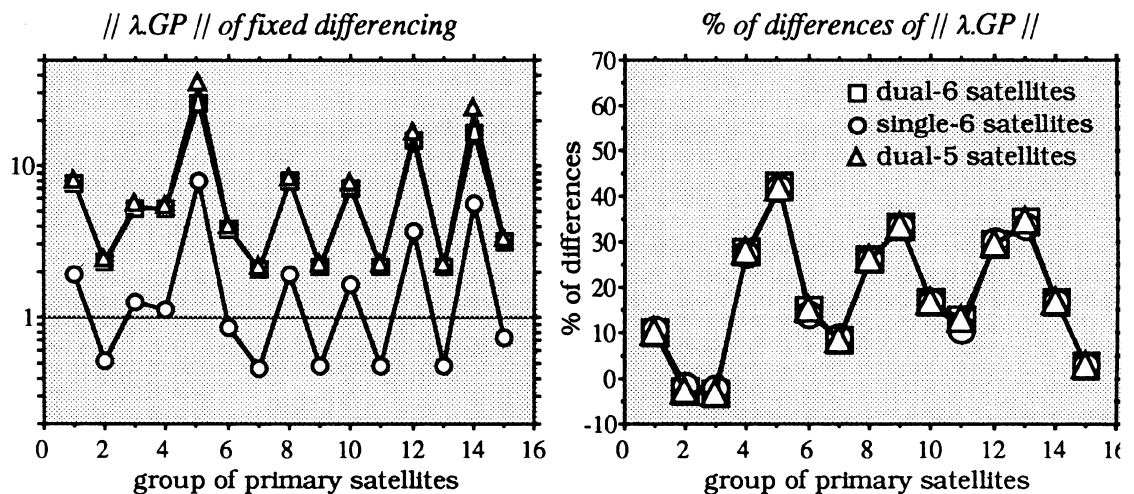


Figure 6.13. The effects of differencing approach on the matrix norm- $\| \lambda.GP \|$ .

The example in Figure 6.13 again illustrates that, the matrix norms  $\| \lambda.GP \|$  are affected by the signal wavelength and the number of satellites as well as other factors such as the observation differencing approach. Differences in the values of  $\| \lambda.GP \|$  due to the differences in the observation differencing approach vary as a function of primary satellites used. Depending on the primary satellites, the percentages of differences could be as much as 45 %. For the same primary satellites used, however, the percentages of differences are more or less the same, within  $\pm 3\%$ , regardless of the signal wavelength and the number of satellites.

With the different observation differencing approach, for the same primary satellites, different satellite ordering of different reference satellite will not affect the volume, shape, and orientation of the physical searching space. It will, however, affect the pattern and spacing of the ambiguity surfaces, as two-dimensionally illustrated in Figure 6.14. This change usually leads to a different number of ambiguity sets to be tested. In the context of mathematical searching space, only the shape and orientation of the space are affected. Its volume remains the same as shown in Appendix V.

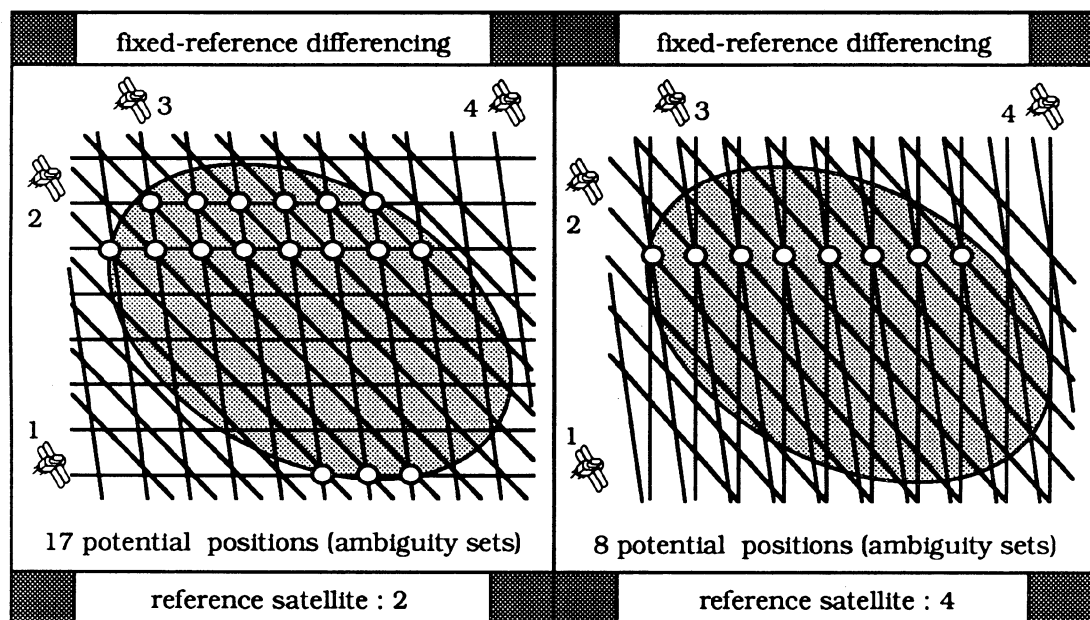


Figure 6.14. The effects of the reference satellite on the number of initial ambiguity sets.

The example from the single-frequency zero-baseline data is given in Table 6.5. The ellipsoidal searching space is sized with 99% confidence level, and the standard deviations of observations as listed in Table 4.3 are used. Note from this table, that the use of different reference satellite could be either smaller, larger, or the same ambiguity sets inside the searching space. However, when the nominal size of the searching space is small, as in the case of Rogue kinematic data processing shown before, the use of different satellites for

differencing does not affect the number of ambiguity sets, as the use of different differencing approaches, although the ambiguity resolution times could still be different.

Table 6.5. The effects of the reference satellite on the number of initial ambiguity sets.

reference satellites	primary satellites PRNs : 18, 2, 11, 6	reference satellites	primary satellites PRNs : 18, 2, 11, 19
	number of ambiguity sets		number of ambiguity sets
18	1403	18	3969
2	1473	2	3955
11	1451	11	3921
6	1451	19	4001
fixed-reference differencing & observed satellites are PRNS : 2, 6, 11, 16, 18, and 19			

With different observation differencing strategies, different pattern and spacing of the surfaces of ambiguities are established. In this case, the ambiguities being tested have to satisfy different geometrical constraints and different powers of some identification criteria. This in turn could lead to different speeds of ambiguity resolution. An example is shown in Figure 6.15 which is based on dual-frequency zero baseline data.

The values of the identification process parameters used to derive the results shown in Figure 6.9, are used in this case. With fixed-reference differencing, the first satellite in order is used as a reference satellite. Note from Figure 6.15 that depending on the primary satellites used, the use of fixed-reference differencing instead of sequential differencing, could either mean slower, faster, or the same speed of ambiguity resolution. Even when the number of ambiguity sets inside the searching space is not affected, different differencing approaches still can lead to different speed of ambiguity resolution, as shown in Table 6.6. The results in this table are based on the Rogue kinematic data described in Chapter 4, and the same values of the identification process parameters given in that chapter are used for both cases of differencing.

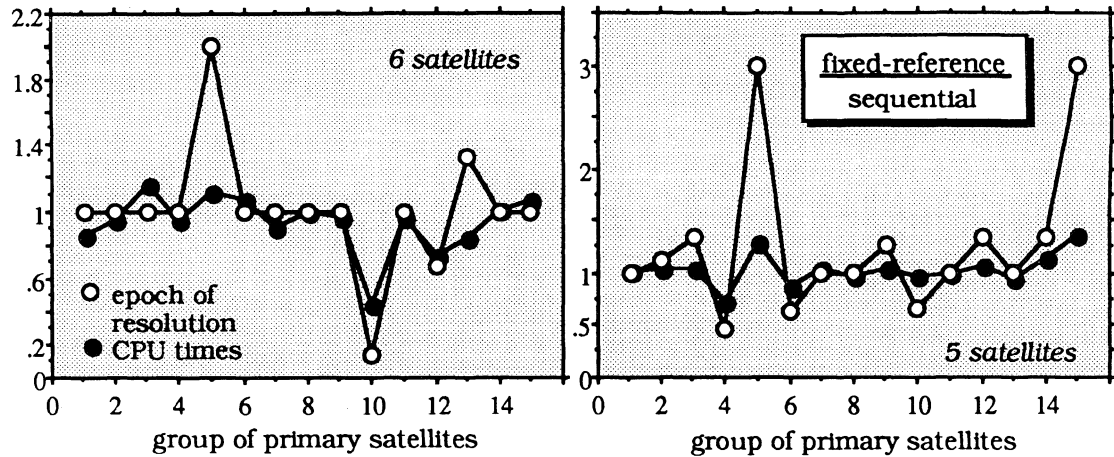


Figure 6.15. The ratio of the ambiguity resolution times between the fixed-reference and sequential differencing approaches.

Table 6.6. The effects of the observation differencing approach on the epoch of on-the-fly ambiguity resolution.

primary satellites	11,12,15,21		11,12,15,23		11,12,21,23		11,15,21,23		12,15,21,23	
	FD	SD	FD	SD	FD	SD	FD	SD	FD	SD
PGC-B1	6	6	13	13	4	4	6	3*	4	2*
PGC-B2	5	6	12	1*	5	5	6	12	4	2*
PGC-B3	4	10	3	3	5	5	4	3*	4	2*
UCLU-B1	1	3	3	3	4	4	3	4	3	3
UCLU-B2	2	2	2	2	4	4	2	2	4	4
UCLU-B3	1	1	1	2	1	1	1	4	1	1

FD = fixed-reference differencing, with 1st satellite in order as a reference.  
SD = sequential differencing. The failure of ambiguity resolution is denoted by \*.

Note from Table 6.6 that the use of sequential differencing instead of fixed-reference differencing could lead to slower ambiguity resolution or even the failure to resolve ambiguities correctly. The ambiguity resolution failures for some cases of the sequential differencing approach related to monitor station PGC, indicate that the values of some identification process parameters, do not properly represent the combined effects of observation geometry and the level of errors and biases in the observations for these

particular cases. Therefore, changing the values of some parameters can be used to avoid the ambiguity resolution failures. For example, if the parameter values of the second and seventh criteria are changed to 0.50 and 0.90 & 0.925, respectively, the ambiguity resolution failures as shown in Table 6.6 can be avoided, as shown in Table 6.7. In this case, however, the ambiguity resolution related to primary satellites PRNs 11, 12, 15, 23 and antenna B3, becomes longer (in terms of epochs) with the changes in the parameter values of those criteria.

Table 6.7. The effects of the differencing approach on the ambiguity resolution epoch (sequential differencing approach).

primary satellites	PGC - B1	PGC - B2	PGC - B3
11,12,15,21	6	6	10
11,12,15,23	13	12	11
11,12,21,23	4	5	5
11,15,21,23	13	12	11
12,15,21,23	13	12	11

As has been pointed out, for the same primary satellites and the same number of observed satellites, different ordering of satellites or different reference satellite used for differencing, could lead to different number of ambiguity sets to be tested, as shown by the example in Table 6.5. Besides, they will also yield different geometrical and computational constraints which have to be satisfied by the ambiguities being tested. Moreover, the characteristics of the observation noises could also be different. As the result, different speed of ambiguity resolution could be obtained, as shown in the example given in Table 6.8. These results correspond to the number of ambiguity sets shown in Table 6.5. The same values of the identification process parameters used in obtaining the results shown in Figure 6.15 are adopted.

Table 6.8. The effects of the reference satellite on the ambiguity resolution times.

reference satellites	primary satellites PRNs : 18, 2, 11, 6		reference satellites	primary satellites PRNs : 18, 2, 11, 19	
	epoch of resolution	CPU times in msec.		epoch of resolution	CPU times in msec.
18	26	809	18	31	1890
2	23	819	2	25	1846
11	23	829	11	26	1985
6	20	707	19	26	2014
fixed-reference differencing & observed satellites are PRNS : 2, 6, 11, 16, 18, and 19					

Even when the use of a different reference satellite does not affect the number of initial ambiguity sets, a different epoch of ambiguity resolution still could be expected. This is shown in Table 6.9. These findings are based on Rogue kinematic data and use the same values of the identification process parameters used in obtaining the results shown in Table 6.6.

Table 6.9. The effects of the reference satellite on the ambiguity resolution times.

reference satellites	epoch of ambiguity resolution			CPU times in milliseconds		
	PGC-B1	PGC-B2	PGC-B3	PGC-B1	PGC-B2	PGC-B3
11	6	5	4	106	93	89
12	4	4	4	81	79	80
15	6	6	4	99	96	79
21	6	6	10	99	96	130
fixed-reference differencing; observed satellites are PRNs: 11,12,15,21, and 23; and the primary satellites are PRNs: 11, 12, 15, and 21.						

### **6.7. The location of satellites.**

The location of satellites, relative to the moving receiver, will affect the ambiguity searching space and the identification process of the correct integer ambiguities. Different location of satellites, therefore, can be expected to lead to different number of initial ambiguity sets and different epochs of ambiguity resolution. Different locations of satellites relative to the moving receiver could result from different locations of the moving receiver, satellites observed, times of observations, or a combination of these variables. In this research study, however, I will primarily concentrate on the effects of temporal variations of satellite locations in ambiguity resolution.

As the relative position between the satellites and the moving receiver changes, the size, shape, and orientation of the ellipsoidal searching space can also be expected to change. The pattern and spacing of the ambiguity surfaces will also change. The number of initial ambiguity sets to be tested, related to certain primary satellites, therefore can be expected to also vary with times of observation, as shown by the example in Figure 6.16. The example is based on the zero baseline data described in Chapter 4. The searching space is sized with 99% confidence level, and the standard deviations as listed in Table 4.3 are used in this case. The time variations of the PDOP values in this case are shown in Figure 6.17.

Figure 6.16 illustrates, that, as expected the trend of time variations of the number of initial ambiguity sets depends on the primary satellites being used. For the same primary satellites, the trend will also depend on the number of observed satellites, while it remains more or less the same for different signal wavelength or different differencing approach as shown in Figure 6.16. Note from Figures 6.16 and 6.17 that, as expected, for certain primary satellites, there is negative correlation between the variations in the number of ambiguity sets and the variations in the PDOP values. When the nominal size of the

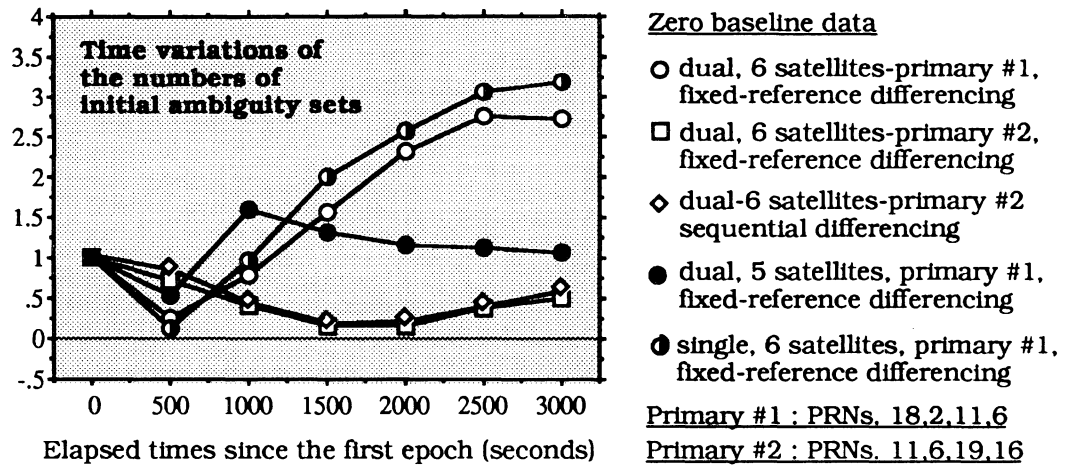


Figure 6.16. Time variations of the number of initial ambiguity sets. Results are expressed as the ratio to the first epoch's number of ambiguities.

ellipsoid is small and the wavelength of the working signal is relatively long, as in the case of Rogue kinematic data, the variations in the number of ambiguity sets can be expected to be relatively small. The example related to station UCLU and antenna B3 is shown in Table 6.10. The time variations of PDOP values in this case are shown in Figure 6.18.

In deriving the results shown in Table 6.10, 99% confidence level is used to size the ellipsoidal searching space, and the standard deviations of the observations listed in Table 4.12 are used in this case. Note from Table 6.10 and Figure 6.18 that the time variations of the number of initial ambiguity sets are relatively small, except for the primary satellites with PRNs 11, 12, 15, and 23. Due to significant time variations of its

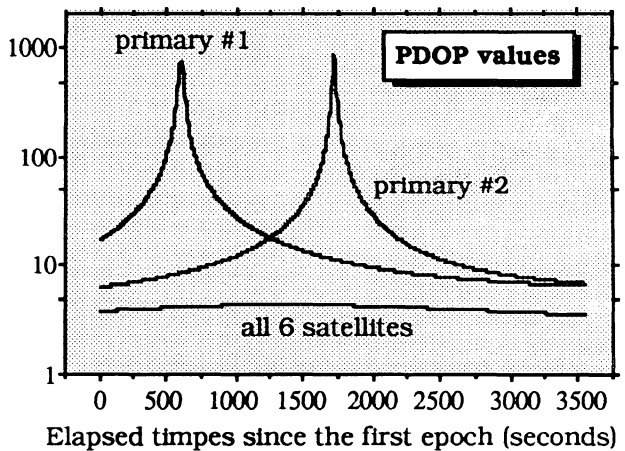


Figure 6.17. Time variations of PDOP values (Trimble zero baseline data).



PDOP values, as shown in Figure 6.18 (left plot), the time variations in the number of ambiguity sets related to this particular primary satellite group are also significant (more than 50 % variations). Its nominal values, however, are small due to larger nominal PDOP values.

Table 6.10. The time variations of the number of initial ambiguity sets (Rogue kinematic data, baseline UCLU - antenna B3, fixed-reference differencing approach).

elapsed times since 1st epoch	PRN number of primary satellites				
	11,12,15,21	11,12,15,23	11,12,21,23	11,15,21,23	12,15,21,23
0	43	17	41	65	37
5 minutes	43	9	43	67	41
10 minutes	43	9	49	65	41
15 minutes	49	7	55	63	41

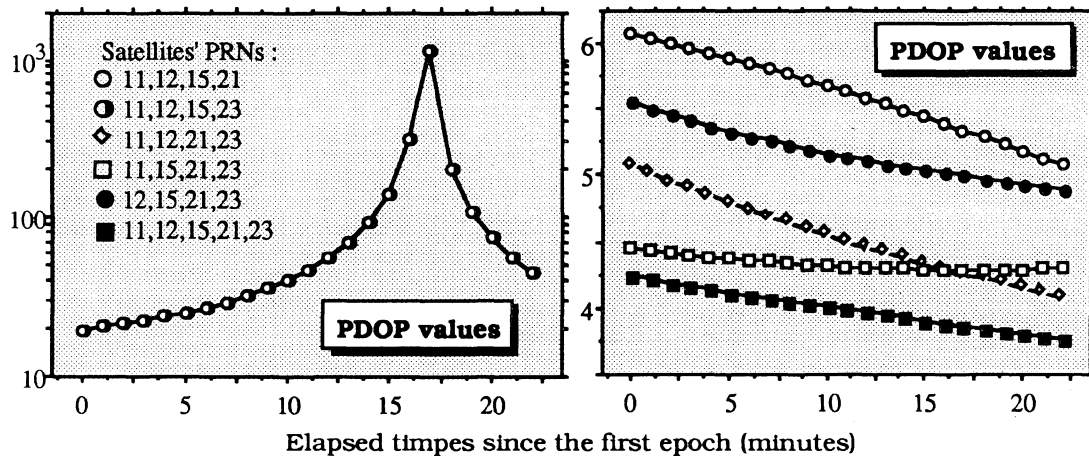


Figure 6.18. Time variations of PDOP values (Rogue kinematic data).

In addition to yielding a different number of initial ambiguity sets, different temporal locations of satellites will also yield different pattern and spacing of the surfaces of ambiguities. Therefore, the ambiguity sets being tested also have to satisfy different geometrical and computational constraints. This in turn can be expected to lead to different speed of ambiguity resolution. The results based on the zero baseline data can be used as an

example, since they are not contaminated by the observation errors and biases. The results are depicted in Figure 6.19. They are based on the number of initial ambiguity sets shown in Figure 6.16, and the values of the identification process parameters used in obtaining the results shown in Figure 6.15.

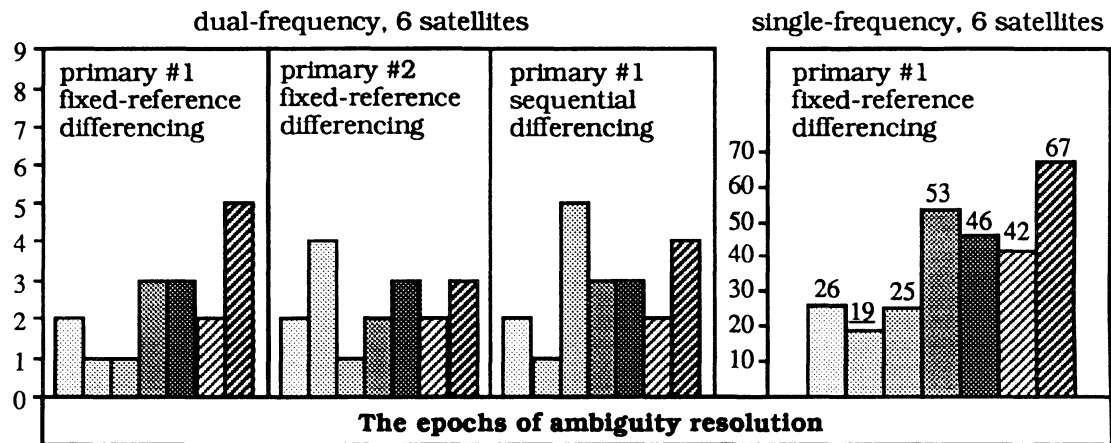


Figure 6.19. The time variations of the ambiguity resolution times (zero baseline data). The underline number inside the figure denotes the ambiguity resolution failure.

The epochs of ambiguity resolution in Figure 6.19 are given for seven cases, respectively. The same values of the identification process parameters are used for all cases. Two consecutive cases are separated in times by 500 seconds ( $\approx 8.3$  minutes). Starting the ambiguity resolution process at different times could either lead to faster, slower, or the same speed of ambiguity resolution, or even to the ambiguity resolution failure. The variations, however, appear more with single-frequency data than dual-frequency data.

If observation errors and biases exist, different temporal locations of satellites also mean different level and characteristics of the errors and biases. An example of this is shown by the time series of the residuals in Figure 6.20. These least-squares residuals of wide-lane phase observations are related to monitor station UCLU and antenna B3 of the Rogue kinematic data, and derived by utilizing the integer ambiguities given in Table 4.15.

Notably, the level of observation errors and biases are generally not the same for the whole. Therefore, depending when the ambiguity resolution is performed, different performance of ambiguity resolution can be expected. An example is shown by the results in Table 6.11.

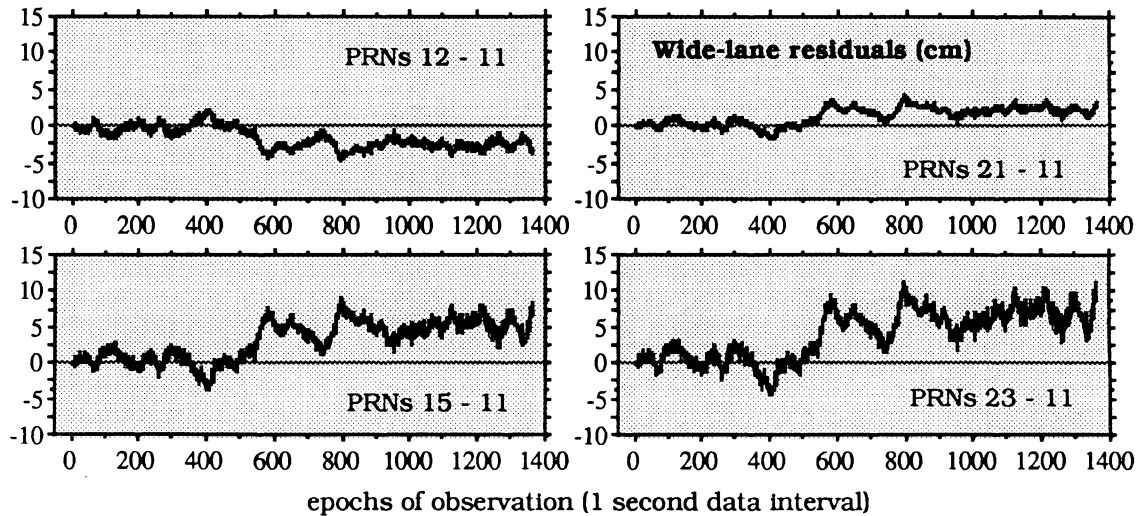


Figure 6.20. The time series of the wide-lane residuals.

Table 6.11. The time variations of the ambiguity resolution times (Rogue kinematic data, baseline UCLU - antenna B3, fixed-reference differencing approach).

elapsed times since 1st epoch	PRN number of primary satellites									
	11,12,15,21		11,12,15,23		11,12,21,23		11,15,21,23		12,15,21,23	
	A	B	A	B	A	B	A	B	A	B
0	1	62	1	52	1	56	1	57	1	56
5 minutes	1*	59	2*	54	4	72	1*	57	1*	50
10 minutes	3*	74	133	1552	5	78	3*	71	3*	66
15 minutes	1*	61	36	434	1*	54	2*	63	4*	73

\* denotes the ambiguity resolution failure.  
A = epoch of ambiguity resolution, B = CPU times in milliseconds.

Results are based on the number of initial ambiguity sets given in Table 6.10, and the values of the identification process parameters listed in Table 4.13. The same identification process parameters are used for all four cases. Two consecutive cases are separated by five minutes time interval. Note from Table 6.11 that, as expected, the parameter values of the identification process used in this case cannot represent the level and characteristics of the observation errors and biases for the whole observation period. This fact is indicated by quite a lot of cases of ambiguity resolution failures, as shown in Table 6.11.

Theoretically speaking, for each case, there will be certain values of the identification process parameters which will yield the fastest successful ambiguity resolution. Knowing these parameter values for each case, however, is not an easy task, since it will depend on quite a lot of factors. If the same parameter values is used for all cases and the ambiguity resolution failures are also avoided, then the pessimistic approach in assigning the parameter values is usually the safest approach to pursue. In the results shown in Table 6.11, if for example the ellipsoidal searching space is sized by 99.5% confidence level, and the values of the 5th, 6th, 7th, and 8th criteria are changed to 0.999, 0.70, 0.95 & 0.96, and 0.9999, respectively, then the ambiguity resolution epochs as listed in Table 6.12 are obtained. In this case, ambiguity resolution failures do not exist anymore.

Table 6.12. The time variations of the ambiguity resolution times (Rogue kinematic data, baseline UCLU - antenna B3, fixed-reference differencing approach).

elapsed times since 1st epoch	PRN number of primary satellites				
	11,12,15,21	11,12,15,23	11,12,21,23	11,15,21,23	12,15,21,23
	epoch of ambiguity resolution (1 second data interval)				
5 minutes	4	3	5	4	4
10 minutes	4	133	12	5	12
15 minutes	33	36	39	43	4

The time variations of the ambiguity resolution epochs, shown by Table 6.12, are not the same for all primary satellites, as theoretically expected. For the same primary satellites, the speed of ambiguity resolution could either be the same, slower, or faster depending on when the ambiguity resolution is performed. Slow but successful ambiguity resolution can be expected to correspond to the times of relatively large observation errors and biases, as indicated by the results shown in Figure 6.20 and Table 6.12. Slow ambiguity resolution can also be expected to occur when the ambiguity resolution is performed with poor primary satellite geometry, as shown by the results in Table 6.12 related to the primary satellites with PRNs 11, 12, 15, and 23. In general, it can be concluded that for fast and reliable ambiguity resolution, one has to choose observation times corresponding to a low level of the observation errors and biases, and relatively good primary satellites geometry as well as using the proper values of the identification process parameters.

## **6.8. Data rate**

The data rate of the observation does not affect the ambiguity searching space. With the same nominal size of the searching spaces, the same observation geometry, i.e., same signal wavelength, same observed satellites, and same primary satellites, and the same starting epoch of ambiguity resolution, the number of initial ambiguity sets to be tested are the same, regardless of the time interval between two consecutive observation epochs. Depending on the satellite geometry's rate of change and the time variations of the errors and biases in observations, the data rate of the observation could effect the speed of ambiguity resolution.

The examples of the effects of the observation data rate on the epoch of ambiguity resolution are given in Table 6.13 and 6.14. The results are based on the Rogue kinematic data described in Chapter 4. In both tables, the ellipsoidal searching spaces are sized with

99% confidence level, and the standard deviations of the observations as listed in Table 4.12 are used. The values of the identification process parameters given in Table 4.13 are used, except for those related to monitor station PGC in Table 6.14. In these latter cases, the parameter values used to derive the results of Table 6.7 are used. In all cases, the first epoch of ambiguity resolution is the first epoch of the observation session.

Note from the examples in Tables 6.13 and 6.14 that in terms of ambiguity resolution epochs, different data rate can lead to the same, slower, or faster ambiguity resolution, or even its failure. In terms of actual time, however, the higher data rate, i.e., the smaller data interval, generally leads to faster ambiguity resolution, and vice versa. In the cases shown in Table 6.13, the effects of different data rate on the epochs of ambiguity resolution are relatively small, except for the cases related to monitor station PGC, antennas B1 and B2, and primary satellites P #2, which are quite affected by a different data rate. These exceptions are probably due to different characteristics of the random errors in the observations and not due to the changes in satellite geometry, since the same case related to antenna B3 is not significantly affected by the different data rates used.

Note also from the results in these two tables that the effects of the data rates on the epoch of ambiguity resolution are also affected by the observation differencing approach used. This is quite obvious since a different differencing approach leads to different level and characteristics of the observation errors and biases and to different observation geometry, i.e., different pattern and spacing of ambiguity surfaces. In the examples shown in Tables 6.13 and 6.14, it can be seen that the effects of the data rates on the ambiguity resolution epochs in the cases related to monitor station PGC becomes more pronounced if the sequential differencing is used instead of fixed reference approach. In the cases related to monitor station UCLU, however, the effects of different data rates are not significantly affected by different observation differencing approach used. This leads to the conclusion

Table 6.13. The effects of data rate on the epoch of on-the-fly ambiguity resolution (Rogue kinematic data with fixed-reference observation differencing).

Data interval	P #1	P #2	P #3	P #4	P #5	P #1	P #2	P #3	P #4	P #5
	PGC - B1					PGC - B2				
1 sec.	6	13	4	6	4	5	12	5	6	4
2 sec.	4	6	5	5	4	5	7	5	5	4
3 sec.	4	4	5	5	4	4	4	4	5	4
4 sec.	4	4	5	4	4	4	3	5	4	4
5 sec.	4	3	5	4	4	4	3	5	4	4
8 sec.	4	3	4	4	4	4	3	4	5	4
10 sec.	4	2*	4	4	4	4	2*	5	5	4
	PGC - B3					UCLU - B1				
1 sec.	4	3	5	4	4	1	3	4	3	3
2 sec.	4	6	4	4	4	1	2	3	3	3
3 sec.	4	4	5	4	4	1	2	4	2	2
4 sec.	4	4	5	5	4	1	2	2	2	2
5 sec.	4	4	4	3	4	1	2	4	3	3
8 sec.	4	3	5	5	4	1	3	4	4	4
10 sec.	3	5	3	3	4	1	2	4	2	2
	UCLU - B2					UCLU - B3				
1 sec.	2	2	4	2	4	1	1	1	1	1
2 sec.	3	3	3	3	3	1	1	1	1	1
3 sec.	2	3	3	3	4	1	1	1	1	1
4 sec.	2	2	2	2	2	1	1	1	1	1
5 sec.	3	2	4	3	4	1	1	1	1	1
8 sec.	2	2	4	2	4	1	1	1	1	1
10 sec.	4	3	4	4	4	1	1	1	1	1
Primary satellites : P #1 (11,12,15,21), P #2 (11,12,15,23), P #3 (11,12,21,23), P #4 (11,15,21,23), P #5 (12,15,21,23) Fixed-reference differencing with 1st satellite in order as the reference satellite. The ambiguity resolution failure is denoted by *.										

Table 6.14. The effects of data rate on the epoch of on-the-fly ambiguity resolution (Rogue kinematic data with sequential observation differencing).

Data interval	P #1	P #2	P #3	P #4	P #5	P #1	P #2	P #3	P #4	P #5
	PGC - B1					PGC - B2				
1 sec.	6	13	4	13	13	6	12	5	12	12
2 sec.	6	6	5	7	7	5	7	5	7	7
3 sec.	5	4	5	5	5	5	4	4	5	5
4 sec.	5	4	5	9	11	5	3	5	11	12
5 sec.	5	3	5	9	9	8	3	5	8	10
8 sec.	5	3	4	5	6	6	3	4	6	9
10 sec.	5	5	4	5	5	5	5	5	5	15
	PGC - B3					UCLU - B1				
1 sec.	10	11	5	11	11	3	3	4	3	3
2 sec.	6	6	4	6	6	4	2	3	3	3
3 sec.	5	4	4	5	14	2	2	4	2	2
4 sec.	5	4	5	11	12	2	2	2	2	2
5 sec.	8	4	4	4	28	3	2	4	3	3
8 sec.	5	3	5	6	7	4	3	4	4	4
10 sec.	3	5	3	5	5	3	2	4	2	2
	UCLU - B2					UCLU - B3				
1 sec.	2	2	4	2	4	1	2	1	4	1
2 sec.	3	3	3	3	3	1	3	1	3	1
3 sec.	2	3	3	3	4	1	3	1	3	1
4 sec.	2	2	2	2	2	1	2	1	2	1
5 sec.	3	2	4	3	4	1	3	1	2	1
8 sec.	2	2	4	2	4	1	4	1	4	1
10 sec.	4	3	4	4	4	1	3	1	3	1
Primary satellites : P #1 (11,12,15,21), P #2 (11,12,15,23), P #3 (11,12,21,23), P #4 (11,15,21,23), P #5 (12,15,21,23) Sequential observation differencing approach.										



that the dependence of the effects of different data rates on the observation differencing used, as in the case of monitor station PGC, are related primarily to the different characteristics of the observation errors and noise and not to the changes in satellite geometry.

As stated before, different locations of satellites could lead to different observation geometry and different level and characteristics of the observation errors and biases. Therefore, the effects of different data rates will also be affected by the different location of satellites. The example is shown by Figure 6.21.

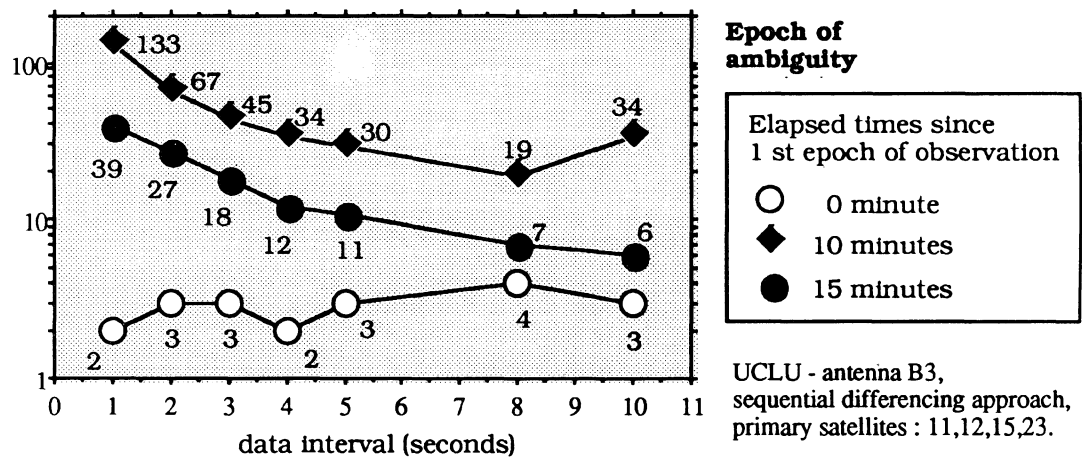


Figure 6.21. The effects of the observation data interval on the epoch of ambiguity resolution as a function of different temporal location of satellites.

The results are based on Rogue kinematic data, related to monitor station UCLU and antenna B3, and primary satellites with PRNs 11, 12, 15, and 23. Three different temporal locations of satellites are considered, with the first epoch of ambiguity resolution at the first epoch of observation, 5 minutes after the first epoch, and 10 minutes after the first epoch, respectively. For the first case, the same values of the identification process parameters as used in deriving the results in Table 6.14 are used, while in the other two cases the parameter values used for obtaining the results in Table 6.12 are used. Figure 6.18 shows

that the primary satellite geometry related to these three cases of satellite locations are not the same, indicated by the differences in the values and trends of their PDOPs. Consequently, the effects of different data rates on the epochs of ambiguity resolution are also different, depending on the location of satellites used. The results in Figure 6.21 also point out that the highest data rate, i.e., the smallest data interval, corresponds to the fastest speed of ambiguity resolution in terms of the actual times of observation, regardless of the satellites' locations.

### **6.9. Number of (secondary) monitor stations**

The number of secondary monitor stations (see Figure 3.2) will affect both the ambiguity searching space and the identification process of the correct ambiguity sets. To construct the ambiguity searching, however, the number of secondary monitor stations will have no affect if the extrawidelaning technique is used to estimate the initial ambiguity set. If the code-derived position is used, then the number of the monitor stations will affect the number of initial ambiguity sets to be tested.

Generally the more monitor stations used, the smaller the number of initial ambiguity sets there will be. The mathematical explanation for this matter is given in Appendix V. Figure 6.22 shows an example based on the single-frequency simulated kinematic GPS data, described in Appendix VI. The example is related to the 8-satellite constellation # 4 (see Figure VI.3).

In this example, one, two, three, and four monitors are related to stations SA; SA and SB; SA, SB, and SC; and SA, SB, SC, and SD, respectively, as shown in Figure VI.1. For more insight into the effects of the number of secondary monitor stations, the simulated GPS data in this case is contaminated only by observation noise. The satellite ephemeris

errors are simulated using the values given in Appendix VI. The ellipsoidal searching spaces are sized with 99% confidence level, and the precision of certain type of observations to all satellites is characterized by the same standard deviation. The standard deviations of the pseudoranges ( $\sigma_p$ ) and carrier phases ( $\sigma_L$ ) observations listed in Table 6.15 are used.

Table 6.15. The standard deviations of L1 C/A-code pseudoranges and phases.

	Monitor stations	Moving receiver
$\sigma_p$	1.0 m	1.5 m
$\sigma_L$	2.00 mm	3.00 mm

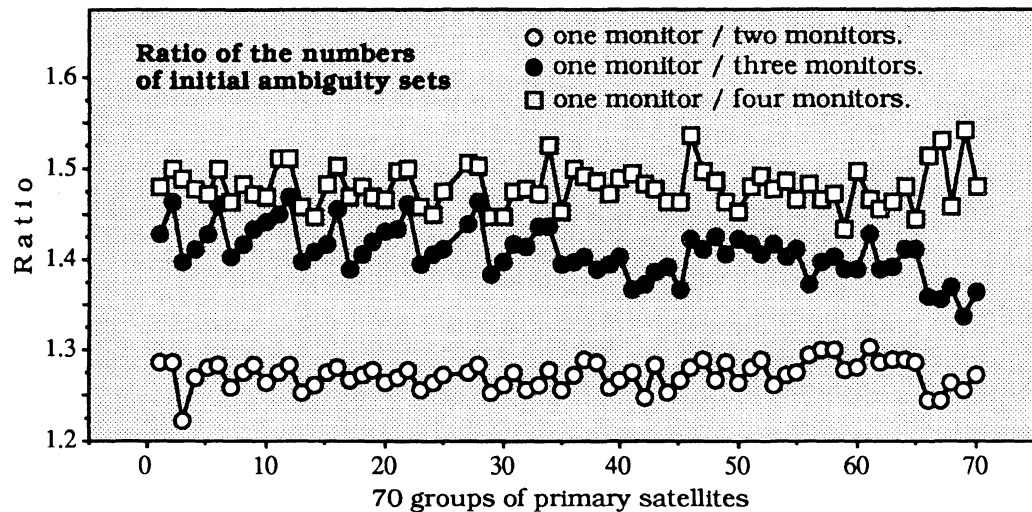


Figure 6.22. The ratio of the number of initial ambiguity sets with respect to the number of secondary monitor stations (single frequency, eight satellites, constellation #4).

According to Figure 6.22, the more secondary monitor stations used, the smaller the number of initial ambiguity sets obtained, regardless of the primary satellites used. The ratios of the numbers of initial ambiguity sets, related to two numbers of monitor stations, however, depend on the primary satellites. The average value of these ratios related to 70

group of primary satellites is more or less the same for all four 8-satellite constellations (see Figure VI.3) as shown by Table 6.16.

Table 6.16. The average of the ratios of the number of initial ambiguity sets with respect to the number of secondary monitor stations.

8-satellite constellation	8-satellite PDOP	The average of the ratios of the initial ambiguity sets related to 70 groups of primary satellites		
		<u>one monitor</u> <u>two monitors</u>	<u>one monitor</u> <u>three monitors</u>	<u>one monitor</u> <u>four monitors</u>
# 1	2.37	1.288	1.408	1.470
# 2	3.17	1.272	1.411	1.466
# 3	2.57	1.283	1.397	1.472
# 4	3.45	1.272	1.409	1.479

The number of secondary monitor stations also affects the identification process of the correct integer ambiguities. Generally, the more secondary monitor stations used, the more geometric constraints ambiguities have to satisfy, i.e., the more stringent the validation and rejection process. This makes the incorrect ambiguity sets more distinguishable and, in turn usually leads to faster ambiguity resolution. The results based on single-frequency simulated kinematic GPS data are shown in Figure 6.23, related to satellite constellation #2 and 30 groups of primary satellites. For the identification process of the correct integer ambiguities, the parameter values listed in Table 6.17 are used.

In Figure 6.23 with single-frequency and 8 observed satellites, the use of two secondary monitor stations can speed up the ambiguity resolution (in terms of epoch) up to four times more the use of only one monitor station. The ratio of improvement depends on the primary satellites used. Note also from the figure that using three or four monitor stations speeds up the ambiguity resolution in a few cases of primary satellites. In general, however, there is no significant improvement over the two monitor station. This is also true for other satellite

constellations, shown in Figure VI.3. Figure 6.24 shows the results of a two monitor station case, related to other satellites constellations.

Table 6.17. The parameter values of the identification process (A for one monitor; B for two, three, and four monitors).

The parameters	A	B
Confidence level of ellipsoidal searching space	0.99	0.99
Confidence level of the first criteria	0.99	0.99
The constant value of the second criteria	0.50	0.50
Confidence level of the third criteria	0.95	0.95
The constant value of the fourth criteria	0.10	0.10
Confidence level of the fifth criteria	0.99	0.99
Minimum individual mapping function value of the sixth criteria	0.80	0.80
Minimum normalized mapping function values of the seventh criteria	0.97 & 0.98	0.97, 0.98, and 0.99
Confidence level of the eight criteria	0.99	0.99
Minimum normalized mapping function value of the assurance criteria	0.995	0.995

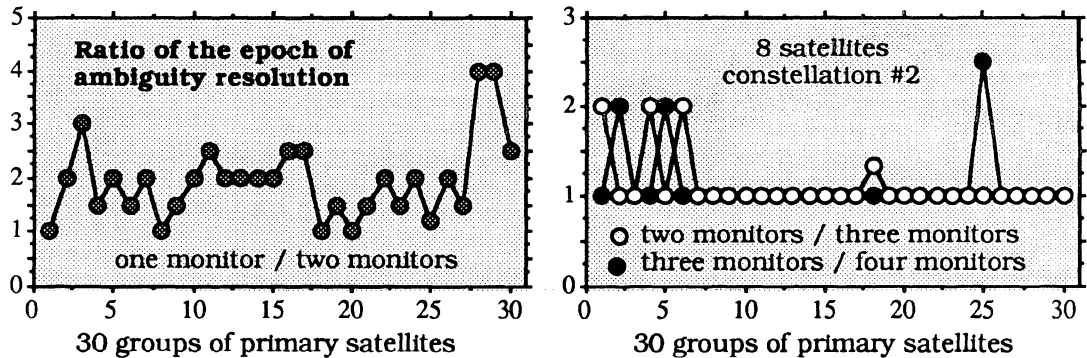


Figure 6.23. The effects of the number of secondary monitor stations on the epochs of ambiguity resolution ( single-frequency, 8 satellites, constellation #2).

Note from Figure 6.24 that the effect of two monitor stations in improving the speed (in terms of resolution epochs) of the ambiguity resolution depends also on the satellite constellation and the primary satellites used. At certain satellite constellations, depending on the primary satellites used, the computation times associated with the use of two monitor stations, could either be slower or faster than single monitor station.

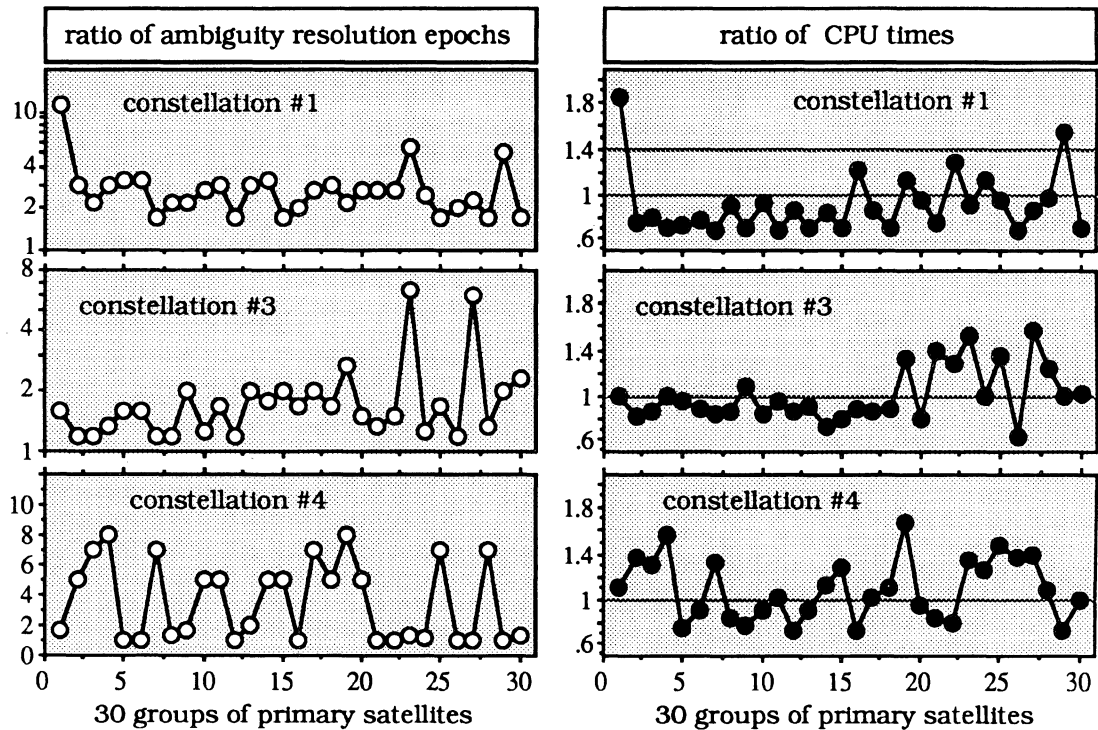


Figure 6.24. The ratios between one monitor and two monitors ambiguity resolution results (single-frequency, 8 satellites).

With a smaller number of observed satellites, it can be expected that the effects of the number of secondary monitor stations on the ambiguity resolution epoch will be different. In this case, the examples related to the cases of seven and six observed satellites are shown in Figures 6.25 and 6.26, respectively. The examples are based on the same simulated kinematic GPS data and the same values of the identification process parameters used in obtaining the results shown in Figure 6.23 and 6.24. Note from Figure 6.25 that

with single frequency data and seven satellites, depending on the primary satellites, the use of three monitor stations can still be beneficial in improving the speed of ambiguity resolution. The use of four monitor stations generally does not produce significant improvement. Although with a few groups of primary satellites, improvements in the ambiguity resolution speed can still be achieved. As shown by examples in Figure 6.26, the general trends with six observed satellites are more or less the same with those in the case of seven observed satellites.

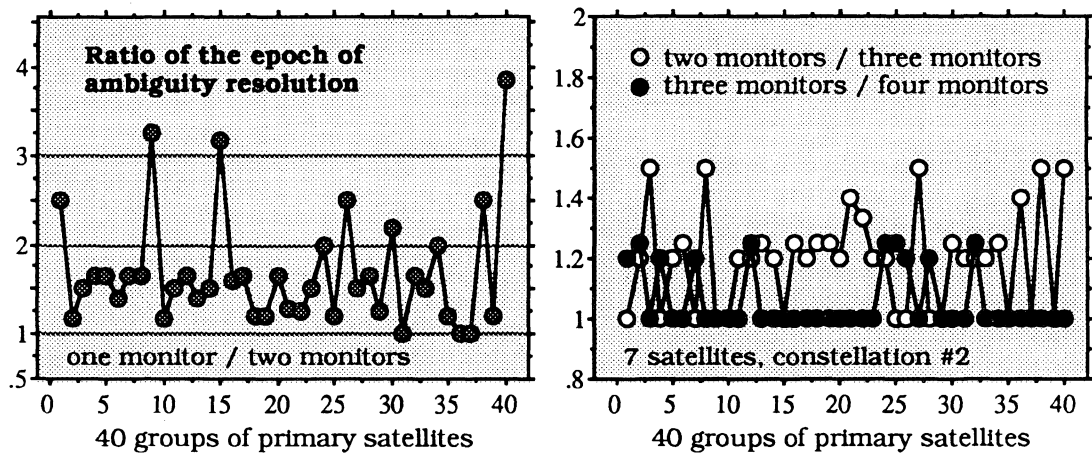


Figure 6.25. The effects of the number of secondary monitor stations on the epochs of ambiguity resolution ( single-frequency, 7 satellites, constellation #2).

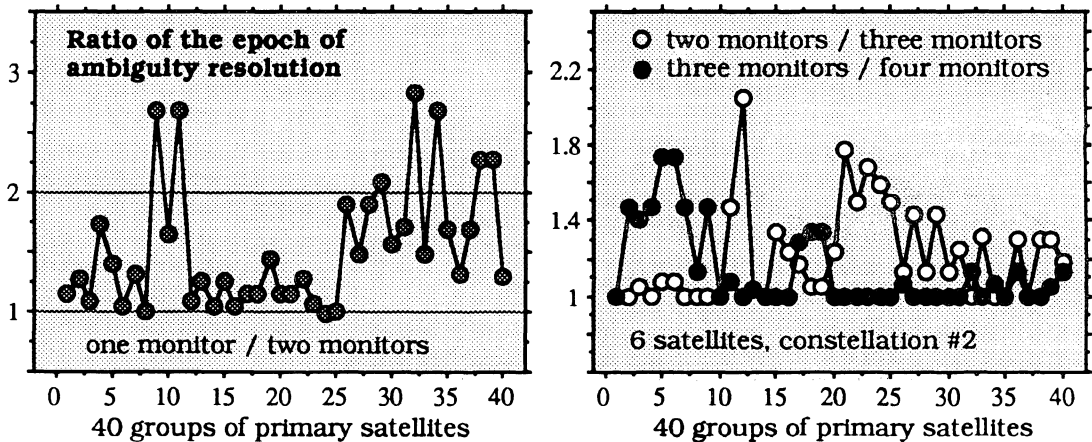


Figure 6.26. The effects of the number of secondary monitor stations on the epochs of ambiguity resolution ( single-frequency, 6 satellites, constellation #2).

Finally, it should be mentioned that, in the case of codeless or dual-frequency data, the required number of secondary monitor stations at certain number of observed satellites can be expected to be fewer than the one required for single frequency data. Some simulation results related to this hypothesis can be seen in *Abidin et. al.* [1991].

#### **6.10. Location of (secondary) monitor stations**

The location of secondary monitor stations will affect the ambiguity resolution process. Although the location of the monitor stations will not affect the size, shape, and orientation of the ellipsoidal searching space, when a code-derived position is used to estimate the initial ambiguities, the center location of the searching space could be affected. In this case, since the code-derived position is estimated using pseudoranges from all monitor stations, then different location of the monitor stations could affect the estimated position. This is mainly caused by the looking-direction dependent errors and biases, such as the ionospheric and tropospheric delays, and the satellite ephemeris errors, for which their effects on the pseudoranges are dependent on the looking directions from the monitor stations to the satellites.

Since location of secondary monitor stations only affects the center location of the searching space, it can be expected that the effects of the monitor station location on the number of initial ambiguity sets will be relatively small. The examples based on the simulated GPS kinematic data used in the previous section is shown in Figure 6.27. In this case, however, the pseudoranges and phases observations are contaminated with the low ionospheric biases computed using the Bent ionospheric model explained in Appendix VI. The examples are related to 8 satellites, 2 monitor stations, and satellite constellation #4 session, which is started approximately around 2.00 p.m. local time.



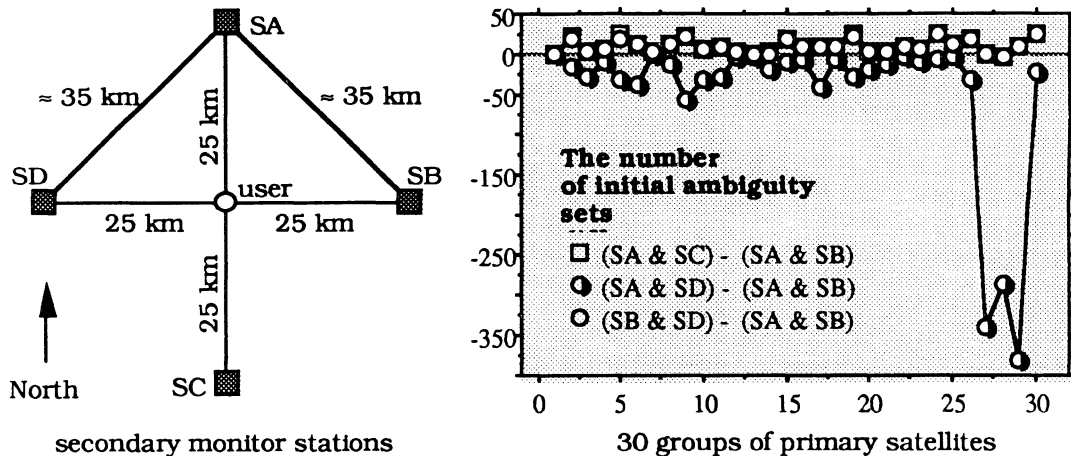


Figure 6.27. The effects of location of secondary monitor stations on the number of initial ambiguity sets ( single-frequency, 8 satellites, 2 monitor stations, constellation #4). In this case, the average number of initial ambiguity sets from four monitor stations and 30 groups of primary satellites is 126,592.

The ellipsoidal searching space is sized with 95% confidence level, and to account for the residual ionospheric delays in the observations, the standard deviations of the observations at every epoch are considered to be elevation-dependent and are computed using equation (4.1). In this case, the zenith standard deviations listed in Table 6.18 are used. Note from Figure 6.27 that the effects of monitor station locations on the number of ambiguity sets are relatively small and are dependent on the primary satellite used.

Table 6.18. Zenith standard deviations of the pseudoranges and phases.

	Monitor stations	Moving receiver
$\sigma_p(90)$	1.0 m	1.5 m
$\sigma_L(90)$	6.00 mm	9.00 mm

Since with different locations of monitor stations, the double difference observations could experience different levels of errors and biases, it is obvious that the location of the monitor

stations could lead to different speed of ambiguity resolution. An example is shown in Figure 6.28. The results are based on the same simulated data used to derive the results shown in Figure 6.27. For the identification correct integer ambiguities, the parameter values listed in Table 6.19 are used. More pessimistic values than those in Table 6.17 are used to account for the residual ionospheric biases in the observations.

Table 6.19. The parameter values of the identification process.

The parameters	Parameter values
Confidence level of ellipsoidal searching space	0.950
Confidence level of the first criteria	0.950
The constant value of the second criteria	1.000
Confidence level of the third criteria	0.950
The constant value of the fourth criteria	0.100
Confidence level of the fifth criteria	0.999
Minimum individual mapping function value of the sixth criteria	0.700
Minimum normalized mapping function values of the seventh criteria	0.900, 0.920, and 0.930
Confidence level of the eight criteria	0.999
Minimum normalized mapping function value of the assurance criteria	0.950

Note from the results in Figure 6.28 that, with the existence of low residual ionospheric delays, the resolution epoch of L1 signal ambiguity is quite significantly affected by the location of the secondary monitor stations. As shown by this example, the effects of the monitor station locations are also dependent on the primary satellites used. The examples in Figure 6.28 suggest that one should carefully place the secondary monitor stations by considering the relative locations of the satellites and the possible residual errors and biases

after applying the corrections derived by the primary monitor stations (refer to Figure 3.2 in Chapter 3).

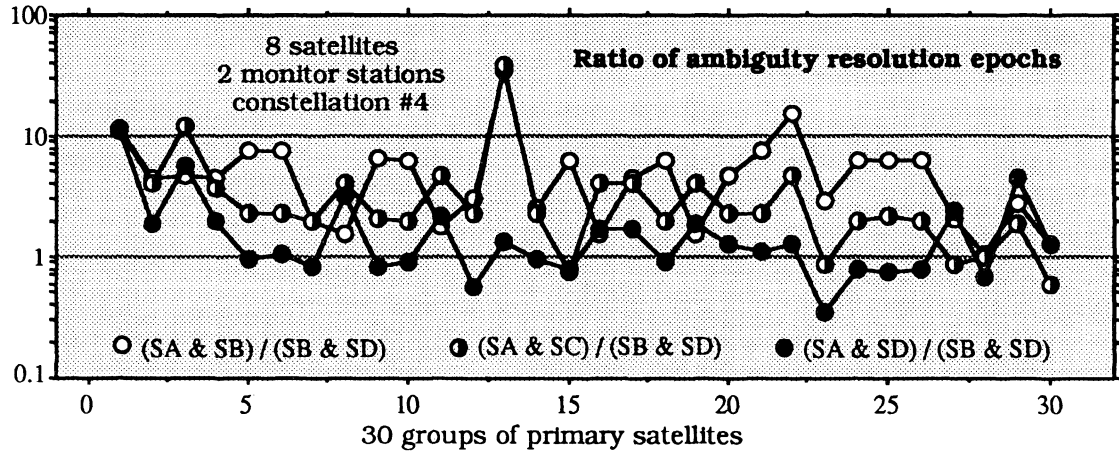


Figure 6.28. The effects of location of secondary monitor stations on the epochs of ambiguity resolution.

The effects of the location of the secondary monitor stations can be expected to be more significant with increases in the level of ionospheric activity and the distances between the monitor stations, which make the effects of satellite ephemeris errors more apparent. In these situations, it is obvious that for fast and reliable ambiguity resolution, the locations of the secondary monitor station have to be judiciously chosen.

## Chapter 7

# SUMMARY, CONCLUSIONS, AND RECOMMENDATIONS

---

---

This final chapter summarizes the research, presents conclusions, and finally recommends some suggestions for future investigations.

### **7.1. Summary of the research.**

The research primarily studied the possibility of performing reliable and fast on-the-fly ambiguity resolution of GPS carrier phase signals. An integrated on-the-fly ambiguity resolution technique was developed. The technique was designed to work with either single-frequency, codeless or dual-frequency GPS data from a minimum of five observed satellites, and it accommodates the use of more than one monitor station. The technique also considers in its formulation existing on-the-fly ambiguity resolution techniques such as the extrawidelaning technique, ambiguity mapping function technique, and least-squares ambiguity searching technique, which are reviewed in Chapter 2. The integrated technique developed utilizes the positive features of the existing techniques along with its own features, which include new validation and rejection criteria. The concept and mathematical formulations of the technique are described in Chapter 3, and its general strategy is depicted in Figure 7.1.

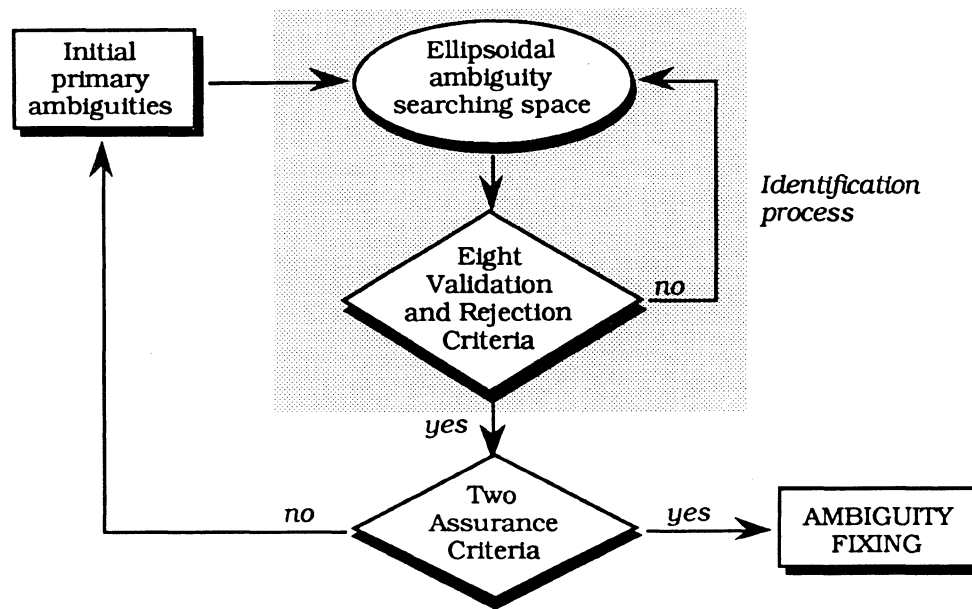


Figure 7.1. General strategy of the integrated on-the-fly ambiguity resolution technique.

The validity of the technique has been verified using static and kinematic GPS data. The static GPS data used are the Trimble zero baseline data and Ashtech short baseline data, and the kinematic data are observed using Rogue receivers involving three antennas on a moving buoy. The integrated technique has been shown to be capable of reliably and quickly resolving initial ambiguities on-the-fly. Under certain conditions, resolution was instantaneous. The results of verification are presented in Chapters 4 and 6, and the summary is shown in Table 7.1. These results are based on one monitor station and certain parameter values of the identification process.

Computational and geometrical aspects of on-the-fly ambiguity resolution have also been studied in this research. The computational aspects studied involve the construction of the ambiguity searching space and the process of identifying the correct ambiguities as shown in Figure 7.2. With ambiguity searching space construction, the advantages of using an ellipsoid rather than a cube for the shape of ambiguity searching space to speed up the ambiguity resolution are investigated and presented.

Table 7.1. Summary of the verification results of the integrated on-the-fly ambiguity resolution technique.

data types	receiver used	baseline length	number of satellites	data rate (seconds)	Basic signal for resolution	Ambiguity resolution	
						epoch	times
<b>static :</b> L1-C/A code, L2-P code, and full wavelength L1 and L2 carrier phases	Trimble geodesist P-receivers	zero	6	5	L1	6	25 sec.
					widelane	2	5 sec.
<b>static :</b> L1-C/A code, full wavelength L1, and half wavelength L2 carrier phases	Ashtech LD-XII	≈ 535 m	5	30	L1	7	180 sec.
					half widelane	4	90 sec.
					double widelane	2	30 sec.
<b>kinematic :</b> L1-P code, L2-P code, and full wavelength L1 and L2 carrier phases	Rogue	≈ 61 km	5	1	widelane	3	2 sec.
		≈ 61 km				4	3 sec.
		≈ 61 km				1	instant
		≈ 157 km				4	3 sec.
		≈ 157 km				4	3 sec.
		≈ 157 km				4	3 sec.

The effects of the size of the ellipsoidal searching space on the speed and reliability of the ambiguity resolution are also studied with respect to the confidence level of the ellipsoid, standard deviations of the observations, and the primary satellites used. With dual frequency data, the effects of the initial ambiguity estimation approaches (the code-derived position approach and extrawidelaning technique) on the size of the searching space is also presented. Characteristics of the validation and rejection criteria employed by the integrated technique in the identification process of the correct integer ambiguities are also studied, particularly their identification power, the numbers and types necessary, and the parameter values used in the process. The Trimble zero baseline data and the Rogue kinematic data are used for the investigations. Results of the investigations are given in Chapter 5.

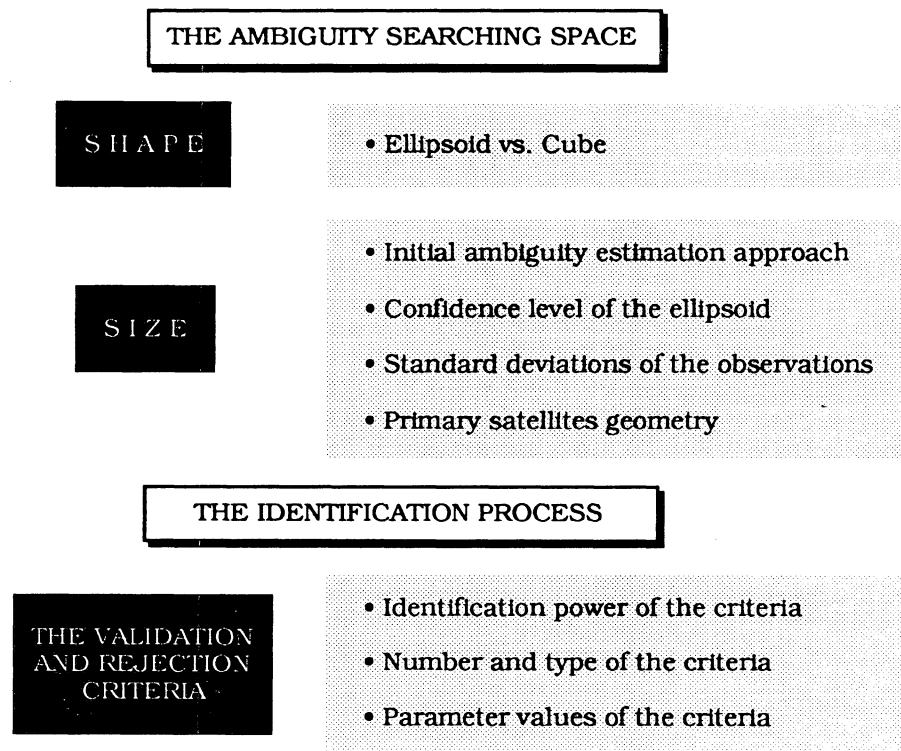


Figure 7.2. The computational parameters of on-the-fly ambiguity resolution.

The speed and reliability of on-the-fly ambiguity resolution will be affected by the observation geometry. In this research, the effects of the observation geometry are investigated with respect to the geometrical parameters listed in Figure 7.3. Static and real kinematic GPS data are used to investigate the geometrical parameters of GPS satellites and observations. For the geometrical parameters related to the secondary monitor stations, the single-frequency simulated kinematic GPS data involving four secondary monitor stations are used for the investigation. The results of the investigations are presented in Chapter 6.

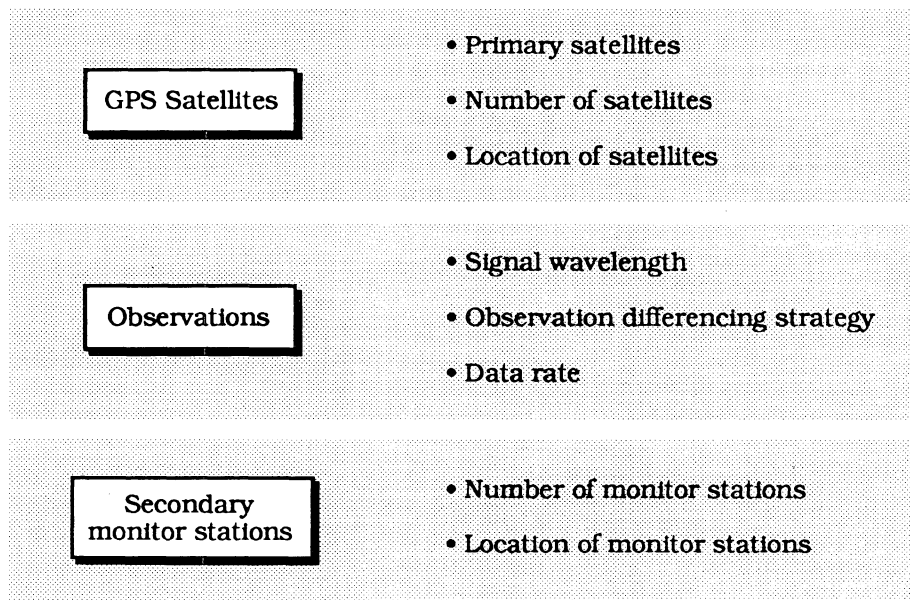


Figure 7.3. The geometrical parameters of the on-the-fly ambiguity resolution.

In explaining the effects of some geometrical parameters of the ambiguity resolution process, the concept of the lines and surfaces of (double-difference) ambiguities are applied. The application of this concept provides a more meaningful interpretation of the ambiguity resolution, as shown in Chapter 6. Finally, it should be noted that a significant number of results are produced during the course of this research. These results, which are summarized and presented in Chapters 4, 5, and 6, give a general idea about the achievable results, prospects, and limitations of on-the-fly ambiguity resolution.



## **7.2. Conclusions of the research**

Based on the investigations done in this research and the results obtained from the data processing, the following conclusions can be drawn.

### **7.2.1. The construction of initial ambiguity searching space**

(1). For fast and reliable on-the-fly ambiguity resolution, an ellipsoidal searching space should be used instead of a cubic searching space. The ellipsoidal searching space will contain a smaller number of ambiguity sets to be tested, which means shorter computation times for ambiguity resolution. This will usually also lead to faster observation times of ambiguity resolution. The ratio of improvement can reach a factor of two, depending on the size of the space.

(2). The initial ambiguity searching space is centred at the initial estimates of ambiguities. In the case of P-code dual frequency data, it is preferable to estimate the initial ambiguities using the code-derived position rather than using the extrawidelaning technique. Moreover, the narrow-lane pseudoranges should be used, due to its lower noise than the other types of pseudoranges. When more than one secondary monitor station is used, the initial ambiguity should be estimated using the pseudoranges from all of the monitor stations. Pseudoranges should always be smoothed to reduce their noise levels by using carrier phase observations.

In the case of C/A code and codeless data, it is more reliable to smooth the pseudoranges for 5 to 10 epochs before constructing the initial searching space instead of constructing the searching space at the very first epoch of observation.

- (3). For fast and reliable on-the-fly ambiguity resolution, the ellipsoidal ambiguity searching space in general should be sized with confidence level between 95% to 99%. The size of searching space should be neither too small (  $\ll 95\%$  ) nor too large (  $\gg 99\%$  ).

The small searching space, although preferable from the computational point of view, is not always reliable. It may not contain the correct ambiguity set, which in turn could lead to the ambiguity resolution failure (the ambiguities are fixed to the incorrect integers) or if not, it will still slow down the ambiguity resolution process.

A large ambiguity searching space, on the other hand, is not preferable from the computational and reliability points of view. Computationally, since the space will contain too many ambiguity sets to be tested, it will lead to longer computation times and usually also to longer observation times of ambiguity resolution. For reliability it is also not preferable since it will contain too many ambiguity sets to be tested which, with certain observation geometry, could lead to ambiguity resolution failures.

#### **7.2.2. The implementation of the validation and rejection criteria.**

- (1). For fast and reliable on-the-fly ambiguity resolution using the integrated technique, all eight validation and rejection criteria should generally be used.
- (2). Different values of the validation and rejection criteria parameters could lead to different computation and observation times of ambiguity resolution, and even to the failure in the ambiguity resolution.

The optimal set of values, which will lead to the fastest and successful on-the-fly ambiguity resolution, however, is not easy to determine. One has to consider quite a lot of factors in determining them, such as the type of data being used, residual observation errors and biases, and observation geometry, i.e., the number of satellites, signal wavelength, number of secondary monitor stations, etc.

In general, however, based on the trial and error selection process adopted in this research, the interval of values listed in Table 7.2 can be considered. Choosing the set of values from these intervals for a particular data set should be done by considering these factors. Pessimistic values are preferable for reliability, but not for computational efficiency and vice versa for the optimistic values.

Table 7.2. The interval values for the identification process parameters.

Criteria	Single frequency	Codeless	Dual frequency
#1	0.95 - 0.99	0.95 - 0.99	0.95 - 0.99
#2	0.10 - 0.40	0.10 - 0.40	0.20 - 0.40
#3	0.95 - 0.99	0.95 - 0.99	0.95 - 0.99
#4	0.05 - 0.10	0.05 - 0.10	0.05 - 0.10
#5	0.990 - 0.999	0.990 - 0.999	0.990 - 0.999
#6	0.80 - 0.90	0.80 - 0.90	0.70 - 0.85
#7	0.97 - 0.99	0.97 - 0.98	0.95 - 0.97
#8	0.9900 - 0.9999	0.9900 - 0.9999	0.9900 - 0.9990
Assurance	0.99 - 0.995	0.98 - 0.99	0.97 - 0.98

### 7.2.3. The effects of the observation geometry.

- (1). The observation geometry, i.e., geometry related to all observation components such as the signal being observed, the satellites, the monitor station(s), and the user, strongly affects the speed and reliability of on-the-fly ambiguity resolution.
- (2). The wavelength of the signal affects the speed and reliability of on-the-fly ambiguity resolution. It will affect both the number of initial ambiguity sets to be tested and the identification process of the correct integer ambiguities. The longer wavelength leads to faster and more reliable resolution of its ambiguities.

In the case of dual-frequency data, the wide-lane signal (wavelength  $\approx 86\text{cm}$ ) should be used as a working signal, while in the case of codeless data one can either use the half wide-lane signal (wavelength  $\approx 43\text{ cm}$ ) or the double wide-lane signal (wavelength  $\approx 163\text{ cm}$ ). Since the levels of the ionospheric effects and the observation noise of the double wide-lane signal are significantly higher than those of the half wide-lane signal, the double wide-lane signal should only be used when the effects of those two variables are relatively insignificant.

- (3). The primary satellites used will affect both the number of initial ambiguity sets to be tested and the identification process of the correct ambiguities. With certain satellite constellations, for fast and reliable ambiguity resolution, one should not use the primary satellites with the smallest or the largest values of NAI1 or PDOP. Instead the primary satellites with the NAI1 or PDOP values (either one of them) close to the averages values related to all possible combination of primary satellites should be used.

- (4). The number of satellites being used affects both the number of initial ambiguity sets to be tested and the identification process of the correct ambiguities. For a given size of the searching space, more satellites means fewer initial ambiguity sets. This in turn leads to faster ambiguity resolution.

In general, in the case of codeless and P-code dual frequency data, five satellites and one monitor station are enough to resolve the ambiguities under one minute of observation times. In the case of C/A code data, at least six satellites are required, unless more than one secondary monitor station are used. In the case of P-code dual-frequency data, ambiguity resolution well under 10 seconds of observation time can also be achieved using one monitor station and five satellites, providing that accurate pseudoranges (as measured by the Rogue receiver) are used.

- (5). The observation differencing strategy, used to perform the double difference observations, affects the speed and reliability of on-the-fly ambiguity resolution. It will affect both the number of initial ambiguity sets to be tested and the identification process of the correct ambiguities. With certain parameter values of the identification process, a different observation differencing strategy could lead to a different speed of ambiguity resolution, and even to the ambiguity resolution failures.

In terms of observation differencing approach, although the sequential differencing sometimes leads to faster ambiguity resolution, the fixed reference differencing in general seems to be more reliable. With certain chosen primary satellites, the reference satellite which corresponds to the smallest or the largest values of  $\|\lambda \cdot GP\|$ , i.e., corresponds to the largest and smallest number of initial ambiguity sets to be tested, should not be used. Instead, for fast and reliable ambiguity resolution, the

satellite that corresponds to a more or less average value of  $\|\lambda.GP\|$  should be used as the reference satellite.

- (6). Within a certain observation period, the speed and reliability of on-the-fly ambiguity resolution will depend on the time when the ambiguity resolution process is started. Generally, if operationally possible, the period of poor satellite geometry (indicated by relatively large value of PDOP) should not be used as the times to perform on-the-fly ambiguity resolution.
- (7). For fast on-the-fly ambiguity resolution, high data rate is necessary. In general, the data rate equal or higher than 1 Hz is preferable. The optimal data rate to be used, however, should also be chosen by considering the types of GPS data and the number of satellites being observed, as depicted in Figure 7.4.

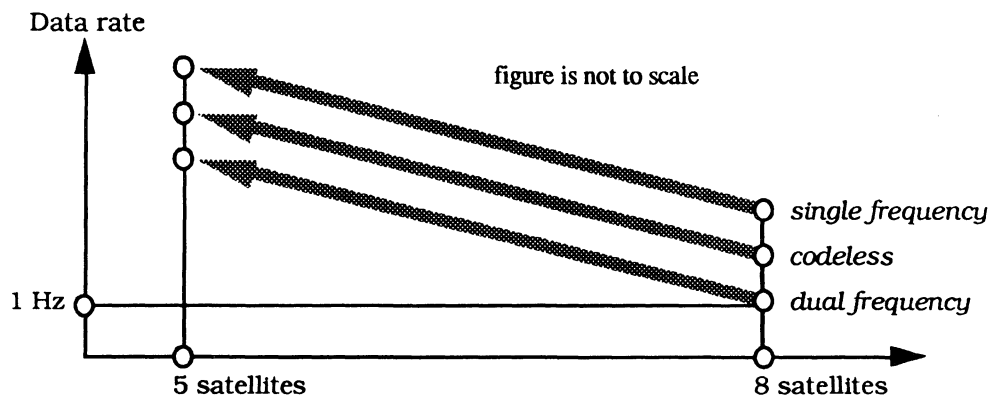


Figure 7.4. Optimal data rate implementation considerations.

- (8). The number of secondary monitor stations affect the number of initial ambiguity sets to be tested and the identification process of the correct ambiguities. If the code-derived position is used to estimate the initial ambiguities, more secondary monitor stations will reduce the number of initial ambiguity sets inside the searching space.

Moreover, with more secondary monitor stations, the ambiguities being tested have to satisfy more geometrical and mathematical constraints. Therefore, the use of more than one monitor stations usually leads to faster ambiguity resolution.

The optimal number of secondary monitor stations to be used, however, depends primarily on the required speed of the ambiguity resolution, the type of data being used, and the number of satellites available. In general, based on the data processing done in this research, using real and simulated GPS data, it can be predicted that to successfully resolve the ambiguities under 30 seconds of observation time (with 1 second data intervals), the maximum optimal number of secondary monitor stations required is three, namely when C/A code data is used with five satellites. When P-code data is used, generally one monitor station is enough, even with five satellites. In the case of a codeless data, maximum of two monitor stations are required when only five satellites are available.

- (9). When more than one secondary monitor station is used, the monitor stations should be located by considering the location of the satellites relative to the moving receiver to minimize the effects of residual ionospheric refraction and satellite ephemeris errors. Whenever possible, monitor stations should also be located as close as possible to the moving receiver.

#### **7.2.4. Instantaneous on-the-fly ambiguity resolution.**

- (1). The speed and reliability of on-the-fly ambiguity resolution are affected by many factors. To achieve successful instantaneous ambiguity resolution, several factors have to be judiciously taken into account, and it is indeed possible to achieve it under certain circumstances. The degree of possibility depends primarily on the accuracy

and precision of the pseudoranges, level of residual observation errors and biases, and observation geometry.

- (2). By using the integrated technique, the instantaneous on-the-fly ambiguity resolution for baseline length of about 60 km is possible with certain satellite geometry, dual-frequency data with accurate and precise P-code pseudoranges (as observed by Rogue GPS receiver), five observed satellites, and relatively small residual errors and biases in the observations with respect to the wavelength of L1 signal, i.e., less than 0.25 cycles.
- (3). Based on the simulated kinematic GPS data, it is predicted that for single frequency data and favourable satellite geometry, instantaneous on-the-fly ambiguity resolution is possible, providing that at least eight satellites are available, two secondary monitor stations are used, and the residual errors and biases in the observations are less than 0.25 cycles of L1 signal.
- (4). A network of primary monitor stations which can provide the user the information for eliminating the effects of satellite ephemeris errors and the ionospheric refraction, is necessary for fast and reliable on-the-fly ambiguity resolution, and is critical for reliable instantaneous on-the-fly ambiguity resolution.

### **7.3. Prospects and limitations of on-the-fly ambiguity resolution**

Based on the results obtained in this research, experiences gained during the course of the research, and theoretical considerations, some points related to the prospects and limitations of on-the-fly ambiguity resolution can be drawn.



### 7.3.1. The prospects

With the full deployment of GPS satellites, users will have enough satellites to perform fast and reliable on-the-fly ambiguity resolution. With full satellite deployment, the better spatial and temporal coverage of the satellites will allow fast and reliable ambiguity resolution in all regions and during all times of the day. If the GLONASS satellites are also considered, then the situation becomes even better [*Chamberlain and Eastwood, 1990*].

The wide-area differential GPS system is intended to provide the users with the information to correct for clock errors, effects of the ionospheric refraction, and satellite ephemeris errors. The realization of this wide-area differential concept will ease the users in performing fast and reliable ambiguity resolution. Besides relying on single-frequency data, the user will also have more flexibility in placing the secondary monitor station(s).

Advancements in the receiver, computer, and data communication technology will certainly improve the performance of on-the-fly ambiguity resolution. In terms of the receiver, it can be expected that the single-frequency GPS receiver which can provide precise and accurate pseudoranges, and can internally suppress the multipath effects [*Meehan and Young, 1992*], might be available in the near future.

Due to the fast development in electronics technology, the availability of faster and more powerful computer and data communication systems can also be expected in the near future. The products of these advancements, will not only improve the performance (speed and reliability) of on-the-fly ambiguity resolution, but will also make the on-the-fly ambiguity resolution much easier and more practical for day-to-day precise real-time kinematic positioning.

Since fast and reliable on-the-fly ambiguity resolution will have a lot of practical applications, as have been described in Chapter 1, it can also be expected that the research in this area will be on going. Therefore, the smarter and more powerful algorithm, i.e., more automatic, more adaptive, taking into account the physical correlation among the observations and the effects of multipath and residual ionospheric bias, etc., can be expected still to come.

### **7.3.2. The limitations**

Although the prospects for on-the-fly ambiguity resolution are quite promising, the implementation of the Anti-Spoofing (A-S) policy degrades the performance of the ambiguity resolution for unauthorized users who are mostly civilians. Since the unauthorized users cannot get access to the P-code and have to work with single-frequency or codeless data, the users should use as many satellites as possible and perhaps two or three secondary monitor stations to achieve fast and reliable on-the-fly ambiguity resolution. The use of GLONASS satellites should also be considered in this case.

Until the receiver which can internally suppress the multipath effects is available, on-the-fly ambiguity resolution performance will be degraded by multipath effects which cannot be eliminated by the information obtained from the primary monitor stations network.

Moreover, if the correction parameters derived by the primary monitor stations network cannot fully represent the ionospheric effects for the local survey area, then the residual ionospheric bias may also degrade the performance of the ambiguity resolution.

#### **7.4. Suggestions and recommendations for future research.**

The research reported in this dissertation did not provide all the answers to the problem of fast and reliable on-the-fly ambiguity resolution, which in itself is a multi faceted problem. Some aspects have not been investigated, such as those related to multipath effects, residual ionospheric delays, and cycle slips, and some of them need more elaborate investigations. Since on-the-fly ambiguity resolution is an important aspect of precise real-time kinematic positioning, research in this area should be continued. The following investigations are recommended to be performed as a continuation of this research.

- (1). In order to have more insight into the performance of the integrated on-the-fly ambiguity resolution technique, a wider variety of kinematic GPS data should be processed. Data from marine, airborne, and land environments observed by various GPS receivers (single-frequency, codeless, and dual-frequency) should be considered, including those related to many secondary monitor stations.
- (2). In conjunction with the above suggestion, effects of the observation geometry on the speed and reliability of on-the-fly ambiguity resolution, which have been investigated in this research, should also be re-investigated with a wider variety of observation geometry in order to get deeper insight into the problem of on-the-fly ambiguity resolution. The effects of using both the GPS and GLONASS satellites should also be investigated.
- (3). The effects of uncompensated observation errors and biases on the performance of on-the-fly ambiguity resolution should be thoroughly investigated and analyzed. The effects of multipath and residual ionospheric delays should be given special attention.

- (4). The effects of the physical correlation among the observations on the performance of on-the-fly ambiguity resolution, which are neglected in this research, should also be investigated.
- (5). The algorithm should be improved, particularly the part related to the assignment of values to the identification process parameters, i.e., the parameters related to the size of ambiguity searching space, the validation and rejection criteria, and the assurance criteria. The assignment should be designed and formulated to be *automatic*, i.e., no user interference is needed, and *adaptive*, i.e., the parameter values automatically changed as the observation geometry and the level of the observation errors and biases change.
- (6). The software code should also be improved. The software code developed here was designed as a research tool, and not to meet the standards of modern, commercial, user-friendly software. Once a production application and algorithm are decided upon, the code should be made computationally more efficient, and more "bullet-proof and user-friendly".

## REFERENCES

---

---

- Abidin, H. Z. and D. E. Wells (1990). "Extrawidelaning for on-the-fly ambiguity resolution: simulation of ionospheric effects." *Proceedings of Second International Symposium on Precise Positioning with the Global Positioning System*, Ottawa, Canada, 3-7 September, pp. 1217-1232.
- Abidin, H. Z. (1990). "Extrawidelaning for on-the-fly ambiguity resolution: simulation of multipath effects." *Proceedings of ION GPS-90 Third International Technical Meeting of the Satellite Division of the Institute of Navigation*, Colorado Springs, Colorado, USA, 17-21 September, pp. 525-533.
- Abidin, H. Z. (1991). "New strategy for on-the-fly ambiguity resolution." *Proceedings of ION GPS-91, Fourth International Technical Meeting of the Satellite Division of the Institute of Navigation*, Albuquerque, New Mexico, 11-13 September, pp. 875-886.
- Abidin, H. Z., D.E. Wells, and A. Kleusberg (1991). "Multi-monitor station on-the-fly ambiguity resolution: Theory and preliminary results." *Proceedings of DGPS '91, First International Symposium on Real Time Differential Applications of the Global Positioning System*, Braunschweig, Federal Republic of Germany, 16-20 September, Volume I, pp. 44-56.
- Abidin, H.Z. (1992). "Multi-monitor station on-the-fly ambiguity resolution: the impacts of satellite geometry and monitor station geometry." *Proceedings of PLANS '92, IEEE Position Location and Navigation Symposium*, Monterey, California, 24-27 March, pp. 412-418.
- Abidin, H.Z., D.E. Wells, and A. Kleusberg (1992). "Some aspects of on-the-fly ambiguity resolution." *Proceedings of Sixth International Geodetic Symposium on Satellite Positioning*, Columbus, Ohio, 17-20 March, Volume II, pp. 660-669.
- Ackermann, F. (1990). "Kinematic GPS camera positioning for aerial triangulation." *Proceedings of Second International Symposium on Precise Positioning with the Global Positioning System*, Ottawa, Canada, 3-7 September, pp. 1155-1168.

- Anderman, A. (1991). "Integrated INS/GPS attitude determination for manned space flight." *Proceedings of ION GPS-91, Fourth International Technical Meeting of the Satellite Division of the Institute of Navigation*, Albuquerque, New Mexico, 11-13 September, pp. 161-170.
- Ashjaee, J. and R. Lorenz (1992). "Precision GPS surveying after Y-code." Paper presented at ION GPS-92, 5th International Technical Meeting of the Satellite Division of the Institute of Navigation, Albuquerque, New Mexico, 16-18 September.
- Auernhammer, H. and T. Muhr (1991). "The use of GPS in agriculture for yield mapping and tractor implement guidance." *Proceedings of DGPS '91, First International Symposium on Real Time Differential Applications of the Global Positioning System*, Braunschweig, Federal Republic of Germany, 16-20 September, Volume II, pp. 455-465.
- Bagley, L.C. and J.W. Lamons (1992). "NAVSTAR Joint Program Office and a status report on the GPS Program ." *Proceedings of Sixth International Geodetic Symposium on Satellite Positioning*, Columbus, Ohio, 17-20 March, Volume I, pp. 21-30.
- Balde, M., C.L.V. Aiken, D.G. Ziegler, J. Hare, S. Cates, and W. Gosnold (1992). "Stop and go kinematic GPS for position control in a large scale gravity survey in North Dakota." *Proceedings of Sixth International Geodetic Symposium on Satellite Positioning*, Columbus, Ohio, 17-20 March, Volume II, pp. 769-777.
- Bishop, G.J., J. A. Klobuchar, and P.H. Doherty (1985). "Multipath effects on the determination of absolute ionospheric time delay from GPS signals." *Radio Science.*, Vol. 20, No. 3, May-June, pp. 388-396.
- Bock, Y., R.I. Abbot, C.C. Counselman III, R.W. King, S.A. Gourevitch (1985). "Three dimensional geodetic control by interferometry with GPS: Processing of GPS phase observables." *Proceedings of the first international symposium on precise position with the Global Positioning System*, Rockville, Md., April. Volume-1, pp. 255-262.
- Bowditch, N. (1981). "Useful tables, calculations, glossary of marine navigation." Vol. II, *The American Practical Navigator*, Publication No. 9, DMAHTC, Washington, D.C., U.S.A.
- Braasch, M.S. and F. van Graas (1991). "Guidance accuracy considerations for real-time GPS interferometry." *Proceedings of ION GPS-91, Fourth International Technical Meeting of the Satellite Division of the Institute of Navigation*, Albuquerque, New Mexico, 11-13 September, pp. 373-386.

- Brown, A. (1989). "Extended differential GPS." *Navigation*, Journal of the Institute of Navigation, Vol. 36, No.3, Fall, pp. 265-285.
- Brown, R.A. (1992). "Instantaneous GPS attitude determination." *Proceedings of PLANS '92, IEEE Position Location and Navigation Symposium*, Monterey, California, 24-27 March, pp. 113-120.
- Brown, R.A. and A.G. Evans (1990). "GPS pointing system performance." *Proceedings of ION GPS-90 Third International Technical Meeting of the Satellite Division of the Institute of Navigation*, Colorado Springs, Colorado, USA, 17-21 September, pp. 645-654.
- Cannon, M.E. (1991). *Airborne GPS/INS with an application to Aerotriangulation*. UCSE Reports Number 20040, Department of Surveying Engineering, The University of Calgary, Calgary, Canada.
- Chamberlain, S.M. and R. A. Eastwood (1990). "Global satellite navigation using both GPS and Glonass." *Proceedings of ION GPS-90 Third International Technical Meeting of the Satellite Division of the Institute of Navigation*, Colorado Springs, Colorado, USA, 17-21 September, pp. 277-286.
- Cohen, C.E. and B.W. Parkinson (1991). "Expanding the performance envelope of GPS-based attitude." *Proceedings of ION GPS-91, Fourth International Technical Meeting of the Satellite Division of the Institute of Navigation*, Albuquerque, New Mexico, 11-13 September, pp. 1001-10011.
- Colombo, Oscar L. (1986). "Ephemeris errors of GPS satellites." *Bulletin Geodesique*, Vol. 60, No. 1, pp. 64-84.
- Committee on Geodesy (1983). *Sea floor referenced positioning: Needs and opportunities*. Panel on ocean positioning, National Research Council, Washington, D.C.
- Counselman, C.C., III, and S.A. Gourevitch (1981). "Miniature Interferometer Terminals for Earth Surveying: Ambiguity and Multipath with Global Positioning System." *IEEE Transactions on Geoscience and Remote Sensing*, Vol. GE-19, No.4, October, pp. 244-252.
- Delikaraoglou, D., H. Dragert, J. Kouba, K. Lochhead and J. Popelar (1990). "The development of a Canadian GPS Active Control System: status of the current array." *Proceedings of Second International Symposium on Precise Positioning with the Global Positioning System*, Ottawa, Canada, 3-7 September, pp. 190-202.
- Dixon, R.C. (1976). *Spread spectrum systems*. John Wiley, New York, U.S.A.

- Dragert, Herb (1992). Personal communications. Pacific Geoscience Centre, Sidney, British Columbia, Canada, 8 May 1991.
- Easton, R.L. (1980). "The Navigation Technology Program ." In *Global Positioning System*. Papers published in Navigation, Volume I. Reprinted by the Institute of Navigation, Washington, D.C., pp. 15-20.
- Euler, H-J. and Goad, C.C. (1991). "On optimal filtering of GPS dual frequency observations without using orbit information" . *Bulletin Geodesique*, Volume 65, Number 2, pp. 130-143.
- Euler, H-J., G.W. Hein, and H. Landau (1991). "Precise real-time differential GPS positioning in decimetre ranges." *Proceedings of DGPS '91, First International Symposium on Real Time Differential Applications of the Global Positioning System*, Braunschweig, Federal Republic of Germany, 16-20 September, Volume II, pp. 466-474.
- Geier, G.J., A. Kleusberg, and S. DeLoach (1990). " Kinematic phase processing techniques in support of dredging operations." *Proceedings of ION GPS-90 Third International Technical Meeting of the Satellite Division of the Institute of Navigation*, Colorado Springs, Colorado, USA, 17-21 September, pp. 85-90.
- Geiger, A. and M. Cocard (1992). "Sea-wave direction detection by GPS." *Proceedings of Sixth International Geodetic Symposium on Satellite Positioning*, Columbus, Ohio, 17-20 March, Volume I, pp. 319-326.
- Georgiadou, Y. and A. Kleusberg (1988). "On carrier signal multipath effects in relative GPS positioning." *Manuscripta Geodaetica*, Vol. 13, pp. 172-179.
- Green, G.B., P.D. Massatt and N.W. Rhodus (1989). "The GPS 21 primary satellite constellation." *Navigation* , Journal of the Institute of Navigation, Vol. 36, No.1, Spring, pp. 9-24.
- Hatch, R. (1982). "The synergism of GPS code and carrier measurements." *Proceedings of the third international geodetic symposium on satellite doppler positioning*. New Mexico State University, Las Cruces, New Mexico, February 8-12. Volume-2, pp. 1213-1231.
- Hatch, R. (1989). "Ambiguity Resolution in the Fast Lane." *Proceedings of ION GPS-1989, Second International Technical Meeting of the Satellite Division of the Institute of Navigation*, Colorado Springs, September 27-29, pp. 45-50.



- Hatch, R. (1990). "Instantaneous ambiguity resolution." *Proceedings of International Association of Geodesy Symposia No. 107 Kinematic Systems in Geodesy, Surveying, and Remote Sensing*, Banff, Canada, 10-13 September, Springer Verlag, New York, pp. 299-308.
- Hatch, R. (1991). "Ambiguity resolution while moving - Experimental results" *Proceedings of ION GPS-91, Fourth International Technical Meeting of the Satellite Division of the Institute of Navigation*, Albuquerque, New Mexico, 11-13 September, pp. 707-713.
- Hatch, R., R. Keegan, T.A. Stansell (1992). "Kinematic receiver technology from Magnavox." *Proceedings of Sixth International Geodetic Symposium on Satellite Positioning*, Columbus, Ohio, 17-20 March, Volume I, pp. 174-183.
- Hein, G.W., H. Landau, and H. Blomenhofer (1991). "Determination of instantaneous sea surface, wave heights, and ocean currents using satellite observations of the Global Positioning System." *Marine Geodesy*, Volume 14, pp. 217-224.
- Hein, G.W., H. Landau, and H. Blomenhofer (1991). "Real-time monitoring of sea level using differential GPS." *Proceedings of DGPS '91, First International Symposium on Real Time Differential Applications of the Global Positioning System*, Braunschweig, Federal Republic of Germany, 16-20 September, Volume II, pp. 383-393.
- Hintz, R.J. and M. Z. Zhao (1989). "Considerations in the implementation of aerotriangulation with GPS derived exposure station positions." *Photogrammetric Engineering and Remote Sensing*. Vol. 55, No. 12, December, pp. 1731-1735.
- Hofmann-Wellenhof, B., and B. W. Remondi (1988). "The antenna exchange: One aspect of high-precision GPS kinematic survey." Presented at the International GPS Workshop, GPS Techniques Applied to Geodesy and Surveying, Darmstadt, F.R.G., 10-13 April.
- Trimble Navigation (1989). *GPS A Guide to the Next Utility*. Sunnyvale, California.
- Hwang, P.Y.C. (1990a). "Kinematic GPS: Resolving integer ambiguities on the fly." *Proceedings of PLANS '90, IEEE Position Location and Navigation Symposium*, Las Vegas, Nev., 20-23 March, pp. 579-586.
- Hwang, P.Y.C. (1990b). "A near-instantaneous initialization method for attitude determination." *Proceedings of ION GPS-90 Third International Technical Meeting of the Satellite Division of the Institute of Navigation*, Colorado Springs, Colorado, USA, 17-21 September, pp. 661-669.

- Jurgens, R.D. and C.E. Rodgers (1992). "Advances in GPS attitude determining technology as developed for the strategic defense command." *Proceedings of PLANS '92, IEEE Position Location and Navigation Symposium*, Monterey, California, 24-27 March, pp. 991-999.
- Kee, Changdon, B.W. Parkinson, and P. Axelrad (1991). "Wide-area differential GPS." *Navigation*, Journal of The Institute of Navigation, Vol. 38, No.2, pp. 123-145.
- Knight, J. and R. Hatch (1990). "Attitude determination via GPS" *Proceedings of International Association of Geodesy Symposia No. 107 Kinematic Systems in Geodesy, Surveying, and Remote Sensing*, Banff, Canada, 10-13 September, Springer Verlag, New York, pp. 168-177.
- Landau, H. (1990). "GPS processing techniques in geodetic networks." *Proceedings of Second International Symposium on Precise Positioning with the Global Positioning System*, Ottawa, Canada, 3-7 September, pp. 373-386.
- Landau, H. and H.J. Euler (1991a). "High-precision real-time differential positioning." *Proceedings of ION GPS-91, Fourth International Technical Meeting of the Satellite Division of the Institute of Navigation*, Albuquerque, New Mexico, 11-13 September, pp. 699-705.
- Landau, H. and H.J. Euler (1991b). "The key to decimetre-level differential GPS navigation: carrier phase ambiguity determination in real-time." *Proceedings of DGPS '91, First International Symposium on Real Time Differential Applications of the Global Positioning System*, Braunschweig, Federal Republic of Germany, 16-20 September, Volume I, pp. 36-43.
- Landau, H. and H.J. Euler (1992). "On-the-fly ambiguity resolution for precise differential positioning." Paper presented at ION GPS-92, 5th International Technical Meeting of the Satellite Division of the Institute of Navigation, Albuquerque, New Mexico, 16-18 September.
- Langley, R. (1992). "*The effect of the ionosphere and troposphere on satellite positioning system.*" Paper presented at the Symposium of Refraction of Transatmospheric Signals in Geodesy, The Hague, Netherlands, 19-22 May.
- Lapine, L.A. (1991). *Analytical calibration of the Airborne Photogrammetric System using a priori knowledge of the exposure station obtained from kinematic Global Positioning System techniques*. Report No. 411. Department of Geodetic Science and Surveying, The Ohio State University, Columbus, Ohio.
- Llewellyn, S.K. and R.B. Bent (1973). "Documentation and description of the Bent ionospheric model." AFCRL-TR-73-0657, SAMSO TR-73-252, Atlantic Science Corporation, Indialantic, Florida.

- Loomis, P. (1989). "A kinematic GPS double-differencing algorithm." *Proceedings of the Fifth International Geodetic Symposium on Satellite Positioning*, DMA, U.S.DoD, NGS, NOAA, Volume II, Las Cruces, N. Mex., 13-17 March, Physical Science Laboratory, New Mexico State University, Las Cruces, N. Mex., pp. 611-620.
- Lucas, J.R. (1987). "Aerotriangulation without ground control." *Photogrammetric Engineering and Remote Sensing*. Vol. 53, No. 3, March, pp. 311-314.
- Mader, G.L. (1990). "Ambiguity function techniques for GPS phase initialization and kinematic solutions." *Proceedings of Second International Symposium on Precise Positioning with the Global Positioning System*, Ottawa, Canada, 3-7 September, pp. 1233-1247.
- Mader, G.L. (1992). "Rapid static and kinematic Global Positioning System solutions using the ambiguity function technique." *Journal of Geophysical Research*, Vol. 97, No. B3, pp. 3271-3283.
- Martin, E.H. (1980). "GPS user equipment error models ." In *Global Positioning System*. Papers published in Navigation, Volume I. Reprinted by the Institute of Navigation, Washington, D.C.
- McIntyre, M.C. (1989). *Design and testing of sea floor geodesy system*. Ph.D. Dissertation, Marine Physical Laboratory, Scripps Institution of Oceanography, University of California, San Diego.
- Meehan, T.K. and L. E. Young (1992). "On-receiver signal processing for GPS multipath reduction." *Proceedings of Sixth International Geodetic Symposium on Satellite Positioning*, Columbus, Ohio, 17-20 March, Volume I, pp. 200-208.
- Merrell, R.L., M.P. Leach, and J.R. Clynch (1989). "Development of an operational GPS controlled aerial photography capability." *Proceedings of the Fifth International Geodetic Symposium on Satellite Positioning*, DMA, U.S.DoD, NGS, NOAA, Volume II, Las Cruces, N. Mex., 13-17 March, Physical Science Laboratory, New Mexico State University, Las Cruces, N. Mex., pp. 634-642.
- Nesbo, I. (1988). "Applications of GPS determined attitude for navigation." *Proceedings of ION GPS-88, First International Technical Meeting of the Satellite Division of the Institute of Navigation*, Colorado Springs, Colorado, USA, 19-23 September, pp. 95-100.
- Nesbo, I. and P. Canter (1990). "GPS attitude determination for navigation." *GPS World*, Volume 1, Number 5, September/October, pp. 36-41.

- Petersen, C. (1991). "Precision GPS navigation for improving agricultural productivity." *GPS World*, Vol. 2, No.1, January, pp. 38-44.
- Purcell Jr., G.H., L.E. Young, S.K. Wolf, T.K. Meehan, C.B. Duncan, S.S. Fisher, F.N. Spiess, G. Austin, D.E. Boegeman, C.D. Lowenstein, C. Rocken, T.M. Kelecy (1990). "Accurate GPS measurement of the location and orientation of a floating platform. *Marine Geodesy*, Volume 14, pp. 255-264.
- Remondi, B.W. (1984). *Using the Global Positioning System (GPS) Phase Observable for Relative Geodesy: Modeling, Processing, and Results*. Doctoral Dissertation. Center for Space Research, University of Texas at Austin, Texas.
- Remondi, B.W. (1990). *Pseudo-Kinematic GPS Results using the Ambiguity Function Method*. NOAA Technical Memorandum NOS NGS-52, Rockville, MD, May.
- Remondi, B.W. (1991). *Kinematic GPS results without static initialization*. NOAA Technical Memorandum NOS NGS-55, Rockville, MD, May.
- Remondi, B.W. (1992a). "Real-time centimeter-accuracy GPS for marine applications." *Proceedings of the U.S. Hydrographic Conference '92*. The Hydrographic Society, Special Publication No. 28, Baltimore, MD, February 25-28.
- Remondi, B.W. (1992b). "Real-time centimeter-accuracy GPS without static initialization." *Proceedings of Sixth International Geodetic Symposium on Satellite Positioning*, Columbus, Ohio, 17-20 March, Volume II, pp. 691-701.
- Rocken, C. and T.M. Kelecy (1992). "High-accuracy GPS marine positioning for scientific applications." *GPS World*, Volume 3, Number 6, June, pp. 42-47.
- Rocken, C., T.M. Kelecy, G.H. Born, L.E. Young, G.H. Purcell Jr., and S.K. Wolf (1990). "Measuring precise sea level from a buoy using the Global Positioning System." *Geophysical Research Letters*, Vol. 17, No. 12, June, November, pp. 2145-2148.
- Schwartz, K.P., C.S. Fraser, and P.C. Gustafson (1984). "Aerotriangulation without ground control." *International Archives of Photogrammetry and Remote Sensing*. Vol. 25, Part A1, pp. 237-250.
- Seeber, G. and G. Wubben (1989). "Kinematic positioning with carrier phases and 'on the way' ambiguity solution ." *Proceedings of the 5th international geodetic symposium on satellite positioning*. New Mexico State University, Las Cruces, New Mexico, March 13-17. Volume-2, pp. 600-610.

- Spiess, F.N. (1985). "Sub-oceanic geodetic measurements.", *IEEE Transactions on Geoscience and Remote Sensing*, Vol. GE-23, No. 4, July, pp. 502-510.
- Spiess, F.N. (1990). "Sea floor geodesy by the year 2000." In *Geodesy in the year 2000*, A report of Committee on Geodesy, Board on Earth Sciences and Resources, National Research Council, Washington, D.C., pp. 100-113.
- Strang, Gilbert (1980). *Linear Algebra and Its Applications* Second edition. Harcourt Brace Jovanovich Publishers, New York.
- Thomas, J.B. (1988). *Functional Description of Signal Processing in the Rogue GPS Receiver* JPL Publication 88-15. Jet Propulsion Laboratory, California Institute of Technology, Pasadena, California. June 1, 1988.
- van Dierendonck, A.J., S.S. Russell, E.R. Kopitzke and M. Birnbaum (1986). "The GPS navigation Message ." In *Global Positioning System*. Papers published in Navigation, Volume I. Reprinted by the Institute of Navigation, Washington, D.C., pp. 55-73.
- van Graas, F. and M. Braasch (1991). "GPS interferometric attitude and heading determination: initial flight test results." *Navigation*, Journal of the Institute of Navigation, Vol. 38, No.4, Winter, pp. 297-316.
- van Graas, F. and M. Braasch (1992). "Real-time attitude and heading determination using GPS." *GPS World*, Volume 3, Number 3, March, pp. 32-39.
- Wilson and Tonnemacher (1992). "A GPS attitude determination system." *Journal of Navigation*, Journal of the Royal Institute of Navigation, Vol. 45, Number 2, May, pp. 192-204.
- Vanicek, P. and E.J. Krakiwsky (1986). *Geodesy: The Concepts*. Second edition. North-Holland, Amsterdam.
- Wells, D.E. (1974). "Doppler satellite control." Technical Report No. 29, Department of Surveying Engineering, University of New Brunswick, Fredericton, N.B., Canada.
- Wells, D.E. (1992). Personal communications. Professor, Department of Surveying Engineering, University of New Brunswick, Canada, July.

- Wells, D.E., N. Beck, D. Delikaraoglou, A. Kleusberg, E.J. Krakiwsky, G. Lachapelle, R.B. Langley, M. Nakiboglu, K.P. Schwarz, J.M. Tranquilla, P. Vanicek (1986). "Guide to GPS positioning." Canadian GPS Associates, Fredericton, N.B., Canada.
- Wells, D.E., W. Lindlohr, B. Schaffrin, E. Grafarend (1987). "GPS design: Undifferenced carrier beat phase observations and the fundamental differencing theorem." Technical Report No. 116, Department of Surveying Engineering, University of New Brunswick, Fredericton, N.B., Canada.
- Wubben, G. (1989). "The GPS adjustment software package GEONAP, concepts and models." *Proceedings of the 5th international geodetic symposium on satellite positioning*. New Mexico State University, Las Cruces, New Mexico, March 13-17. Volume-1, pp. 452-461.
- Wubben, G. (1991). *Zur Modellierung von GPS-Beobachtungen für die hochgenaue Positionsbestimmung*. Ph.D. Dissertation (in German). Institut für Erdmessung, University of Hannover, Federal Republic of Germany.
- Wysocki, J. (1991). "GPS and selective availability - the military perspective". *GPS World*. July/August 1991, pp. 38-44.
- Young, L.E., S.C. Wu, and T.H. Dixon (1987). "Decimetre GPS positioning for surface element of sea floor geodesy system." *Proceedings of International Symposium on Marine Positioning INSMAP '86*, D. Reidel, Boston, pp. 223-232.
- Ziegler, D.G., R.L. Hunt, and C.L.V. Aiken (1992). "Rapid GPS positioning of a gravity survey in the South Georgia basin, Georgia, using the two occupation rapid static ambiguity function technique." *Proceedings of Sixth International Geodetic Symposium on Satellite Positioning*, Columbus, Ohio, 17 - 20 March, Volume II, pp. 759-768.

## Appendix I

# LINEAR COMBINATIONS OF GPS OBSERVATIONS

---



---

The actual GPS observables are the in-phase carrier component (carrier phase,  $\phi$ ) and code modulation travel time ( $\Delta t$ ) of the L1 and L2 signals. The frequencies of the signals,  $f_1$  and  $f_2$ , and their wavelengths,  $\lambda_1$  and  $\lambda_2$ , are :

$$\begin{aligned}
 f_1 &= 154 \times 10.23 \text{ MHz} = 1575.42 \text{ MHz} , \\
 f_2 &= 120 \times 10.23 \text{ MHz} = 1227.60 \text{ MHz} , \\
 \lambda_1 &\approx 19.0 \text{ cm} , \quad \lambda_2 \approx 24.4 \text{ cm} .
 \end{aligned}
 \tag{I.1}$$

One can acquire some or all of the observables, depending on the type of receiver being used. These observations can be related to the receiver position (x,y,z) and the other variables through observation equations such as:

$$P_i = \rho + d\rho + dtrop + dion_i + (dt - dT) + MP_i + \phi P_i , \tag{I.2}$$

$$L_i = \rho + d\rho + dtrop - dion_i + (dt - dT) + MC_i - \lambda_i \cdot N_i + \phi C_i , \tag{I.3}$$

where :

$$\begin{aligned}
 P_i &= c \cdot \Delta t_i = \text{code pseudorange at } f_i \text{ frequency (m), (i = 1, 2),} \\
 L_i &= \lambda_i \cdot \phi_i = \text{carrier range at } f_i \text{ frequency (m), (i = 1,2),} \\
 \rho &= \text{geometric distance between the receiver (x,y,z) and} \\
 &\quad \text{the satellite (m),}
 \end{aligned}$$

$c$	=	the speed of light in a vacuum (m/s),
$\lambda$	=	wavelength of the signal (m) = $c / f$ (frequency),
$d\rho$	=	range error caused by ephemeris errors (m),
$d_{\text{trop}}$	=	tropospheric delay (m),
$d_{\text{ion}_i}$	=	ionospheric delay at $f_i$ frequency (m),
$dt, dT$	=	receiver and satellite clock offsets and errors (m),
$MP_i, MC_i$	=	multipath effects in $P_i$ and $L_i$ observation (m),
$N_1, N_2$	=	cycle ambiguities of L1 and L2 carrier phases (cycles), and
$\sigma P_i, \sigma C_i$	=	noise in $P_i$ and $L_i$ observations (m) .

### I.1. Linear combination of phase observations

The other artificial phase observations can be created from the aforementioned actual phase observations by linearly combining the respective phases. Detailed explanations of various combinations of L1 and L2 phases can be found in *Wubben* [1989]. In the following, some of the combinations used in this investigation are explained, namely, double wide-lane, wide-lane, semi wide-lane, narrow-lane, and ionospheric signal observations.

For the resolution of carrier phase ambiguities, the following characteristics of the resulting linear combination phases are desired:

- the ambiguity is an integer,
- the wavelength is reasonable, not too short, preferably long,
- the ionospheric effect is small, and
- the measurement noise is kept small.

Given  $\phi_1$  and  $\phi_2$  as the observed phases of L1 and L2 signals expressed in cycles, the linear combinations which keep the carrier phase ambiguities as integer numbers can be formulated as follows :



$$\phi_{n,m} = n.\phi_1 + m.\phi_2 , \quad (I.4)$$

where n and m are integers. The *ambiguity of the linear combination*  $N_{n,m}$ , is related to the ambiguities of L1 and L2 signals,  $N_1$  and  $N_2$ , as follows:

$$N_{n,m} = n.N_1 + m.N_2 . \quad (I.5)$$

The *frequency and the wavelength of the linear combination* signal,  $f_{n,m}$  and  $\lambda_{n,m}$ , can also be expressed as a function of the frequencies and wavelengths of L1 and L2 signals as follows:

$$f_{n,m} = n.f_1 + m.f_2 , \quad \frac{1}{\lambda_{n,m}} = \frac{n}{\lambda_1} + \frac{m}{\lambda_2} . \quad (I.6)$$

The linear combination signal can also be expressed in the range units as:

$$L_{n,m} = \lambda_{n,m} \cdot \phi_{n,m} = \frac{n.f_1.L_1 + m.f_2.L_2}{n.f_1 + m.f_2} . \quad (I.7)$$

The above equation can also be used to express the linear combination of the pseudorange observations. Note also from the above equation, that the linear combination process will only alter the *frequency-dependent* errors and biases, such as the ionospheric advances, measurement noise, and multipath. The magnitudes of the *frequency-independent* errors

and biases, such as ephemeris errors, clock errors and offsets, and tropospheric delays, will still be the same for the linear combination signal as for the L1 and L2 signals.

In the case of **the ionospheric effects**, if the magnitudes of the ionospheric effects (either delays or advances) on the L1 and L2 (code or phase) observations are denoted as  $dion_1$  and  $dion_2$ , then the magnitude of the ionospheric effect on the linear combination  $dion_{n,m}$  can be written using equation (I.7) above as follows:

$$dion_{n,m} = \frac{n.f_1.dion_1 + m.f_2.dion_2}{n.f_1 + m.f_2} \quad (I.8)$$

Considering only the first order ionospheric effects,  $dion_1$  and  $dion_2$  can be formulated in length units as follows:

$$dion_1 = \frac{C}{f_1^2} \quad , \quad dion_2 = \frac{C}{f_2^2} \quad , \quad (I.9)$$

where C is a constant whose value is dependent on the electron content encountered by the signal traveling from the satellite to the receiver. If equation (I.9) is substituted into equation (I.8), then the following equation for the linear combination can be established:

$$dion_{n,m} = \frac{C}{f_1.f_2} \cdot \left( \frac{n.f_2 + m.f_1}{n.f_1 + m.f_2} \right) \quad (I.10)$$

Note in the above equation that, depending on integers n and m, the magnitudes of  $dion_{n,m}$  will be different. Their values also could be either positive or negative, which, in the case of phase observations, means that the linear combination signal could either be advanced or

delayed by the ionosphere. Based on equations (I.9) and (I.10), the magnitude of the ionospheric effect on the linear combination can be written as function of the magnitude of ionospheric effect on L1 signal, as follows:

$$\text{dion}_{n,m} = \text{isf} \cdot \text{dion}_1 \quad , \quad (\text{I.11})$$

where the *ionospheric scale factor*, *isf*, can be formulated as:

$$\text{isf} = \frac{f_1}{f_2} \cdot \left( \frac{n \cdot f_2 + m \cdot f_1}{n \cdot f_1 + m \cdot f_2} \right) \quad . \quad (\text{I.12})$$

The linear combination process will also alter the **noise level** of the observations. If the noise in the L1 and L2 phases are characterized by the same standard deviation in cycle units,  $\sigma_\phi$ , then the standard deviation of the linear combination phase in length units  $\sigma(L_{n,m})$  can be written, based on equation (I.4) and (I.7), as follows:

$$\sigma(L_{n,m}) = \lambda_{n,m} \cdot \sqrt{n^2 + m^2} \cdot \sigma_\phi \quad . \quad (\text{I.13})$$

Based on the above equation, the noise level of the linear combination phase can be written as a function of the noise level of L1 phase in length units as follows:

$$\sigma(L_{n,m}) = \text{nsf} \cdot \sigma(L_1) \quad , \quad (\text{I.14})$$

where the *noise scale factor*, *nsf*, can be formulated as:

$$\text{nsf} = \frac{\lambda_2 \cdot \sqrt{n^2 + m^2}}{n \cdot \lambda_2 + m \cdot \lambda_1} \quad (\text{I.15})$$

Equations (I.4) to (I.15) above are derived by considering the dual-frequency data. With **codeless data**, the half-wavelength L2 signal is observed rather than the full wavelength signal. The frequency and wavelength of the half-wavelength L2 signal, denoted in this case as  $f_{2c}$  and  $\lambda_{2c}$ , will take the following values:

$$\begin{aligned} f_{2c} &= 2 \cdot f_2 = 2455.20 \text{ MHz} , \\ \lambda_{2c} &= \lambda_2 / 2 \approx 24.4 \text{ cm} . \end{aligned} \quad (\text{I.16})$$

In order to be valid for the codeless data, the parameters  $f_2$  and  $\lambda_2$  in equations (I.4) to (I.15) should be replaced with  $f_{2c}$  and  $\lambda_{2c}$ . Also the ambiguity of L2 signal  $N_2$ , should be denoted as  $N_{2c}$  since its value will be different, i.e., two times larger than  $N_2$ .

The examples of some linear combination signals with their wavelengths, ionospheric scale factors, and noise scale factors are shown in Tables I.1 and I.2. Table I.1 is for the dual-frequency data and Table I.2 is for the codeless data.

In the case of dual-frequency data, two linear combination signals, *wide-lane* and *narrow-lane*, play important roles in ambiguity resolution, particularly in extrawidelaning technique of ambiguity resolution [Wubben, 1989]. They will be discussed in more detailed in subsection I.2. In the case of codeless data, three linear combination signals can be considered to be used in the ambiguity resolution process, namely *semi*, *half* and *double wide-lane* signals.

Table I.1. Some examples of linear combination phases of dual-frequency data.

n	m	$\lambda_{n,m}$ in cm	isf	nsf	note
-14	18	732.6	350.4	877.9	very long wavelength
-7	9	1465.3	350.4	877.9	very long wavelength
-3	4	162.8	18.2	42.8	double wide-lane signal
-2	3	56.4	5.5	10.7	
-1	2	34.1	2.8	4.0	semi wide-lane
0	1	24.4	1.6	1.3	L2 signal
1	-1	86.2	-1.3	6.4	wide-lane signal
1	0	19.0	1.0	1.0	L1 signal
1	1	10.7	1.3	0.8	narrow-lane
2	-2	43.1	-1.3	6.4	half wide-lane
4	-3	11.4	0.09	3.0	low ionospheric effects
5	-4	10.1	-0.07	3.4	low ionospheric effects

Table I.2. Some examples of linear combination phases of codeless data.

n	m	$\lambda_{n,m}$ in cm	isf	nsf	note
-14	9	732.6	-316.7	640.8	very long wavelength
-9	6	54.3	-14.7	30.8	
-6	4	81.4	-14.7	30.8	
-3	2	162.8	-14.7	30.8	double wide-lane signal
-1	1	34.1	-0.6	2.5	semi wide-lane
0	1	12.2	0.4	0.6	L2 signal
1	0	19.0	1.0	1.0	L1 signal
2	-1	43.1	3.1	5.1	half wide-lane
5	-3	58.6	9.5	17.9	
11	-7	209.3	71.6	143.4	long wavelength

As shown in Table I.2, a double wide-lane signal has reasonably long wavelength, desirable for ambiguity resolution. However, it is more affected by ionospheric refraction, and also it has the highest noise level compared to semi and half wide-lane signals. Among the three, the semi wide-lane is the least affected by the ionosphere and also has the lowest noise level. Its wavelength, however, is the shortest. Considering the ionospheric activity, the separation between the monitor station and moving receiver, and the noise level of the observations, one therefore has to trade off the aforementioned factors in choosing the signal to be used in the ambiguity resolution process.

## I.2. Wide-lane and narrow-lane combinations

In the case of dual-frequency data, two linear combination signals play important roles in the ambiguity resolution process, namely the wide-lane and narrow-lane observations. In the integrated technique proposed in this research, the wide-lane signal is used as a working signal for ambiguity resolution in the case of dual-frequency data, and the narrow-lane signal is used to assist the ambiguity resolution of the L1 and L2 signals afterward. Both signals are also used in the extrawidelaning technique of ambiguity resolution which also is incorporated in the integrated technique of ambiguity resolution.

As indicated in Table I.1, the *wide-lane carrier phase* ( $\phi_{\Delta}$ ) and *narrow-lane carrier phase* ( $\phi_{\Sigma}$ ) observations are constructed from the phase observations of L1 and L2 signals as follows:

$$\phi_{\Delta} = \phi_1 - \phi_2 \quad ; \quad \phi_{\Sigma} = \phi_1 + \phi_2, \quad (I.17)$$

where  $\phi_1$  and  $\phi_2$  are expressed in the unit of cycles. Their wavelengths are about 86.2 cm and 10.7 cm, respectively. The above equations imply the following relation for the cycle-ambiguities of the signals:

$$N_{\Delta} = N_1 - N_2 \quad ; \quad N_{\Sigma} = N_1 + N_2. \quad (I.18)$$

Note from the above equation the existence of *the even-odd relation* between the wide-lane and narrow-lane integer ambiguities, i.e.,

$$\begin{array}{l} N_{\Delta} \text{ is even} \quad \longrightarrow \quad N_{\Sigma} \text{ has to be even,} \\ N_{\Delta} \text{ is odd} \quad \dashrightarrow \quad N_{\Sigma} \text{ has to be odd.} \end{array}$$

This even-odd relation implies that when the ambiguity of one of these combinations is resolved, the effective wavelength of the other combination is increased by a factor of 2, and can therefore be resolved more easily. For example, when  $N_{\Sigma}$  can be resolved, then the effective wavelength of wide-lane will increase to 172.5 cm, and  $N_{\Delta}$  can be resolved much easier. This is the basic idea of the *extrawidelaning technique* of ambiguity resolution [Wubben, 1989]. Also, if the wide-lane ambiguity can be resolved, then the effective wavelength of narrow-lane will increase to 21.4 cm, which is close to the wavelength of L2 signal, but with lower noise level and ionospheric effects than the L2 signal.

In terms of length units, the *wide-lane* and *narrow lane carrier ranges* can be formulated based on equation (I.7) before as:

$$L_{\Delta} = \lambda_{\Delta} \cdot \phi_{\Delta} = \frac{f_1 \cdot L_1 - f_2 \cdot L_2}{f_1 - f_2} = \frac{154}{34} L_1 - \frac{120}{34} L_2 \quad , \quad (I.19)$$

$$L_{\Sigma} = \lambda_{\Sigma} \cdot \phi_{\Sigma} = \frac{f_1 \cdot L_1 + f_2 \cdot L_2}{f_1 + f_2} = \frac{154}{274} L_1 + \frac{120}{274} L_2 \quad . \quad (I.20)$$

In the same manner, the *wide-lane* and *narrow-lane pseudorange observations* can be formulated as follows:

$$P_{\Delta} = \frac{f_1 \cdot P_1 - f_2 \cdot P_2}{f_1 - f_2} \quad ; \quad P_{\Sigma} = \frac{f_1 \cdot P_1 + f_2 \cdot P_2}{f_1 + f_2} \quad . \quad (I.21)$$

Equations (I.19) to (I.21) show that the frequency-independent errors in wide-lane and narrow-lane observations, such as clock errors, tropospheric effect, and ephemeris error, are equal to those in the code and phase observations in either L1 or L2 frequency. The frequency-dependent errors, such as ionospheric effect, multipath, and observation noise, are modified according to the above equations. Particularly for the ionospheric effect, these artificial observations, i.e., wide-lane and narrow-lane pseudoranges and carrier ranges, are affected by the same magnitude. However, the narrow-lane pseudoranges and wide-lane carrier ranges are delayed by the ionosphere, and the wide-lane pseudoranges and narrow-lane carrier ranges are advanced. The observation equations for wide-lane and narrow-lane pseudorange and carrier range observations can then be written down as :

$$P_{\Delta} = \rho + d\rho + dtrop - dion_{\Delta/\Sigma} + (dt - dT) + MP_{\Delta} + \vartheta P_{\Delta} \quad , \quad (I.22)$$

$$P_{\Sigma} = \rho + d\rho + dtrop + dion_{\Delta/\Sigma} + (dt - dT) + MP_{\Sigma} + \vartheta P_{\Sigma} \quad , \quad (I.23)$$

$$L_{\Delta} = \rho + d\rho + dtrop + dion_{\Delta/\Sigma} + (dt - dT) + MC_{\Delta} - \lambda_{\Delta} \cdot N_{\Delta} + \vartheta C_{\Delta} \quad , \quad (I.24)$$

$$L_{\Sigma} = \rho + d\rho + dtrop - dion_{\Delta/\Sigma} + (dt - dT) + MC_{\Sigma} - \lambda_{\Sigma} \cdot N_{\Sigma} + \vartheta C_{\Sigma} \quad . \quad (I.25)$$



The other linear combination of GPS observations used in the extrawidelaning technique is the *ionospheric signal* defined as [Wubbena, 1989]:

$$L_{is} = L_{\Sigma} - L_{\Delta} . \quad (I.26)$$

If equations (I.24) and (I.25) are substituted in equation (I.26), the following formulation for the ionospheric signal is obtained:

$$\begin{aligned} L_{is} &= -2.dion_{\Delta/\Sigma} - \lambda_{\Sigma}.N_{\Sigma} + \lambda_{\Delta}.N_{\Delta} + Bias + Noise , \\ &= -\frac{2.f_1.f_2}{f_1^2 - f_2^2} (dion_2 - dion_1) - \lambda_{\Sigma}.N_{\Sigma} + \lambda_{\Delta}.N_{\Delta} + Bias + Noise , \end{aligned} \quad (I.27)$$

where :

$$Bias = MC_{\Sigma} - MC_{\Delta} , \quad \text{and} \quad Noise = \vartheta C_{\Sigma} - \vartheta C_{\Delta} .$$

From equations (I.27), it can be seen that the ionospheric signal observation does not contain any geometric information. It relates the wide-lane cycle ambiguity with the narrow-lane cycle ambiguity, the properties of which are important in performing the extrawidelaning technique of ambiguity resolution.

### I.3. Semi, half, and double wide-lane signals

In the case of codeless data, the integrated ambiguity resolution technique proposed in this research used either semi wide-lane, half wide-lane, or double wide-lane signals. Their wavelength as shown in Table I.2 are about 34.1 cm, 43.1 cm, and 162.8 cm, respectively.

The *semi wide-lane carrier phase* ( $\phi_{s\Delta}$ ), *half wide-lane carrier phase* ( $\phi_{\Delta/2}$ ), and *double wide-lane carrier phase* ( $\phi_{2\Delta}$ ) are constructed from the L1 phase ( $\phi_1$ ) and half-wavelength L2 phase ( $\phi_{2c}$ ) using the following relations:

$$\phi_{s\Delta} = -\phi_1 + \phi_{2c} \quad , \quad (I.28)$$

$$\phi_{\Delta/2} = 2\phi_1 - \phi_{2c} \quad , \quad (I.29)$$

$$\phi_{2\Delta} = -3\phi_1 + 2\phi_{2c} \quad , \quad (I.30)$$

where  $\phi_1$  and  $\phi_{2c}$  are expressed in the unit of cycles. The above equations imply the following relation for the cycle-ambiguities of the signals:

$$N_{s\Delta} = -N_1 + N_{2c} \quad , \quad (I.31)$$

$$N_{\Delta/2} = 2N_1 - N_{2c} \quad , \quad (I.32)$$

$$N_{2\Delta} = -3N_1 + 2N_{2c} \quad . \quad (I.33)$$

In terms of length units, the semi wide-lane, half wide-lane, and double wide-lane carrier ranges can be formulated, by basing on equation (I.7), as follows:

$$L_{s\Delta} = \lambda_{s\Delta} \cdot \phi_{s\Delta} = \frac{-f_1 \cdot L_1 + f_{2c} \cdot L_{2c}}{-f_1 + f_{2c}} = \frac{-77}{43} L_1 + \frac{120}{43} L_{2c} \quad , \quad (I.34)$$

$$L_{\Delta/2} = \lambda_{\Delta/2} \cdot \phi_{\Delta/2} = \frac{2 \cdot f_1 \cdot L_1 - f_{2c} \cdot L_{2c}}{2 \cdot f_1 - f_{2c}} = \frac{154}{34} L_1 - \frac{120}{34} L_{2c} \quad , \quad (I.35)$$

$$L_{2\Delta} = \lambda_{2\Delta} \cdot \phi_{2\Delta} = \frac{-3 \cdot f_1 \cdot L_1 + 2 \cdot f_{2c} \cdot L_{2c}}{-3 \cdot f_1 + 2 \cdot f_{2c}} = \frac{-231}{9} L_1 + \frac{240}{9} L_{2c} \quad (I.36)$$

Note from the above equations that, among the three linear combination signals, the double wide-lane range will have the highest noise level, and the semi wide-lane will have the lowest one. The double wide-lane will also be the most affected by ionospheric refraction, and the semi wide-lane will be the least affected, as also shown in Table I.2. Double and semi wide-lane signal will be delayed by the ionosphere, while the half wide-lane signal will be advanced.

## Appendix II

### CODE SMOOTHING USING THE CARRIER PHASES

---

---

The use of carrier phases for smoothing the (code) pseudoranges was first proposed by Hatch [1982], and has become the widely used code-smoothing technique for GPS kinematic positioning. The technique is supposed to effectively reduce noise level and the multipath effect in pseudorange observations. The carrier smoothed pseudoranges are computed based on the weighted least-squares adjustment technique [*Vanicek and Krakiwsky, 1986*].

If at epoch  $k$  the observed and smoothed pseudoranges are denoted as  $P_k$  and  $\hat{P}_k$  and the Doppler observation (between-epoch single-difference carrier phases) as  $D_{k-1,k}$ , and the physical correlation among the measurements are neglected, then the following sequential relations for the smoothed pseudorange and its variance can be derived:

$$\hat{P}_k = \left( \frac{w_1}{w_1 + w_2} \right) P_k + \left( \frac{w_2}{w_1 + w_2} \right) (\hat{P}_{k-1} + D_{k-1,k} + 2 \text{dion}_{k-1,k}) \quad , \quad (\text{II.1})$$

$$\sigma^2(\hat{P}_k) = \frac{1}{w_1 + w_2} \quad , \quad (\text{II.2})$$

where :

$$w_1 = \frac{1}{\sigma^2 (P_k)} ; \quad (II.3)$$

$$w_2 = \frac{1}{\sigma^2 (\hat{P}_{k-1}) + \sigma^2 (D_{k-1,k}) + 4 \sigma^2 (dion_{k-1,k})} . \quad (II.4)$$

The magnitude of ionospheric advance experienced by  $D_{k-1,k}$  is  $dion_{k-1,k}$ , and is included to make the ionospheric delays the same for both raw and smoothed pseudoranges. When dual-frequency data is available, this ionospheric advance can be computed based on dual-frequency Doppler observations. With single frequency data, this ionospheric advance can be estimated to a certain accuracy based on the ionospheric model. The remaining ionospheric refraction, however, will bias the yielded smoothed pseudoranges.

The smoothing process is started by taking the first observed pseudorange and its variance as the first smoothed values. The carrier smoothed pseudorange is simply the normalized weighted average of the observed and predicted pseudoranges, where the weights change with time. The smoothing process changes the magnitude of the frequency-dependent errors (except for the ionospheric delay) such as noise and multipath. The ionospheric delay (in the case of dual-frequency data) and other frequency-independent errors, such as tropospheric delay, clock errors, and ephemeris errors, are the same for smoothed and raw pseudoranges. Since the variance of the smoothed pseudorange gets smaller with time, after a certain time period the noise level of the smoothed pseudorange will become much lower than the original pseudorange observation and the effect of multipath (if it exists) should also be reduced.

As well as the biasing effect of ionospheric refraction in the case of single frequency data, there are other problems related to this smoothing process. The first is the occurrence of cycle slips. When cycle slips occur between two epochs, unless they can somehow be corrected (which is a difficult task in real-time kinematic mode), the Doppler observations cannot be used for smoothing the pseudorange, and the smoothing should be reset. This means a degradation in the accuracy of the smoothed pseudorange. The undetected cycle slips (usually small) also corrupt the smoothing process.

The second problem involves multipath effects. If multipath occurs when the weight of the observed pseudorange is still large, then the effect of multipath will contaminate the smoothed pseudoranges, not just at that epoch but also at several subsequent epochs. This contamination propagates in the manner expressed by equation (I.1). Therefore this smoothing technique should be used with care, and it should be considered only as an optional step instead of a compulsory one.

## Appendix III

### COVARIANCE MATRIX OF MULTI STATION DOUBLE-DIFFERENCE OBSERVATIONS

---

---

In this research of on-the-fly ambiguity resolution, the double-difference observations related to some monitor stations and satellites are used. Accordingly, the covariance matrix of the double-difference observations has to be constructed. In this case, only *mathematical correlations* among the observations are taken into account. The physical correlations among the observations, however, are ignored in this research since they are very difficult to model, particularly in real-time. Physical correlations require another intensive study.

When on-the-fly ambiguity resolution uses more than one monitor station, two groups of monitor stations are used, namely *primary* and *secondary* groups of monitor stations (see Figure 4.1). In this research, the primary group of monitor stations is considered as a user-independent system, established to provide users with information for correcting observation biases. The user only deals with the GPS observations of the secondary monitors stations and the user itself. Therefore, the examples and the notations used in constructing the covariance matrix in this appendix is restricted to the use of secondary group of monitor stations. The concept and mathematical methodologies, however, are valid for general multi station cases as well.

In this derivation of the covariance matrix, some secondary monitor stations and satellites are used, and, with the moving receiver, they are denoted whenever necessary as:

moving receiver : 2 ,  
 monitor stations : 1, 3, 4, ..., k ( n monitor stations ) , and  
 satellites : a, b, c, ... , z ( ns satellites ).

Two types of observations are used, namely pseudoranges and carrier phases (in the length units they are denoted as P and L). For simplicity, however, the term observation will be used and denoted as *obs* in this appendix. The single-differencing between stations will be denoted with symbol  $\Delta$ , and the single-differencing between satellites with symbol  $\nabla$ . Accordingly, the station-satellite double-differencing will be denoted with symbol  $\nabla\Delta$ .

### III.1. Covariance matrix of one-way observations

The covariance matrix of one-way observations related to a certain monitor station or the moving receiver and ns number of satellites is formulated as:

$$C(\text{obs}_k) = \text{diagonal} \left[ (\sigma_k^a)^2, (\sigma_k^b)^2, \dots, (\sigma_k^z)^2 \right]. \quad (\text{III.1})$$

with the dimension of (ns,ns). Note in the above equation that the physical correlations between the observations to different satellites are ignored.

In the case of n monitor stations, the covariance matrix of the whole one-way observation can be written as follows:



$$C(\text{obs})_n = \begin{bmatrix} C(\text{obs}_1) & O & O & O \\ & C(\text{obs}_2) & O & O \\ & & \dots & \dots \\ \text{symmetric} & & & C(\text{obs}_n) \end{bmatrix} \quad (\text{III.2})$$

In the above equation, O is the zero matrix with dimension (ns,ns), and the dimension of the covariance matrix  $C(\text{obs})_n$  is (n+1)ns by (n+1)ns.

### III.2. Covariance matrix of between-station single-difference observations

If n secondary monitor stations are used, the single-differencing between stations is performed in the format of :

(moving receiver - monitor station #1),  
 (moving receiver - monitor station #2),  
 ....., and  
 (moving receiver - monitor station #n).

In terms of station numbering, it is performed as (2-1), (2-3), ....., (2-n). The covariance matrix of between-station single difference observations involving all monitor stations  $C(\Delta\text{obs})_n$ , then can be computed as :

$$C(\Delta\text{obs})_n = (J_\Delta)_n \cdot C(\text{obs})_n \cdot (J_\Delta)_n^T \quad , \quad (\text{III.3})$$

where  $(J_\Delta)_n$  is between-station single-difference Jacobian matrix involving n monitor stations with the following structure:



differencing [Bock *et al.*, 1985], however, will destroy the integer nature of the ambiguities, and therefore is not considered in this research. If  $n_s$  satellites : a,b,c, ..., z, are observed, the sequential differencing is performed as (b-a),(c-b),(d-c), and so on; and the fixed differencing is performed as (b-a),(c-a),(d-a), and so on.

In the case of  $n$  monitor stations and  $n_s$  satellites, the covariance matrix of station-satellite double-difference observations  $C(\nabla\Delta\text{obs})_n$  can be computed as follows:

$$C(\nabla\Delta\text{obs})_n = (J_{\nabla})_n \cdot C(\Delta\text{obs})_n \cdot (J_{\nabla})_n^T, \quad (\text{III.7})$$

where  $(J_{\nabla})_n$  is between-satellite single-difference Jacobian matrix involving  $n$  monitor stations. In the above equation, matrix  $(J_{\nabla})_n$  with dimension of  $n(n_s-1)$  by  $n(n_s)$  can be formulated as:

$$(J_{\nabla})_n = \begin{bmatrix} J_{\nabla} & \mathbf{0} & \mathbf{0} & \dots & \mathbf{0} \\ \mathbf{0} & J_{\nabla} & \mathbf{0} & \dots & \mathbf{0} \\ \mathbf{0} & \mathbf{0} & J_{\nabla} & \dots & \mathbf{0} \\ \dots & \dots & \dots & \dots & \dots \\ \mathbf{0} & \mathbf{0} & \mathbf{0} & \dots & J_{\nabla} \end{bmatrix}, \quad (\text{III.8})$$

where  $J_{\nabla}$  is between-satellite single-difference Jacobian matrix with dimension of  $(n_s-1, n_s)$ . With sequential differencing, matrix  $J_{\nabla}$  will have the following structure :

$$J_{\nabla} = \begin{bmatrix} -1 & 1 & 0 & 0 & \dots & 0 \\ 0 & -1 & 1 & 0 & \dots & 0 \\ 0 & 0 & -1 & 1 & \dots & 0 \\ \dots & \dots & \dots & \dots & \dots & \dots \\ 0 & 0 & 0 & \dots & -1 & 1 \end{bmatrix}, \quad (\text{III.9})$$

and, in the case of fixed differencing, it can be formulated as:

$$J_{\nabla} = \begin{bmatrix} -1 & 1 & 0 & 0 & \dots & 0 \\ -1 & 0 & 1 & 0 & \dots & 0 \\ -1 & 0 & 0 & 1 & \dots & 0 \\ \dots & \dots & \dots & \dots & \dots & \dots \\ -1 & 0 & 0 & 0 & \dots & 1 \end{bmatrix} . \quad (\text{III.10})$$

If equations (III.5) and (III.8) are substituted to equation (III.7), then the covariance matrix  $C(\nabla\Delta\text{obs})_n$ , with dimension  $n(ns-1)$  by  $n(ns-1)$ , can be rewritten as:

$$C(\nabla\Delta\text{obs})_n = \begin{bmatrix} C(\nabla\Delta\text{obs}_{12}) & C(\nabla\text{obs}_2) & C(\nabla\text{obs}_2) & C(\nabla\text{obs}_2) \\ & C(\nabla\Delta\text{obs}_{32}) & C(\nabla\text{obs}_2) & C(\nabla\text{obs}_2) \\ & & \dots & \dots \\ \text{symmetric} & & & C(\nabla\Delta\text{obs}_{n2}) \end{bmatrix} . \quad (\text{III.11})$$

The main diagonal sub matrices in equation (III.11) are defined as follows:

$$\begin{aligned} C(\nabla\Delta\text{obs}_{12}) &= J_{\nabla} \cdot C(\Delta\text{obs}_{12}) \cdot J_{\nabla}^T , \\ C(\nabla\Delta\text{obs}_{32}) &= J_{\nabla} \cdot C(\Delta\text{obs}_{32}) \cdot J_{\nabla}^T , \\ &\dots, \\ C(\nabla\Delta\text{obs}_{n2}) &= J_{\nabla} \cdot C(\Delta\text{obs}_{n2}) \cdot J_{\nabla}^T , \end{aligned} \quad (\text{III.12})$$

whereas the off diagonal sub matrix, which can be considered as some kind of correlation matrix is formulated as:

$$C(\nabla\text{obs}_2) = J_{\nabla} \cdot C(\text{obs}_2) \cdot J_{\nabla}^T . \quad (\text{III.13})$$

In this context of integrated on-the-fly ambiguity resolution equation (III.11), the observations denoted by obs could be pseudoranges or phases observations, and the structure of the covariance matrix is also valid for the case of primary satellites.

## Appendix IV

### HISTOGRAM AND TIME SERIES OF THE ANTENNAS' DISTANCE DIFFERENCES

---

---

This appendix is a supplement to Chapter 4. It presents the histogram and time series of the distance differences between the computed distances and the corresponding known distances of the three GPS antennas on the moving buoy. The distance differences are computed with respect to monitor stations PGC and UCLU and the signals: wide-lane, narrow-lane, ionospheric free linear combination, L1-signal, and L2-signal. The geometry of the monitor stations and the antennas on the buoy can be seen in Figures 4.1 and 4.3. For a certain monitor station and a specific signal, the distance differences at each epoch is computed using the following steps:

- estimate the Cartesian coordinates of the three antennas, i.e.,  $X_{B1}$ ,  $X_{B2}$  and  $X_{B3}$ , using the 'unambiguous' double-difference phase observations,
- compute the distances between the antennas :

$$\begin{aligned}d_{12} &= \| X_{B1} - X_{B2} \| , \\d_{13} &= \| X_{B1} - X_{B3} \| , \text{ and} \\d_{23} &= \| X_{B2} - X_{B3} \| ,\end{aligned}\tag{IV.1}$$

- compute the distance differences as follows:

$$\begin{aligned}\delta d_{12} &= d_{12} - \hat{d}_{12} , \\ \delta d_{13} &= d_{13} - \hat{d}_{13} , \quad \text{and} \\ \delta d_{23} &= d_{23} - \hat{d}_{23} ,\end{aligned}\tag{IV.2}$$

where  $\hat{d}_{12}$ ,  $\hat{d}_{13}$ , and  $\hat{d}_{23}$  denote the known distances between the antennas. The histogram and time series of these distance differences,  $\delta d_{12}$ ,  $\delta d_{13}$ , and  $\delta d_{23}$ , are shown in the following Figures IV.1 to IV.10.

Narrow-lane signal, Monitor station : UCLU

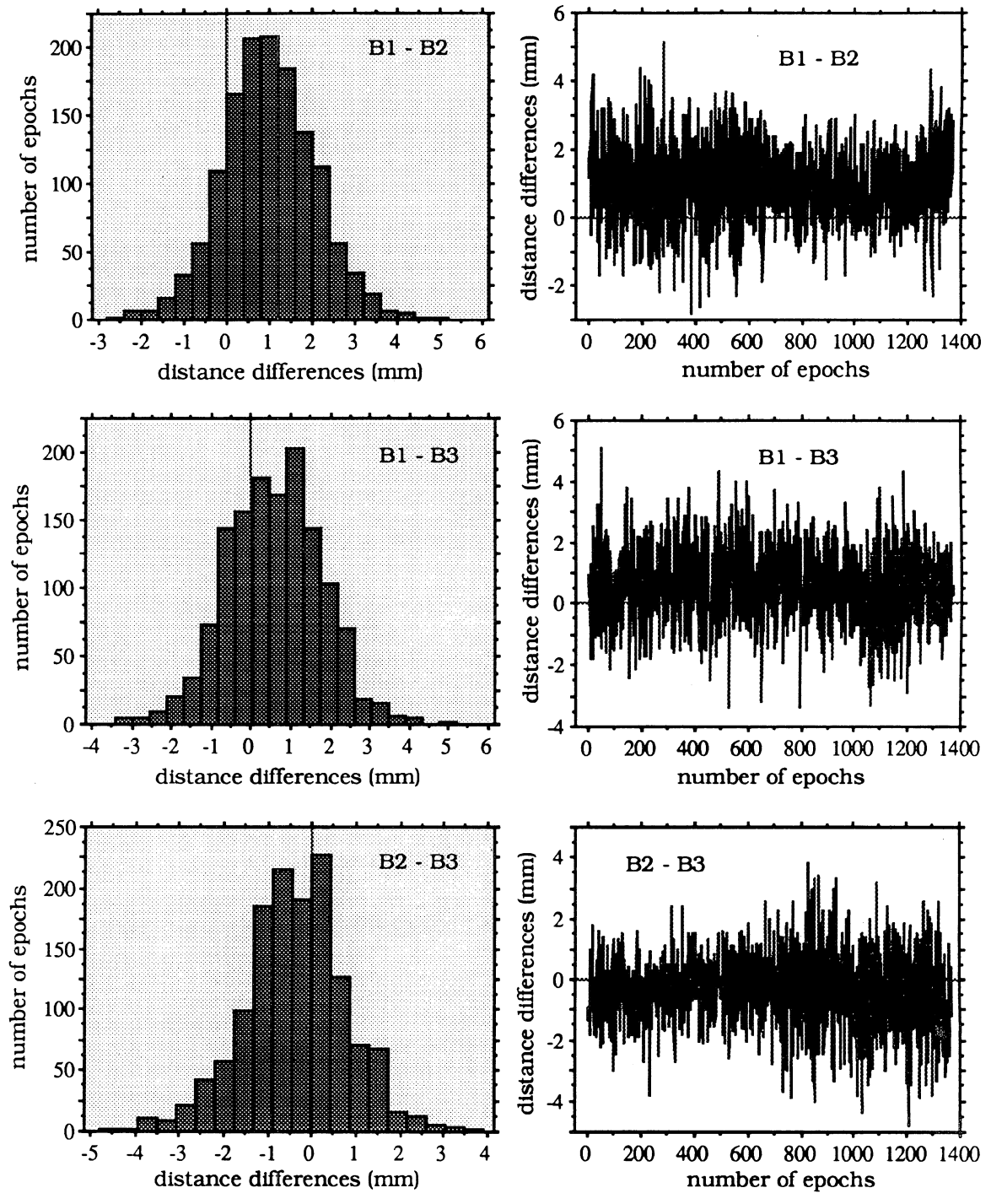


Figure IV.1. The differences of the antennas' distances on the buoy between the distances derived from the fixed ambiguity solution and their 'known' distances (narrow-lane signal, monitor station: UCLU).

Narrow-lane signal, Monitor station : PGC

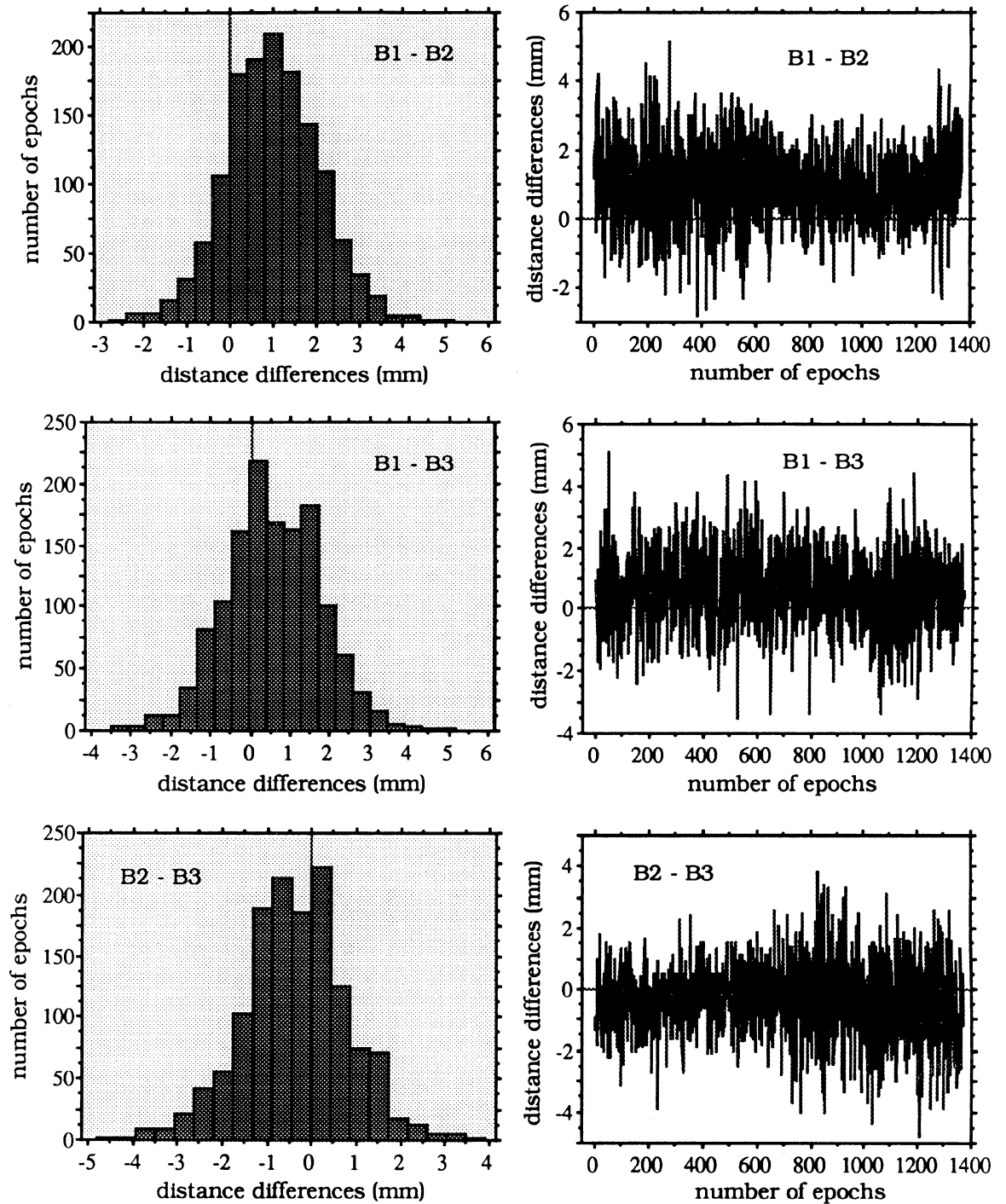


Figure IV.2. The differences of the antennas' distances on the buoy between the distances derived from the fixed ambiguity solution and their 'known' distances (narrow-lane signal, monitor station: PGC).



Wide-lane signal, Monitor station : UCLU

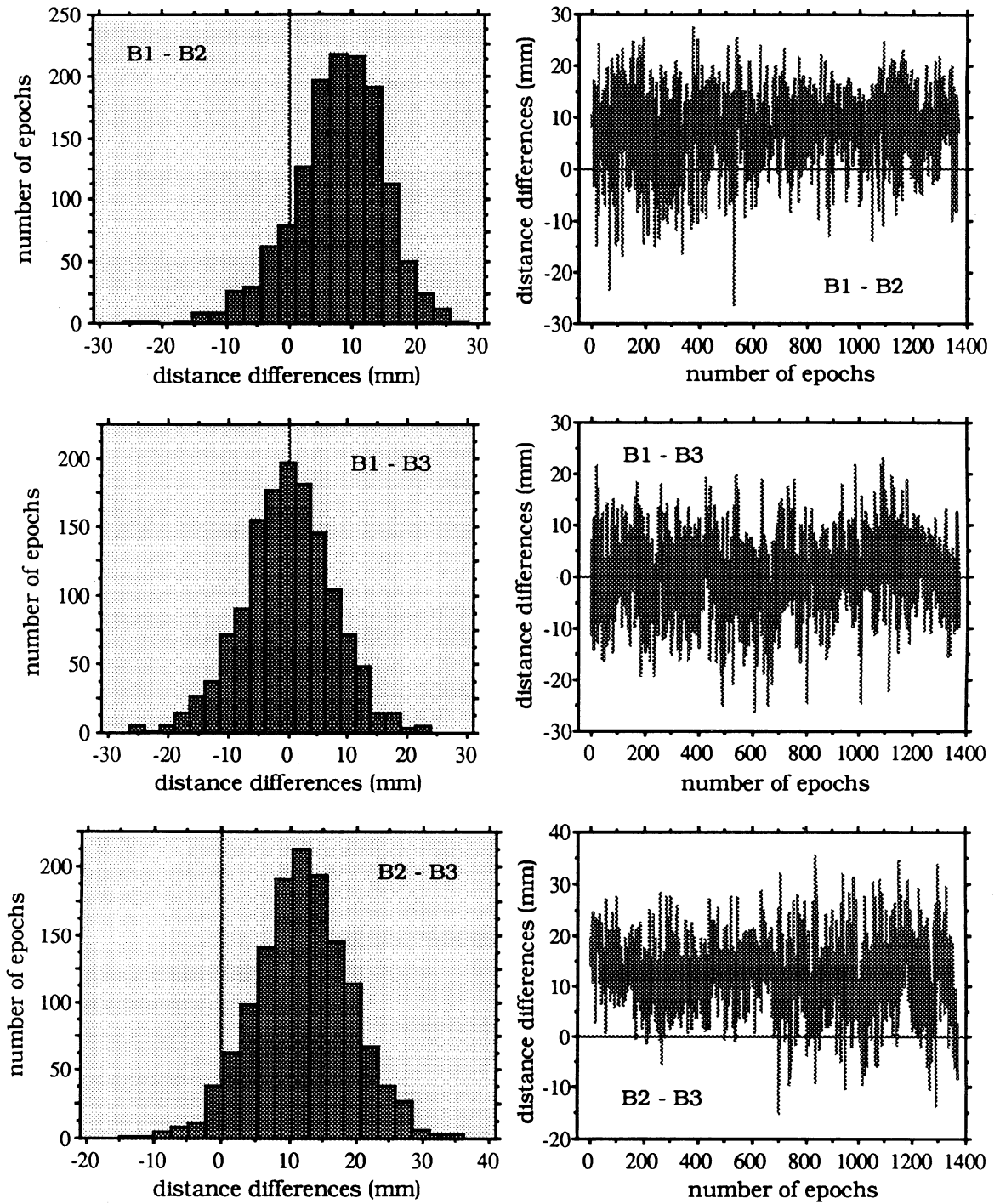


Figure IV.3. The differences of the antennas' distances on the buoy between the distances derived from the fixed ambiguity solution and their 'known' distances (wide-lane signal, monitor station: UCLU).

Wide-lane signal, Monitor station : PGC

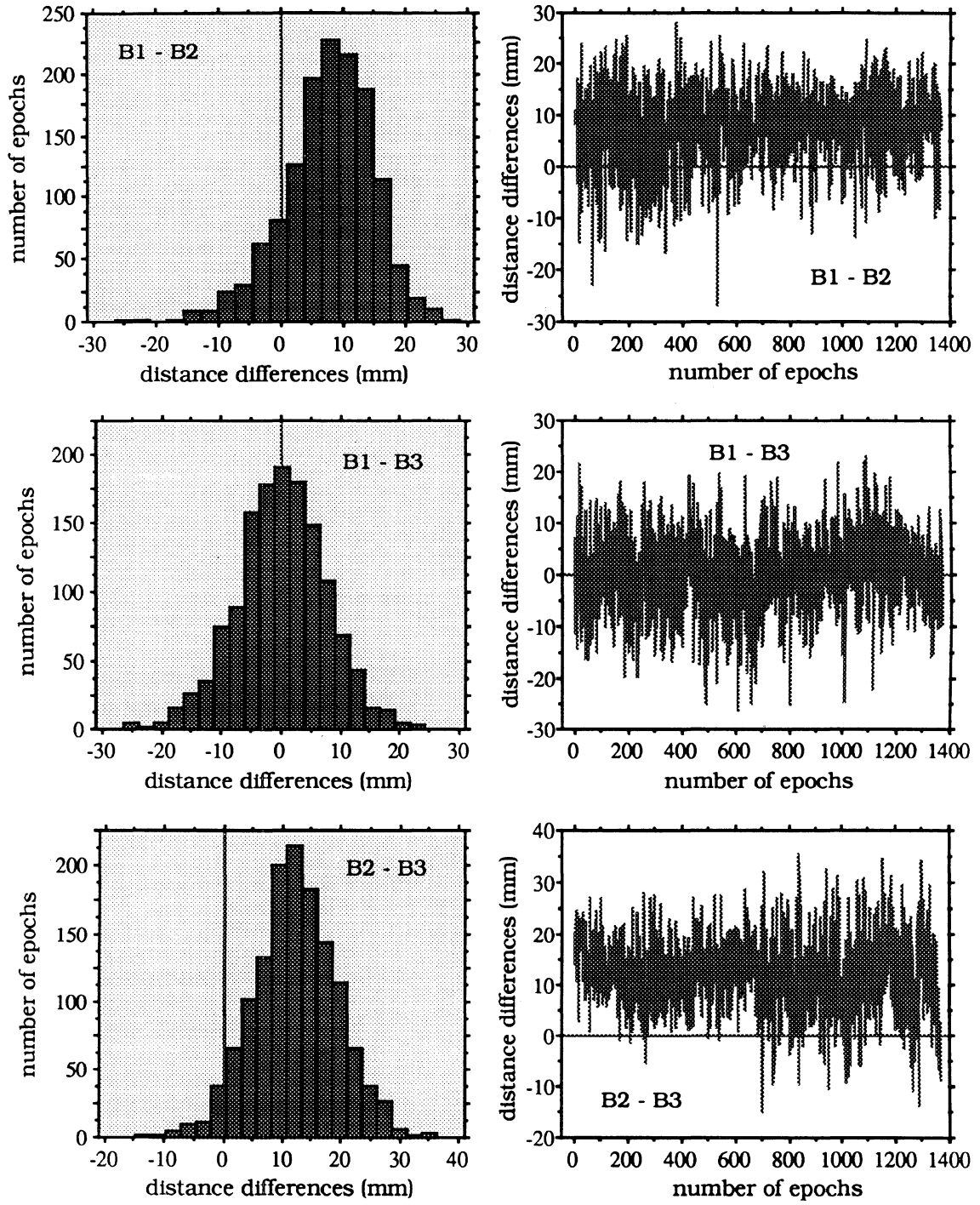


Figure IV.4. The differences of the antennas' distances on the buoy between the distances derived from the fixed ambiguity solution and their 'known' distances (wide-lane signal, monitor station: PGC).

Ionospheric-free linear combination, Monitor station : UCLU

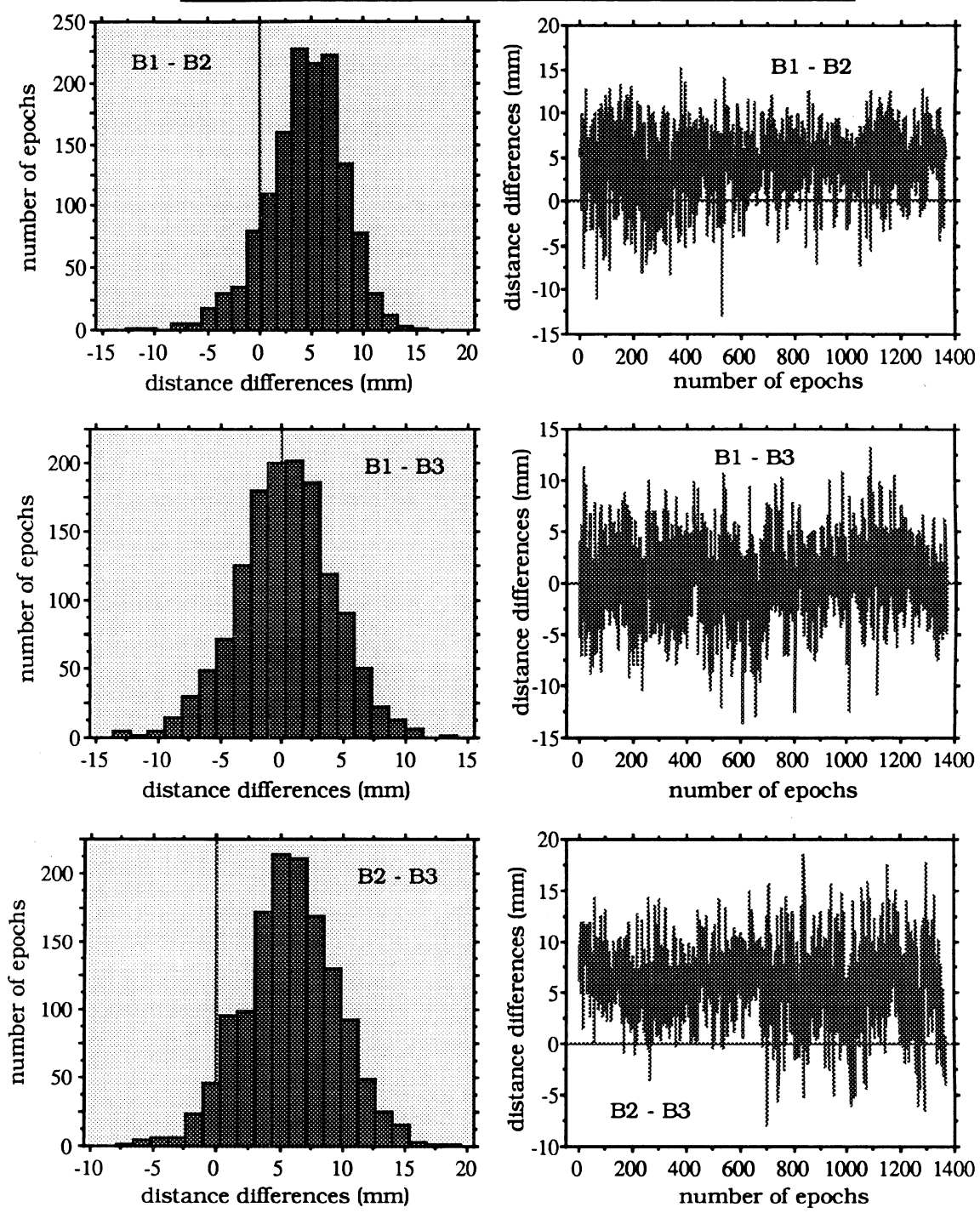


Figure IV.5. The differences of the antennas' distances on the buoy between the distances derived from the fixed ambiguity solution and their 'known' distances (ionospheric-free linear combination, monitor station: UCLU).

Ionospheric-free linear combination, Monitor station : PGC

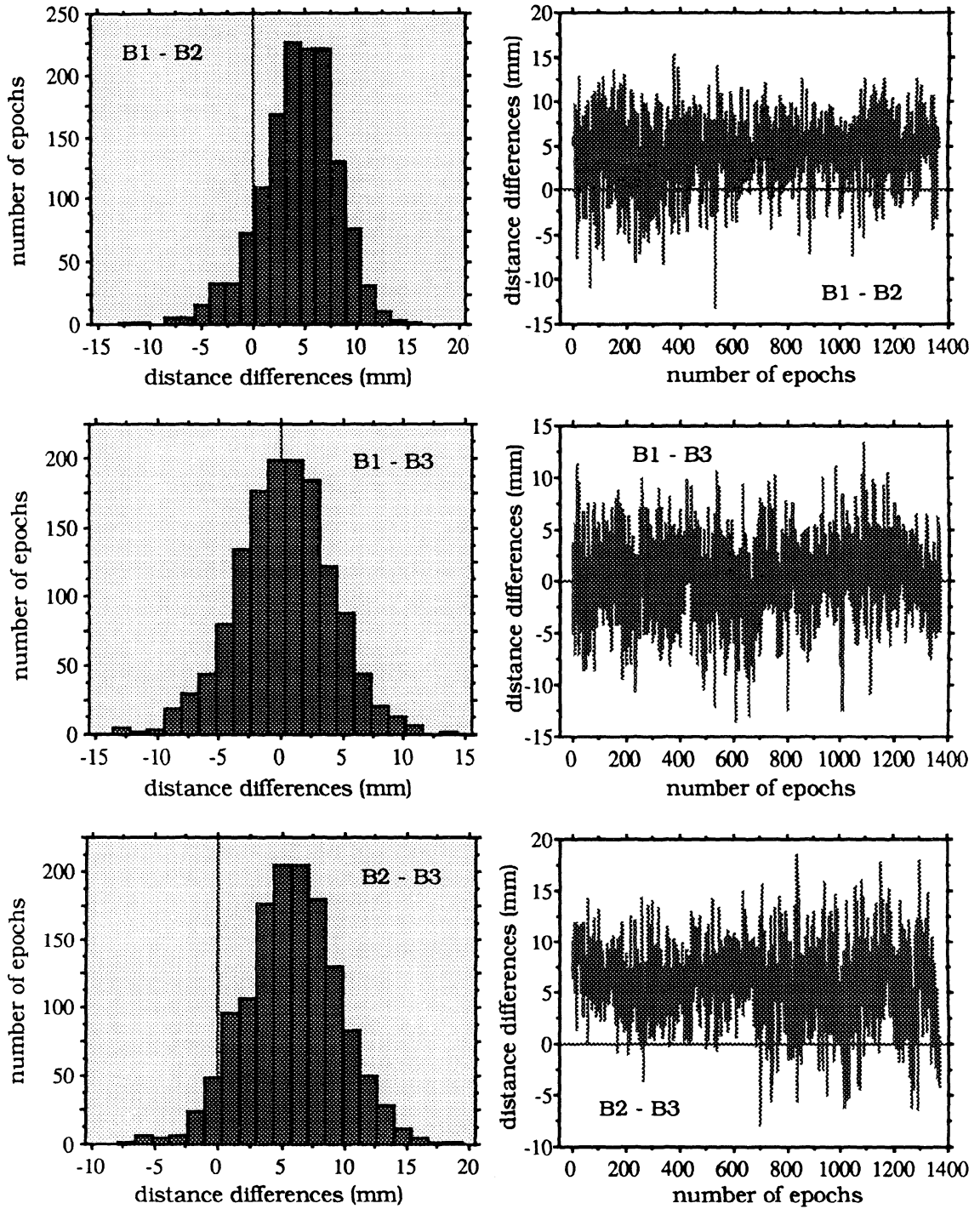


Figure IV.6. The differences of the antennas' distances on the buoy between the distances derived from the fixed ambiguity solution and their 'known' distances (ionospheric-free linear combination, monitor station: PGC).

L1 - signal, Monitor station : UCLU

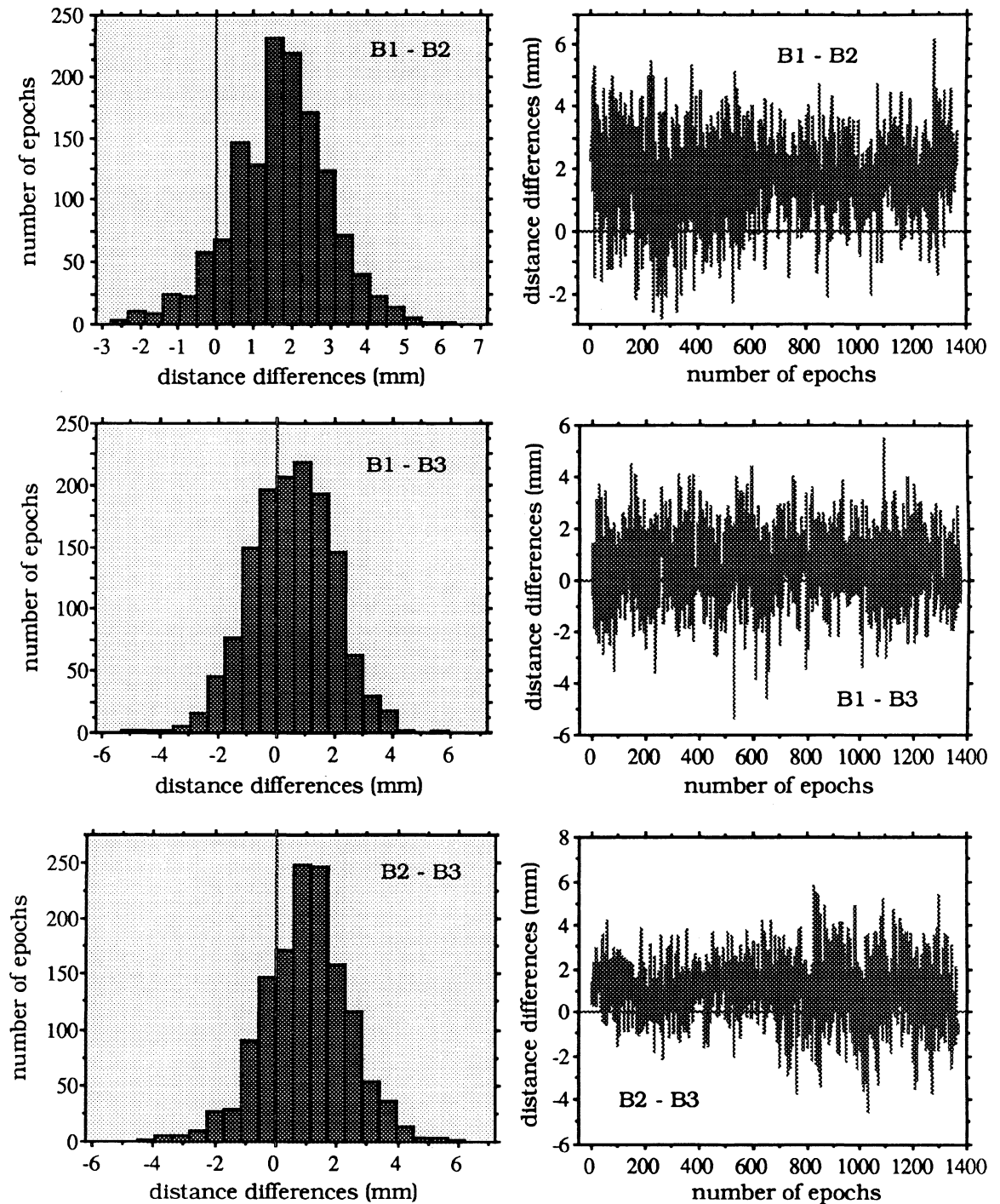


Figure IV.7. The differences of the antennas' distances on the buoy between the distances derived from the fixed ambiguity solution and their 'known' distances (L1 - signal, monitor station: UCLU).

L1 - signal, Monitor station : PGC

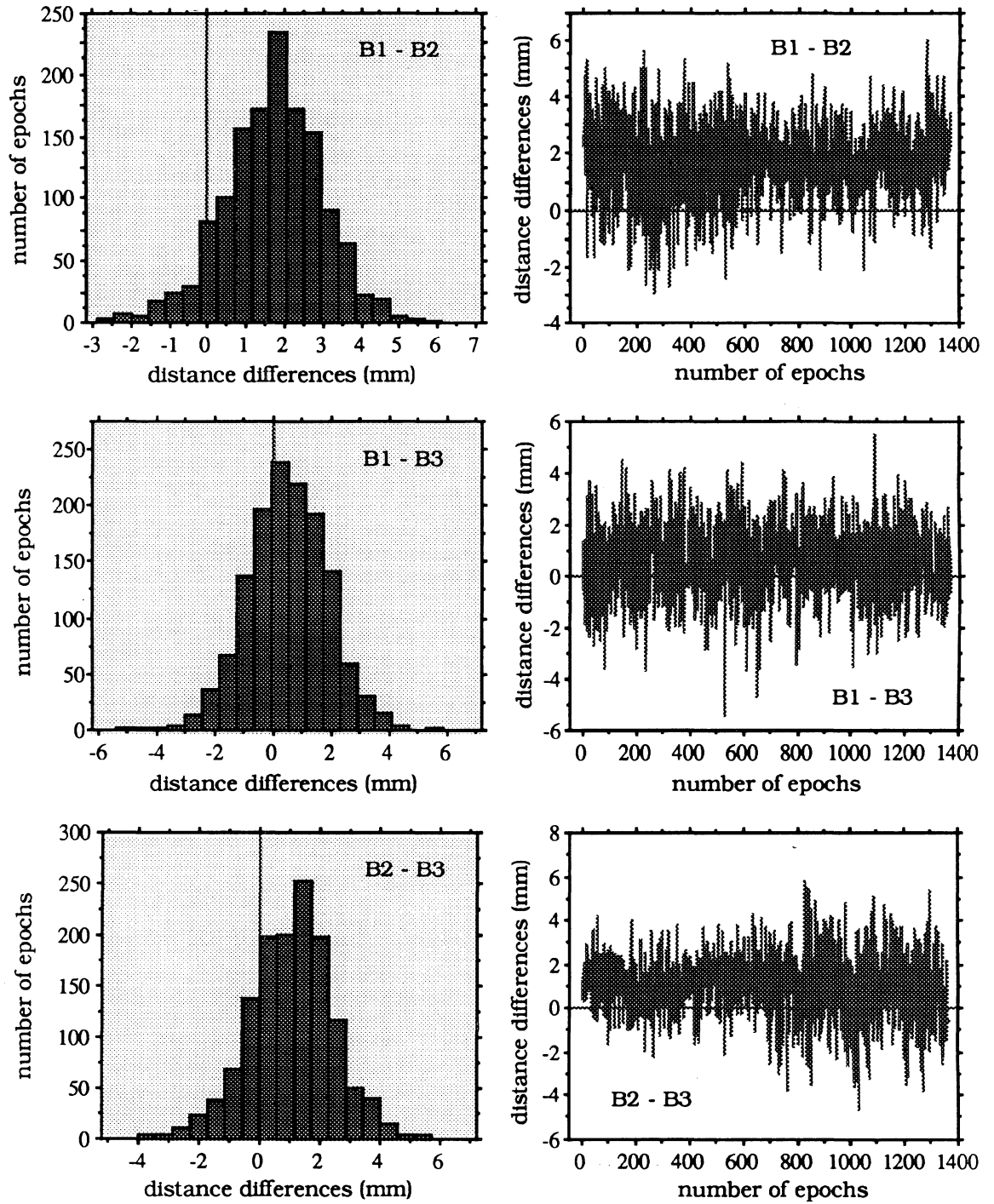


Figure IV.8. The differences of the antennas' distances on the buoy between the distances derived from the fixed ambiguity solution and their 'known' distances (L1 - signal, monitor station: PGC).

L2 - signal, Monitor station : UCLU

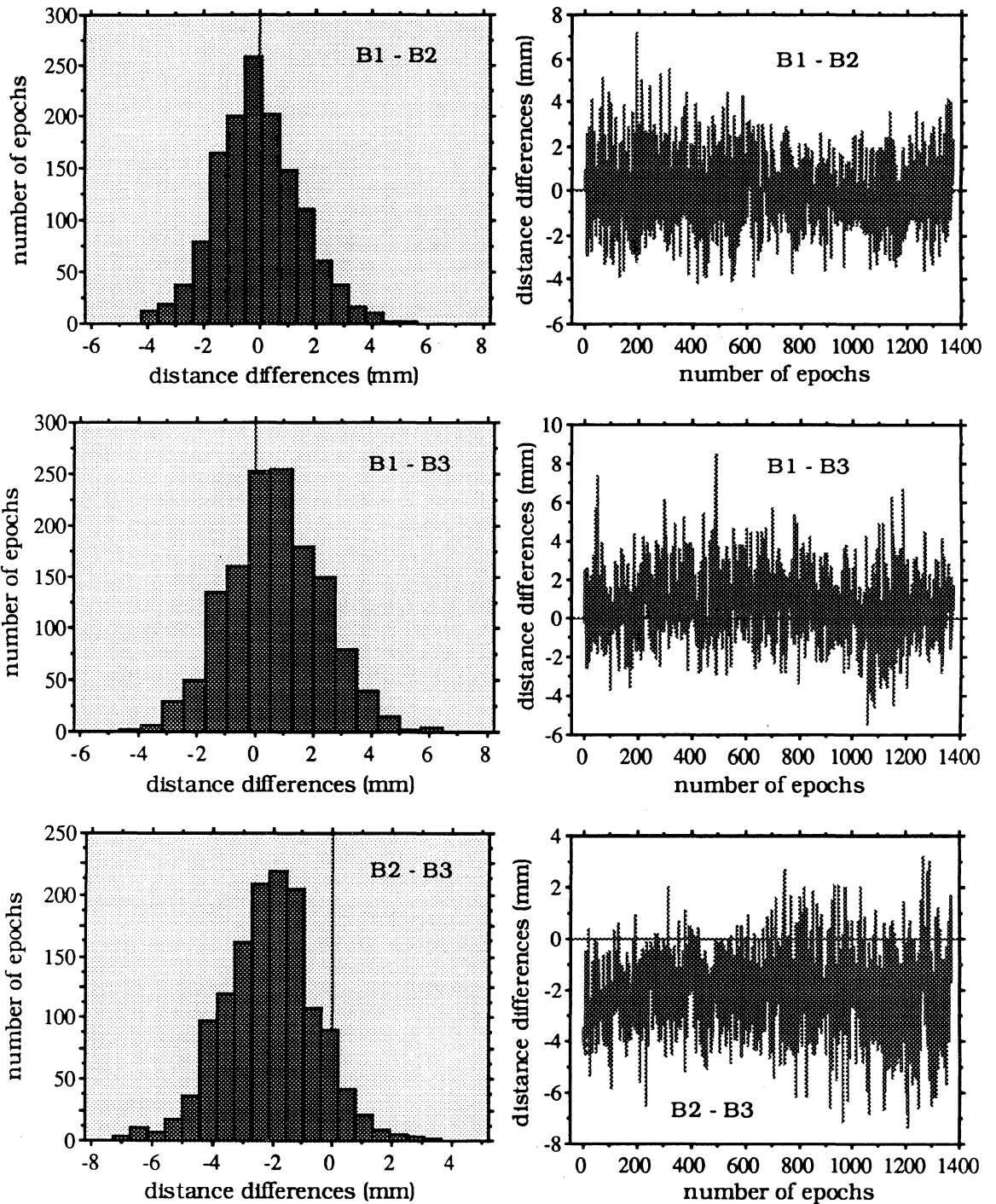


Figure IV.9. The differences of the antennas' distances on the buoy between the distances derived from the fixed ambiguity solution and their 'known' distances (L2 - signal, monitor station: UCLU).

L2 - signal, Monitor station : PGC

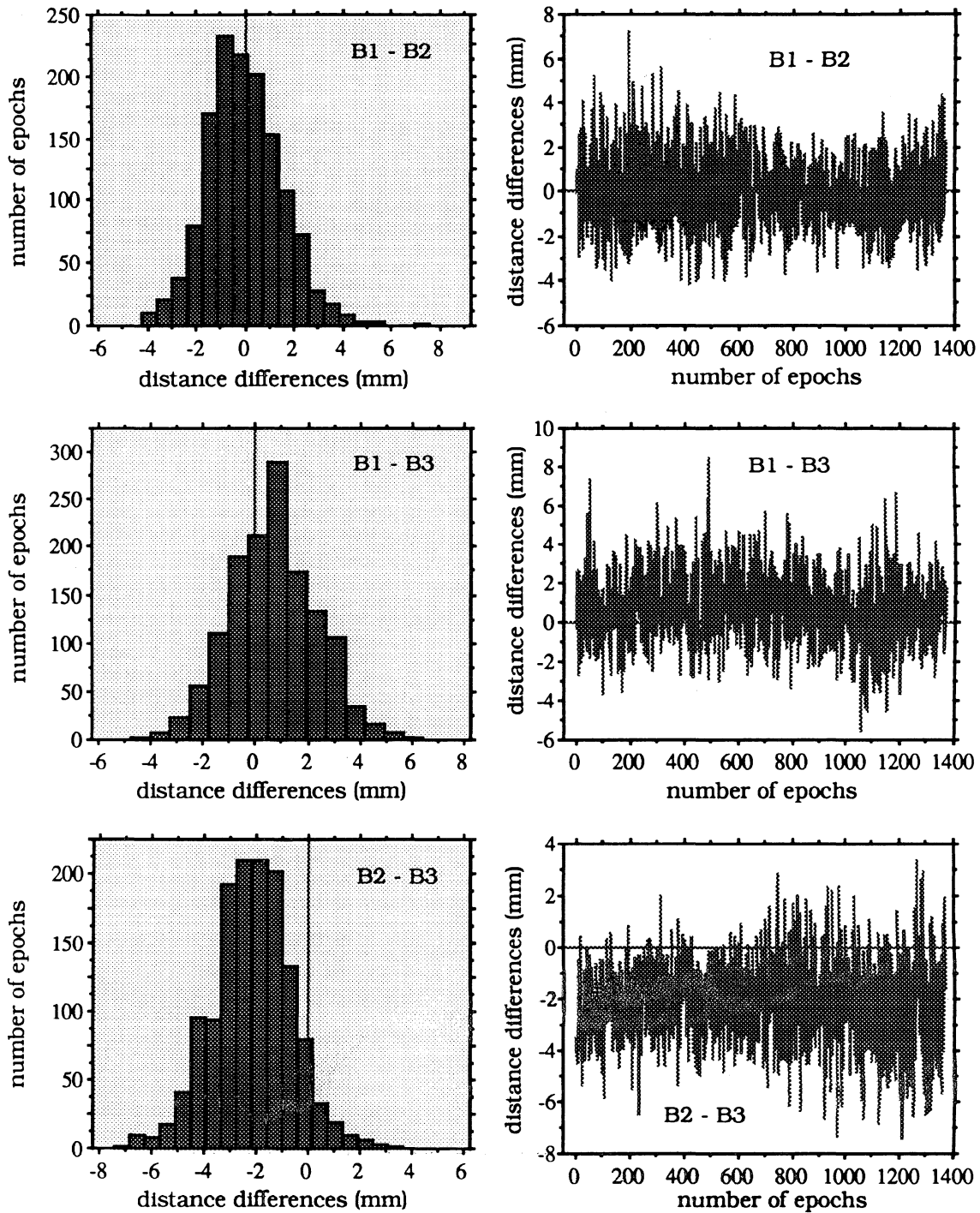


Figure IV.10. The differences of the antennas' distances on the buoy between the distances derived from the fixed ambiguity solution and their 'known' distances (L2 - signal, monitor station: PGC).



## Appendix V

### THE EFFECTS OF GEOMETRICAL PARAMETERS ON THE AMBIGUITY SEARCHING SPACE

---

---

As described in Chapter 6, observation geometry affects the speed and reliability of on-the-fly ambiguity resolution. Observation geometry, which in this research is represented by some geometrical parameters, will affect both the ambiguity searching space and the identification process of the correct ambiguities. In Chapter 6, the effects of the geometrical parameters on the ambiguity resolution has been explained in general and the ambiguity resolution results have also been presented. In summary, the effects of geometrical parameters on the initial ambiguity mathematical and physical searching spaces can be tabulated in Tables V.1 and V.2.

In this appendix, a more detail explanation about the effects of some of these geometrical parameters on the ambiguity searching space will be given, particularly from a mathematical point of view. The geometrical parameters will not be explained in the same order as in Chapter 6, and their effects will be explained in the context of mathematical ambiguity searching space. The effects on the physical ambiguity searching space should be easily understood by using explanations of the mathematical ambiguity searching space.

Table V.1. The effects of the geometrical parameters on the initial mathematical ambiguity searching space

Geometrical parameters	Centre	Volume	Shape	Orientation
Signal wavelength	√	√	√	√
Primary satellites	X	√	√	√
Number of satellites	√	√	√	√
Observation differencing strategy	X	X	√	√
Location of satellites	√	√	√	√
Data rate	X	X	X	X
Number of secondary monitor stations	√	√	√	√
Location of secondary monitor stations	√	X	X	X
√ = has an affect.      X = has no affect				

Table V.2. The effects of the geometrical parameters on the initial physical ambiguity searching space

Geometrical parameters	Centre	Volume	Shape	Orientation	Pattern
Signal wavelength	√	√	√	√	√
Primary satellites	X	√	√	√	√
Number of satellites	√	√	√	√	√
Observation differencing strategy	X	X	X	X	√
Location of satellites	√	√	√	√	√
Data rate	X	X	X	X	X
Number of secondary monitor stations	√	√	√	√	√
Location of secondary monitor stations	√	X	X	X	X
√ = has an affect.      X = has no affect Pattern = ( pattern of / distances between ) the surfaces of ambiguities					

### V.1. The number of secondary monitor station.

The mathematical searching space is defined in equation (3.2), and is rewritten in the following :

$$(\nabla\Delta N_{12} - \nabla\Delta N_{12}^o)^T \cdot C^{-1}(\nabla\Delta N_{12}^o) \cdot (\nabla\Delta N_{12} - \nabla\Delta N_{12}^o) < \chi^2_{3,1-\alpha} \quad , \quad (V.1)$$

As explained before, the above equation represents the ellipsoid centered at the initial primary ambiguities related to first secondary monitor station ( $\nabla\Delta N_{12}^o(i)$ ,  $i=1,3$ ). These initial ambiguities are estimated using the code derived position. The volume, shape, and orientation of the ellipsoid is governed by the covariance matrix of the initial ambiguities,  $C(\nabla\Delta N_{12}^o)$ , which itself depends on the covariance matrix of the code derived position.

The code derived position is estimated using all code observations. Its accuracy, therefore, depends on the number of secondary monitor station being used as do the initial primary ambiguities which are estimated using this position. In other words, the number of the monitor stations will affect the centre of the initial mathematical ambiguity searching space.

The covariance matrix of the initial ambiguities is computed using equation (3.4), and it depends on the covariance matrices of the code derived position,  $(C(X_c)_n)$ , involving  $n$  secondary monitor stations. The covariance matrix of code-derived position  $C(X_c)_n$  is computed using equations (3.5) - (3.7) in Chapter 3. For the sake of comparison with single monitor station case, it can be shown that, if all monitor station observations are characterized with one standard deviation value and all moving receiver observation with another value, then the covariance matrix of all code observations,  $C(\nabla\Delta P)_n$ , formulated by equation (3.7), and its inverse, can be reformulated as follows :

$$C(\Delta\nabla P)_n = \begin{bmatrix} C(\Delta\nabla P_{12}) & \tau.C(\Delta\nabla P_{12}) & \tau.C(\Delta\nabla P_{12}) & \tau.C(\Delta\nabla P_{12}) \\ & C(\Delta\nabla P_{12}) & \tau.C(\Delta\nabla P_{12}) & \tau.C(\Delta\nabla P_{12}) \\ & & \dots\dots\dots & \dots\dots\dots \\ \text{symmetric} & & & C(\Delta\nabla P_{12}) \end{bmatrix}, \quad (V.2)$$

$$C^{-1}(\Delta\nabla P)_n = \frac{1}{c_1} \begin{bmatrix} c_2.C^{-1}(\Delta\nabla P_{12}) & -\tau.C^{-1}(\Delta\nabla P_{12}) & -\tau.C^{-1}(\Delta\nabla P_{12}) & -\tau.C^{-1}(\Delta\nabla P_{12}) \\ & c_2.C^{-1}(\Delta\nabla P_{12}) & -\tau.C^{-1}(\Delta\nabla P_{12}) & -\tau.C^{-1}(\Delta\nabla P_{12}) \\ & & \dots\dots\dots & \dots\dots\dots \\ \text{symmetric} & & & c_2.C^{-1}(\Delta\nabla P_{12}) \end{bmatrix}. \quad (V.3)$$

In equations (V.2) and (V.3) above, the parameters  $\tau$ ,  $c_1$ , and  $c_2$  are defined as follows:

$$\tau = \frac{\sigma^2(P) \text{ of moving receiver}}{\sigma^2(P) \text{ of monitor station} + \sigma^2(P) \text{ of moving receiver}}, \quad (V.4)$$

$$c_1 = (1 - \tau) \cdot \{ 1 + (n-1)\tau \}, \quad (V.5)$$

$$c_2 = \{ 1 + (n-2)\tau \}, \quad (V.6)$$

where  $n$  is the number of secondary monitor stations. If the above equations are substituted into equation (3.5), the covariance matrix of the code derived position involving all monitor stations expressed by equation (3.5), can be simplified to the following equation:

$$C(X_c)_n = sf \cdot \{ A_c^T \cdot C^{-1}(\nabla\Delta P_{12}) \cdot A_c \}^{-1}, \quad (V.7)$$

or :

$$C(X_c)_n = sf \cdot C(X_c), \quad (V.8)$$

where  $C(X_c)$  is the covariance matrix involving only one secondary monitor station and  $sf$  is the scale factor which has the following formulation:

$$sf = \frac{1 + (n - 1)\tau}{n}. \quad (V.9)$$

Inserting equation (V.7) into equation (3.4), the covariance matrix of the initial ambiguities involving n monitor stations can be rewritten as follows:

$$C(\nabla\Delta N_{12}^o) = \frac{1}{\lambda^2} \cdot \{ sf \cdot A_p \cdot C(X_c) \cdot A_p^T + C(\nabla\Delta L_{p12}) \} \quad , \quad (V.10)$$

Since the value of  $\tau$  is always smaller than 1, then for  $n = 2$  or greater, the value of  $sf$  will always be smaller than 1. For  $n = 1$ , its value will be equal to 1. In general, the value of  $\tau$  will have the following range:

$$0 < \tau \leq 1 \quad . \quad (V.11)$$

Figure V.1 shows that at a certain value of  $\tau$ , the values of the scale factor  $sf$  decreases as more monitor stations are used.

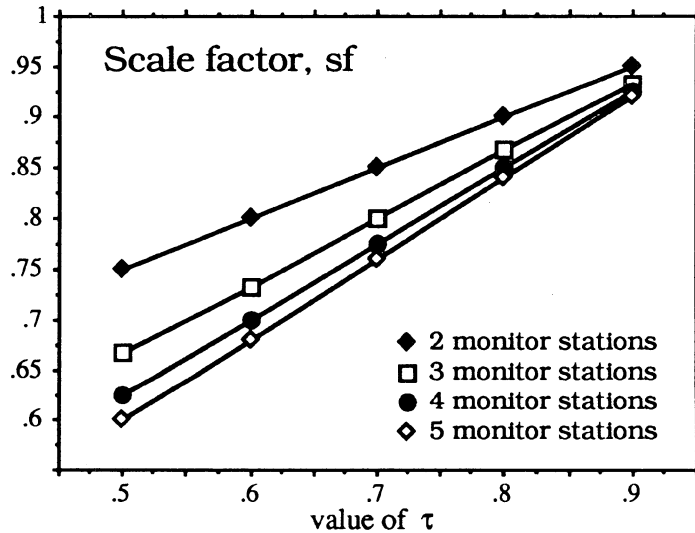


Figure V.1. Some values of the scale factor  $sf$

As expressed by equation (3.16), the **volume** of the ellipsoidal mathematical searching space is a function of the determinant of covariance matrix  $C(\nabla\Delta N_{12}^o)$ :

$$\text{Volume} \sim \sqrt{\det ( C(\nabla\Delta N_{12}^0) )} . \quad (\text{V.12})$$

In terms of the eigenvalues of matrix  $C(\nabla\Delta N_{12}^0)$ , equation (V.11) can be rewritten as:

$$\text{Volume} \sim \sqrt{\kappa_1 \cdot \kappa_2 \cdot \kappa_3} , \quad (\text{V.13})$$

where  $\kappa_1, \kappa_2$ , and  $\kappa_3$  are the eigenvalues. If the covariance matrix related to one monitor station is denoted as  $C(\nabla\Delta N_{12}^0)_1$ , and the following symmetric matrices are defined:

$$A = \frac{1}{\lambda^2} \cdot A_p \cdot C(X_c) \cdot A_p^T , \quad (\text{V.14})$$

$$B = \frac{1}{\lambda^2} \cdot C(\nabla\Delta L_{p12}) , \quad (\text{V.15})$$

then the following relations of the determinants of the matrices can be established:

$$\det ( C(\nabla\Delta N_{12}^0)_1 ) = \det (A) + \det (B) , \quad (\text{V.16})$$

$$\det ( C(\nabla\Delta N_{12}^0) ) = sf^3 \cdot \det (A) + \det (B) . \quad (\text{V.17})$$

Since A and B are positive definite matrices, then:

$$\det (A) > 0 \quad \text{and} \quad \det (B) > 0 . \quad (\text{V.18})$$

Based on equation (V.11) and (V.16) to (V.18), the following inequality can be realized:

$$\det ( C(\nabla\Delta N_{12}^0) ) < \det ( C(\nabla\Delta N_{12}^0)_1 ) , \quad (\text{V.19})$$

which then leads to the following relation:

$$\text{Volume (n)} < \text{Volume (1)} , \quad (\text{V.20})$$

where Volume (n) and Volume (1) are the volumes of the ellipsoidal searching spaces related to the use of n and one secondary monitor station, respectively. From equation (V.20), it can be concluded that the more secondary monitor stations used the smaller the searching space volume, and the fewer the number of initial ambiguity sets to be tested.

The **shape** of the ellipsoidal searching space will be determined by the ratio of the eigenvalues of the covariance matrix of the initial ambiguities. If the eigenvalues of  $C(\nabla \Delta N_{12}^0)$ , ordered with their increasing magnitudes, are denoted as  $\kappa_1, \kappa_2$ , and  $\kappa_3$ , and the eigenvalues of  $C(\nabla \Delta N_{12}^0)_1$  are denoted as  $\kappa_4, \kappa_5$ , and  $\kappa_6$ , then the two corresponding ellipsoidal spaces will have the same shape if:

$$\frac{\kappa_2}{\kappa_1} = \frac{\kappa_5}{\kappa_4}, \quad \frac{\kappa_3}{\kappa_1} = \frac{\kappa_6}{\kappa_4}, \quad \text{and} \quad \frac{\kappa_3}{\kappa_2} = \frac{\kappa_6}{\kappa_5} . \quad (\text{V.21})$$

With n monitor stations, based on equations (V.16) and (V.17), the following relation can be expressed :

$$\text{tr} ( C(\nabla \Delta N_{12}^0) ) < \text{tr} ( C(\nabla \Delta N_{12}^0)_1 ) , \quad (\text{V.22})$$

where  $\text{tr} (\bullet)$  is the trace of matrix  $(\bullet)$ , i.e., the sum of the diagonal elements of the matrix.

The above relation will lead to the following relation:

$$\kappa_1 + \kappa_2 + \kappa_3 < \kappa_4 + \kappa_5 + \kappa_6 . \quad (\text{V.23})$$

Since the covariance matrices  $C(\nabla \Delta N_{12}^0)$  and  $C(\nabla \Delta N_{12}^0)_1$  are positive definite matrices, then all eigenvalues,  $\kappa_1, \kappa_2, \dots, \kappa_6$ , will be greater than zero. Therefore, by also considering equations (V.23), then the following relation cannot exist :

$$\kappa_1 = \kappa_4, \quad \kappa_2 = \kappa_5, \quad \text{and} \quad \kappa_3 = \kappa_6 . \quad (\text{V.24})$$

Moreover, from the theory of matrix algebra, it is known that, if for example  $C$  is a  $m$  by  $m$  matrix with eigenvalues  $\kappa_1, \kappa_2, \dots$ , and  $\kappa_m$ , then matrix  $kC$  with  $k$  as a scalar will have eigenvalues  $k\kappa_1, k\kappa_2, \dots$ , and  $k\kappa_m$ . Based on equations (V.16) and (V.17), it can be seen that:

$$C(\nabla\Delta N_{12}^o) \neq s \cdot C(\nabla\Delta N_{12}^o)_1, \quad (V.25)$$

where  $s$  is any positive scalar. This non-uniform scaling and the non-existence of the relation expressed by equation (5.24), will lead to the conclusion that the relation expressed by equation (V.21) also cannot be valid. This means that the shape of ellipsoidal searching space will be affected by the number of secondary monitor stations used.

The **orientation** of the ellipsoidal searching space can be represented by three eigenvectors of the covariance matrix of  $(\nabla\Delta N_{12}^o)$ . The three eigenvectors are orthogonal to each other and their directions coincide with the semi axis of the ellipsoid.

If the three eigenvectors of  $C(\nabla\Delta N_{12}^o)$  are denoted as  $e_1, e_2$ , and  $e_3$ , and the three eigenvectors of  $C(\nabla\Delta N_{12}^o)_1$  are denoted as  $e_3, e_4$ , and  $e_6$ , then the following relations can be written:

$$\begin{aligned} C(\nabla\Delta N_{12}^o) \cdot e_1 &= \kappa_1 \cdot e_1, & C(\nabla\Delta N_{12}^o)_1 \cdot e_4 &= \kappa_4 \cdot e_4, \\ C(\nabla\Delta N_{12}^o) \cdot e_2 &= \kappa_2 \cdot e_2, & C(\nabla\Delta N_{12}^o)_1 \cdot e_5 &= \kappa_5 \cdot e_5, \\ C(\nabla\Delta N_{12}^o) \cdot e_3 &= \kappa_3 \cdot e_3, & C(\nabla\Delta N_{12}^o)_1 \cdot e_6 &= \kappa_6 \cdot e_6. \end{aligned} \quad (V.26)$$

In the above equations, if:

$$C(\nabla\Delta N_{12}^o) = s \cdot C(\nabla\Delta N_{12}^o)_1, \quad (V.27)$$

where  $s$  is any positive scalar, then the following relations exists:



$$\begin{aligned}
\kappa_1 &= s \cdot \kappa_4 \quad , & e_1 &= e_4 \quad , \\
\kappa_2 &= s \cdot \kappa_5 \quad , & e_2 &= e_5 \quad , \\
\kappa_3 &= s \cdot \kappa_6 \quad , & e_3 &= e_6 \quad .
\end{aligned}
\tag{V.28}$$

By using  $n$  secondary monitor stations, however, equation (V.27) is not valid, as can be realized from equation (V.16) and (V.17). Therefore, in this case the following relationship does not exist:

$$e_1 = e_4 \quad , \quad e_2 = e_5 \quad , \quad \text{and} \quad e_3 = e_6 \quad . \tag{V.29}$$

Hence, the orientation of the ellipsoidal searching space is affected by the number of secondary monitor stations used.

## V.2. The number of satellites

The number of satellites affects the centre, volume, shape, and orientation of the mathematical ambiguity searching space. As the number of secondary monitor stations, the number of satellites affects the searching space through the covariance matrix of the code derived position. For the sake of simplicity, only one secondary monitor stations is considered. The fixed differencing approach is used with the first satellite in order as a reference satellite. All observations are assumed to have the same precision. The covariance matrix of the code derived position, therefore, will have the following formulation:

$$C(X_c)_1 = 2\sigma^2 \cdot (A_c^T \cdot (J_{\nabla} \cdot J_{\nabla}^T)^{-1} \cdot A_c)^{-1} \quad , \tag{V.30}$$

where  $\sigma$  is the standard deviation of one-way code observations, and  $J_{\nabla}$  ( $ns-1, ns-1$ ) is the between-satellite single-difference Jacobian matrix formulated in equation (III.10), where  $ns$  is the number of observed satellites. It can be shown that :

$$J_{\nabla} \cdot J_{\nabla}^T = \begin{bmatrix} 2 & 1 & 1 & \dots & 1 \\ 1 & 2 & 1 & \dots & 1 \\ 1 & 1 & 2 & \dots & 1 \\ \vdots & \vdots & \vdots & \ddots & \vdots \\ 1 & 1 & 1 & 1 & 2 \end{bmatrix} , \quad (V.31)$$

and

$$(J_{\nabla} \cdot J_{\nabla}^T)^{-1} = \frac{1}{ns} \begin{bmatrix} ns-1 & -1 & -1 & \dots & -1 \\ -1 & ns-1 & -1 & \dots & -1 \\ -1 & -1 & ns-1 & \dots & -1 \\ \vdots & \vdots & \vdots & \ddots & \vdots \\ -1 & -1 & -1 & -1 & ns-1 \end{bmatrix} . \quad (V.32)$$

Equation (V.32) can be reformulated as:

$$(J_{\nabla} \cdot J_{\nabla}^T)^{-1} = I - \frac{1}{ns} \cdot S , \quad (V.33)$$

where  $I (ns-1, ns-1)$  is an identity matrix and  $S$  is the square matrix  $(ns-1, ns-1)$  in which all of its elements are equal to 1:

$$S = \begin{bmatrix} 1 & 1 & 1 & \dots & 1 \\ 1 & 1 & 1 & \dots & 1 \\ 1 & 1 & 1 & \dots & 1 \\ \vdots & \vdots & \vdots & \ddots & \vdots \\ 1 & 1 & 1 & 1 & 1 \end{bmatrix} . \quad (V.34)$$

Substituting equation (V.33) into equation (V.30), the following formulation for the covariance matrix of the code derived position is obtained:

$$C(X_c)_1 = 2\sigma^2 \cdot (A_c^T \cdot A_c - \frac{1}{ns} \cdot A_c^T \cdot S \cdot A_c)^{-1} . \quad (V.35)$$

The design matrix of the between-satellite single difference observations,  $A_c$ , can be formulated in the cartesian coordinate system as a function of the direction cosines to the satellites. These direction cosines are defined as in Figure V.2.

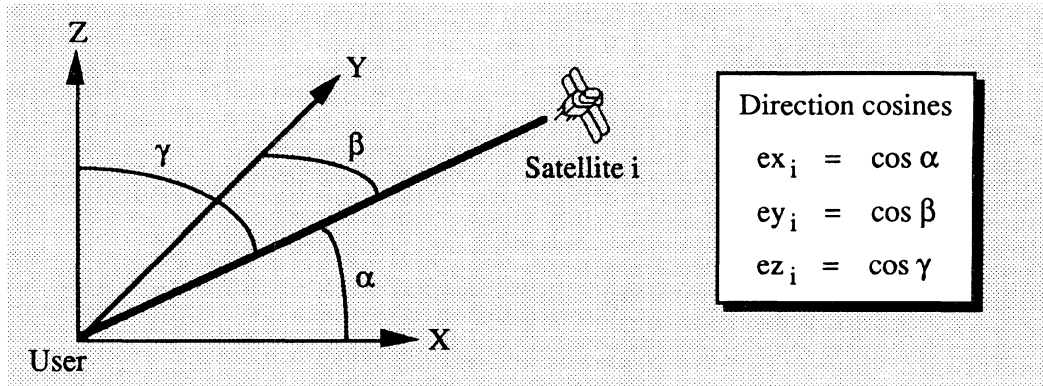


Figure V.2. Direction cosines to the satellite.

If  $n_s$  number of satellites are observed and the first satellite in order is taken as the reference satellite, then the design matrix  $A_c$  can be formulated as:

$$A_c = \begin{bmatrix} ex_2 - ex_1 & ey_2 - ey_1 & ez_2 - ez_1 \\ ex_3 - ex_1 & ey_3 - ey_1 & ez_3 - ez_1 \\ \dots\dots\dots & \dots\dots\dots & \dots\dots\dots \\ ex_{n_s} - ex_1 & ey_{n_s} - ey_1 & ez_{n_s} - ez_1 \end{bmatrix} = \begin{bmatrix} ex_{12} & ey_{12} & ez_{12} \\ ex_{13} & ey_{13} & ez_{13} \\ \dots & \dots & \dots \\ ex_{1n_s} & ey_{1n_s} & ez_{1n_s} \end{bmatrix} \quad (V.36)$$

It can be shown that:

$$A_c^T \cdot A_c = \begin{bmatrix} \sum_{j=2}^{n_s} (ex_{1j})^2 & \sum_{j=2}^{n_s} (ex_{1j} \cdot ey_{1j}) & \sum_{j=2}^{n_s} (ex_{1j} \cdot ez_{1j}) \\ & \sum_{j=2}^{n_s} (ey_{1j})^2 & \sum_{j=2}^{n_s} (ey_{1j} \cdot ez_{1j}) \\ \text{symmetry} & & \sum_{j=2}^{n_s} (ez_{1j})^2 \end{bmatrix} \quad (V.37)$$

From equation (V.34), it can be seen that  $S$  is a singular matrix. Hence, the following relations exist :

$$\det(S) = 0 \quad (V.38)$$

and  $\det(A_c^T \cdot S \cdot A_c) = 0 \quad (V.39)$

Based on equation (V.35) and (V.39), therefore :

$$\det (C(X_c)_1) \sim \det ((A_c^T \cdot A_c)^{-1}) \sim \frac{1}{\det (A_c^T \cdot A_c)} . \quad (V.40)$$

In equation (V.37), the trace of matrix  $(A_c^T \cdot A_c)$  becomes larger with an increase in the number of observed satellites, i.e., :

$$\text{tr} (A_c^T \cdot A_c) \uparrow \quad \text{as} \quad ns \uparrow . \quad (V.41)$$

where  $\uparrow$  denotes the value increase. If the eigenvalues of matrix  $(A_c^T \cdot A_c)$  are denoted as  $\kappa_1$ ,  $\kappa_2$ , and  $\kappa_3$ , then the relation shown by the above equation will lead to the following relationship:

$$(\kappa_1 + \kappa_2 + \kappa_3) \uparrow \quad \text{as} \quad ns \uparrow . \quad (V.42)$$

Since  $(A_c^T \cdot A_c)$  is positive definite matrix, and therefore it has positive eigenvalues, the above relation will lead to the following relation:

$$(\kappa_1 \cdot \kappa_2 \cdot \kappa_3) \uparrow \quad \text{as} \quad ns \uparrow , \quad (V.43)$$

or 
$$\det (A_c^T \cdot A_c) \uparrow \quad \text{as} \quad ns \uparrow . \quad (V.44)$$

Based on equation (V.40) and the above equation, then:

$$\det (C(X_c)_1) \downarrow \quad \text{as} \quad ns \uparrow , \quad (V.45)$$

where  $\downarrow$  denote the value decrease. The above equation then leads to:

$$\det (C(\nabla \Delta N_{12}^0)_1) \downarrow \quad \text{as} \quad ns \uparrow , \quad (V.46)$$

and therefore based on equation (V.12), the following relation is obtained:

$$\text{Volume} \downarrow \quad \text{as} \quad n_s \uparrow \quad . \quad (\text{V.47})$$

From the above relation it can be concluded that the volume of the ellipsoidal searching space becomes smaller as the number of observed satellite increases. With the shape and orientation of the searching space, the same arguments that have been used in the case of the number of secondary monitor stations can be used to verify that the number of satellites will also affect the shape and orientation of the searching space.

### V.3. Primary satellites

With the same number of observed satellites, different primary satellites will lead to a different volume, shape, and orientation of the searching space. For the sake of explanations, all observations are considered to have the same precision, and the fixed reference differencing approach is used to create the double difference observation with the first satellite in order is taken as a reference satellite.

The mathematical searching space is constructed using the covariance matrix of initial estimates of the ambiguities rewritten in the following:

$$C(\nabla\Delta N_{12}^o) = \frac{1}{\lambda^2} \cdot \{ A_p \cdot C(X_c)_n \cdot A_p^T + C(\nabla\Delta L_{p12}) \} \quad . \quad (\text{V.48})$$

Primary satellites affect the searching space through the design matrix  $A_p$ , while the matrices  $C(X_c)_n$  and  $C(\nabla\Delta L_{p12})$  remain unchanged. If, for example, two groups of primary satellites are considered (the first group, satellites 1, 2, 3, and 4; the second group, satellites : 1, 2, 3, and 5), then two corresponding design matrices are obtained:

$$A_p(1) = \begin{bmatrix} ex_{12} & ey_{12} & ez_{12} \\ ex_{13} & ey_{13} & ez_{13} \\ ex_{14} & ey_{14} & ez_{14} \end{bmatrix}, \quad A_p(2) = \begin{bmatrix} ex_{12} & ey_{12} & ez_{12} \\ ex_{13} & ey_{13} & ez_{13} \\ ex_{15} & ey_{15} & ez_{15} \end{bmatrix}, \quad (V.49)$$

where (1) and (2) denote the values related to the first and second group of primary satellites, respectively. Since for the user at or near the Earth's surface two different GPS satellites will always have different direction cosines, then:

$$A_p(1) \neq A_p(2) \quad , \quad (V.50)$$

and therefore

$$\det ( A_p(1) ) \neq \det ( A_p(2) ) \quad . \quad (V.51)$$

From the theory of linear algebra, it is known that the determinant of the matrix is equal to the determinant of its transpose. Therefore, based on equations (V.48) and (V.51), the following relation will follow:

$$\det ( C(\nabla\Delta N_{12}^o) (1) ) \neq \det ( C(\nabla\Delta N_{12}^o) (2) ) \quad , \quad (V.52)$$

which then will obviously lead to the following relation:

$$\text{Volume (1)} \neq \text{Volume (2)} \quad . \quad (V.53)$$

Therefore, it can be concluded that the volume of the ambiguity searching space will be affected by the primary satellites used. With the shape and orientation of the searching space, the same arguments that have been used with the number of secondary monitor stations can be used to prove that the shape and orientation of the searching space will also be affected by the primary satellites used.

#### V.4. Observation differencing strategy.

The observation differencing strategy includes the differencing approach used to create the double difference observations (fixed-reference or sequential differencing), the satellite ordering, and the reference satellite used in the case of fixed-reference differencing. For the sake of explanation, only one secondary monitor station is considered.

If there are  $ns$  observed satellites, the fixed-reference differencing with the first satellite in order as the reference satellite, is performed as: 2 - 1, 3 - 1, 4 - 1, ...,  $ns - 1$ ; and the sequential differencing is performed as: 2 - 1, 3 - 2, 4 - 3, ...,  $ns - (ns-1)$ .

For the above two differencing schemes, the following relations, involving the matrices used in constructing the ambiguity searching space, can be established:

$$A_p(s) = E_p \cdot A_p(f) , \quad (V.54)$$

$$A_c(s) = E_c \cdot A_c(f) , \quad (V.55)$$

$$J_{\nabla}(s) = E_c \cdot J_{\nabla}(f) , \quad (V.56)$$

$$C(\nabla\Delta L_{p12})(s) = E_c \cdot C(\nabla\Delta L_{p12})(f) \cdot E_c^T , \quad (V.57)$$

where (f) and (s) denote the parameters related to the fixed-reference and sequential differencing approaches, respectively; and  $E_p$  (3,3) and  $E_c$  ( $ns-1, ns-1$ ) are the matrices which have the following structure:

$$E_p = \begin{bmatrix} 1 & 0 & 0 \\ -1 & 1 & 0 \\ 0 & -1 & 1 \end{bmatrix} , \quad E_c = \begin{bmatrix} 1 & 0 & 0 & \dots & 0 \\ -1 & 1 & 0 & \dots & 0 \\ 0 & -1 & 1 & \dots & 0 \\ \dots & \dots & \dots & \dots & \dots \\ 0 & 0 & 0 & -1 & 1 \end{bmatrix} . \quad (V.58)$$

Note from the above equation that:

$$\det (E_p) = 1 , \quad \det (E_c) = 1 , \quad (V.59)$$

which will then lead to the following relations:

$$\det (A_p (s)) = \det (A_p (f)) , \quad (V.60)$$

$$\det (A_c (s)) = \det (A_c (f)) , \quad (V.61)$$

$$\det (J_{\nabla} (s)) = \det (J_{\nabla} (f)) , \quad (V.62)$$

$$\det (C(\nabla \Delta L_{p12}) (s)) = \det (C(\nabla \Delta L_{p12}) (f)) . \quad (V.63)$$

If the above equations are substituted into equations (V.30) and (V.48), the following relations can be established:

$$\det (C(X_c)_1 (s)) = \det (C(X_c)_1 (f)) , \quad (V.64)$$

$$\det (C(\nabla \Delta N_{12}^o) (s)) = \det (C(\nabla \Delta N_{12}^o) (f)) , \quad (V.65)$$

which then lead to the following relation:

$$\text{Volume (s)} = \text{Volume (f)} . \quad (V.66)$$

Therefore, the use of either fixed-reference or sequential differencing approach will lead to the same volume of the ambiguity searching space, considering that other geometrical parameters, such as the number of observed satellites and the primary satellites used, are the same.



If the eigenvalues of  $C(\nabla\Delta N_{12}^0)(s)$ , ordered with their increasing magnitudes, are denoted as  $\kappa_1, \kappa_2$ , and  $\kappa_3$ , and the eigenvalues of  $C(\nabla\Delta N_{12}^0)(f)$  are denoted as  $\kappa_4, \kappa_5$ , and  $\kappa_6$ , then based on equation (V.65), the following relation is valid:

$$\kappa_1 \cdot \kappa_2 \cdot \kappa_3 = \kappa_4 \cdot \kappa_5 \cdot \kappa_6 \quad . \quad (V.67)$$

In order to check whether the shape and orientation of the ellipsoidal searching space are affected by the use of different differencing approaches, one must also check the relation between the corresponding traces of the matrices,  $C(\nabla\Delta N_{12}^0)(s)$  and  $C(\nabla\Delta N_{12}^0)(f)$ .

Based on equation (V.30), it can be shown that, for the sequential differencing approach, the following relation can be written:

$$C(X_c)_1(s) = 2\sigma^2 \cdot \{ A_c(s)^T \cdot (J_{\nabla}(s) \cdot J_{\nabla}(s)^T)^{-1} \cdot A_c(s) \}^{-1} \quad . \quad (V.68)$$

Substituting equations (V.54) - (V.56) into the above equation, the following relations can be established:

$$\begin{aligned} C(X_c)_1(s) &= 2\sigma^2 \cdot \{ [E_c \cdot A_c(f)]^T \cdot [(E_c \cdot J_{\nabla}(f)) \cdot (E_c \cdot J_{\nabla}(f))^T]^{-1} \cdot [E_c \cdot A_c(f)] \}^{-1} \quad , \\ &= 2\sigma^2 \cdot \{ A_c(f)^T \cdot E_c^T \cdot (E_c^T)^{-1} \cdot (J_{\nabla}(f) \cdot J_{\nabla}(f)^T)^{-1} \cdot E_c^{-1} \cdot E_c \cdot A_c(f) \}^{-1} \quad , \\ &= 2\sigma^2 \cdot \{ A_c(f)^T \cdot (J_{\nabla}(f) \cdot J_{\nabla}(f)^T)^{-1} \cdot A_c(f) \}^{-1} \quad , \\ &= C(X_c)_1(f) \quad . \end{aligned} \quad (V.69)$$

With the covariance matrix of the initial estimates of ambiguities, by considering the same precision for all phase observations (characterized by standard deviation  $\sigma$ ), the following relations can also be written :

$$\begin{aligned}
C(\nabla\Delta N_{12}^o)(s) &= \frac{1}{\lambda^2} \cdot \{ A_p(s) \cdot C(X_c)_1(s) \cdot A_p(s)^T + 2\sigma^2 \cdot J_{\nabla}(s) \cdot J_{\nabla}(s)^T \} \quad , \\
&= \frac{1}{\lambda^2} \cdot \{ E_p \cdot A_p(f) \cdot C(X_c)_1(f) \cdot A_p(f)^T \cdot E_p^T + 2\sigma^2 \cdot E_p \cdot J_{\nabla}(f) \cdot J_{\nabla}(f)^T \cdot E_p^T \} \quad , \\
&= \frac{1}{\lambda^2} \cdot E_p \cdot \{ A_p(f) \cdot C(X_c)_1(f) \cdot A_p(f)^T + 2\sigma^2 \cdot J_{\nabla}(f) \cdot J_{\nabla}(f)^T \} \cdot E_p^T \quad , \\
&= E_p \cdot C(\nabla\Delta N_{12}^o)(f) \cdot E_p^T \quad . \tag{V.70}
\end{aligned}$$

From the above equation, it can be realized that:

$$\text{tr}(C(\nabla\Delta N_{12}^o)(s)) \neq \text{tr}(C(\nabla\Delta N_{12}^o)(f)) \quad , \tag{V.71}$$

which then lead to the following relation:

$$\kappa_1 + \kappa_2 + \kappa_3 \neq \kappa_4 + \kappa_5 + \kappa_6 \quad . \tag{V.72}$$

Since all eigenvalues are positive, then, based on equations (V.67) and (V.72), it can be concluded that the observation differencing approach used will affect the shape and orientation of the ellipsoidal mathematical searching space.

Finally, it should be noted that, by using the same arguments as presented by equations (V.54) to (V.72), it can be shown that different satellite ordering and different reference satellites used for fixed-reference differencing will only affect the shape and orientation of the mathematical ambiguity searching space, as in the case of the other differencing approach. The volume of the ambiguity searching space will not be affected.

## Appendix VI

# SIMULATED GPS KINEMATIC DATA

---

---

As well as using real static and kinematic GPS data, the simulated GPS kinematic data is used to study the effects of the number and location of the secondary monitor stations on the performance of on-the-fly ambiguity resolution technique.

### **VI.1. Simulating the code and phase observations**

In this simulation, four stations are considered as secondary monitor stations and the moving receiver is assumed to be installed in a marine vessel moving along certain simulated trajectory. The relative position of the secondary monitor stations with respect to the initial position of moving receiver is shown in Figure VI.1. along with the simulated trajectory of the moving receiver. The pitch, roll, and heave data used to characterize the dynamics of vehicle-sea interaction is the real data observed off the shore of Nova Scotia. The GPS observations are simulated with one second data interval. The WGS-84 ellipsoidal GPS antenna coordinates of the four secondary monitor stations and the initial coordinates of moving receiver used in this simulation are listed in Table VI.1.

The one-way code and phase observations from the stations on the ground, either monitor station or moving receiver, to the satellites on the sky can be simulated based on equations (I.2) and (I.3).

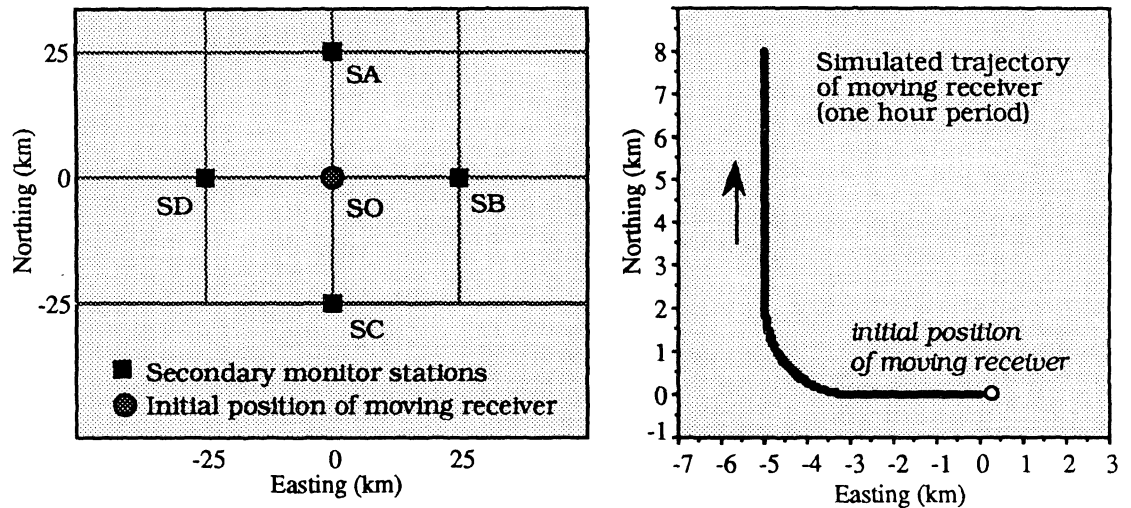


Figure VI.1. Relative positions of the secondary monitor stations and the simulated trajectory of the moving receiver.

Table VI.1. The GPS antenna coordinates of the stations for simulation.

Station	Latitude	Longitude	Ellipsoidal height (metres)
SO	48° 00' 00.00000"	-123° 00' 00.00000"	-15.00
SA	48° 13' 29.40705"	-123° 00' 00.00000"	-9.00
SB	47° 59' 58.24148"	-122° 39' 53.98315"	-9.00
SC	47° 46' 30.56112"	-123° 00' 00.00000"	-9.00
SD	47° 59' 58.24148"	-123° 20' 11.28617"	-9.00

In simulating the errors and biases affecting observations, only ionospheric refraction, ephemeris errors, and observation noises are taken into account. Since working observations are station-satellite double-difference observations, no (receiver and satellite) clock offsets and fractional uncalibrated initial phases are taken into account. It is assumed that the effects of tropospheric refraction can be greatly reduced by correction based on surface measurements of meteorological data and also, to a certain extent, by observation differencing. With multipath, it can be assumed that the antennas are placed on the 'multipath-free' sites and the ground absorber planes are utilized to further reduce the

multipath effects. However, it should be noted that our computer program to simulate the GPS data used in this research is equipped with the capability to simulate the tropospheric delay based on Hopfield model and the multipath errors based on algorithms described in *Georgiadou and Kleusberg [1988]* and *Bishop et al. [1985]*. Therefore, in simulating the code and phase observations ( $P_i$  and  $L_i$ ), equations (I.2) and (I.3) are simplified into the following equations:

$$P_i = \rho + d\rho + \text{dion}_i + \vartheta P_i, \quad (\text{VI.1})$$

$$L_i = \rho + d\rho - \text{dion}_i - \lambda_i \cdot N_i + \vartheta C_i, \quad (\text{VI.2})$$

where  $\rho$  is geometric range between the antenna and the satellite,  $d\rho$  is range error caused by ephemeris errors,  $\text{dion}$  is the bias caused by the ionospheric refraction,  $\lambda$  is the wavelength of the signal,  $N$  is the integer cycle ambiguity of the phase observation, and  $\vartheta P$  and  $\vartheta C$  are the noises in code and phase observations. Subscript  $i$  denotes the signal frequency used which corresponds to L1 and/or L2 signals.

## **VI.2. Computing the geometric range between the antenna and satellite**

The geometric distance between the satellite receiver's antenna and the satellite can be easily computed from the coordinates of the antenna and satellite. The coordinates of the antenna at every epoch are computed based on the simulated trajectory shown in Figure VI.1, the assumed antenna height above sea surface, and the dynamics of the vessel represented by pitch, roll, and heave parameters. The coordinates of the observed satellites are computed based on the broadcast ephemeris of the satellites [*van Dierendonck, 1986*]. The computation of the geometric ranges at every epoch are performed by iteration and its general step is shown in Figure VI.2.

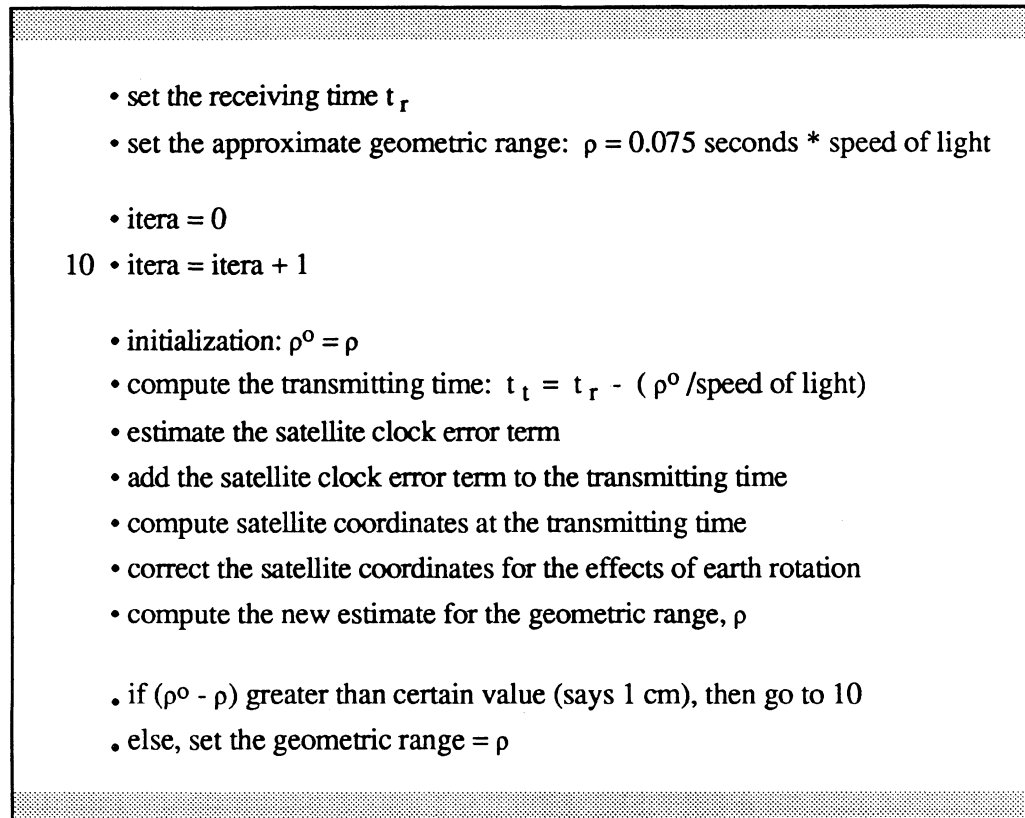


Figure VI.2. Computing the geometric range between the antenna and the satellite.

When simulating data from GPS satellites, the 21 primary satellite constellation is used. It consists of 24 satellite positions, with 4 satellites in each of six 55 degree inclined equally spaced orbital planes [Green *et al.*, 1989]. The orbital parameters of the satellites used for the simulation is given in Table VI.2. In this simulation, the satellites are numbered from 1 to 24. Note that these numbers are not related to the actual PRN numbers of the satellites. The date of simulation is 1 January 1991, and the data interval is one second. On this particular day, four eight-satellite constellations were considered, with one-hour observation periods in the evening (4:30 - 5:30 p.m), night (11:30 p.m - 12:30 a.m.), morning (7:30 - 8:30 a.m), and afternoon (2:00 - 3:00 p.m.), respectively. The satellite polar plots for these four constellations are shown in Figure VI.3.

Table VI.2. 21 Primary SV (GPS) constellation ephemerides  
(classical coordinates - km/deg, epoch = 1989. 11. 26. 0. 0. 0.0);  
from [Green et al., 1989].

No.	Plane	a	e	i	$\Omega$	$\omega$	M
1	A1	26609.0	0.	55.0	325.730284	0.	190.96
2	A2	26609.0	0.	55.0	325.730284	0.	220.48
3	A3	26609.0	0.	55.0	325.730284	0.	330.17
4	A4	26609.0	0.	55.0	325.730284	0.	83.58
5	B1	26609.0	0.	55.0	25.7302839	0.	249.90
6	B2	26609.0	0.	55.0	25.7302839	0.	352.12
7	B3	26609.0	0.	55.0	25.7302839	0.	25.25
8	B4	26609.0	0.	55.0	25.7302839	0.	124.10
9	C1	26609.0	0.	55.0	85.7302839	0.	286.20
10	C2	26609.0	0.	55.0	85.7302839	0.	48.94
11	C3	26609.0	0.	55.0	85.7302839	0.	155.08
12	C4	26609.0	0.	55.0	85.7302839	0.	183.71
13	D1	26609.0	0.	55.0	145.730284	0.	312.30
14	D2	26609.0	0.	55.0	145.730284	0.	340.93
15	D3	26609.0	0.	55.0	145.730284	0.	87.06
16	D4	26609.0	0.	55.0	145.730284	0.	209.81
17	E1	26609.0	0.	55.0	205.730284	0.	11.90
18	E2	26609.0	0.	55.0	205.730284	0.	110.76
19	E3	26609.0	0.	55.0	205.730284	0.	143.88
20	E4	26609.0	0.	55.0	205.730284	0.	246.11
21	F1	26609.0	0.	55.0	265.730284	0.	52.42
22	F2	26609.0	0.	55.0	265.730284	0.	165.83
23	F3	26609.0	0.	55.0	265.730284	0.	275.52
24	F4	26609.0	0.	55.0	265.730284	0.	305.04
a = semimajor axis, e = eccentricity, i = inclination, $\Omega$ = right ascension of ascending node, $\omega$ = argument of perigee, M = mean motion.							

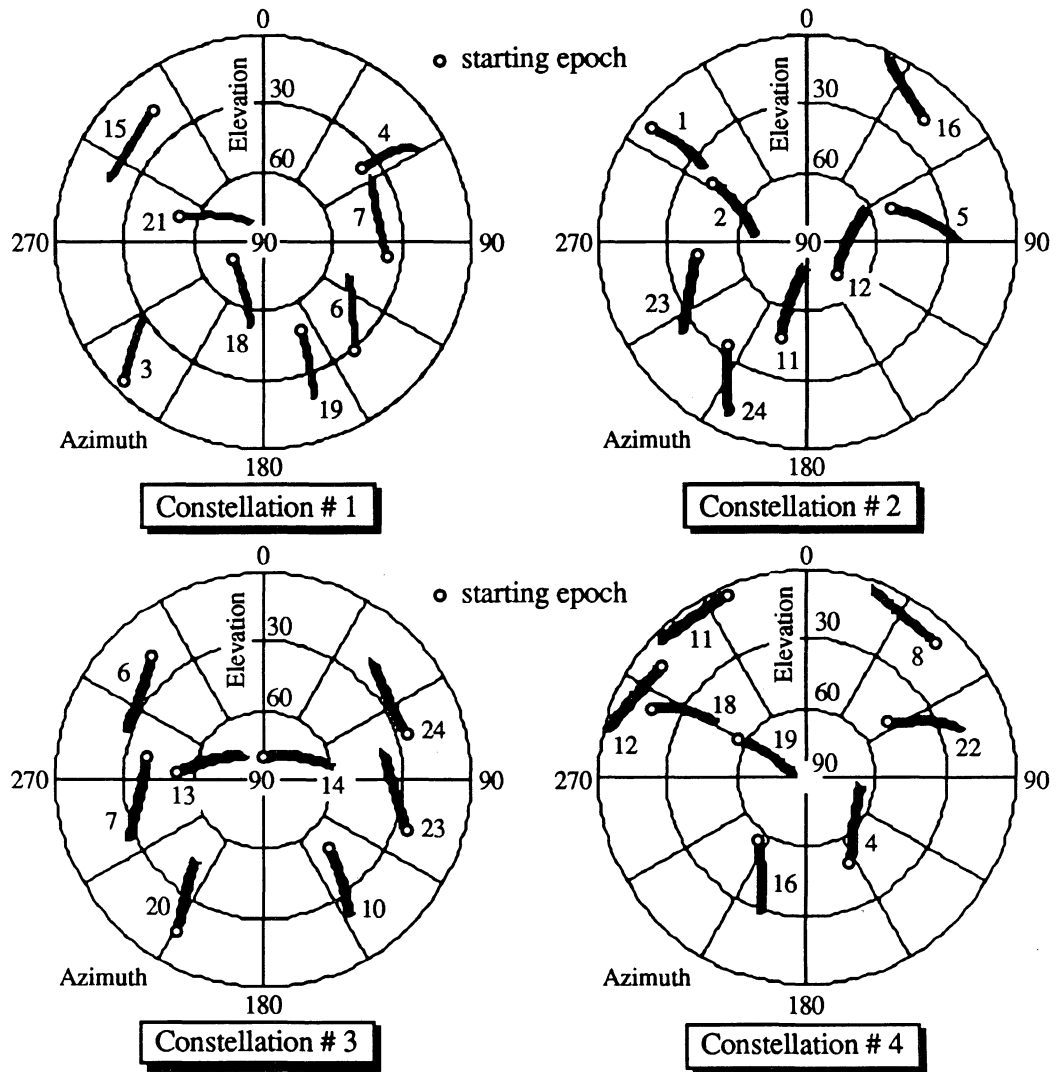


Figure VI.3. GPS satellites polar plot seen from initial position of the moving receiver.

### VI.3. Simulating the satellite ephemeris errors

The coordinates of the GPS satellites can be computed using the satellite broadcast ephemeris. Errors in the ephemeris will affect the accuracy of the computed satellite coordinates. Ephemeris errors can originate from two sources [Colombo, 1986]: (1). the imprecise estimation of the position and velocity of the satellite at the initial state, which is due to errors in tracking data, station coordinates, force models etc. used for this



estimation, and (2). the use of incorrect force models to integrate the equations of motion onwards from this initial state. In this simulation, the ephemeris errors of a satellite for a certain time period is characterized by three error components, namely *along-track*, *across track*, and *radial* components as shown in Figure VI.4.

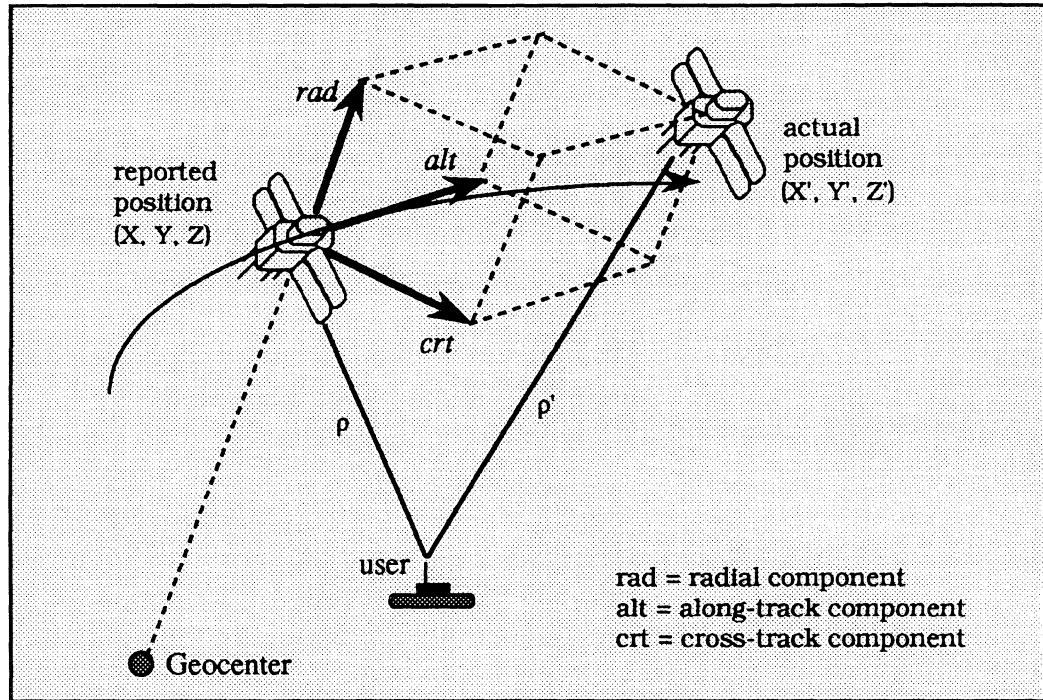


Figure VI.4. Satellite ephemeris errors (picture is not to scale).

Each satellite is randomly assigned with certain values of these three error components, and these values are considered constant for the observation session (in our simulation, a session is usually 1 hour). For each satellite, the constant values of the errors components are assigned as:

$$\begin{aligned}
 \text{rad}(i) &= \sigma_{\text{rad}} \cdot \mathcal{R}_1(0,1,i) \quad , i = 1, \text{ns} \\
 \text{alt}(i) &= \sigma_{\text{alt}} \cdot \mathcal{R}_2(0,1,i) \quad , i = 1, \text{ns} \\
 \text{crt}(i) &= \sigma_{\text{crt}} \cdot \mathcal{R}_3(0,1,i) \quad , i = 1, \text{ns}
 \end{aligned}
 \tag{VI.3}$$

where  $\sigma_{\text{rad}}$ ,  $\sigma_{\text{alt}}$ , and  $\sigma_{\text{crt}}$  are the values to characterize the level of ephemeris errors, and  $\mathcal{R}_1(0,1,i)$  is  $i$ th real number of the normally distributed random variables with zero mean and unit standard deviation  $\mathcal{R}_1(0,1)$ . In this simulation, the values of 2.0 m, 5.0 m, and 3.0 m are assigned to  $\sigma_{\text{rad}}$ ,  $\sigma_{\text{alt}}$ , and  $\sigma_{\text{crt}}$ , respectively.

In this simulation, the effects of satellite ephemeris errors in code and phase observations,  $d\rho$ , is computed using the following relation :

$$d\rho = \rho' - \rho \quad , \quad (\text{VI.4})$$

where  $\rho'$  and  $\rho$  are the geometric ranges computed based on actual and reported position of the satellite, respectively. The computation of  $\rho$  is explained in Figure IV.2. The actual position of the satellite,  $(X',Y',Z')$ , itself can be computed based on the satellite position computed using the broadcast ephemeris,  $(X,Y,Z)$ , and its ephemeris error components (rad,alt,crt) using the following formulation:

$$\begin{bmatrix} X' \\ Y' \\ Z' \end{bmatrix} = \begin{bmatrix} X \\ Y \\ Z \end{bmatrix} + \text{ROT} \cdot \begin{bmatrix} \text{rad} \\ \text{alt} \\ \text{crt} \end{bmatrix} \quad , \quad (\text{VI.5})$$

where ROT (3,3) is the transformation matrix which can be defined in terms of the rotation matrices  $R_1(\alpha)$  and  $R_3(\alpha)$  as follows:

$$\text{ROT} = R_3(-\lambda) \cdot R_1(-i) \cdot R_3(-u) \quad . \quad (\text{VI.6})$$

In the above equation,  $u$  is the *argument of latitudes* (argument of perigee + true anomaly),  $i$  is the *satellite inclination*, and  $\lambda$  is the *longitude of ascending node*. These three parameters can be computed based on the satellite ephemeris. If the definition of the

rotation matrices  $R_1(\alpha)$  and  $R_3(\alpha)$  [Vanicek & Krakiwsky, 1986] are substituted into equation (VI.6), the following elements of matrix ROT can be obtained:

$$\begin{aligned}
 \text{ROT (1,1)} &= \cos(\lambda).\cos(u) - \sin(\lambda).\sin(u).\cos(i) \\
 \text{ROT (1,2)} &= -\cos(\lambda).\sin(u) - \sin(\lambda).\cos(u).\cos(i) \\
 \text{ROT (1,3)} &= \sin(\lambda).\sin(i) \\
 \text{ROT (2,1)} &= \sin(\lambda).\cos(u) + \cos(\lambda).\sin(u).\cos(i) \\
 \text{ROT (2,2)} &= -\sin(\lambda).\sin(u) + \cos(\lambda).\cos(u).\cos(i) \\
 \text{ROT (2,3)} &= -\cos(\lambda).\sin(i) \\
 \text{ROT (2,1)} &= \sin(u).\sin(i) \\
 \text{ROT (2,2)} &= \cos(u).\sin(i) \\
 \text{ROT (2,3)} &= \cos(i)
 \end{aligned}
 \tag{VI.7}$$

#### VI.4. Simulating the ionospheric biases

The ionospheric biases caused by the ionospheric refraction are simulated based on the standard Bent ionospheric model [Llewellyn and Bent, 1973]. It is an empirical world-wide model capable of predicting the ionospheric electron density profile and the corresponding delay and directional changes of the signal due to ionospheric refraction. The model is a result of extensive investigation based on a vast ionospheric data included over 50,000 topside soundings, 6,000 satellite measurements of electron density, and over 400,000 bottomside soundings; extended over the period of 1962 to 1969, covering the minimum to a maximum of a solar cycle. Built into the model are the combined influences of geographical and geomagnetic effects, solar activity, local time, and seasonal variations. The model has a prediction accuracy of about 75 - 80% at mid-latitudes.

Three levels of solar activity are considered in this simulation, and the parameters involved are listed in Table IV.3. To appreciate the different levels of ionospheric activity used, the monthly time series of the mean sunspot number is also given in Figure VI.5.

Table VI.3. Ionospheric simulation parameters.

Activity level	Date	F	F <sub>12</sub>	S <sub>12</sub>
High	11 January 1980	264.4	200.1	163.9
Medium	11 January 1983	144.1	148.5	92.8
Low	11 September 1986	67.9	72.9	12.3

F = the daily solar flux (10.7 cm flux).  
F<sub>12</sub> and S<sub>12</sub> = the 12-month running averages of solar flux and sunspot number.

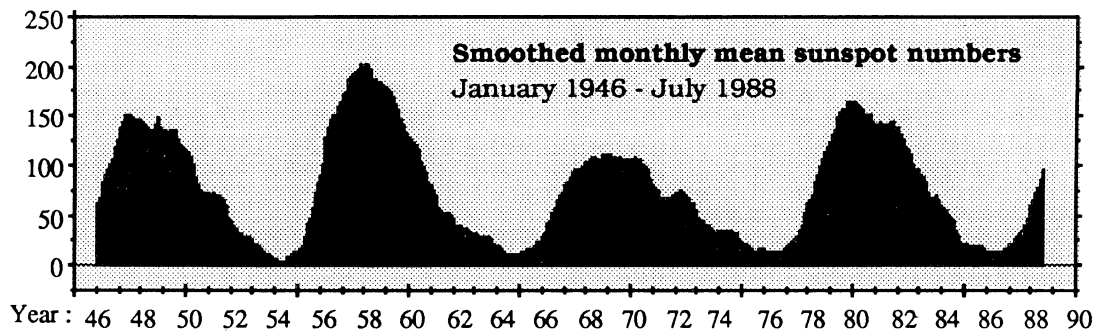


Figure VI.5. Smoothed (12-month running averages) monthly mean sunspot numbers.

### VI.5. Simulating the observation noises

The observation noises are modeled as Gaussian random variables with zero mean and certain standard deviations. At every epoch  $t$ , the noise of the pseudoranges ( $\vartheta P$ ) and phases ( $\vartheta C$ ) observations related to monitor station  $m$ , moving receiver  $v$ , satellite  $j$ , and signal  $i$ , are determined using the following relations:

$$\begin{aligned}
\vartheta P_{i,m}^j(t) &= \sigma_{P_{i,m}} \cdot \mathcal{R}_k(0,1,t) , \\
\vartheta P_{i,v}^j(t) &= \sigma_{P_{i,v}} \cdot \mathcal{R}_1(0,1,t) , \\
\vartheta C_{i,m}^j(t) &= \sigma_{L_{i,m}} \cdot \mathcal{R}_m(0,1,t) , \\
\vartheta C_{i,v}^j(t) &= \sigma_{L_{i,v}} \cdot \mathcal{R}_n(0,1,t) .
\end{aligned}
\quad k \neq 1 \neq m \neq n , \quad (VI.8)$$

In the above equation,  $\sigma_{P_{i,m}}$ ,  $\sigma_{P_{i,v}}$ ,  $\sigma_{L_{i,m}}$ , and  $\sigma_{L_{i,v}}$  are the standard deviation values used to characterize the level of the observation noises.  $\mathcal{R}_k(0,1,t)$  is the real number with index  $t$  of the normally distributed random variables with zero mean and unit standard deviation  $\mathcal{R}_k(0,1)$ .

In this thesis, only the single frequency data is simulated to study the effects of the number and location of the secondary monitor stations on the ambiguity resolution. The standard deviation values listed in Table VI.4 are used to determine the magnitudes of the observation noises at every epoch.

Table VI.4. Standard deviations of the simulated single-frequency data.

$\sigma_{P_{i,m}}$	$\sigma_{P_{i,v}}$	$\sigma_{L_{i,m}}$	$\sigma_{L_{i,v}}$
1.0 m	1.5 m	2.0 mm	3.0 mm

### VI.6. Simulating the integer cycle ambiguity

The integer cycle ambiguity of one-way L1 and L2 carrier phase observations ( $N_1$  and  $N_2$ ), related to satellite  $j$  and a monitor station  $m$  or a moving receiver  $v$ , are simulated by using the following relations:

$$\begin{aligned}
N_{2,m}^j &= 60,000 \cdot \text{PRN}(j) , \\
N_{2,v}^j &= 120,000 \cdot \text{PRN}(j) , \\
N_{1,m}^j &= (77/60) \cdot N_{2,m}^j = 77,000 \cdot \text{PRN}(j) , \\
N_{1,v}^j &= (77/60) \cdot N_{2,v}^j = 154,000 \cdot \text{PRN}(j) .
\end{aligned}
\tag{VI.9}$$

In the above equations, PRN is the Pseudo Random Number of the satellite, which is also an integer. The above relations are adopted for easy verification of integer ambiguities fixed by the ambiguity resolution technique. Notably, by utilizing the above equations, the double-difference integer ambiguities will always be the multiplication of 1,000, regardless of the between-satellite observation differencing strategy used and the signals being used, i.e., L1, L2, wide-lane, narrow-lane, double wide-lane, semi wide-lane, or half wide-lane signals.

## Appendix VII

# GLOSSARY OF GPS TERMINOLOGY

---

---

This appendix is intended to provide an explanation of the GPS terminology used in this dissertation. The glossary of GPS terminology presented here is originally taken from [Wells *et al.*, 1986], and then modified by the author.

\* \* \*

**Ambiguity.** *See* Carrier beat phase ambiguity

**Anti-Spoofing (A-S).** A-S is a procedure to prevent the counterfeiting of the precise P-code. It is done by switching the P-code into the classified Y-code, which can only be decrypted by the authorized users, i.e., U.S. and allied military forces, and approved civilian users. The unauthorized users (mostly civilian) can access only C/A code in this situation. *See* Y-code.

**Bandwidth.** A measure of the width of the spectrum of a signal (frequency domain representation of a signal) expressed in Hertz.

**Baseline.** A baseline consists of a pair of stations for which simultaneous GPS data has been collected.

**Beat frequency.** Either of the two additional frequencies obtained when signals of two frequencies are mixed, equal to the sum or difference of the original frequencies, respectively. For example, in the identity,

$$\cos A \cos B = (\cos(A+B) + \cos(A-B))/2,$$

the original signals are A and B and the beat signals are A+B and A-B. The term Carrier Beat Phase refers only to the difference A-B, where A is the incoming Doppler-shifted satellite carrier signal, and B is the nominally constant-frequency reference signal generated in the receiver.

**Between-epoch difference.** The difference between two measurements (carrier phases or codes) made by the same receiver on the same signal (same satellite, same frequency), but at different time epochs.

**Between-frequency difference.** The instantaneous difference between two measurements (carrier phases or codes) made by the same receiver observing signals from the same satellite at two (or more) different frequencies.

**Between-receiver (between-station) difference.** The instantaneous difference between two measurements (carrier phases or codes) made at two receivers simultaneously observing the same received signal (same satellite, same frequency).

**Between-satellite difference.** The instantaneous difference between two measurements (carrier phases or codes) made by the same receiver observing two satellite signals simultaneously (same frequency).



**Binary pulse code modulation.** Pulse modulation using a string (code) of binary numbers. This coding is usually represented by ones and zeros with definite meanings assigned to them, such as changes in phase or direction of a wave [*Dixon, 1976*].

**Binary biphasic modulation.** Phase changes on a constant frequency carrier of either  $0^\circ$  or  $180^\circ$  (to represent binary 0 or 1, respectively). These can be modelled by  $y = A(t) \cos (wt + \phi)$ , where the amplitude function  $A(t)$  is a sequence of +1 and -1 values (to represent  $0^\circ$  and  $180^\circ$  phase changes, respectively). [*Dixon, 1976*].

**Broadcast Ephemeris.** The satellite orbital information that is transmitted to the user in the navigation message. It is used to estimate the current satellite position .

**Carrier.** A radio wave having at least one characteristic (e.g., frequency, amplitude, phase) which may be varied from a known reference value by modulation [*Bowditch, 1981*].

**Carrier frequency.** The frequency of the unmodulated fundamental output of a radio transmitter [*Bowditch, 1981*].

**Carrier beat phase.** The phase of the signal which remains when the incoming Doppler-shifted satellite carrier signal is beat (the difference frequency signal is generated) with the nominally constant-frequency reference signal generated in the receiver.

**Carrier beat phase ambiguity.** The uncertainty in the initial measurement, which biases all measurements in an unbroken sequence. The ambiguity consists of three components :

$$\alpha_i, \beta^j, \text{ and } N_1^j$$

where

$\alpha_i$  is the fractional initial phase in the receiver

$\beta^j$  is the fractional initial phase in the satellite (both due to various contributions to phase bias, such as unknown clock phase, circuit delays, etc.), and

$N_1^j$  is an integer cycle bias in the initial measurement.

**Channel.** A channel of a GPS receiver consists of the radio frequency, digital hardware, and the software required to track the signal from one GPS satellite at one of the two GPS carrier frequencies.

**Chip.** The minimum time interval of either a zero or a one in a binary pulse code.

**C/A-code.** The standard (Coarse/Acquisition, or Clear/Access) GPS code—a sequence of 1023 pseudo-random binary biphasic modulations on the GPS carrier at a chip rate of 1.023 MHz, thus having a code repetition period of one millisecond.

**Complete instantaneous phase measurement.** A measurement of carrier beat phase which includes the integer number of cycles of carrier beat phase since the initial phase measurement. *See* Fractional instantaneous phase measurement.

**Control segment.** A world-wide network of GPS monitoring and control stations that ensure the accuracy of satellite positions and their clocks [*Trimble Navigation*, 1989].

**Correlation-type channel.** A GPS receiver channel which uses a delay lock loop to maintain an alignment (correlation peak) between the replica of the GPS code generated in the receiver and the incoming code.

**Cycle slip.** A cycle slip is a discontinuity of an integer number of cycles in the measured carrier beat phase resulting from a temporary loss-of-lock in the carrier tracking loop of a GPS receiver.

**Delay lock.** The technique whereby the received code (generated by the satellite clock) is compared with the internal code (generated by the receiver clock) and the latter shifted in time until the two codes match. Delay lock loops can be implemented in several ways, for example, tau dither and early-minus-late gating.

**Differenced measurements.** *See* Between-epoch difference, Between-frequency difference, Between-receiver difference, and Between-satellite difference. Many combinations of differences are possible. The difference and its order, should be specified in describing a processing method (for example receiver-satellite double differences).

**Dilution of precision (DOP).** A description of the purely geometrical contribution to the uncertainty in a kinematic position fix, given by the expression

$$\text{DOP} = \text{TRACE}(A^T A)^{-1},$$

where  $A$  is the design matrix for the solution (dependent on satellite/receiver geometry). The DOP factor depends on the parameters of the position fix solution. Standard terms in the case of kinematic GPS are:

GDOP	(three position coordinates plus clock offset in the solution)
PDOP	(three coordinates)
HDOP	(two horizontal coordinates)
VDOP	(height only)
TDOP	(clock offset only), and
HTDOP	(horizontal position and time).

**Doppler shift.** The apparent change in frequency of a received signal due to the rate of change of the range between the transmitter and receiver. *See* Carrier beat phase.

**Double-difference observation.** The difference between two single-difference observations. *See* single-difference observation.

**Fast switching channel.** A switching channel with a sequence time short enough to recover (through software prediction) the integer part of the carrier beat phase.

**Fractional instantaneous phase measurement.** A measurement of the carrier beat phase which does not include any integer cycle count. It is a value between zero and one cycle. *See* Complete instantaneous phase measurement.

**Frequency band.** A range of frequencies in a particular region of the electromagnetic spectrum [*Wells, 1974*].

**Frequency spectrum.** The distribution of amplitudes as a function of frequency of the constituent waves in a signal [*Wells, 1974*].

**GLONASS.** GLONASS (Global Navigation Satellite System) is the Soviet satellite navigation system, quite similar to GPS. In the operational phase, the GLONASS space segment is planned to comprise 24 satellites, eight satellites spaced evenly in each of six nearly circular orbital planes, which have 64.8 degree inclination. The satellites are at an altitude of 19,100 kilometres with an orbital period of 11 hours and 15 minutes.

**Ionosphere.** The region of the Earth's atmosphere in which ionizing radiation causes electrons to exist in sufficient quantities to affect the propagation of radio waves [*Langley, 1992*]. It extends from an altitude of about 50 km to about 2,000 km.

**Ionospheric refraction.** A signal travelling through the ionosphere experiences a propagation time different from that which would occur in a vacuum. Phase advance depends on electron content and affects carrier signals. Group delay depends on dispersion in the ionosphere as well, and affects signal modulation (codes). The phase advance and group delay are of the same magnitude, but opposite sign.

**Kinematic positioning.** Kinematic positioning refers to applications in which a trajectory (of a ship, ice field, tectonic plate, etc.) is determined.

**Lane.** The area (or volume) enclosed by adjacent lines (or surfaces) of zero phase of either the carrier beat phase signal, or of the difference between two carrier beat phase signals. On the earth's surface, a line of zero phase is the locus of all points for which the observed value would have an exact integer value for the complete instantaneous phase measurement. In three dimensions, this locus becomes a surface.

**L-band.** The radio frequency band extending from 390 MHz to (nominally) 1550 MHz [Bowditch, 1981].

**Multipath error.** An error resulting from interference between radiowaves which have travelled between the transmitter and the receiver by two paths of different electrical lengths [Bowditch, 1981].

**Multichannel receiver.** A receiver containing many channels.

**Multiplexing channel.** A receiver channel which is sequenced through a number of satellite signals (each from a specific satellite and at a specific frequency) at a rate which is synchronous with the satellite message bit-rate (50 bits per second or 20 milliseconds per bit). Thus, one complete sequence is completed in a multiple of 20 milliseconds.

**Observing session.** The period of time over which GPS data is collected simultaneously by two or more receivers.

**One-way observation.** Observation of a certain signal, involving one receiver and one satellite.

**Outage.** The occurrence in time and space of a GPS Dilution of Precision value exceeding a specified maximum.

**P-code.** The Precise (or Protected) GPS code—a very long (about  $10^{14}$  bit) sequence of pseudo-random binary biphasic modulations on the GPS carrier at a chip rate of 10.23 MHz which does not repeat itself for about 267 days. Each one-week segment of the P-code is unique to one GPS satellite and is reset each week.

**Phase lock.** The technique whereby the phase of an oscillator signal is made to become a smoothed replica of the phase of a reference signal by first comparing the phases of the two signals and then using the resulting phase difference signal to adjust the reference oscillator frequency to eliminate phase difference when the two signals are next compared. The smoothing time span occurs over approximately the inverse of the bandwidth. Thus a 40 hertz loop bandwidth implies an approximately 25 millisecond smoothing time constant.

**Point positioning.** Determination of the position of the point(s) based on only one receiver measurements.

**Precise positioning service (PPS).** The navigation and positioning service provided by dual-frequency P-code, with the effects of Selective Availability and Anti-Spoofing counteracted. PPS is intended for U.S. military and authorized users. See Selective Availability and Anti-Spoofing.

**Pseudo-random noise (PRN) code.** Any of a group of binary sequences that exhibit noise-like properties, the most important of which is that the sequence has a maximum autocorrelation at zero lag [Dixon, 1976].

**Pseudo-random noise (PRN) code number.** PRN number of a satellite denotes which of the available 37 seven-day segments of P-code pseudorandom noise signal is presently used by each particular satellite. The number is used as one way to identify the individual GPS satellite.

**Pseudorange.** The time shift required to align (correlate) a replica of the GPS code generated in the receiver with the received GPS code, scaled into distance by the speed of light. This time shift is the difference between the time of signal reception (measured in the receiver time frame) and the time of emission (measured in the satellite time frame).

**Relative positioning.** The determination of relative positions between two or more receivers which are simultaneously tracking the same radiopositioning signals (e.g., from GPS). It is sometimes also called *differential positioning*. In this type of positioning, one or more receivers are located at the station(s) with known coordinates, usually called monitor stations or reference sites.

**Satellite constellation.** The arrangement in space of the complete set of satellites of a system like GPS.

**Satellite configuration.** The state of the satellite constellation at a specific time, relative to a specific user or set of users.

**Selective availability (SA).** SA is a technique intended to protect precise, real-time GPS data for authorized users only, i.e., U.S. and allied military forces and approved civilians [Wysocki, 1991]. SA is implemented by a combination of degraded satellite orbital information ( $\epsilon$ -type SA) and satellite clock dithering ( $\delta$ -type SA).

**Simultaneous measurements.** Measurements referred to time frame epochs which are either exactly equal or else so closely spaced in time that the time misalignment can be accommodated by correction terms in the observation equation, rather than by parameter estimation.

**Single-difference observation.** The difference between two one-way observations. It could be related to different epochs, different frequencies, different receivers, or different satellites. *See* one-way observation.

**Slow switching channel.** A switching channel with a sequencing period which is too long to allow recovery of the integer part of the carrier beat phase.

**Spread spectrum systems.** A system in which the transmitted signal is spread over a frequency band much wider than the minimum bandwidth needed to transmit the information being sent [Dixon, 1976].

**Squaring-type channel.** A GPS receiver channel which multiplies the received signal by itself to obtain a second harmonic of the carrier, which does not contain the binary biphase code modulation.

**Standard positioning service (SPS).** The navigation and positioning service provided by the single-frequency C/A code, affected by Selective Availability. SPS is intended primarily for civil GPS users. *See* Selective Availability and Anti-Spoofing.



**Static positioning.** Positioning applications in which the positions of points are determined without regard for any trajectory they may or may not have.

**Switching channel.** A receiver channel which is sequenced through a number of satellite signals (each from a specific satellite and at a specific frequency).

**Troposphere.** The lower part of the Earth's atmosphere, where temperature decreases with an increase in altitude [*Langley, 1992*]. It extends from the Earth's surface to an altitude of about 9 to 16 km (its thickness is not everywhere the same). The propagation of electromagnetic signals will be affected due to the presence of neutral atoms and molecules in the troposphere.

**Tropospheric delay.** The troposphere delays the GPS signals. Unlike the ionosphere, the troposphere is not dispersive for frequencies below 30 GHz, and therefore the group and phase delays are the same.

**Y-code.** A classified code, which is the modulo two sum of the P-code and the encryption code W [*Ashjaee and Lorenz, 1992*]. See Anti-Spoofing.

# V I T A

---

---

- Candidate's full name : Hasanuddin Zainal Abidin.
- Place and date of birth : Jakarta, Indonesia, August 8, 1960.
- Permanent address : Department of Geodesy,  
Bandung Institute of Technology,  
Ganesha St. # 10,  
Bandung 40132, Indonesia.
- Schools attended : Elementary School of Gleumpang Minyeuk,  
Aceh, Indonesia, 1966 - 1968.
- Elementary School of Ciputat,  
Jakarta, Indonesia, 1968 - 1971.
- Junior High School # 87,  
Jakarta, Indonesia, 1972 - 1974.
- High School # 29,  
Jakarta, Indonesia, 1975 - 1977.
- Universities attended : Department of Electrical Engineering,  
Bandung Institute of Technology, Indonesia,  
1978 - 1979.
- Department of Geodesy,  
Bandung Institute of Technology, Indonesia,  
1980 - 1985, Ir (1985).
- Department of Surveying Engineering,  
University of New Brunswick, Fredericton, Canada,  
1986 - 1989, M.Sc.Eng. (1989).
- Department of Surveying Engineering,  
University of New Brunswick, Fredericton, Canada,  
1989 - 1992, Ph.D. candidate.

## PUBLICATIONS :

- Abidin, H. Z. (1988). "Real-time marine differential kinematic GPS - Comparison of positioning methods." *Proceedings of The Institute of Navigation Satellite Division Student Paper Competition*, Colorado Springs, Colorado, USA, 19-23 September, pp. 1-22.

- Abidin, H. Z. and D.E. Wells (1989). "Real-time marine instantaneous velocity determination using differential GPS." *Proceedings of the fifth international geodetic symposium on satellite positioning*. New Mexico State University, Las Cruces, New Mexico, March 13-17. Volume II, pp. 1009-1018.
- Abidin, H. Z. and D. E. Wells (1990). "Extrawidelaning for on-the-fly ambiguity resolution : simulation of ionospheric effects." *Proceedings of Second International Symposium on Precise Positioning with the Global Positioning System*, Ottawa, Canada, 3-7 September, pp. 1217-1232.
- Abidin, H. Z. (1990). "Extrawidelaning for on-the-fly ambiguity resolution : simulation of multipath effects." *Proceedings of ION GPS-90 Third International Technical Meeting of the Satellite Division of the Institute of Navigation*, Colorado Springs, Colorado, USA, 17-21 September, pp. 525-533.
- Abidin, H. Z. (1991). "New strategy for 'on the fly' ambiguity resolution." *Proceedings of ION GPS-91, Fourth International Technical Meeting of the Satellite Division of the Institute of Navigation*, Albuquerque, New Mexico, 11-13 September, pp. 875-886.
- Abidin, H. Z., D.E. Wells, and A. Kleusberg (1991). "Multi monitor station on-the-fly ambiguity resolution: Theory and preliminary results." *Proceedings of DGPS '91, First International Symposium on Real Time Differential Applications of the Global Positioning System*, Braunschweig, Federal Republic of Germany, 16-20 September, Volume I, pp. 44-56.
- Abidin, H.Z. (1992). "Multi-monitor station on-the-fly ambiguity resolution: the impacts of satellite geometry and monitor station geometry." *Proceedings of PLANS '92, IEEE Position Location and Navigation Symposium*, Monterey, California, 24-27 March, pp. 412-418.
- Abidin, H.Z., D.E. Wells, and A. Kleusberg (1992). "Some aspects of on-the-fly ambiguity resolution." Paper presented at Sixth International Geodetic Symposium on Satellite Positioning, Columbus, Ohio, 17-20 March.